

UNIVERSITY  

---

OF CENTRAL  

---

LANCASHIRE



Developing a physiologically relevant blood brain  
barrier model for the study of drug disposition in  
glioma.

By

Swati Ashok Kumar

A thesis submitted in partial fulfilment for the requirements for the degree of  
Doctor of Philosophy at the University of Central Lancashire

July 2015

# STUDENT DECLARATION FORM



## Concurrent registration for two or more academic awards

I declare that while registered as a candidate for the research degree, I have not been a registered candidate or enrolled student for another award of the University or other academic or professional institution

---

## Material submitted for another award

I declare that no material contained in the thesis has been used in any other submission for an academic award and is solely my own work

---

## Collaboration

Where a candidate's research programme is part of a collaborative project, the thesis must indicate in addition clearly the candidate's individual contribution and the extent of the collaboration. Please state below:

**Signature of Candidate**

A handwritten signature in black ink, appearing to read "Skumar", written over a horizontal line.

**Type of Award**

**Doctor of Philosophy (PhD)**

**School**

**School of Pharmacy and Biomedical Science**

# Abstract

The blood brain barrier is a highly selective physical, transport and metabolic barrier, that limits the disposition of drugs to the CNS; a pertinent problem to the successful treatment of glioma. There has been an emergence of cell based *in vitro* models as potential tools to predict the *in vivo* permeation of therapeutics at the BBB, however most of the available models have only been characterised for just the physical barrier and not the metabolic barrier comprised of efflux transporters and drug metabolising enzymes. In addition, a review of all the available models found that there was a lack of multicellular models cultured using all human components. There was an urgent need to develop a model which is physiologically relevant and focusses on the metabolic barrier present at the blood and brain junctions with a goal to delivering chemotherapeutics to CNS tumours. The aim of the study was to design an all human, fully characterised and physiologically relevant *in vitro* BBB model for the prediction of permeability of drugs across the blood brain barrier to glioma. Cell cultures investigated included the glioma cell lines (U87MG, 1321N1), non-cancerous cell lines (SVGP12, hCMEC/D3), glioma short term cultures (BTNW914, BTNW370) human endothelial culture (HBMEC), human astrocytes (HA) and human pericytes (HBVP). The cell cultures were characterised and studied for the expression of activity levels for efflux transporters; ABCB<sub>1</sub> and ABCG<sub>2</sub> and drug metabolising enzymes; CYP3A4 and CYP2D6. The culturing conditions of cells was optimised by using human serum, human fibronectin to maximise the expression and activity of these proteins. The cell showing high expression and activity were used to design the mono-, co- and tri- culture *in vitro* BBB model on a transwell insert. The models were assessed on the basis of TEER, tight junction protein expression and expression and activity of efflux transporter and DMEs. These models were also constructed on 3D Alvetex scaffolds and exposed to shear stress by dynamic perfusion. Finally model was used to screen permeability of novel lipid NPs and a glioma specific targeting aptamer SA43. The human primary cultures (HBMEC, HBVP and HA) were selected to model the BBB and the tri-culture model gave the highest TEER of 258  $\Omega/\text{cm}^2$ . The tri-culture model on alvetex scaffold with perfusion showed a TEER of 769  $\Omega/\text{cm}^2$ . The screening of NPs found the docetaxel and curcumin lipid NPs were permeable through the barrier. In future, the developed BBB model will be further characterised and used commercially for screening of novel glioma therapeutics and drug delivery systems.

# List of figures

Figure 1.1 A) Tumour invading healthy brain tissue. B) Tumour pressing on the healthy tissue and causing increased pressure within the brain (Abrey and Mason, 2003).....	1
Figure 1.2 Illustration of the ten capabilities of cancer cells acquired during development of cancer (Hanahan and Weinberg, 2000; Hanahan and Weinberg, 2011). .....	3
Figure 1.3 Types of neuroglial tumours classified by the cell of origin (Huse and Holland, 2010). .....	6
Figure 1.4 Genetic pathways to primary (de novo) and secondary glioblastomas at the population level (Grzmil and Hemmings, 2010) .....	7
Figure 1.5 Pathways for the development of primary and secondary GBM showing genetic alterations in types of glioma. ....	8
Figure 1.6 Cancer survival rates.....	12
Figure 1.7 The neurovascular unit of the Blood Brain Barrier (Hartz and Bauer, 2010). ...	16
Figure 1.8 Diagrammatic representation of the cerebral capillary highlighting the structure of BBB comprising of TJs in the interendothelial cleft and high numerical density of TJs (Burns <i>et al.</i> , 1981). .....	17
Figure 1.9 Assembly of transmembrane proteins, occluding, claudins forming the TJs between the endothelial cells (Chou and Messing, 2008).....	18
Figure 1.10 Schematic illustration of transport across the brain endothelial cells (Wong <i>et al.</i> , 2013). .....	21
Figure 1.11 Schematic representation of drug disposition within the body (Gunaratna, 2000). .....	22
Figure 1.12 Different phases involved in drug metabolism.....	23
Figure 1.13 The proportion of drugs metabolised by various enzymes in the Phase I metabolism process. ....	24
Figure 1.14 The proportion of drugs metabolised by various enzymes in the Phase II metabolism process. ....	25
Figure 1.15 A) Absorption spectra for cytochrome P450 and the shift in the absorption spectrum due to its ferrous–carbon monoxide complex (Munro <i>et al.</i> , 2007). B) Structure of a porphyrin ring with a covalently bound haem in CYP enzymes (Johnston <i>et al.</i> , 2011)..	26

Figure 1.16 Schematic representation of metabolic pathway of a carcinogen causing tumour genesis (Oyama <i>et al.</i> , 2004).....	33
Figure 1.17 Carrier-mediated transport machineries (efflux and the influx transporters) at the BBB sites of the BBB (Omidi and Barar, 2012).....	34
Figure 1.18 Measurement of TEER using an EVOM-2.....	41
Figure 1.19 Diagrammatic representation of the electric resistance and capacitance across the cell monolayer in Cellzscope. ....	42
Figure 1.20 Monolayer of cells through which the ECIS reads the membrane capacitance and resistance. ....	43
Figure 1.21 Summary of the conducted experiments.....	48
Figure 2.1 Diagrammatic representation of a transwell insert. ....	70
Figure 2.2 A scheme of the proposed <i>in vitro</i> BBB transwell models.....	73
Figure 2.3 Diagrammatic representation of transwell insert used for permeability assay. ...	77
Figure 2.4 Diagrammatic representation of brain tumour barrier .....	81
Figure 3.1 Growth analysis of human cell lines.....	86
Figure 3.2 Light microscopy images of cells on day 3 of growth.....	87
Figure 3.3 Growth analysis of primary cultures.....	88
Figure 3.4 Light microscopy images of cells on day 5 of the exponential phase of growth.....	89
Figure 3.5 Fluorescence staining of cell lines for GFAP and HLA. ....	90
Figure 3.6 DAB staining of patient derived short term culture BTNW914.....	93
Figure 3.7 DAB staining of patient derived short term culture BTNW370.....	94
Figure 4.1 Concentration of protein extracted with respect to time in the exponential growth phase of cell lines. ....	103
Figure 4.2 Standard linear plot of BSA (mg/mL) vs. absorbance at 612 nm.....	104
Figure 4.3 Standard linear plot of BSA (mg/mL) vs. absorbance at 612 nm.....	105
Figure 4.4 Standard linear plot of BSA (mg/mL) vs. absorbance at 612 nm.....	106
Figure 4.5 Standard linear plot of BSA (mg/mL) vs. absorbance at 612 nm.....	107
Figure 4.6 Western blots showing expression of CYP3A4 (57 kDa). ....	110
Figure 4.7 Densitometry analysis of the blots showing expression of CYP3A4. ....	110
Figure 4.8 Western blots showing expression of CYP2D6 (57 kDa). ....	111
Figure 4.9 Densitometry analysis of the blots showing expression of CYP2D6. ....	112
Figure 4.10 Western blots showing expression of ABCB <sub>1</sub> efflux transporter (170 kDa)..	113

Figure 4.11 Densitometry analysis of the blots showing semi-quantitation of the ABCB <sub>1</sub> efflux transporter.....	113
Figure 4.12 Western blots showing expression of ABCG <sub>2</sub> efflux transporter (72 kDa). ..	114
Figure 4.13 Densitometry analysis of the blots showing expression of ABCG <sub>2</sub> efflux transporter. ....	115
Figure 4.14 Expression of the efflux transporters and drug metabolising enzymes in HA (human astrocyte) in different culturing conditions.....	117
Figure 4.15 Densitometry analysis of the blots showing expression of efflux transporters and DMEs in HA cells. ....	119
Figure 4.16 Expression of the efflux transporters and drug metabolising enzymes in HBVP (pericyte cells) in various culturing conditions. ....	120
Figure 4.17 Densitometry analysis of the blots showing expression of efflux transporters and DMEs in HBVP cells. ....	122
Figure 4.18 Expression of the efflux transporters and drug metabolising enzymes in HBMEC (endothelial cell) primary culture in various culturing conditions.....	123
Figure 4.19 Densitometry analysis of the blots showing expression of efflux transporters and DMEs in HBMEC cells.....	125
Figure 4.20 Activity of efflux transporters in different cells. ....	129
Figure 4.21 Activity of efflux transporters in U87MG cells (grade IV glioma).....	132
Figure 4.22 Activity of efflux transporters in 1321N1 cells (grade IV glioma). ....	134
Figure 4.23 Activity of efflux transporters in SVGp12 cells (foetal glial cells).....	136
Figure 4.24 Activity of efflux transporters in HBMEC. ....	138
Figure 4.25 Activity of efflux transporters in HA cells. ....	140
Figure 4.26 Activity of efflux transporters in HBVP cells. ....	142
Figure 4.27 Activity of efflux transporters in hCMEC/D3 cells.....	144
Figure 4.28 Standard plot of concentration of fluorescence <i>verses</i> HFC metabolite concentration. ....	146
Figure 4.29 Standard plot of concentration of fluorescence <i>verses</i> metabolite AHMC. ...	146
Figure 4.30 Activity of CYP3A4 metabolism of BFC to HFC at different protein concentration in bacosomes. ....	148
Figure 4.31 Activity of CYP2D6 metabolism of AMMC to AHMC at different protein concentrations of bacosome. ....	149

Figure 4.32 A Activity of CYP3A4 enzyme at different BFC substrate concentration with respect to time .....	151
Figure 4.33 Michaelis Menton plot determining the rate of metabolism <b>A</b> CYP3A4 <b>B</b> CYP2D6 .....	153
Figure 4.34 Activity CYP3A4 metabolism of 25 $\mu$ M BFC to HFC in 1 mg/ mL cell lines and short term cultures .....	155
Figure 4.35 Activity CYP2D6 metabolism of 25 $\mu$ M AMMC to AHMC in 1 mg/ml cell lines and short term cultures .....	156
Figure 5.1 Mean of five measurements of TEER within each well .....	166
Figure 5.2 Mean of three measurements of TEER for intra-replicates of an experiment ..	167
Figure 5.3 Mean of three measurements of TEER for inter-replicates of an experiment ..	167
Figure 5.4 Effect of co- and tri cultivation on the induction of TEER in hCMEC/D3 monolayers of <i>in vitro</i> BBB models measured by the EVOM probe. ....	169
Figure 5.5 Comparison between TEER values measured by EVOM for all of the hCMEC/D3 co- and tri- culture models. ....	170
Figure 5.6 Western blots for TJs proteins expression in hCMEC/D3 mono-, co- and tri-cultures .....	171
Figure 5.7 Densitometry analysis of TJs proteins expression in hCMEC/D3 mono-, co- and tri- cultures .....	172
Figure 5.8 TEER measurements of endothelial (hCMEC/D3) monoculture in 2D ECIS model .....	173
Figure 5.9 TEER measurements of endothelial cells (hCMEC/D3) and astrocytes (SC-1800) co-culture in 2D ECIS model .....	174
Figure 5.10 TEER measurements of endothelial cells (hCMEC/D3) and pericytes (HBVP) co-culture in 2D ECIS model. The graph is an average of the data from two separate experiments. ....	175
Figure 5.11 TEER measurements of endothelial cells (hCMEC/D3), astrocytes (SC1800) and pericytes (HBVP) tri-culture in 2D ECIS model. ....	176
Figure 5.12 Comparison of TEER measured for co- and tri- culture 2D models set up on the ECIS array .....	178
Figure 5.13 Western blots for TJs proteins expression in hCMEC/D3 mono-, co- and tri-cultures setup on the ECIS array .....	179

Figure 5.14 Densitometry analysis of TJs proteins expression in hCMEC/D3 mono-, co- and tri- cultures setup on the ECIS array. ....	180
Figure 5.15 <b>A.</b> TEER measurements <b>B.</b> Capacitance of endothelial (hCMEC/D3) monoculture in 3D model. ....	182
Figure 5.16 <b>A:</b> TEER measurements <b>B:</b> Capacitance of endothelial cells (hCMEC/D3) and astrocytes (SC-1800) co-culture in 3D model.....	183
Figure 5.17 <b>A.</b> TEER measurements and <b>B.</b> Capacitance of endothelial cells (hCMEC/D3) and pericytes (HBVP) co-culture in 3D model. ....	184
Figure 5.18 <b>A.</b> TEER measurements and <b>B.</b> Capacitance of endothelial cells (hCMEC/D3), astrocytes (SC1800) and pericytes (HBVP) tri-culture in 3D model.....	185
Figure 5.19 Comparison of all the TEER measurements in different co- and tri- culture 3D models set up on the Cellzscope. ....	187
Figure 5.20 Western blots for TJs protein expression in hCMEC/D3 mono-, co- and tri- cultures set up on Cellzscope. ....	188
Figure 5.21 Densitometry analysis of TJs proteins expression in hCMEC/D3 mono-, co- and tri- cultures set up on Cellzscope. ....	189
Figure 5.22 Effect of co- and tri cultivation on the induction of TEER in HBMEC monolayers of <i>in vitro</i> BBB models. ....	191
Figure 5.23 Comparison of TEER values between all the HBMEC co- and tri- culture models. ....	193
Figure 5.24 Western blots for TJs proteins expression in HBMEC mono-, co- and tri- cultures. ....	194
Figure 5.25 Densitometry analysis of TJs proteins expression in HBMEC mono-, co- and tri- cultures. ....	195
Figure 5.26 Effect of foetal calf serum and human serum on the induction of TEER in HBMEC co- and tri-culture <i>in vitro</i> BBB models. ....	197
Figure 5.27 Comparison between TEER values obtained from HBMEC co- and tri-cultures of <i>in vitro</i> BBB models grown in foetal calf serum and human serum in. ....	198
Figure 5.28 Western blots for TJs protein expression in HBMEC co- and tri-cultures of <i>in vitro</i> BBB models grown in foetal calf serum and human serum. ....	199
Figure 5.29 Densitometry analysis of TJs proteins expression in HBMEC co- and tri-cultures of <i>in vitro</i> BBB models grown in foetal calf serum and human serum.....	200

Figure 5.30 Comparison of TEER values between co- and tri-culture models of HBMEC in Alvetex scaffold with and without perfusion (sheer flow).....	202
Figure 5.31 Comparison of TEER measurements in co- and tri- cultures of HBMEC with perfused alvetex scaffold, static alvetex scaffold and static polycarbonate insert of BBB models. ....	204
Figure 5.32 Western blots for TJs proteins expression in HBMEC tri-cultures set up on different inserts.....	205
Figure 5.33 Densitometry analysis of TJs proteins expression in HBMEC tri-cultures set up on different inserts.....	206
Figure 5.34 Effect of location of pericyte on the induction of TEER in tri- or co-culture <i>in vitro</i> BBB models.....	208
Figure 5.35 Comparison of TEER values between HBMEC and HA (in-contact) co-culture with different location of pericyte.....	209
Figure 5.36 Western blots of TJs proteins expression in HBMEC co- and tri-cultures with different location of HBVP. ....	210
Figure 5.37 Densitometry of TJs proteins expression in HBMEC co-, tri-cultures with different location of HBVP. ....	211
Figure 5.38 Expression of efflux transporters in different <i>in vitro</i> BBB models.....	213
Figure 5.39 Densitometry of efflux transporters in different <i>in vitro</i> BBB models. <b>A.</b> ABCB <sub>1</sub> . <b>B.</b> ABCG <sub>2</sub> .....	214
Figure 5.40 Activity of ABCB <sub>1</sub> efflux transporter in different <i>in vitro</i> BBB models.....	215
Figure 5.41 Activity of ABCG <sub>2</sub> efflux transporter in different <i>in vitro</i> BBB models. ....	216
Figure 5.42 Expression of drug metabolising enzymes in different <i>in vitro</i> BBB models.	217
Figure 5.43 Densitometry of drug metabolising enzymes in different <i>in vitro</i> BBB models. ....	218
Figure 5.44 Measurement of fluorescent HFC formation by CYP3A4 with respect to time in different <i>in vitro</i> BBB models.....	220
Figure 5.45 Measurement of AMHC formation by CYP2D6 in different <i>in vitro</i> BBB models. ....	221
Figure 5.46 Expression and activity of efflux transporter in both tri-culture <i>in vitro</i> BBB models. ....	224
Figure 5.47 Activity of ABCB <sub>1</sub> and ABCG <sub>2</sub> in the different designed tri-culture models.	225

Figure 5.48 Expression and activity of drug metabolising enzyme in both tri-culture <i>in vitro</i> BBB models. ....	227
Figure 5.49 Activity of CYP3A4 and CYP2D6 in the different designed tri-culture models. ....	228
Figure 6.1: Permeability of FITC-dextran across different models at time intervals 1 h, 2 h and 3 h.....	243
Figure 6.2: Standard plot of fluorescence <i>versus</i> concentration of FITC-dextran measured at excitation wavelength 492 nm and emission wavelength 518 nm. The data points are means of three replicates (n=3). ....	244
Figure 6.3: Percentage cell viability of endothelial cells relative to vehicle control after treatment with three different concentrations of docetaxel loaded lipid nanoparticle at time points 24 h, 48 h and 72 h determine by the MTS assay. ....	246
Figure 6.4: Percentage cell viability of endothelial cells relative to vehicle control after treatment with three different concentrations of lipid nanoparticle at time points 24 h, 48 h and 72 h as measured by the MTS assay.....	248
Figure 6.5: Percentage cell viability of endothelial cells relative to vehicle control after treatment with three different concentrations of NPs and SA43 aptamer at time points 24 h, 48 h and 72 h as measured by the MTS assay.....	250
Figure 6.6: Permeability of aptamers SA43 (10nM) and FITC-dextran across different <i>in vitro</i> BBB tri-culture model [HBMEC, HA (in contact) and HBVP (out of contact)] at time intervals 1 h, 2 h & 3 h.....	251
Figure 6.7 Time course TEER measurement of tri-culture BBB model to study the effect of NPs on the resistance of the barrier.....	253
Figure 7.1 Comparison of TEER values in tri-culture model with GBM spheroids (basolateral side) compared to tri-culture alone without GBM. ....	263
Figure 7.2 Comparison of expression between GBM spheroids and monolayer.....	264
Figure 7.3 NPs uptake by spheroids on tri-culture with GBM (basolateral side). ....	267
Figure 7.4 BBB structure <i>in vivo</i> . a) normal BBB model b) BBB model when leaky. ....	269
Figure 8.1 Schematic overview of the permeability pathways across the endothelial barrier (Kroll and Neuwelt, 1998). ....	281

# List of tables

<i>Table 1.1 Synopsis of clinical data of primary and secondary glioblastoma (Nakada et al., 2011).</i> .....	6
<i>Table 1.2 WHO Grading of Tumours of the Central Nervous System (Louis et al., 2007) ...</i>	9
<i>Table 1.3: Summary of nuclear receptor activating target gene (Hedlund et al., 2001).</i> ....	27
<i>Table 1.4 Various CYP isoforms found localised in specific regions of the brain (Meyer et al., 2007)</i> .....	29
<i>Table 1.5 Chemotherapeutics for treatment of glioma and CYPs involved in their metabolism.</i> .....	32
<i>Table 1.6 ABC transporters involved in drug resistance and cancer therapy (Hartz and Bauer, 2010).</i> .....	36
<i>Table 1.7 List of patented models of in vitro BBB (Toth et al., 2011).</i> .....	44
<i>Table 2.1 Summary of cell culture supplements used.</i> .....	51
<i>Table 2.2 List of rabbit polyclonal primary antibodies, their concentration and dilutions used for immunostaining.</i> .....	56
<i>Table 2.3 List of concentrations and dilutions and incubation period of rabbit polyclonal primary antibodies used for DAB staining.</i> .....	57
<i>Table 2.4 List of concentration and dilution of rabbit polyclonal primary antibodies (Abcam, UK) and secondary antibody used for probing nitrocellulose membrane blots.</i> .....	63
<i>Table 2.5 The layout of the chip in the ECIS plate. E: endothelial cells, A: astrocytes, P: pericytes and ECM: extra cellular matrix.</i> .....	75
<i>Table 2.6 List of NPs, aptamer and Evans blue concentration used for toxicity screening.</i>	78
<i>Table 2.7 List of NPs and their concentrations used for the cellular uptake studies.</i> .....	80
<i>Table 2.8 Concentration of NPs used in the BTB model permeability studies.</i> .....	82
<i>Table 4.1 Summary of the protein concentration of cell lines using different extraction protocol.</i> .....	108
<i>Table 4.2 Summary of the % expression of different protein relative to standard culturing conditions.</i> .....	126
<i>Table 4.3 Rate of CYP3A4 and CYP2D6 enzyme at 25 <math>\mu</math>M substrate concentration in cell lines, primary and short term cultures.</i> .....	157
<i>Table 5.1 Rate of enzyme activity at 25 <math>\mu</math>M [S]</i> .....	222

<i>Table 5.2 Rate of enzyme activity at 25 <math>\mu</math>M [S]</i> .....	228
<i>Table 6.1 Apparent permeability value of the in vitro BBB models</i> .....	244
<i>Table 6.2 Papp of the NPs and SA43 aptamer</i> .....	251

# Acknowledgement

I First and above all, I praise God, the almighty for providing me this opportunity and granting me the capability to proceed successfully. This thesis is a result of assistance and guidance of several people. I would therefore like to offer my sincere thanks to all of them.

My heartfelt gratitude to my Director of Studies, Dr. Jane Alder. She patiently provided the vision, encouragement, motivation, enthusiasm and advice necessary for me to proceed through the PhD. She has been a strong and supportive adviser and has given me the freedom to pursue independent work. I appreciate her endless efforts in correcting my thesis and give me providing constructive criticism. I could not have imagined having a better mentor for my PhD study and it is an honour to be her first PhD student.

I would also like to thank my supervisor, Dr. Lisa Shaw, for her help and support and her innovative ideas that helped in structuring this research. I would like to acknowledge Dr. Clare Lawrence for their guidance and expertise which helped me to overcome difficulties during my degree. I appreciate their help and support all throughout my project, especially their contributions during the write up of my thesis. I would like to thank Professor Robert Lea for his guidance and supervision during my degree.

I would like to thank Dave Griffiths for his kind help with the histology work and patiently talking me through all the methods. I cannot thank him enough for taking time out to help me do my experiment. I would like to thank Professor Kamalinder Singh and Dr. Kai-Wai Wan for kindly donating their synthesised nanoparticles for the study. I would also like to thank Dr. Julie Shorrocks for all the tissue culture training and the help she provided me the microscope and flow cytometer. I would like to thank Peter Bentley, for keeping track all my orders and delivering them to me them as soon as possible. I would like to acknowledge Dr. Mohit Arora for his help and inputs during the three years of my degree. A big thanks to the Clare Altham for helping me with all the paperwork throughout the PhD, from registration to submission, she has been very helpful.

I would like to acknowledge the contribution of Dr. Zaynah Maherally and Dr. Helen Fillmore from the University of Portsmouth. I would like to thank Professor Geoff Pilkington for giving me the opportunity and welcoming me to work in his lab. The time spent working in the labs in Portsmouth, helped me to deepen my knowledge understanding of the subject.

I would like to thank my biggest support and the driving force which enabled me to finish this degree, MY FAMILY. I would like to dedicate my thesis to my parents; Ashok Kumar and Suman Kumar, my aunty Ekta and my sister Somya, these people made me believe that I could do it. I would like to express my deepest respect and most sincere gratitude to my parents for their endless encouragement, financial support and love, never holding me back from achieving my dreams throughout my life. A big thanks to all members of my big family

and especially my two little cousins, Krattika and Kaniskha who always brought a smile to face.

I would like to thank Dr. Saurabh Prabhu, for being such an understanding friend, loving brother and an amazing cook. He made living away from family less difficult by being the best housemate and always cheered me up when I was low.

I would like to thank the authors of scientific videos uploaded on YouTube, it served as an excellent way to learn new methods and understand the protocols. And finally, I would like to thank my friends in India and in the UK, Kini Shah, Alisha Sheth, Richa Tanna, Nitya Malladi, Kanksha Bhuta, Lestin Sebastian, Michelle Rudd, Sneha Subramanian, you all have made this journey worth it!

# List of Abbreviations

ABC	ATP binding cassette transporters
ABM-2	Astrocyte basal media
ADH	Antidiuretic hormone
AGM-2	Astrocyte Growth Media-2 Single quotes
AHMC	3-[2-(N,N-diethyl-N-methylammonium)ethyl]-7-hydroxy-4-methylcoumarin
AhR	Hydrocarbon receptor
AJs	Adherens junction
ALDH	Aldehyde dehydrogenase
AMMC	3-[2-(N, N-diethyl-N-methylammonium) ethyl]-7-methoxy-4-methylcoumarin
APS	Ammonium persulphate
ATP	Adenosine triphosphate
BBB	Blood brain barrier
BCRP	Breast cancer resistance protein
BFC	7-benzyloxy-4-trifluoromethyl- coumarin
BSA	Bovine serum albumin
BTNW	Brain Tumour North-West
BUI	Brain uptake index
CAR	Constitutively active receptor
Ccl	Capacitance
CD34	Cluster of differentiation

CNS	Central nervous system
CYP450	Cytochrome P450
DIV	Dynamic in vitro
DMEM	Dulbecco's modified eagle's medium
DMEs	Drug metabolising enzymes
DMSO	Dimethyl sulphoxide
DNA	Deoxyribonucleic acid
DPD	Dihydropyrimidine dehydrogenase
EBM-2	Endothelial basal media
ECIS	Electric cell-substrate impedance sensing system
EGM	Endothelial growth medium
ECM	Extracellular matrix
EGFR	Epidermal growth factor receptor
EGM-2	Endothelial Growth Media-2 Single quotes
EMA	Epithelial membrane marker
EMEM	Eagle's minimum essential medium
EORTC	European organization for research and treatment of cancer
EVOM-2	Epithelial Voltohmmeter
FBS	Foetal bovine serum
FDA	Food and Drug Administration
Fe <sup>+2</sup>	Ferrous
Fe <sup>+3</sup>	Ferric
FITC	Fluorescein isothiocyanate
FXR	Farnesoid X-activated receptor

GBM	Glioblastoma multiforme
GFAP	Glial fibrillary acidic protein
GLUT-1	Glucose transporter
GST	Glutathione-S-transferases
HA	Human astrocytes
HBMEC	Human microvascular endothelial cells
HBSS	Hank's balanced salt solution
HBVP	Human brain vascular pericytes
HFC	7-hydroxy-4-trifluoromethylcoumarin
HLA	Human leukocyte antigen
HMT	Histamine N-methyltransferase
HS	Human serum
LAT-1	Large neutral amino acid
SLC	Solute carrier
MDR	Multi drug resistance
MRC	Medical research council
NADPH	Nicotinamide adenine dinucleotide phosphate
Nanoparticles	NPs
NAT1 & NAT2	N-acetyltransferase isoenzymes
NCIC	National cancer Institute of Canada
NEAA	Non-essential amino acid
NHS	National health services
NICE	national institute of for health and care excellence
NQO1	NAD(P)H dehydrogenase [quinone] 1

OATP	Organic anion transporting polypeptides
OCT	Organic cation transport protein
PBS	Phosphate buffered saline
PCGS	Pericyte cell growth supplement
PCM	Pericyte cell medium
PDGFR	Platelet derived growth factor receptor
PFA	Paraformaldehyde
PPAR	Peroxisome proliferator activated receptor
PTEN	Phosphatase and tensin homolog
PXR	Preganane X receptor
RFU	Relative fluorescent units
RIPA buffer	Radioimmunoprecipitation assay buffer
SDA PAGE	Sulphate polyacrylamide gel electrophoresis
SXR	Steroid and xenobiotic receptor
TBS	Tris buffered saline
TEER	Trans endothelial electrical resistance
TEMED	Tetramethylethylenediamine
TJs	Tight junctions
TP53	Tumour protein 53
TPMT	Thiopurine methyltransferase
UGTs	glucuronosyltransferase
VEGF	Vascular endothelial growth factor
ZO-1	Zonula occludens protein 1

# Table of Contents

1. Introduction.....	1
1.1 Brain tumour.....	1
1.1.1 Classification of brain tumour.....	2
1.2 Hallmarks of cancer.....	3
1.3 Glioma.....	5
1.3.1 Types of Glioma.....	5
1.3.2 Grades of Glioma.....	7
1.3.3 Epidemiology.....	10
1.3.4 Treatment.....	11
1.3.5 Prognosis.....	12
1.4 Blood brain barrier.....	15
1.4.1 Physical barrier.....	16
1.4.2 Transport across the Blood Brain Barrier.....	20
1.5 Drug metabolism and Disposition at the BBB.....	21
1.5.1 Phase I and II metabolism.....	24
1.5.2 CYP Localisation and Activity in the Brain.....	28
1.5.3 Cytochrome P450 and Brain tumours.....	31
1.5.4 Transporters at the BBB.....	33
1.6 <i>In vitro</i> modelling of the BBB.....	40
1.6.1 Assessment of <i>in vitro</i> BBB models.....	40
1.6.2 Current existing BBB models.....	43
1.7 Rationale for the project.....	45
1.7.1 Aim.....	46
1.7.2 Objectives.....	47
1.7.3 Overview.....	47

<b>2. Materials and Methods</b> .....	50
2.1 Tissue Culture.....	50
2.1.1 Cell Lines .....	50
2.1.2 Media and Supplements .....	50
2.1.3 Cryopreserving and Thawing Cells.....	52
2.1.4 Subculturing of Cells .....	53
2.2 Cell Counting .....	53
2.2.1 Spheroid Culture .....	54
2.2.2 Growth Curves .....	55
2.3 Immunostaining of cells .....	55
2.3.1 Fixation of cells.....	55
2.3.2 Fluorescent immunostaining .....	56
2.3.3 3,3-Diaminobenzadine (DAB) staining .....	57
2.4 Protein extraction .....	58
2.4.1 Protein linearity experiment.....	58
2.4.2 Optimisation of protein extraction method .....	58
2.4.3 Polycarbonate transwell and alvetex scaffold inserts.....	59
2.5 Protein quantification by Bradford assay .....	60
2.6 Western blotting .....	60
2.6.1 Sample preparation.....	61
2.6.2 Gel electrophoresis.....	61
2.6.3 Transfer of proteins .....	62
2.6.4 Visualisation of transferred proteins .....	62
2.6.5 Probing antibodies and detection of proteins .....	63
2.7 Activity assay for drug metabolising enzymes (CYP3A4 and CYP2D6).....	64
2.7.1 Protein linearity optimisation.....	65

2.7.2	Substrate linearity optimisation .....	65
2.7.3	Enzyme kinetic study .....	66
2.8	Activity assay for efflux transporter (ABCB <sub>1</sub> and ABCG <sub>2</sub> ).....	68
2.9	Co-culture on transwell for BBB model.....	70
2.9.1	Alvetex perfusion BBB model .....	73
2.9.2	Electric Cell-substrate Impedance Sensing (ECIS) for BBB model.....	74
2.9.3	Cellzscope for BBB model.....	75
2.10	Testing integrity of designed co-culture models .....	76
2.10.1	Measurement of TEER.....	76
2.10.2	Permeability of FTIC dextran .....	76
2.10.3	Permeability of nanoparticles (NPs) across the BBB models.....	77
2.11	Brain tumour barrier .....	80
2.11.1	TEER measurement .....	81
2.11.2	Permeability of NPs tested in BTB model. ....	81
2.12	Statistical Analyses.....	82
<b>3.</b>	<b>Characterisation of continuous and primary cell lines. ....</b>	<b>84</b>
3.1	Introduction .....	84
3.2	Results .....	85
3.2.1	Growth kinetics and morphology of continuous cell lines.....	85
3.2.2	Growth kinetics and morphology of short-term cultures .....	87
3.2.3	Characterisation by immunocytochemistry .....	89
3.3	Discussion and conclusion .....	95
<b>4.</b>	<b>Characterisation of drug metabolising enzymes and transporters expression and activity. ....</b>	<b>101</b>
4.1	Introduction .....	101
4.2	Results .....	102
4.2.1	Protein linearity experiment.....	102

4.2.2	Protein extraction method optimisation .....	103
4.2.3	Protein expression profile for different cell lines.....	109
4.2.4	Activity levels of efflux transporters.....	127
4.2.5	Activity levels of drug metabolising enzymes .....	145
4.3	Discussion and conclusion .....	158
<b>5.</b>	<b>Development of the blood brain barrier model.....</b>	<b>164</b>
5.1	Introduction .....	164
5.2	Results .....	165
5.2.1	Validation of the TEER Instrumentation .....	165
5.2.2	Optimising experimental conditions .....	190
5.2.3	Expression and activity of proteins in designed <i>in vitro</i> BBB models. ....	212
5.2.4	Comparison of expression and activity of proteins between Alvetex perfusion and transwell tri-culture model .....	222
5.3	Discussion and conclusion .....	229
<b>6.</b>	<b>Functionality of the tri-culture as an <i>in vitro</i> BBB model .....</b>	<b>240</b>
6.1	Introduction .....	240
6.2	Results .....	241
6.2.1	FITC-Dextran permeability assay .....	241
6.2.2	Screening of nanoparticles and aptamer .....	245
6.3	Discussion and conclusion .....	254
<b>7.</b>	<b>Developing a brain tumour barrier model .....</b>	<b>261</b>
7.1	Introduction .....	261
7.2	Results .....	262
7.2.1	TEER measurements.....	262
7.2.2	Expression of Efflux transporters and DMEs in GBM spheroids.....	263
7.2.3	Testing of NPs in the developed BTB model.....	265
7.3	Discussion and conclusion .....	268

<b>8. Discussion</b> .....	272
8.1 General discussion.....	272
8.2 Limitations of the project .....	283
8.3 Future works.....	284
8.4 Conclusion.....	286
<b>9. References</b> .....	287
<b>10. Appendices</b> .....	310

# CHAPTER 1

# 1. Introduction

## 1.1 Brain tumour

A brain tumour is defined as an abnormal mass or growth of cells in the brain arising from rapidly proliferating cells (Vescovi *et al.*, 2006). These proliferating cells interfere and damage the healthy brain tissue and cause increased intracranial pressure (Figure 1.1). The term brain tumour covers a wide range of benign and malignant tumour types. Benign brain tumours are slow growing, are unlikely to recur or spread to other parts of the brain and can be typically treated with surgery depending on location (Duffner *et al.*, 1985). Malignant brain tumours have a high mitotic index and are likely to metastasise to other parts of the brain and the spinal cord (Graham and Cloughesy, 2004). Malignant tumours are more likely to recur after surgery and therefore require radiotherapy and chemotherapy post tumour resection.

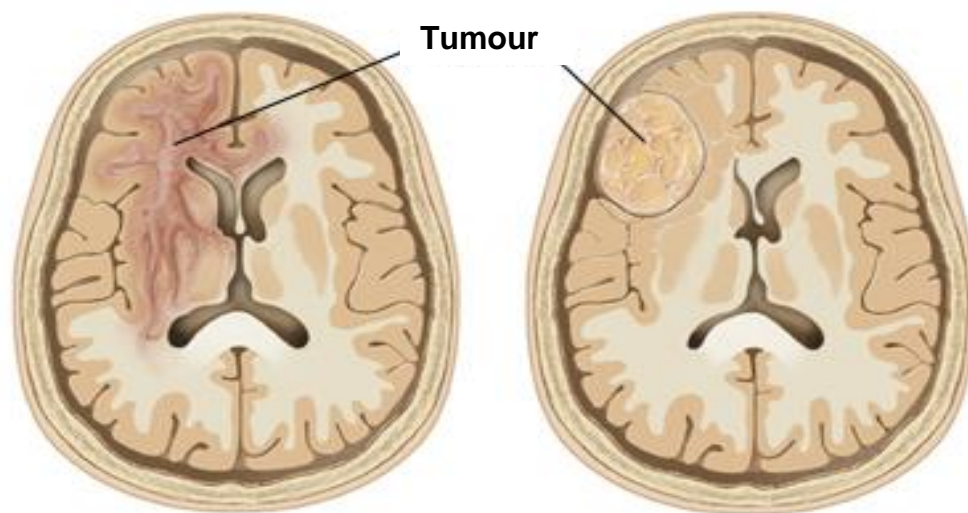


Figure 1.1 A) Tumour invading healthy brain tissue. B) Tumour pressing on the healthy tissue and causing increased pressure within the brain (Abrey and Mason, 2003).

### 1.1.1 Classification of brain tumour

The most fundamental differentiation of a brain tumour is between primary intracranial lesion, metastatic and secondary brain tumour (Abrey and Mason, 2003). The categories, primary (*de novo*) and secondary are more conceptual than diagnostic (Kleihues and Ohgaki, 1999). These terminologies were first used by a German neurologist Hans-Joachim Scherer, who defined primary (*de novo*) as a tumour that lacked an identifiable precursor lesion and arose from a single step malignant transformation (Scherer, 1940; Scherer, 1938; Ohgaki and Kleihues, 2013). Secondary tumours were defined as progressive tumours which develop from a less malignant or a benign precursor (Scherer, 1940; Scherer, 1938).

Brain metastases are ten times more common than primary brain tumours and are estimated to occur in up to 30 % of patients diagnosed with a solid brain tumour (Nathoo *et al.*, 2004). For the adult population, the percentage of cases where brain metastatic tumour commonly originate from is as follows: lung; (50 %) breast (15 - 20 %), unknown primary tumour (10 – 15 %), melanoma (10 %), and colon (5 %) (Wen and Loeffler, 2000; Bouffet *et al.*, 1997). In children, common sources include the sarcomas, neuroblastoma, and germ cell tumours (Wen and Loeffler, 2000; Gil-Gil *et al.*, 2014).

## 1.2 Hallmarks of cancer

The study of cancer involves the recognition of cellular morphological changes, malignant transformations and sequential acquisition of genetic alterations (Kleihues and Ohgaki, 1999). The cancer cell was initially thought to acquire six biological capabilities during multistep development of the tumour as seen in Figure 1.2. In 2011, Hanahan and Weinberg proposed an additional four new hallmarks including deregulation of metabolic pathways to generate energy, evasion of the immune system, chromosomal abnormalities and the role of chronic local inflammation to aid progression of the cancer (Hanahan and Weinberg, 2011).

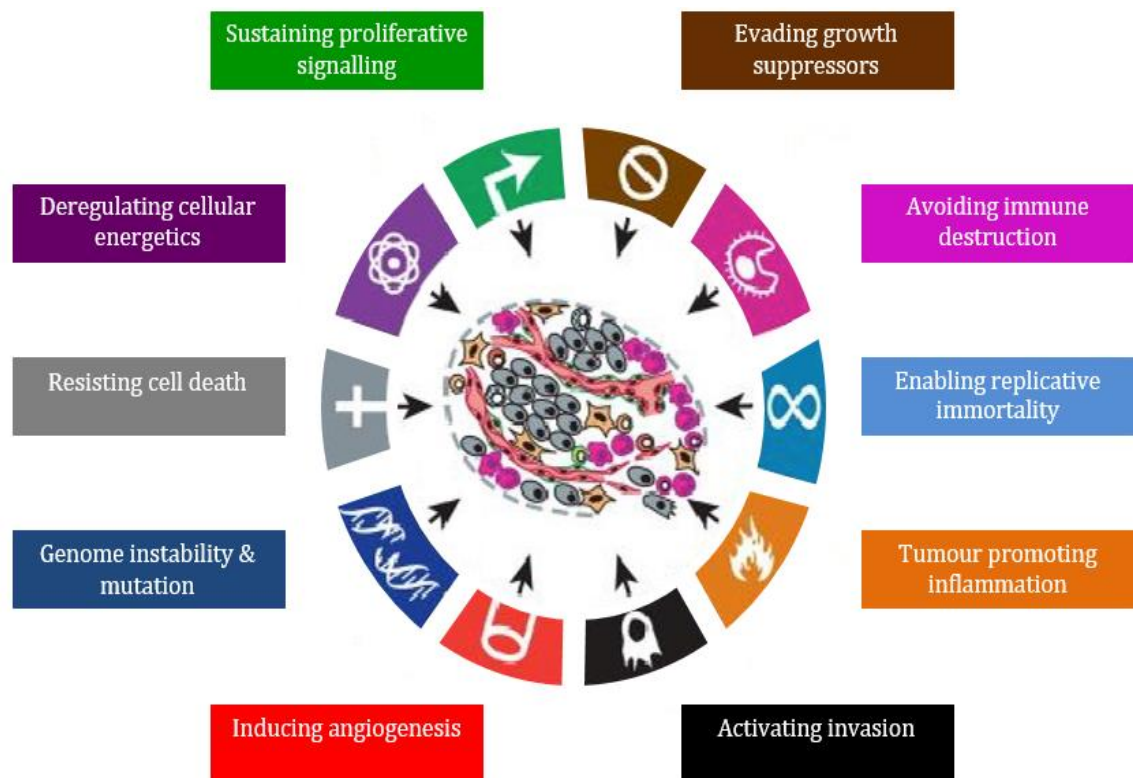


Figure 1.2 Illustration of the ten capabilities of cancer cells acquired during development of cancer (Hanahan and Weinberg, 2000; Hanahan and Weinberg, 2011).

All of the aforementioned hallmarks illustrated in Figure 1.2 play an integral role in the biological development and growth of cancer, however the most fundamental trait of cancer cells is the ability to sustain chronic proliferation. The cancer cells are able to evade growth

suppressors such as PTEN, tumour suppressors such as TP53 and cell cycle regulators cyclin D and phosphoinositide 3-kinase (PI3K). Phosphatase and tensin homolog (PTEN) is a protein coded by the *PTEN* gene, which regulates the cell cycle by preventing growth and multiplication of cells (Rodríguez-Escudero *et al.*, 2011). Tumour protein 53 (TP53), also known as p53, is a tumour suppressor protein which regulates the cell cycle (Ohgaki and Kleihues, 2007; Rivlin *et al.*, 2011). The cancer cells show unregulated proliferation and promote cell division via over expression or over activity of activating growth factor receptors such as epidermal growth factor receptor (EGFR) (ErbB-1, HER1) and platelet derived growth factor receptor (PDGFR). Activated EGFR and PDGFR triggers intrinsic tyrosine kinase activity and downstream signalling cascades, resulting in increased DNA synthesis and cell proliferation (Ohgaki and Kleihues, 2013). Angiogenesis is required for the formation of new tumour vasculature, an important factor in the development of cancer. The *VEGF* gene which encodes for vascular endothelial growth factor (VEGF) is commonly upregulated in cancer. Angiogenic signalling proteins such as VEGF, bind to receptors expressed on the outside of endothelial cells, inducing vasculogenesis and angiogenesis.

The malignant cancer cell possesses the unique property of metastasis which, unlike the benign cancer cell, involves the invasion and migration of cells and contributes largely to the lethality of cancer. The complex metastasis cascade involves the mechanism of physical translocation of cancer cell from the primary source of origin and its colonisation at the distant tissue (Fidler, 2003), and this normally takes place via the blood or lymphatic system (Karnezis *et al.*, 2012). It is responsible for about 90% of the cancer associated mortality but yet has remained the most poorly understood component of cancer pathogenesis (Chaffer and Weinberg, 2011). Migration is often associated with down regulation of genes encoding cell

adhesion proteins associated with cytotaxis (E-cadherin) and up regulation of genes associated with migration and inflammation (N-cadherin) (Hanahan and Weinberg, 2011).

## 1.3 Glioma

The central nervous system is derived from neuroepithelium which has differentiated into glial restricted precursor cells or neuron restricted precursor cells (Figure 1.3). Gliomas are a heterogeneous group of neoplasms originating from the glial cells of the central nervous system (Eggstein *et al.*, 2004). Glioma contributes to 31 % of all types of brain tumours and more than 50 % of primary brain tumours (Louis *et al.*, 2007).

### 1.3.1 Types of Glioma

The human brain is comprised of a complex network of neurons and glial cells. The gliomas are classified into various types based on the cell of origin, for example, astrocytes, oligodendrocytes, ependymal cells, and microglia, as shown in Figure 1.4 (Louis *et al.*, 2007; Huse and Holland, 2010).

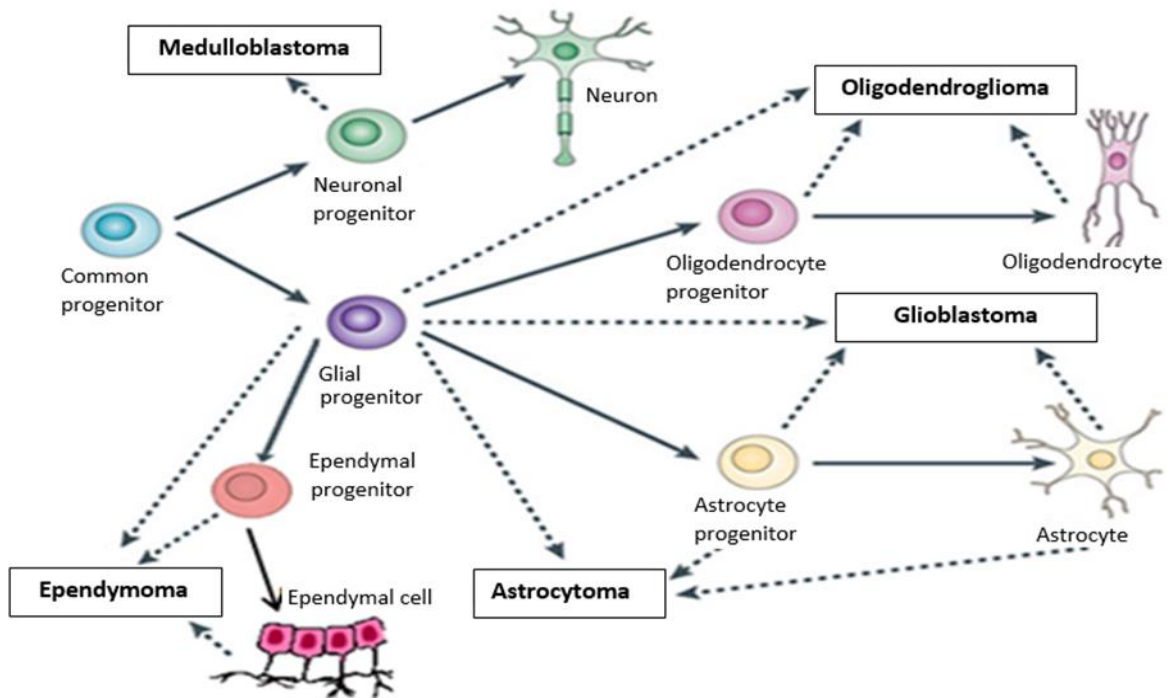


Figure 1.3 Types of neuroglial tumours classified by the cell of origin (Huse and Holland, 2010).

Primary and secondary gliomas are distinct disease entities which affect different age groups as described in Table 1.1. Primary glioblastoma tend to be more prevalent in men, occur later in life and exhibit a short clinical history prior to surgery compared to secondary glioblastoma, which on average appear earlier in life, are more prevalent in women and have a longer presenting clinical history prior to surgery.

Table 1.1 Synopsis of clinical data of primary and secondary glioblastoma (Nakada et al., 2011).

	Primary glioblastoma	Secondary glioblastoma
Clinical onset	<i>de novo</i>	secondary
Preoperative clinical history	1.7 months	53 months (astrocytoma)
Sex ratio (male: female)	1.4	0.8
Age at diagnosis	55	39

Primary and secondary glioblastoma develop through different genetic pathways identified by distinct mRNA and protein expression profiles (Ohgaki and Kleihues, 2007). Multiple genetic alterations have been observed in the major signalling pathways which result in tumour growth and progression Figure 1.4. The genetic alterations significantly differ in primary and secondary glioblastoma. The *TP53* mutations are frequent, with alterations observed in 65 % of secondary glioblastomas and 28 % of primary glioblastomas (Figure 1.4).

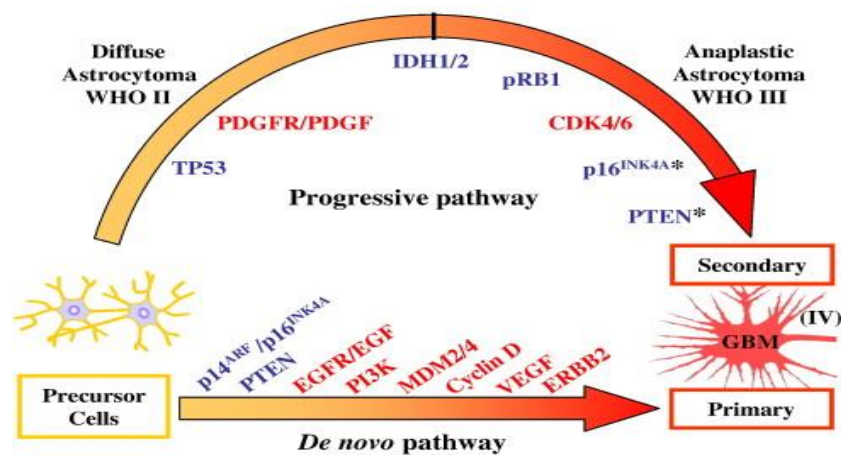


Figure 1.4 Genetic pathways to primary (de novo) and secondary glioblastomas at the population level (Grzmil and Hemmings, 2010)

### 1.3.2 Grades of Glioma

The biological behaviour of a neoplasm can be predicted by histological grading, which plays a key role in determining treatment options and prognosis for the patient. The World Health Organisation (WHO) in 2007 categorised tumours on a scale of malignancy from grades I to IV, where the most benign was designated as grade I and the most malignant was designated grade IV as described in Table 1.2.

According to the WHO, grading was based on factors such as the mitotic index, vascularity, invasive potential and the presence of necrotic potential (Louis *et al.*, 2007). Grade I referred to lesions with a low proliferative potential and possibility of cure after surgical resectioning

of the tumour. Grade II included neoplasms which in spite of low level proliferative activity were infiltrative in nature and tended to recur and progress to a higher grade of malignancy. Grade III designation was for neoplasms and lesions with histological malignancy, nuclear atypia and mitotic activity. Grade IV was assigned to cytologically malignant neoplasms which were mitotically active and associated with pre- and post-operative disease evolution having a fatal outcome (Louis *et al.*, 2007). Grade IV is the most malignant tumour type contributing to 51.9 % of primary brain tumour cases (Moore and Kim, 2010). The WHO grade I and II are referred as “low grade glioma” whereas WHO grade III and IV are “high grade glioma” (Abrey and Mason, 2003). Until recently, the classification of glioma has been strictly based on the morphology of the astrocytic tumour, however lately the WHO guidelines have mentioned the importance of molecular pathogenesis for consideration in the classification (Vartanian *et al.*, 2014). As seen in Figure 1.5, the genetic alteration seen in different types of primary and secondary glioma.

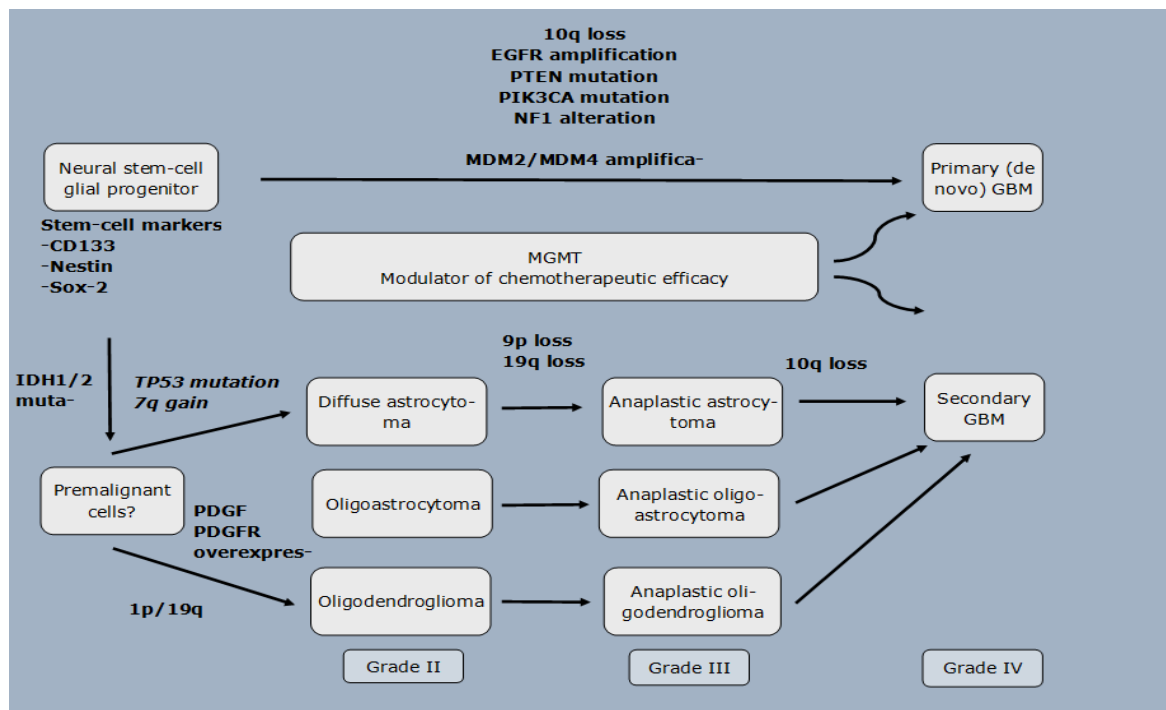


Figure 1.5 Pathways for the development of primary and secondary GBM showing genetic alterations in types of glioma.

Table 1.2 WHO Grading of Tumours of the Central Nervous System (Louis et al., 2007)

Tumour	Grade			
	I	II	III	IV
<b>Astrocytic Tumours</b>				
Subependymal giant cell astrocytoma	•			
Pilocytic astrocytoma	•			
Pilomyxoid astrocytoma		•		
Diffuse astrocytoma		•		
Pleomorphic xanthoastrocytoma		•		
Anaplastic astrocytoma			•	
Glioblastoma				•
Giant cell glioblastoma				•
Gliosarcoma				•
<b>Oligodendroglial tumours</b>				
Oligodendroglioma		•		
Anaplastic oligodendroglioma			•	
<b>Oligoastrocytic tumours</b>				
Oligoastrocytoma		•		
Anaplastic oligoastrocytoma			•	
<b>Ependymal tumours</b>				
Subependymoma	•			
Myxopapillary ependymoma	•			
Ependymoma		•		
Anaplastic ependymoma			•	

### 1.3.3 Epidemiology

Brain tumours account for 2 % of all the cancers diagnosed in adults. Each year in the UK, approximately 4,400 people are diagnosed with brain tumours (Jemal *et al.*, 2010). Gliomas account for more than 50 % of primary brain tumours (Grier and Batchelor, 2006). The rate of incidence of primary brain tumours increases steadily with increasing age, whereas the survival rate decreases with increase in age of the patient (Schwartzbaum *et al.*, 2006). The global incidence of malignant primary brain tumours in males is 5.8 per 100,000 and in females is 4.1 per 100,000 (Schwartzbaum *et al.*, 2006). In Europe, over a 12 month period in 2008, 4,785 people were diagnosed with malignant brain tumours and 4,552 people were diagnosed with other non-invasive types of brain tumour (Crocetti *et al.*, 2012).

A number of epidemiological studies have revealed that certain occupations such as physicians, farmers, firefighters, workers of petroleum industries have an increased brain tumour risk (Gomes *et al.*, 2011). These occupation involve exposure to carcinogens such as radiation and chemicals such as petrochemicals, nitriles, nitrites, amides, lead, vinyl chloride, benzene, n-hexane, polycyclic aromatic hydrocarbons, polychlorinated biphenyls, N-nitroso, however, no epidemiological analyses have led to identification of a single environmental carcinogen which could be unequivocally linked to brain tumour development (Ohgaki and Kleihues, 2005). In Europe, cases of primary brain tumour comprising of high grade glioma and brain metastasis observed range from 4.5 to 11.2 cases per 100,000 in men and from 1.6 to 8.5 per 100,000 in women (Crocetti *et al.*, 2012).

### 1.3.4 Treatment

The standard form of treatment comprises of surgical resectioning of the tumour followed by multimodal regimen of radiotherapy and chemotherapy (Eyupoglu *et al.*, 2013){(NICE), 2007 #879}. Surgery and radiation continue to be the prime modalities of therapy for malignant brain tumours. Chemotherapy is another option for the treatment of glioma, but the role of such a therapy in malignant gliomas has been inconclusive (Kim and Glantz, 2006). Various chemotherapy drugs used for glioma include procarbazine, lomustine, temozolomide and vincristine (Brown *et al.*, 1993; Swartz *et al.*, 2014). In 2005, Stupp *et al.*, presented results of a randomised study conducted by EORTC (European Organization for Research and Treatment of Cancer) and NCIC (National Cancer Institute of Canada), comparing the median patient survival time following concomitant temozolomide chemotherapy and radiotherapy, to radical radiotherapy alone. It was found that temozolomide and radiotherapy combined increased the median survival period from 12.1 months (radiotherapy alone) to 14.6 months (Stupp *et al.*, 2005). Carmustine and temozolomide implants are recommended by the NICE guidelines as a possible treatment for people with newly diagnosed high-grade glioma, but only if 90 % or more of their tumour has been removed (NICE, 2008). Aggressive surgery followed by radiation therapy and adjuvant chemotherapy continues to offer glioblastoma patients the best hope of long-term survival (Reni *et al.*, 2001; Grover *et al.*, 2014).

### 1.3.5 Prognosis

A report by Rachet *et al.*, (2012) stated that over the past four decades, brain tumour treatment has not increased brain tumour patient median survival time, compared to patients with other types cancer, for example colon cancer, where a 10-fold increase in median survival time was observed over the same period (Figure 1.6).

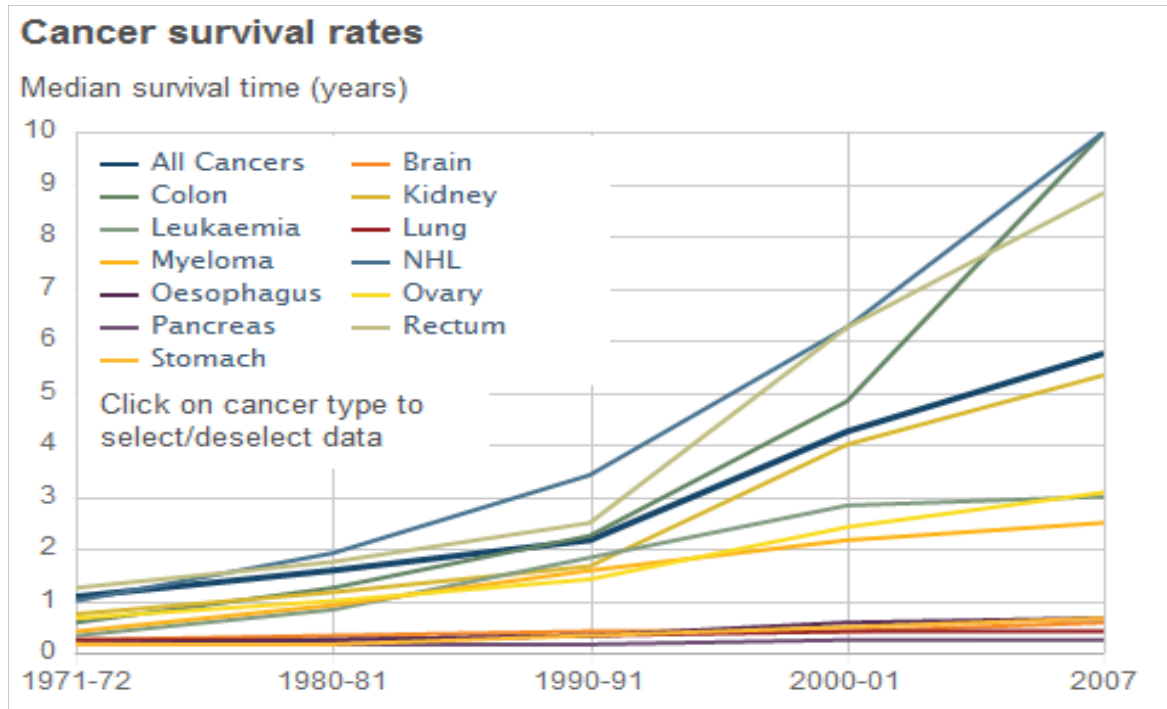


Figure 1.6 Cancer survival rates.

Data provided in the graph are for adults aged 15-99 diagnosed in England and Wales which predicts the survival estimates. Brain tumour shows insignificant increase in the median survival rate over three decades (Rachet *et al.*, 2009).

There is a marked variability in prognosis amidst glioma patients due to the various factors including: 1) characteristics of the tumour and influence on patient, 2) characteristics of the patient, 3) factors related to the influence of the tumour on the patient and 3) factors related to treatment (Loiseau, 1996).

### 1.3.5.1 Characteristics of the tumour linked to prognosis

Glioma comprises of cellular, molecular, genetic, epigenetic, and metabolic heterogeneity which poses challenges for existing therapeutics and personalised medicine (Vartanian *et al.*, 2014). For example the presence of aggressive infiltrating cells at the glioma margin, residual cells remaining following glioma resection and cancer stem-like cells capable of repopulating a glioma all contribute to increasing the likelihood of recurrence and poor patient prognosis (Taylor, 2010; Inda *et al.*, 2014). Histological grading has an influence on prognosis, for example the 5-year survival rate of grade IV glioblastoma patients is less than 3 % whereas for low grade pilocytic astrocytoma is 75 % (Burkhard *et al.*, 2003; Brimelow, 2011).

### 1.3.5.2 Characteristics of the patient linked to prognosis

In glioma, factors which largely influence the survival duration of the patient are age and functional status (Gupta and Sarin, 2002). The prognosis for patients with glioma aged 65 years or older is very poor. Only ~2% of patients as compared to 30% of those under the age of 45 years at GM diagnosis show a survival period of more than 2 years (Schwartzbaum *et al.*, 2006).

### 1.3.5.3 Factors related to treatment and prognosis

The major challenges of glioma treatment include tumour heterogeneity, location, subpopulations of resistant cells, aggressive relapse and poor efficacy of chemotherapy, again age is an important factor in prognosis, with respect to tolerance of radio- and chemotherapy regimens (Stummer and Kamp, 2009). In a clinical trial conducted by the Medical Research Council (MRC), Brada *et al.*, (2001) reported that high grade glioma patients did not show any significant survival benefits after treatment with procarbazine,

lomustine, vincristine chemotherapy post-radiotherapy compared to radiotherapy on its own (Medical Research Council Brain Tumor Working, 2001). As previously mentioned in Section 1.3.5 Stupp *et al.*, have shown that concomitant use of TMZ with radiotherapy in newly diagnosed glioblastoma multiforme (GBM) patient increases survival benefit significantly with minimal additional toxicity (Stupp *et al.*, 2005). The two-year survival rate was increased from 10.4 % (radiotherapy alone) to 26.5 % (radiotherapy plus temozolomide). The multitude of possible reasons for poor response to chemotherapy have been the focus of brain tumour research for many years and are discussed further in Section 1.5. It is essential to understand the working of the underlying drug metabolism involved, to develop effective glioma therapeutic for improving the prognosis of the glioma. From here on in, this thesis will focus on the influence of drug metabolising enzymes and efflux transporters at the BBB and the role of the physical, transport and metabolic barrier imposed by the BBB in reducing the CNS bioavailability of chemotherapeutics at the site of action.

## 1.4 Blood brain barrier

The studies of Paul Ehrlich in 1882 suggested the concept of blood brain barrier (BBB) providing evidence of the separation between circulation and CNS (Banks, 1999). In the early 1970's, Oldendorf introduced the concept of brain uptake index (BUI), to quantify the permeability of the BBB and to predict the rate of entry of different compounds (Oldendorf, 1971). The BBB has since been described as a dynamic biological barrier which restricts the passage of blood-borne drugs, neurotoxic substances and peripheral immune cells from entering the brain, while selectively facilitating the transport of nutrients across the BBB into the brain (Shen and Zhang, 2010; Gynther, 2010). The physical protective barrier is due to the presence of tight junctions between endothelial cells at the blood and brain junction and the biological barrier controls the entry of molecules via tightly regulated transporters (Agarwal *et al.*, 2008; Pardridge, 2005; Shen and Zhang, 2010). The BBB is also responsible for homeostasis of the microenvironment in the neural parenchyma and normal functioning of the brain (Eggstein *et al.*, 2004).

The BBB is present in all the regions in brain except the circumventricular organs where the blood vessels show fenestrations for diffusion (Ballabh *et al.*, 2004; Gynther, 2010). The unique feature of the BBB lies in the structure of the neurovascular unit and the cerebral micro-vascular endothelial cells; these include additional cellular components such as astrocytes, perivascular microglia and pericytes that surround brain capillaries (Figure 1.7). The endothelial cells, astrocytic feet and the pericytes are compactly arranged and tightly integrated with the brain parenchyma on a common basement membrane (Banks, 1999) (Figure 1.7). All these components contribute to the maintenance of functional and structural integrity of the BBB (Nakagawa *et al.*, 2007a; Goldstein, 1988)

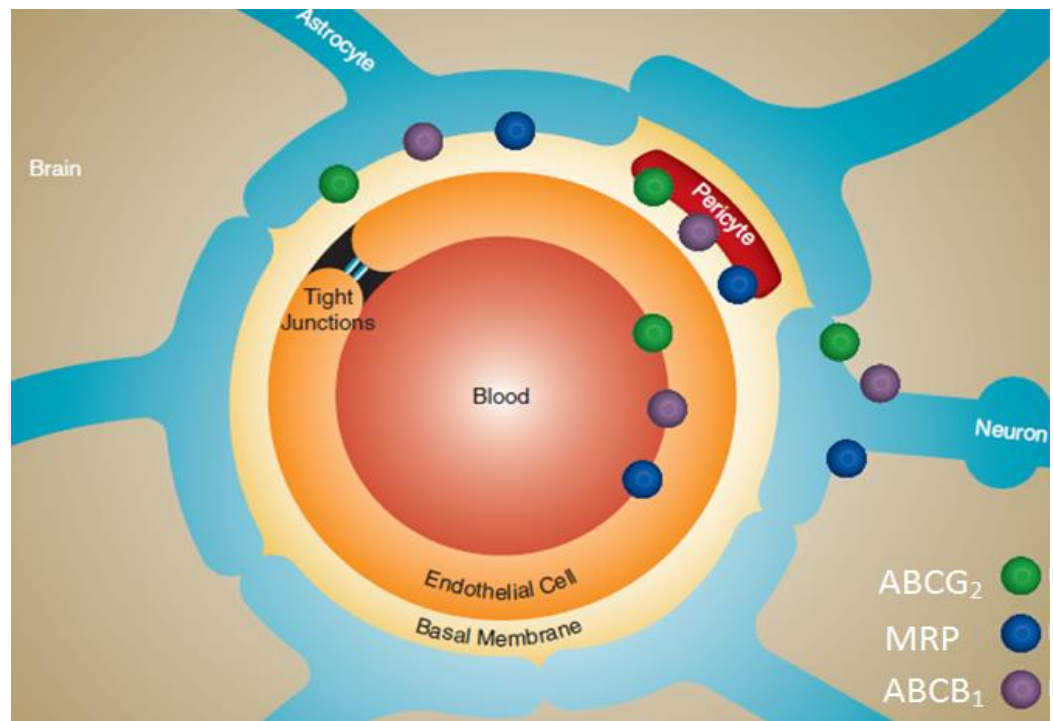


Figure 1.7 The neurovascular unit of the Blood Brain Barrier (Hartz and Bauer, 2010).

## 1.4.1 Physical barrier

The BBB comprises of different physical barriers which comprises of the different cell types and the located at the BBB.

### 1.4.1.1 Endothelial Cells and Tight Junctions

The BBB comprises of a very thin and compact continuous layer of endothelial cells between the blood capillary and parenchymal cells of the brain (Figure 1.8). The thickness of the cell layer that separates the luminal and abluminal membrane is about 200 nm and therefore it takes a short time for a substance to pass through the BBB into the brain parenchyma (Pardridge, 1999; Burns *et al.*, 1981). The specific characteristics distinguishing the cerebral endothelial cells from the peripheral endothelial cells is the presence of complex tight junctions (TJs) and the large number of mitochondria, which suggests high energy

metabolism in the brain endothelium and very low pinocytotic and transcytotic activity (Burns *et al.*, 1981) (Figure 1.8).

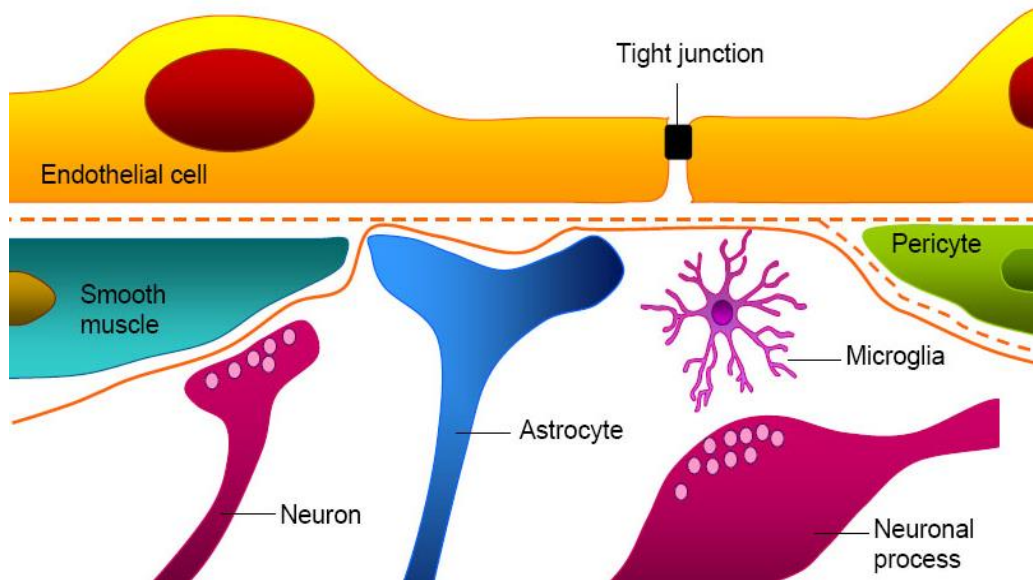


Figure 1.8 Diagrammatic representation of the cerebral capillary highlighting the structure of BBB comprising of TJs in the interendothelial cleft and high numerical density of TJs (Burns *et al.*, 1981).

The cerebral endothelial cells form TJs with each other, characterised by a high trans endothelial electrical resistance (TEER) of 1500 – 2000  $\Omega \cdot \text{cm}^2$  (Zenker *et al.*, 2003). The TJs proteins have been proposed to have two mutually exclusive functions: a fence function which prevents the mixing of membrane proteins between the apical and basolateral membranes; and a gate function which controls the paracellular passage of ions and solutes in between cells (Hartsock and Nelson, 2008). These proteins form the structural and functional integrity of the BBB via interaction of numerous plasma proteins that seal the paracellular pathway (Eggstein *et al.*, 2004; Stamatovic *et al.*, 2008). The TJs comprises of the transmembrane proteins claudin and occludin. These proteins interact with the cytoplasmic accessory proteins that link to the primary cytoskeleton protein actin, to maintain structural and functional integrity of the endothelium (Abbott, 2002) (Figure 1.9).

Occludin was found to interact with zonula occludens protein 1 (ZO-1) and is responsible for stabilising the tight junction. Claudin 1/3, 5 and 12 expressed in the BBB, appear to contribute to the high TEER (Abbott *et al.*, 2006b). The interaction of these plasma membrane proteins regulates and allows paracellular transport to be modulated in response to different stimuli. In epithelial cells, TJs and adherens junctions are strictly separated from each other, but in endothelial cells these junctions are intermingled (Cecchelli *et al.*, 1999; Miller, 2002). Adherens junctions contribute to stabilising and tightening endothelial cell structure (Luissint *et al.*, 2012b). It has been reported that ZO-1 and catenin interact with each other, suggesting that TJs and AJs function together to maintain the BBB integrity (Luissint *et al.*, 2012a).

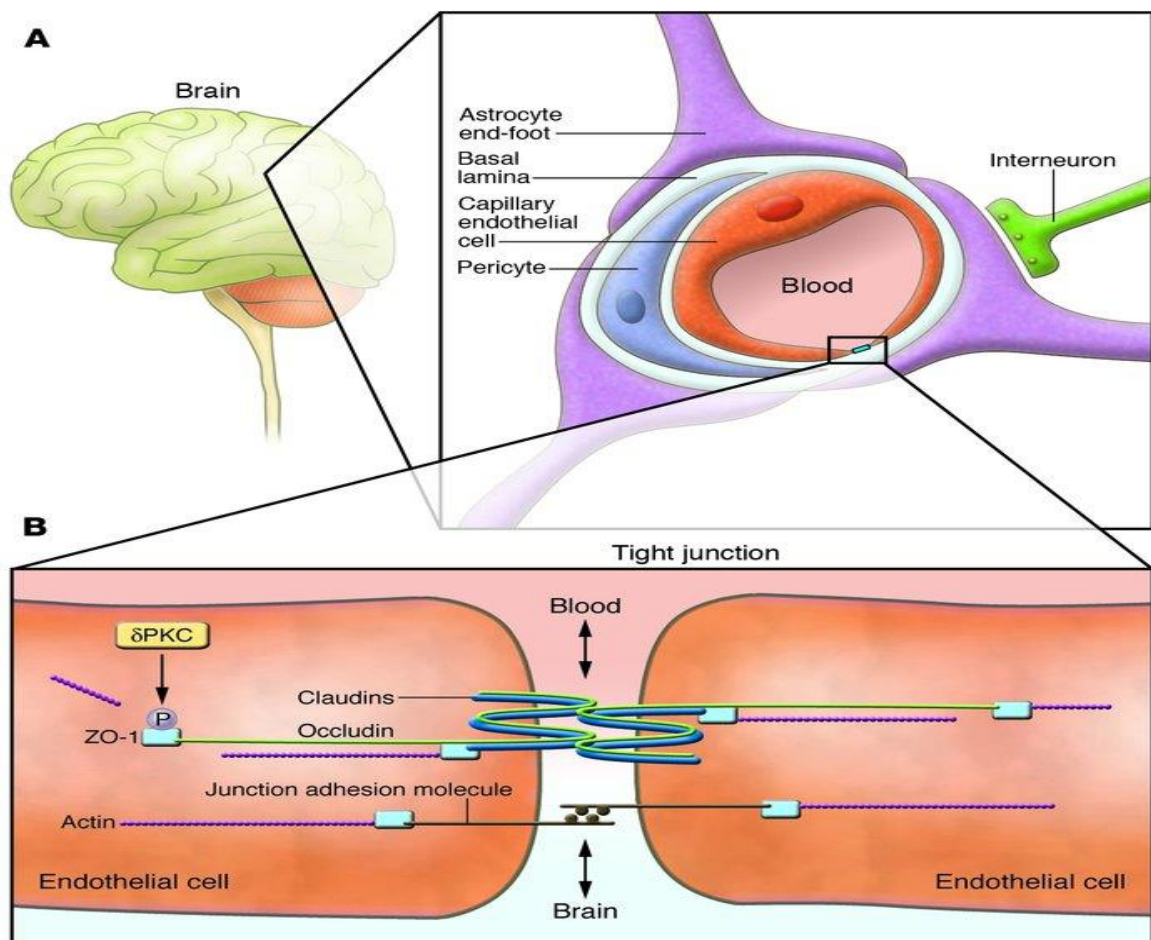


Figure 1.9 Assembly of transmembrane proteins, occluding, claudins forming the TJs between the endothelial cells (Chou and Messing, 2008).

#### 1.4.1.2 Astrocytes

Astrocytes are characteristic star shaped glial cells of the brain and spinal cord. The end feet of the astrocytes encircle 90-99 % of capillaries formed by the endothelial cells (Bauer *et al.*, 2004; Sobue *et al.*, 1999; Pardridge, 1999) (Figure 1.9). The astrocytes were initially thought to play a structural role, but it has since been recognised that astrocytes contribute to the development and maintenance of the BBB (Burns *et al.*, 1981; Wolburg *et al.*, 1994). Three categories of functions performed by astrocyte include guidance and support of neuronal migration during development, maintenance of the neural microenvironment, and modulation of immune reactions by serving as antigen-presenting cells (Montgomery, 1994). Astrocytes are a major source of extracellular matrix such as fibronectin, laminin and cytotactin. The cells secrete extracellular matrix (ECM) which plays an important role in maintaining integrity of the BBB (Kimelberg and Nedergaard, 2010).

#### 1.4.1.3 Pericytes

Pericytes are undifferentiated, contractile connective tissue cells that are located surrounding the endothelial cell layers of the brain capillary network (Allt and Lawrenson, 2000) (Figure 1.9). Pericytes, along with the endothelial cells, play a crucial role in the formation and functionality of the relatively permeable barrier. Pericytes are responsible for tight junction formation and vesicle trafficking among the endothelial cells (Nakagawa *et al.*, 2009b; Nakagawa *et al.*, 2007a; Nakagawa *et al.*, 2007b).

## 1.4.2 Transport across the Blood Brain Barrier

There are four major mechanisms of transport routes across the BBB: 1) passive diffusion (transcellular lipophilic route or paracellular aqueous route); 2) active transport; 3) endocytosis (receptor mediated or adsorptive) and 4) transcytosis or exocytosis (receptor mediated or adsorptive (Xiao and Gan, 2013). The expression of tight junction and other cell membrane domains between endothelial cells, seal the paracellular pathway leaving the transport of essential nutrients, blood gases and removal of xenobiotic molecules to the transcellular pathway (Hitchcock, 2008). Small lipophilic molecules can passively diffuse across the lipid bilayer Small, highly lipophilic, uncharged, small molecules (mol. wt  $\leq$  800 Da) can penetrate the BBB by passive diffusion via the transcellular lipophilic route, but, in many cases, the molecules are returned to the blood by efflux pumps (Wong *et al.*, 2013).

More polar, charged molecules may require access through the specialised active transporters such as GLUT-1 and LAT-1 (Begley, 2004). The movement of hydrophilic substances is facilitated by various endogenous transporter mechanisms located at the luminal and abluminal membrane of brain endothelial cells at the junction of the blood and brain (explained in detail in Section 1.5.4) (de Boer and Gaillard, 2007) (Loscher and Potschka, 2005c; Loscher and Potschka, 2005a; Loscher and Potschka, 2005b). Larger macromolecules may require receptor mediated (ATP-dependent) or adsorptive endocytosis and transcytosis routes (Gynther, 2010). All these pathways play an important role in maintaining the BBB integrity, however drug delivery across the BBB may be significantly impeded by the presence of the physical and metabolic barrier (Bodó *et al.*, 2003; Borges-Walmsley *et al.*, 2003; Chang, 2003; Banks, 1999) (Figure 1.10).

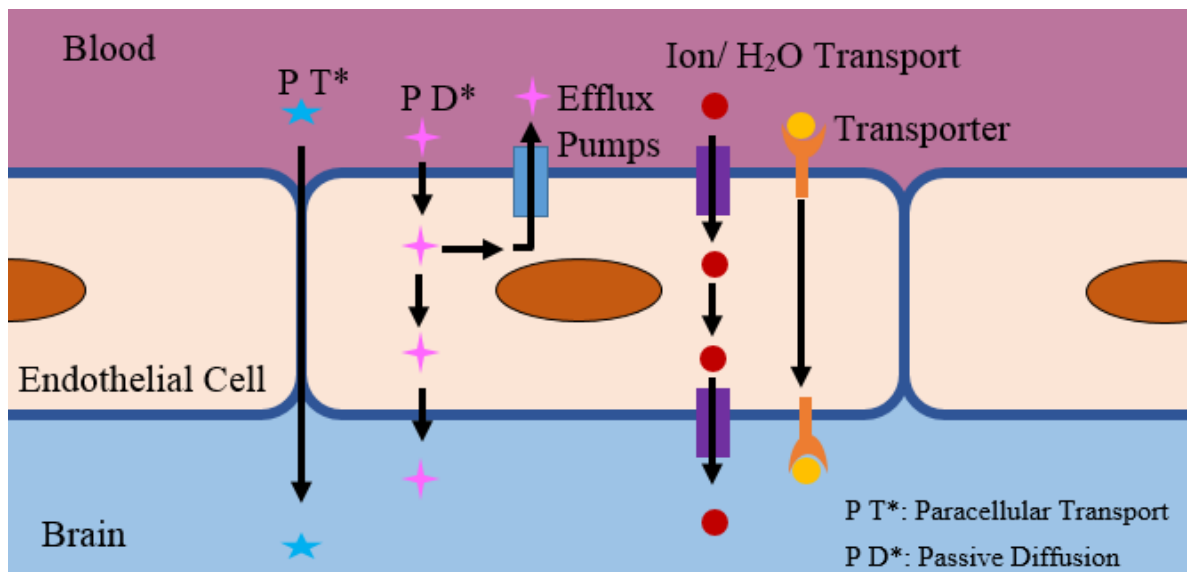


Figure 1.10 Schematic illustration of transport across the brain endothelial cells (Wong *et al.*, 2013).

## 1.5 Drug metabolism and Disposition at the BBB

The human body is exposed to numerous xenobiotics which may be harmful and therefore an elaborate detoxification system has evolved to detoxify and inactivate these foreign compounds. Following absorption into the bloodstream, xenobiotics are distributed by binding to plasma proteins and transported by blood flow to various tissues (Benedetti *et al.*, 2009). A drug is either eliminated directly through urine or bile or indirectly through biochemical transformation by enzymes in the liver and other tissues. Metabolism involves biotransformation of the xenobiotic into new more polar and often inactive chemical entities thus forming a metabolite which can be readily eliminated from the body (Lin and Lu, 1997).

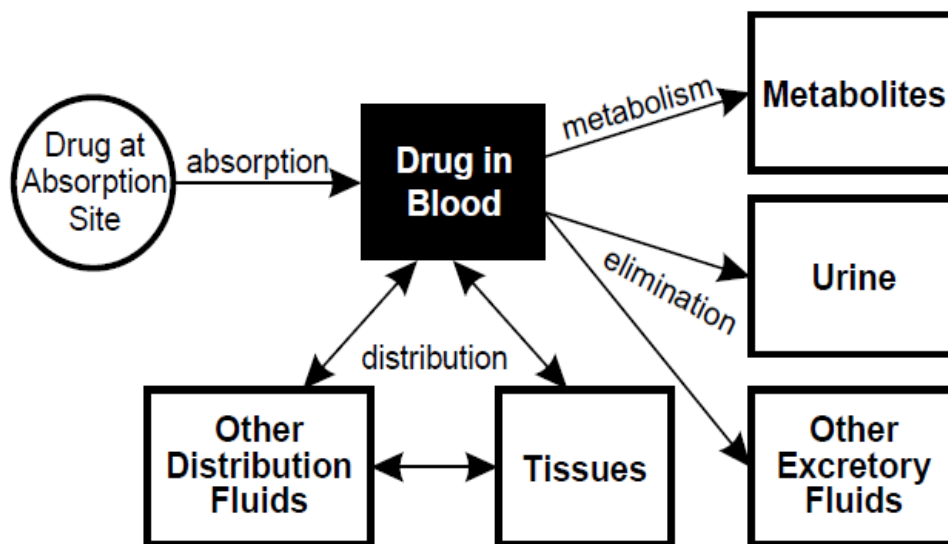


Figure 1.11 Schematic representation of drug disposition within the body (Gunaratna, 2000).

In 1959, Williams classified the drug metabolic reactions that are catalysed by enzymes into two general phases: Phase I and Phase II (Williams, 1959) (Figure 1.12). Since then, transport processes have also been classified as key process involved in the clearance of xenobiotics where drug uptake by transporters were referred to as Phase 0 and drug efflux by transporters were referred to as Phase III (Ritschel and Kerns, 2004).

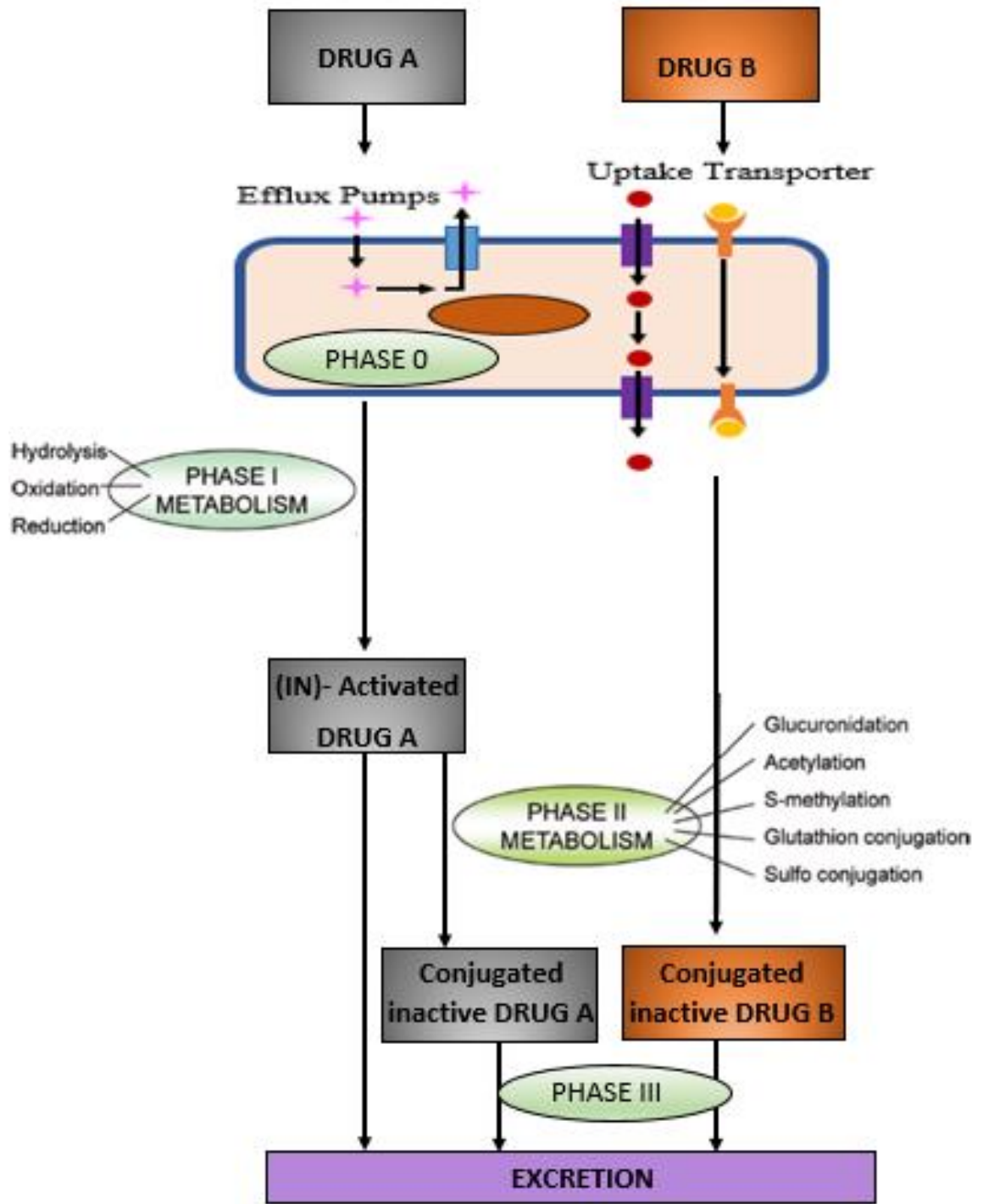


Figure 1.12 Different phases involved in drug metabolism

### 1.5.1 Phase I and II metabolism

In phase I reactions, the drug is broken down which involves unmasking, removal or addition of chemically reactive functional group as a result of oxidation, reduction or hydrolysis reactions. This biotransformation of the drug increases the polarity of the compound enabling its faster elimination from the body (Lin and Lu, 1997). Phase I reactions normally inactivate a parent drug, however occasionally reactive metabolites are formed which are more chemically active than the parent drug. Activation of the drug can also take place in cases where the drug administered is in its prodrug form (Benedetti *et al.*, 2009; Rajkumar *et al.*, 1998). These reactions are primarily catalysed by cytochrome P450 enzymes (CYPs) (Deenen *et al.*, 2011b) (Figure 1.13), but other Phase I drug metabolising enzymes include monoamine oxidase, flavin containing monooxygenase, alcohol dehydrogenase, aldehyde dehydrogenase, xanthine oxidase, peroxidase, NADPH-cytochrome P450 reductase, esterases, amidases and epoxide hydrolase.

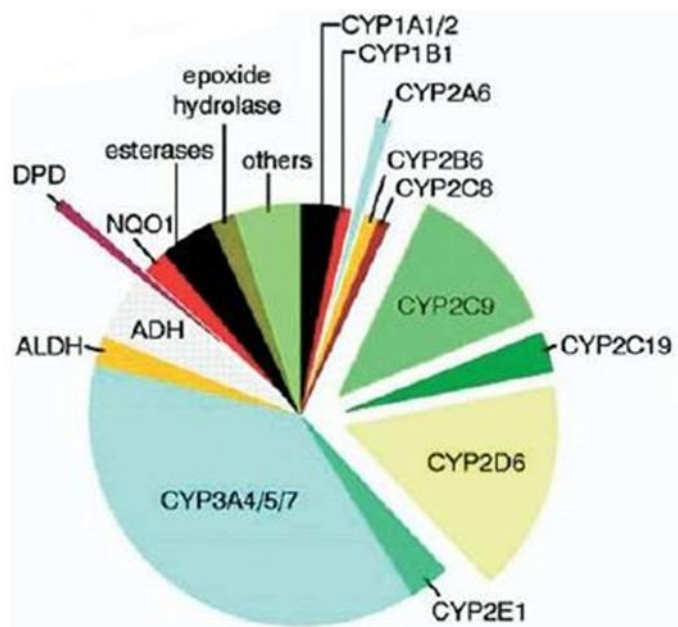


Figure 1.13 The proportion of drugs metabolised by various enzymes in the Phase I metabolism process.

The enzymes included are cytochrome P450 enzymes, aldehyde dehydrogenase (ALDH), Antidiuretic hormone (ADH), dihydropyrimidine dehydrogenase (DPD) NAD(P)H dehydrogenase [quinone] 1 (NQO1) and other metabolic enzymes (Juran *et al.*, 2006).

In Phase II metabolism, the drug or the phase I metabolite is conjugated with an endogenous group, thus inactivating, and further increasing the polarity of the drug enabling water soluble metabolites, to be readily excreted from the body in urine or bile (Ritschel and Kerns, 2004). The conjugation reaction involves acylation, glucuronidation, sulphation, glutathione conjugation and methylation requiring the participation of various enzyme groups as seen in Figure 1.14 (Williams, 1959; Xu *et al.*, 2005).

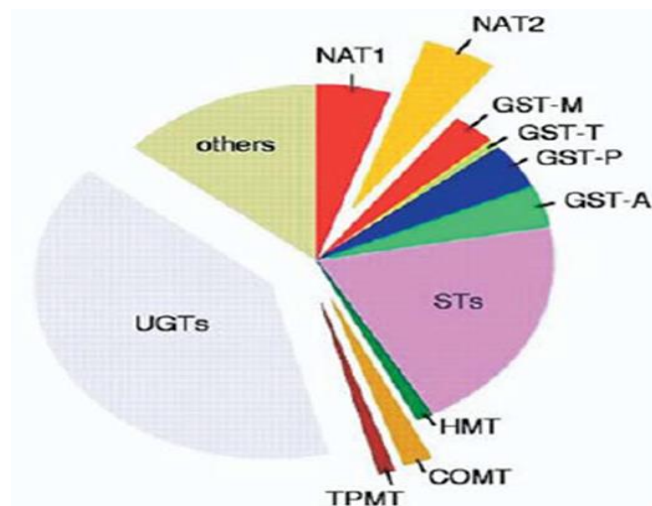


Figure 1.14 The proportion of drugs metabolised by various enzymes in the Phase II metabolism process.

The enzymes included are glucuronosyltransferase (UGTs), thiopurine methyltransferase (TPMT), histamine N-methyltransferase (HMT), N-acetyltransferase isoenzymes (NAT1 and NAT2), Glutathione-S-transferases (GST) (Juran *et al.*, 2006).

### 1.5.1.1 Cytochrome P450 enzyme system.

Cytochrome P450 enzymes (CYPs) are a super-family of thiolate-coordinated heme containing monooxygenase proteins with a molecular weight of approximately 50 Kd. The CYPs are believed to have been in existence for over 3.5 billion years (Gonzalez and Gelboin, 1994). Endogenously, the CYPs play a role in the synthesis and metabolism of neurotransmitters, prostaglandins, vitamin D and cholesterol (Nebert *et al.*, 2013). A subset

of these enzymes are also involved in the synthesis and metabolism of steroid hormones like oestrogen and testosterone (steroidogenesis) in the adrenal glands, gonads and peripheral tissue (Daniel and Timothy, 2006). CYPs are also responsible for metabolising a vast range of xenobiotics which include, 70-80% of prescribed drugs, drugs of abuse and toxins (Ferguson and Tyndale, 2011; Hedlund *et al.*, 2001). CYPs have been found to cause activation of procarcinogens or inactivation of carcinogens during the tumorigenic processes (Oyama *et al.*, 2004). CYPs are located either in the membrane of rough endoplasmic reticulum or in the inner membrane of the mitochondria (Meyer *et al.*, 2007). As seen in Figure 1.15B, cytochromes contain iron protoporphyrin I and when the ferrous haem complex is reduced to the ferric state and bound to carbon monoxide the pigment absorbs light at 450 nm, hence the nomenclature of these enzymes is cytochrome P450 (Figure 1.15A). The gene nomenclature of CYP3A4 was defined as follows: CYP represents the cytochrome P450 superfamily; 3 represents the gene family, defined by  $\geq 40\%$  homology in the amino acid sequence; A represents the gene subfamily, defined by  $\geq 55\%$  homology in the amino acid sequence and 4 represents the individual gene number, defined by a unique amino acid sequence.

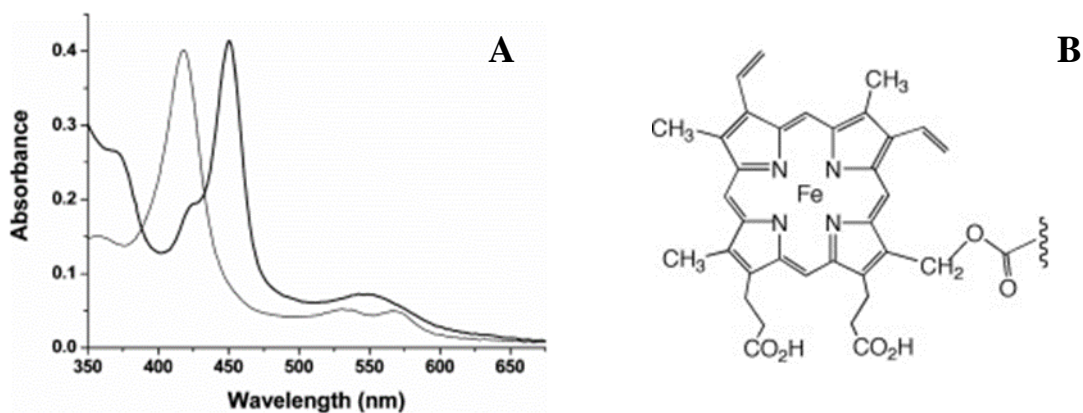


Figure 1.15 A) Absorption spectra for cytochrome P450 and the shift in the absorption spectrum due to its ferrous-carbon monoxide complex (Munro *et al.*, 2007). B) Structure of a porphyrin ring with a covalently bound haem in CYP enzymes (Johnston *et al.*, 2011).

### 1.5.1.2 Induction and Regulation of CYP P450 Enzyme

Inducing CYP enzyme expression increases metabolism and decreases the bioavailability of drug, thus potentially affecting the chemotherapeutic effect of the drug (Meyer *et al.*, 2007).

Induction of CYP enzymes has a significant effect on the drug metabolism, drug-drug interaction, toxicity and carcinogenicity of foreign substances (Kapoor *et al.*, 2007).

The CYPs are regulated by a complex mechanism which includes the transcriptional, post-transcriptional and post-translational mechanisms. Most of the genes of CYP enzymes are transcriptionally activated by xenobiotics. The xenobiotics act by a receptor dependent mechanism via either a aryl hydrocarbon receptor (AhR), constitutively active receptor (CAR), Farnesoid X-activated receptor (FXR), Pregnane X receptor (PXR) or peroxisome proliferator activated receptor (PPAR) as seen in Table 1.3 (Hedlund *et al.*, 2001). Cytosolic steroid receptor, once bound to nuclear receptor such as AhR are activated by the xenobiotic binding in the cytoplasm which causes translocation to the nucleus, whereupon it binds to a co-activator and another nuclear receptor. This complex can then bind to a xenobiotic response element on the promotor of the CYP or transporter gene, leading to increased mRNA transcription and subsequent translation resulting in an increase in CYP protein.

Table 1.3: Summary of nuclear receptor activating target gene (Hedlund *et al.*, 2001).

Target Gene	Nuclear Receptor
<i>ABCB<sub>1</sub></i>	PXR, CAR
<i>CYP3A4</i>	PXR, CAR, GR, HNF4 $\alpha$ , VDR, FXR
<i>CYP 2E1</i>	PXR, CAR, GR
<i>CYP 2B6</i>	PXR, CAR

## 1.5.2 CYP Localisation and Activity in the Brain

The percentage of CYP expression in the brain relative to the rest of the body is relatively low at 0.5-2 % (Ferguson and Tyndale, 2011); CYPs however, play an important role in onset of drug action due to pharmacological activation or inactivation via metabolism of CNS therapeutics (Mann *et al.*, 2012; Agarwal *et al.*, 2008). The brain comprises of regions of different cell types, density and function with a variable pattern of CYP expression. Expression is also dependent on individual genotype and exposure to environmental inducers or repressors (see Section 1.5.1.2) (Miksys and Tyndale, 2009; Strobel *et al.*, 2001; Dutheil *et al.*, 2008). As seen in Table 1.4; various CYP isoforms are found to localise in specific regions of the brain in human, rat and mouse and the cell type and potentially affect the metabolism in the brain microenvironment (Strobel *et al.*, 1995). It has been proven that the more localised the enzyme becomes, the greater its impact on the xenobiotic concentration in those localised area of the brain (Britto and Wedlund, 1992; Rieder *et al.*, 1998).

Table 1.4 Various CYP isoforms found localised in specific regions of the brain (Meyer et al., 2007)

<b>P450 Isoform</b>	<b>Species</b>	<b>Brain region</b>
CYP1A1	Mouse	Abundant
CYP1A1/2	Rat	Striatum, Hypothalamus, Cerebral Cortex, Cerebellum
CYP1A1	Human	Brain cortex
CYP1B1	Human	Temporal lobe
CYP2B1	Rat	Blood-brain barrier, Brain stem, Frontal cortex, Striatum, Olfactory tubercle
CYP2B6	Human/ Rat	Cerebellum, Hippocampus
CYP2B10	Mouse	Hippocampus
CYP2C11	Rat	Abundant
CYP2C29	Mouse	Blood-brain barrier
CYP2D4	Rat	Olfactory bulb, substantia nigra, cerebellum
CYP2D6	Human	Cortex, Hippocampus, Cerebellum
CYP2E1	Rat/Human	Cerebellum,
CYP2G	Rat	Olfactory bulb
CYP2J9	Mouse	Hippocampus, Cerebellum, Brainstem, Cerebral Cortex
CYP3A11	Mouse	Hippocampus, Cerebellum, Olfactory bulb, Hypothalamus
CYP3A13	Mouse	Hippocampus, Cerebellum, Olfactory bulb, Hypothalamus
CYP3A4	Human	Hypothalamus, cerebellum and olfactory lobes
CYP4A	Rat	Cortex, Cerebellum, Brainstem, Hypothalamus
CYP4x1	Human/Mouse	Brain barriers
CYP7B2	Rat/Mouse	Hippocampus

Astrocytes have been shown to participate in the metabolic activity of the BBB (Bauer *et al.*, 2004; Kido *et al.*, 2002), hence, astrocytes have been largely co-cultured with endothelial cells in *in vitro* models used to study the BBB. Pericytes cells also express certain metabolic enzymes like  $\gamma$ -glutamyl transpeptidase and glutamyl aminopeptidase that contribute to the metabolism at the BBB (Gynther, 2010). CYPs are also expressed in neurons, however, total CYP content in astrocytes is 2.7 fold higher than that in neurons (Kapoor *et al.*, 2007). The CYP expression in glial cells does not show stringent region dependent expression pattern as seen in the neuronal CYPs (Dutheil *et al.*, 2008). For the purpose of this thesis, the focus of further study was on the isoforms CYP2D6 and CYP3A4 as these two isoforms are responsible for metabolism of approximately 50 % of all prescribed drugs (Williams, 1959)(Williams, 2004).

#### 1.5.2.1 CYP2D6

Approximately 2 % of total CYP2D6 is expressed in the brain (Mann *et al.*, 2012). CYP2D6 metabolises about 20 % - 25 % of the drugs administered for neurological diseases, predominantly centrally acting opioids, and also neurotoxins and endogenous chemicals (Ingelman-Sundberg, 2004; Miksys and Tyndale, 2004). The expression of CYP2D6 varies for each individual due to polymorphic gene expression causing inter-individual variability in the sensitivity towards anticancer therapy and altered rate of metabolism of endogenous substrates (van Schaik, 2008). Compared to liver, characterisation of CYP2D6 enzyme activity in the brain is difficult, due to low levels of CYP2D6 activity and variation depending on the regions of the brain (Britto and Wedlund, 1992). The CYP2D6 is found to be localised in the cortex, hippocampus and cerebellum regions of the brain which contribute to 2 %, 7% and 2.8 % respectively distribution of glioma (CBTRUS 2012).

### 1.5.2.2 CYP3A4

CYP3A4 is the largest sub-family of all the cytochrome P450 enzymes and is responsible for metabolism of more than 50 % of centrally acting drugs (Strobel *et al.*, 2001). CYP3A4 has localised expression and is observed in areas sensitive to steroid hormones, which include hypothalamus, cerebellum and olfactory lobes (Miksys and Tyndale, 2004). The distribution of glioma shows hypothalamus, cerebellum and olfactory lobes. The nuclear receptor, pregnane X receptor (PXR) is known to regulate the expression of CYP3A4 in the brain (Agarwal *et al.*, 2008).

CYP3A4 and the ABC transporter ABCB<sub>1</sub> have common substrates, inhibitors and inducers and are often co-expressed which leads to an additive response to modulators of metabolism (van Schaik, 2008). CYP3A4 expression shows inter-individual variability which has a large impact on metabolism of low therapeutic index anticancer drugs, such as vincristine, irinotecan and etoposide. The variability of CYP3A4 can cause significant consequences, such as poor toxicity profile in the case of low CYP3A4 activity and poor efficacy leading to resistance in ultra-high CYP3A4 metabolism (Robertson *et al.*, 2003). An extensive study of the expression and function of the localised CYPs is essential for developing effective treatment of glioma and prediction of response to therapy.

## 1.5.3 Cytochrome P450 and Brain tumours

### 1.5.3.1 Role in CNS Drug Metabolism

Few CYPs have been identified in the tumour cells of the brain relative to expression elsewhere in the brain. Certain chemotherapeutics such as vinblastine, cisplatin, lomustine are metabolised by CYPs which causes activation or in-activation of the drug (Table 1.5).

Hence, study of the CYPs expressed by the blood brain barrier, non-cancerous brain cells and tumour cells could help determine the tumour sensitivity towards anticancer therapeutics (Oyama *et al.*, 2004).

*Table 1.5 Chemotherapeutics for treatment of glioma and CYPs involved in their metabolism.*

Drug	CYP enzyme	Reference
Vincristine	CYP 3A4	(Egbelakin <i>et al.</i> , 2011)
Procarbazine	CYP 2B6	(Rodríguez-Escudero <i>et al.</i> , 2011)
Irinotecan	CYP 3A4	(Lu and Cederbaum, 2008)
Temozolomide	CYP 1A1, 1A2, 2E1	(Long and Dolan, 2001)
Cisplatin	CYP 2E1	(Najar <i>et al.</i> , 2011)
Etoposide	CYP 3A4, 1A2	(Najar <i>et al.</i> , 2011)
Ifosfamide	CYP 2B6	(Kerbusch <i>et al.</i> , 2001)
Tamoxifen	CYP2D6	(Ingelman-Sundberg, 2004)

### 1.5.3.2 Role in Tumour development

The CYPs have been observed to participate in the development and progression of a tumour (McFadyen *et al.*, 2004). Carcinogens such as poly aromatic hydrocarbons (see Section 1.3.3) exposed to cells are often metabolised and bioactivated by CYP enzymes. DNA binding metabolites are produced due to activation of carcinogens by the CYPs as depicted in Figure 1.16. The DNA binding metabolites, frequently contain electrophiles or free radicals, capable of binding to electron rich regions in DNA or cysteine residues in protein causing carcinogenicity or cell death (Gonzalez and Gelboin, 1994).

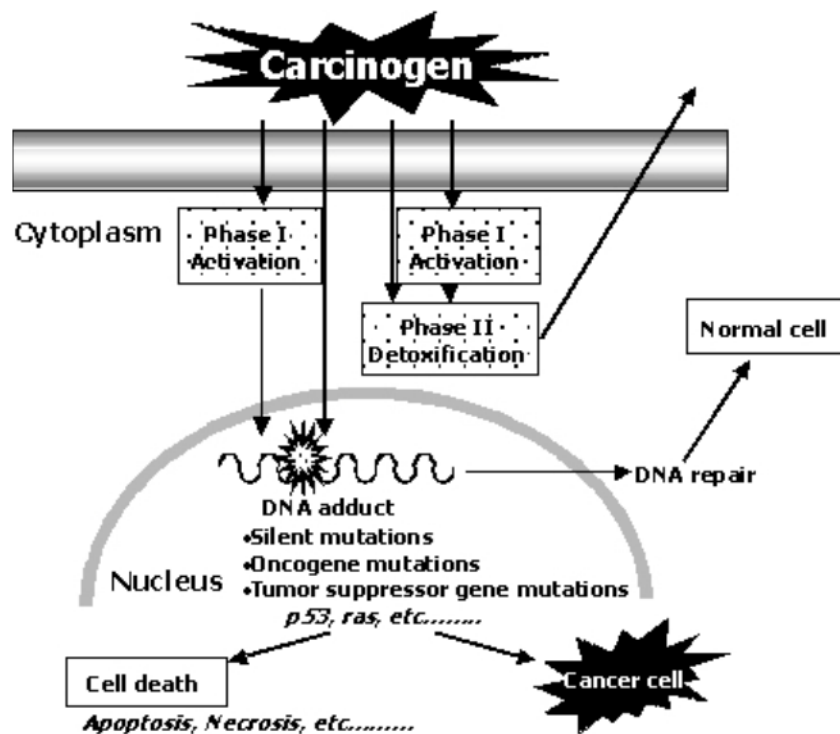


Figure 1.16 Schematic representation of metabolic pathway of a carcinogen causing tumour genesis (Oyama *et al.*, 2004).

### 1.5.4 Transporters at the BBB

An overview of the transporters at the brain and blood junction localised mainly in the luminal membrane of brain capillary endothelial cells can be seen in Figure 1.17 (Dean *et al.*, 2001). The endogenous role of these transporters, is to contribute to the transport barrier, which regulates the transport of essential nutrients across the BBB. For example, essential polar nutrients are transported bidirectionally via GLUT1 (glucose carrier) and large neutral amino acid (LAT1), L-system (amino acid carriers) (Abbott, 2002).

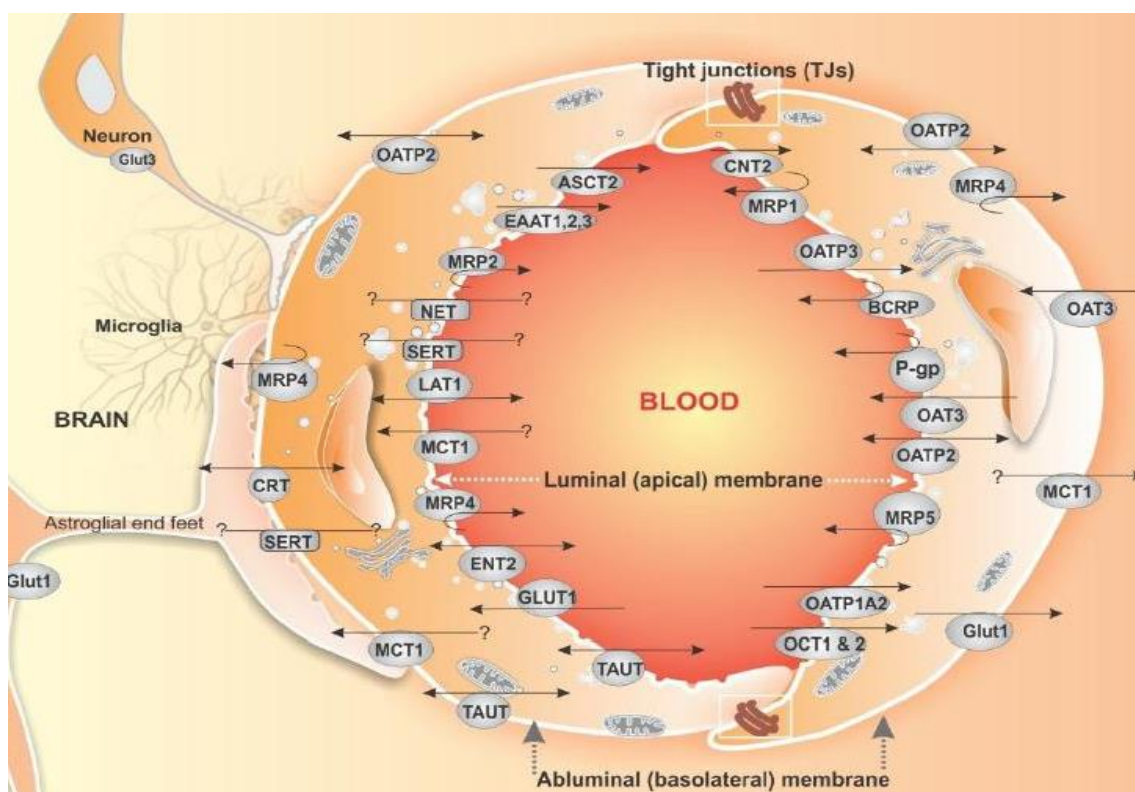


Figure 1.17 Carrier-mediated transport machineries (efflux and the influx transporters) at the BBB sites of the BBB (Omidi and Barar, 2012).

Phase 0 and Phase III metabolism involves the role of drug uptake and efflux transporters respectively, namely the solute like carrier (SLC) uptake transporters and ATP binding cassette (ABC) efflux transporters. These two processes affect the bioavailability and distribution of drugs and hence are important factors to be considered during drug metabolism (Borges-Walmsley *et al.*, 2003; Nelson and Gordon, 1983). Phase III is concerned with the elimination of the drug or metabolite from a cell back into circulation or bile by an ATP dependent efflux transporter (Ishikawa *et al.*, 2004). Efflux transporters, along with metabolising enzymes of xenobiotics, are an important protective mechanism against toxic and potentially harmful xenobiotics (Fromm, 2004). Efflux transporters are however, commonly associated with reducing bioavailability of a drug and play a central role in restricting brain uptake and extrusion of xenobiotics (Loscher and Potschka, 2005a; Loscher and Potschka, 2005b; Löscher and Potschka, 2005).

#### 1.5.4.1 Phase 0: Uptake Transporters

Solute carrier (SLC) transporters are a group large group of membrane transporters encoded by 55 different gene families. Four gene families under the SLC transporters category function as sugar transporters known as the glucose transporter (GLUT) family. High expression of glucose transporter (GLUT-1) has been associated with tumour angiogenesis and glioma proliferation. This has been proposed as a surrogate marker for prediction of patient outcome as increased glucose transport would coincide with the increased metabolic demands of aggressive tumour (Jensen and Chkheidze, 2011). Organic anion transporting polypeptides (OATP) and organic cation transport protein (OCT) are influx transporters of the SLC family and glioma drugs such as imatinib and methotrexate are substrates for OCT-1 (Roth *et al.*, 2012).

#### 1.5.4.2 Phase III: Efflux transporters

ATP-binding cassette (ABC) are one of the largest transmembrane protein superfamilies comprising of 48 transmembrane proteins which are further divided into 7 sub-families based on organisation of domains and amino acid homology ABCA to ABCG (Loscher and Potschka, 2005b; Dean *et al.*, 2001). The endogenous role of the ABC transporters family includes antigen presentation, detoxification, lipid transport and leukotriene transport (Higgins and Linton, 2003). These transporters utilise energy from ATP and transport molecules across the cell membrane. ABCB<sub>1</sub> and ABCG<sub>2</sub> are two prominent members of the ABC family expressed on brain endothelial cells, which safeguard the blood brain barrier limiting the entry of xenobiotics (Agarwal *et al.*, 2011; Pardridge, 2003; Pardridge, 2005).

A number of transporters of the ABC family were identified as multi-drug resistant proteins, where alteration in the expression of these transporters caused a change in the clearance of

clinically important drugs at the BBB (*Table 1.6*) (Gerk and Vore, 2002). ABCB<sub>1</sub> and ABCG<sub>2</sub> are transporters that actively efflux a wide range of lipophilic compounds and limit the drug uptake of the endothelial cells by effluxing substances out of the cells into the blood capillaries (Dean *et al.*, 2001; Lockhart *et al.*, 2003). Recently, research has focussed on ABCB<sub>1</sub> and ABCG<sub>2</sub> and their role as a barrier for the disposition of glioma therapeutics to the CNS.

*Table 1.6 ABC transporters involved in drug resistance and cancer therapy (Hartz and Bauer, 2010).*

Protein	Gene	Substrates
P-glycoprotein	ABCB <sub>1</sub>	Colchicine, doxorubicin, vinblastine, digoxin, paclitaxel
BCRP	ABCG <sub>2</sub>	Mitoxantrone, topotecan, doxorubicin, rodamine, daunorubicin

#### 1.5.4.2.1 Regulation of Efflux transporters

The regulation of expression of efflux transporters is done in a highly dynamic manner. The expression of efflux transporters are under tight transcriptional regulation by group of orphan nuclear receptors such as pregnane X receptor (PXR) in rodents and steroid and xenobiotic receptor [SXR] constitutive androstane receptor (CAR), and farnesoid X-activated receptor (FXR) in humans (Synold *et al.*, 2001; Schuetz and Strom, 2001; Ekins and Erickson, 2002; Sonoda *et al.*, 2003). The transcriptional regulation occurs by binding of the xenobiotic to orphan nuclear receptors by the same mechanism as outlined in Section 1.5.1.2 (Scotto, 2003). The presence of a xenobiotic results in upregulation of efflux transporter expression, hence increasing efflux activity of the drug out of the cell, enabling adaptation to the changing environment, and promoting tissue detoxification and protection (Miller, 2010), however this induction mechanism is considered as the main reason for CNS pharmacoresistance (Borges-Walmsley *et al.*, 2003; Mertsch and Maas, 2002).

### 1.5.4.3 ABCB<sub>1</sub> Transporter

ABCB<sub>1</sub> (also called as P-glycoprotein, MDR-1) was discovered as a prototypic transporter in 1970s and was found to be involved in resistance to anticancer therapeutics (Juliano and Ling, 1976). ABCB<sub>1</sub> acts as an energy dependent extrusion pump, predominantly localised on the luminal surface of the endothelial cells, which have polyspecificity for a large number of chemotherapeutics drugs of the CNS as its substrate (Allt and Lawrenson, 2000). ABCB<sub>1</sub> has a predominant role as the gate keeper of the blood brain barrier (Demeule *et al.*, 2002). Cordon-Carlo *et al.*, (1989) first identified expression of ABCB<sub>1</sub> in the endothelial cells of the BBB junction using immunohistochemistry, which suggested the protein was an operative component of the BBB (Cordon-Cardo *et al.*, 1989). ABCB<sub>1</sub> was also found to be expressed in the intestine, liver, kidney, brain and placenta (Staud *et al.*, 2010). ABCB<sub>1</sub> serves as a defence mechanism by protecting the brain from intoxication of potentially harmful lipophilic xenobiotics, which otherwise would penetrate into the brain by simple diffusion (Schinkel, 1999).

There are several isoforms of human ABCB<sub>1</sub>: type I also known as ‘‘MDR 1 Pgp’’ encoded by the *ABCB1* gene, with high activity which causes a drug resistance phenotype. Type II also known as ‘‘MDR2 Pgp’’ is encoded by the *MDR2* gene, and expressed in the canalicular membrane of hepatocytes and functions as a phosphatidylcholine translocase (Begley, 2004; Bodó *et al.*, 2003; Schinkel, 1999). ABCB<sub>1</sub> shows various functional polymorphisms and is considered the most important ABC transporter in humans for drug disposition (Fromm, 2004; Deenen *et al.*, 2011a).

Three major functions of ABCB<sub>1</sub> have been elucidated: i) expression in the luminal membrane of enterocytes limits the entry of drug in the body post oral administration. ii)

expression in the canalicular membrane of hepatocytes and in luminal membrane of proximal tubule in the kidneys promotes the elimination of drug in the blood in to the bile and urine, and most importantly, iii) expression at the BBB restricts the accumulation of substrates in the endothelial cells. ABCB<sub>1</sub> activity limits the entry of ABCB<sub>1</sub> substrate drugs such as colchicine, doxorubicin, vinblastine, digoxin, paclitaxel, which are potentially beneficial for the treatment of gliomas or any CNS related diseases (Gaillard and de Boer, 2000; Bendayan *et al.*, 2002). ABCB<sub>1</sub> activity is likely to be a determinant of the success of drug therapy, where increased activity results in bioavailability and low intracellular drug concentration (De Lange, 2004; Fromm, 2004). The expression of these ATP dependent transporters causes removal of its substrate out of the cell, which for the treatment of brain cancer results in ineffective therapeutic concentration.

For example, a number of studies have illustrated the role of ABCB<sub>1</sub> for drug penetration of anticancer drugs such as doxorubicin, paclitaxel and vinblastine by studying *ABCB1* knockout mice. Kemper *et al.*, reported that the drug concentration in the knockdown mice was higher than that in the wild type mice (Kemper *et al.*, 2003; Begley, 2004). Burgio *et al.*, showed the impact of ABCB<sub>1</sub> inhibitor on the access of etoposide to rat brain by brain microdialysis (Burgio *et al.*, 1998). Schinkel *et al.*, observed that when *ABCB1* knockdown mice were treated for a mite infestation by ivermectin (neurotoxic antiparasite drug), all mice died due to accumulation of ivermectin in the brain, hence concluded that ABCB<sub>1</sub> played a crucial role as an efflux transporter (Schinkel, 1999).

#### 1.5.4.4 ABCG<sub>2</sub> Transporter

ABCG<sub>2</sub> (also called breast cancer resistance protein (BCRP) or mitoxantrone resistance protein, MRP) is another member of the ABC superfamily and plays an important role in the

transport of substance across the BBB (Bhatia *et al.*, 2012). It was first discovered in a breast cancer cell line which was chemotherapy resistant, hence it was also called a breast cancer receptor protein (Noguchi *et al.*, 2009; Doyle and Ross, 2003). Similar to ABCB<sub>1</sub>, ABCG<sub>2</sub> is predominantly found on the luminal membrane of the BBB and is responsible for efflux of xenobiotics and protection the brain from hazardous substances (Cornford and Hyman, 2005; Warren *et al.*, 2009). ABCG<sub>2</sub> is also found to localise in the placenta, bile caniculi, colon, small bowel, and brain micro-vessel endothelium (Haimeur *et al.*, 2004; Cooray *et al.*, 2002). The expression of ABCG<sub>2</sub> transporter in endothelial cells was reported by Eisenblatter *et al.* (Eisenblatter and Galla, 2002; Eisenblatter *et al.*, 2003). Eisenblätter *et al.* (2003), have demonstrated the active extrusion of daunorubicin from porcine brain endothelial cells is mediated mainly by ABCG<sub>2</sub> compared to ABCB<sub>1</sub> suggesting an important role of ABCG<sub>2</sub> in the efflux transport of xenobiotics from the brain (Eisenblatter *et al.*, 2003). A number of studies were done to understand the role of ABCG<sub>2</sub> as a transport barrier at the BBB. ABCG<sub>2</sub> showed over expression in *mdr1a* knockout mice. Cisternino *et al.* (2004), reported that mice when treated with GF120918 (ABCG<sub>2</sub> inhibitor) showed increased penetration of ABCG<sub>2</sub> substrate prazosin and mitoxantrone in the brain (Cisternino *et al.*, 2004). ABCG<sub>2</sub> is a physiological transporter at the BBB that restricts the permeability of the brain to its substrates *in vivo* and plays an important role in disposition of glioma therapeutics in out of the brain. Similar studies were carried out by Lee *et al.* (2005), indicating that ABCG<sub>2</sub> played a role in active efflux of dehydroepiandrosterone sulphate and mitoxantrone in mice (Lee *et al.*, 2005).

## 1.6 *In vitro* modelling of the BBB

Recently, there has been an emphasis on the need to gradually shift from *in vivo* testing to *in vitro* systems with the aim to reduce, refine and replace animal models in research and development. For specific and detailed understanding of the drug metabolism and transport in the CNS, *in vitro* analysis of CYP and transporter activity is a valuable tool for the accurate prediction of the *in vivo* drug disposition if the therapeutics are substrates for the CYPs or transporter proteins (Kapoor *et al.*, 2007; Meyer *et al.*, 2007).

The full characterisation of BBB *in vitro* is vital for the extrapolation of understanding of typical and atypical neurological function *in vivo*. Research on the BBB has been focussed on developing effective drug delivery for neurological disorders. Currently, the FDA mandates screening of novel therapeutic compounds in animal models to assess the effect of drugs on the CNS (Crofton *et al.*, 2004). Traditional CNS drug validation studies in animals involve study of behavioural/sensory changes and examination of histological samples from the brain tissue of the animal (Coecke *et al.*, 2005). Such studies involve large investment of money, care and housing of animals and ethical issues. To avoid such labour intensive and expensive testing in the CNS drug development, there has been a need to design an *in vitro* model for high throughput screening of novel CNS therapeutics (Xu *et al.*, 2011).

The complexity involved in modelling an *in vitro* BBB with characteristics and microenvironment mimicking the *in vivo* structure is a significant hurdle (Malina *et al.*, 2009).

### 1.6.1 Assessment of *in vitro* BBB models

Since there are numerous hurdles in the development of *in vitro* BBB model, it is essential to develop robust methods for the assessment of the designed models. The measurement of

trans endothelial electrical resistance (TEER) is a simple method for determining the formation of TJs between endothelial cells adhered to the basement membrane (Gaillard and de Boer, 2000; Wilhelm *et al.*, 2011a). TEER can quantitatively measure the tightness of the barrier and acts as a surrogate marker of the health of the cells by measuring the electrical resistance and capacitance across the BBB (Hayashi *et al.*, 2004; Garberg *et al.*, 2005a; Nakagawa *et al.*, 2007a; Nakagawa *et al.*, 2009a).

Traditionally, chopstick electrodes were used to measure the TEER across the cell monolayer, comprised of two electrodes, one shorter than the other, placed in different chambers of the insert to give a reading of the resistance developed across cells grown on a transwell insert as a BBB mimic (Figure 1.18).



Figure 1.18 Measurement of TEER using an EVOM-2

Another method used to measure TEER in similar set up is the Cellzscope. Cellzscope provides real time TEER measurements across cells grown on a transwell insert by placing an electrode on each side of the membrane, one in the upper compartment and one in the lower, and application of a small AC voltage can measure the electric impedance of the cell

system, as seen in Figure 1.19. Apart from TEER values, cellscope also provides real time capacitance values of the model parameter which provides additional information about the cell layer properties. The two quantities, resistance TEER and capacitance ( $C_{cl}$ ), are combined to give the complex impedance  $Z$  of the cell layer.

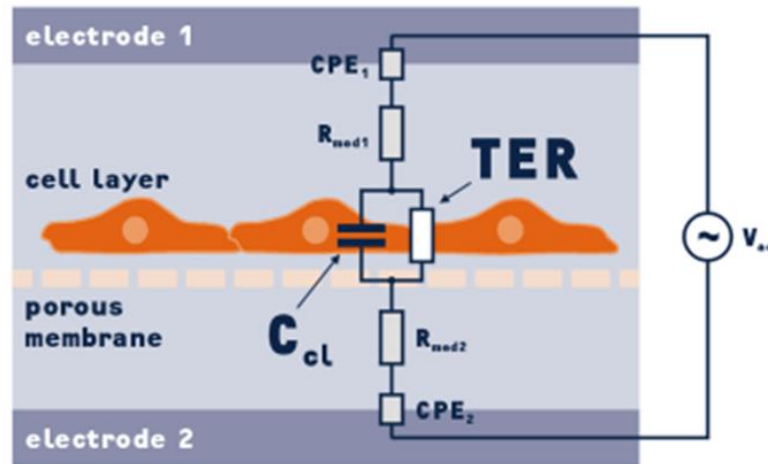


Figure 1.19 Diagrammatic representation of the electric resistance and capacitance across the cell monolayer in Cellscope.

The final system used to measure the TEER, is the electric cell-substrate impedance sensing (ECIS) system, which measures in real-time, the activities of cells grown in tissue culture. In addition, information on morphological changes, cell locomotion, and cell cytoskeleton changes can be detected. ECIS measures TEER from one end of the designed model, therefore it can only measure TEER in two-dimensional BBB models from a monolayer of cells (Figure 1.20).

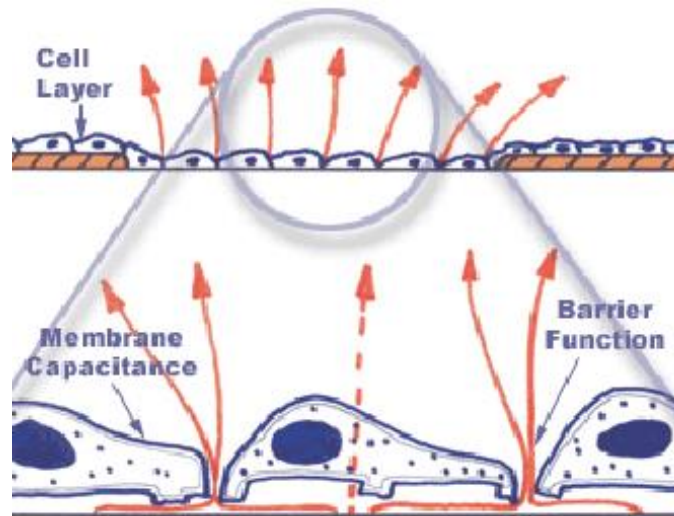


Figure 1.20 Monolayer of cells through which the ECIS reads the membrane capacitance and resistance.

To assess the permeability of molecules through the formed BBB barrier, the flux of fluorescent tagged molecules can be measured across the transwell BBB model (Hoffmann *et al.*, 2011). Carman *et al.* (2011), described the use of dextran tagged with FITC to determine the passive permeability across the barrier (Carman *et al.*, 2011).

Immunohistochemistry using fluorescent labelled antibody can be utilised to observe the formation, expression and localisation of the tight junction proteins under altered growth conditions, thereby helping to optimising the model (Eigenmann *et al.*, 2013).

## 1.6.2 Current existing BBB models

An ideal *in vitro* model should exhibit properties such as reproducibility of solute permeability, restrictive paracellular transport, functional expression of transporters, easy to culture and have a physiologically relevant architecture (Wilhelm *et al.*, 2011b; Berezowski *et al.*, 2004a). Lately, there has been an impressive increase in BBB modelling with a wide range of variations in the type of BBB models designed with difference in species, type of

culture, cell line, culturing conditions, as shown in Table 1.7 (Toth et al., 2011). Modelling of BBB includes different methods such as *in silico* (computer-aided) models, static mono-, co and tri-cultures, use of various dynamic or flow associated mono-, co- and tri-cultures (Cucullo et al., 2007).

Table 1.7 List of patented models of *in vitro* BBB (Toth et al., 2011).

No.	Cell types used	TEER	Major Novelty	reference
1	2 cell types: primary brain endothelial cells and astrocytes	> 200 $\Omega$ /cm <sup>2</sup>	BBB model tightened by cAMP signalling	Rubin et al, 1991
2	3 cell types: primary brain endothelial cells, astrocytes & pericytes	> 350-600 $\Omega$ /cm <sup>2</sup>	Triple co-culture to mimic the anatomical BBB	Niwa et al, 2007
3	2 cell types: primary brain or embryonic stem cell derived endothelial cells and neural progenitor cells	> 100-250 $\Omega$ /cm <sup>2</sup>	Multicellular BBB model	Shusta et al, 2008
4	1 cell type: monolayer of immortalized bovine brain endothelial cell line	NA	Immortalized brain endothelial cell line	Yazdanian et al, 2000
5	2 cell type: temperature sensitive immortalized rat brain endothelial cell line, and rat astrocyte cell lines	>106 $\Omega$ /cm <sup>2</sup>	Co-culture of conditionally immortalized cell lines	Terasaki et al, 2001
6	1 cell type: monolayer of human brain endothelial cell line	>40 $\Omega$ /cm <sup>2</sup>	Human BBB model	Couraud et al, 2006
7	1 cell line: monolayer of mouse primary or immortalized endothelial cells	NA	BBB model tightened by Wnt/ $\beta$ catenin signalling	Dejana et al, 2010
8	1 cell line: co-culture of brain endothelial cells and astrocytes under luminal flow condition	NA	Dynamic BBB model	Janigro et al, 2003

From the above tabulated models, it can be summarised that, there is a need to develop a three dimensional model which recapitulates the neurovascular unit and which can have a balance of high TEER values and low permeability. It should also essentially be cost effective

and easy to maintain giving high throughput results, so that it can be used commercially for screening cancer therapeutics.

## 1.7 Rationale for the project

The main aim in designing a physiologically relevant *in vitro* BBB model is for studying the cellular *in vivo* mechanisms involved in the disposition of drug across the BBB. This would help in predicting the bioavailability of drug across the blood brain barrier. The activity of drug efflux transporters in the BBB contribute considerably to chemotherapy resistance frequently observed when treating gliomas. Various experimental and diagnostic tools have been designed to study the drug efflux transporter function in the brain by designing an *in vitro* model for the BBB. All the *in vitro* and *in vivo* methods used to study drug efflux transporters show considerable differences in the substrate and inhibitor specificity from one species to another (Cecchelli *et al.*, 1999; Dehouck *et al.*, 1992). To avoid hampering extrapolation of efflux transporters in different species, it has been recommended that the materials used for the designing the model should be derived from human tissue (Garberg *et al.*, 2005a). This may provide unambiguous information on transporter function at the blood brain barrier (Loscher and Potschka, 2005c).

Two experimental approaches have been used for studying transport mechanism in the endothelial cells of the blood brain barrier. The first experimental approach was used to study the accumulation of compounds in the cells which explains the transport of compounds in and out of the cell (Takakura *et al.*, 1991; Reichel *et al.*, 2003). The second approach was to set up involved the culturing of brain endothelial cells in monolayer on the filter membrane. This method is largely used in the *in vitro* model designing of the blood brain barrier (Cecchelli *et al.*, 1999). The study of the blood brain barrier function using *in vitro* models

was initially done by investigation in brain capillaries which were isolated from rat brain. Thereafter, the brain capillaries have been isolated from various species like pig, cow, fish have been used (Reichel *et al.*, 2003). The capillaries isolated include the brain endothelial cells, basement membrane ensheathing pericytes and attached astrocytic process. The TEER value of *in vitro* model is compared to *in vivo* model to determine the development of a successful *in vitro* model of the BBB. Since then a number of models have been designed however, all of them failed to reach the level of tightness that is reported in the blood brain barrier *in vivo* (Garberg *et al.*, 2005b).

The penetration of drugs into the human brain through the blood-brain barrier (BBB) is a major obstacle limiting the development of successful neuro pharmaceuticals. This restricted permeability is due to the delicate intercellular junctions, efflux transporters and metabolising enzymes present at the BBB. The pharmaceutical industry and academic research rely heavily on permeability studies conducted in animals and *in vitro* models of the BBB (Shawahna *et al.*, 2012). Therefore, designing a model which predicts drug efficacy and toxicity of brain tumour drug treatment is highly important. The model should be a bridge between the *in vitro* and *in vivo* studies.

### 1.7.1 Aim

To develop a fully characterised, physiologically relevant and functional *in vitro* model for prediction of permeability of drugs across the blood brain barrier. The designed model will be used to study drug metabolism and transport in glioma, and hence prediction of the efficacy of novel drugs, nanoparticles for the treatment of glioma.

## 1.7.2 Objectives

- To study growth characteristics and phenotype of the cell lines and short term cultures to be used for the development of the BBB model.
- To study protein expression profiles of drug metabolising enzymes (CYP3A4 and CYP2D6) and efflux transporters (ABCB<sub>1</sub> and ABCG<sub>2</sub>) in cancerous and non-cancerous cell lines and short term cultures in various culture conditions and optimise the culture conditions for maximal expression
- To study the activity profiles of drug metabolising enzymes (CYP3A4 and CYP2D6) and efflux transporters (ABCB<sub>1</sub> and ABCG<sub>2</sub>) in cancerous and non-cancerous cell lines and short term cultures in various culture conditions optimise the culture conditions for maximal activity.
- To develop an *in vitro* BBB model of human origin using short term cultures by different modelling systems and determine the best developed model by assessing their protein expression profiles for TJs, efflux transporters and DMEs and activity profiles.
- To validate the developed model for different characteristics of a BBB model and test its efficiency using nanoparticles and aptamers.
- To develop a brain tumour barrier BTB model by studying the effect of tumour cells in a BBB model.

## 1.7.3 Overview

As seen in Figure 1.21, the flow chart shows an overview of the study conducted in developing a fully characterised physiologically relevant *in vitro* BBB model.

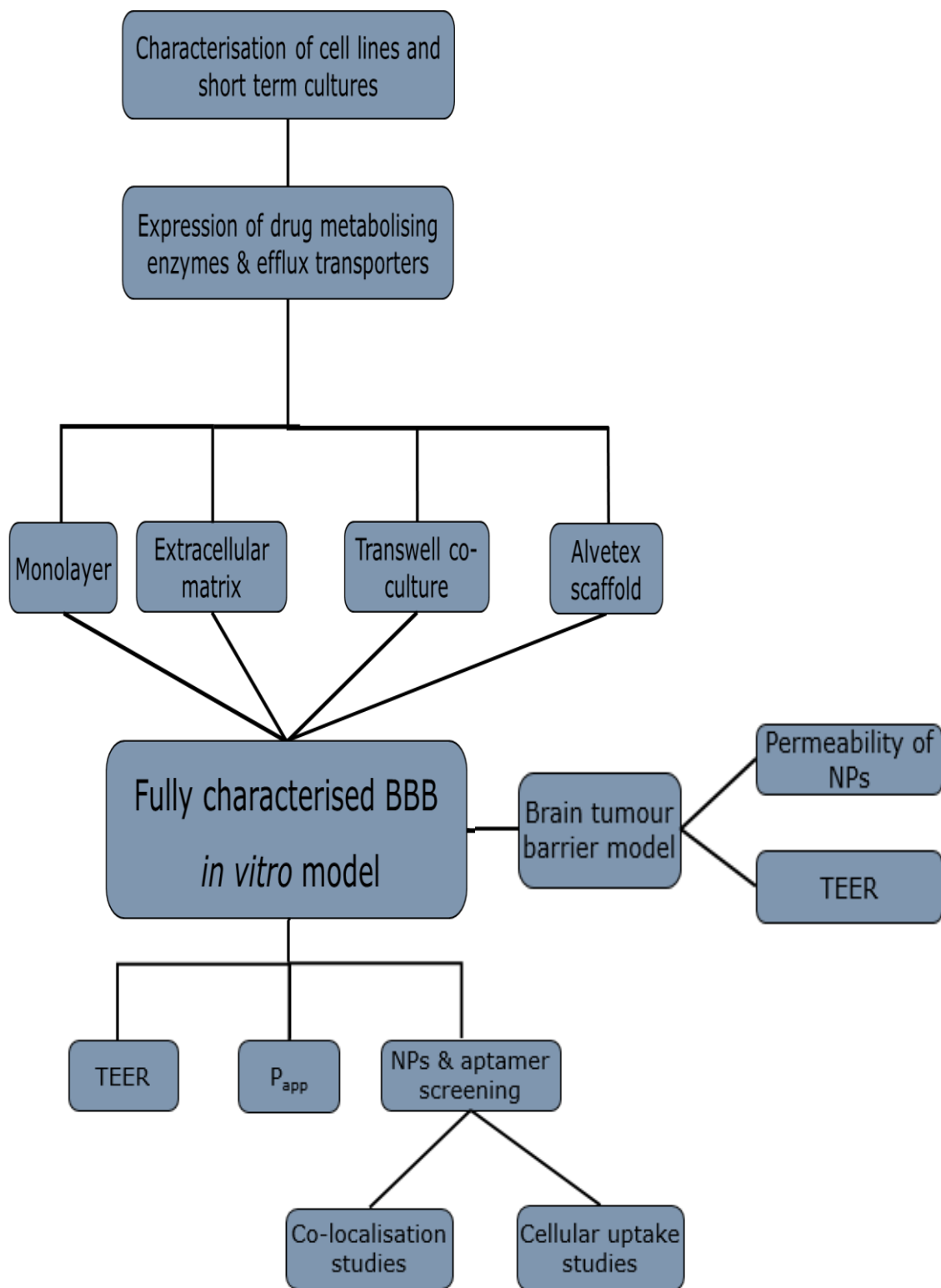


Figure 1.21 Summary of the conducted experiments.

# CHAPTER 2

## 2. **Materials and Methods**

### 2.1 Tissue Culture

#### 2.1.1 Cell Lines

Immortalised human cell lines 1321N1 (malignant astrocytoma, sub-clone of grade IV U118MG), U87MG (astrocytoma grade IV/glioblastoma), SVGp12 (non-cancerous foetal astrocyte) were obtained from the European Collection of Cell Cultures (ECACC, Salisbury, UK). The immortalised human cerebral microvascular endothelial cell line (hCMEC/D3) cell line and short term human astrocyte culture (SC1800) were a generous donation from the Neuro oncology Department of University of Portsmouth. The hCMEC/D3 is a cell line generated from primary human brain capillary endothelial cells via a lentiviral vector system (Urich *et al.*, 2012). In addition, commercially available short-term cell lines derived from primary tissue including human microvascular endothelial cells (HMBEC), human brain vascular pericytes (HBVP) and human astrocytes (HA) were purchased from (Sciencell, Buckingham, UK). Short-term cell lines BTNW914 (female, aged 67, GBM patient) and BTNW370 (female, aged 65, gliosarcoma grade IV patient) were established from human glioma biopsies obtained from the Brain Tumour North-West (BTNW) tissue bank at Royal Preston Hospital. Informed patient consent, NHS and university ethical approval was obtained for the study of glioma phenotype.

#### 2.1.2 Media and Supplements

All cell culture media and supplements used for cell culture were purchased from Lonza, Nottingham, UK unless otherwise mentioned (Table 2.1). Phosphate buffered saline (PBS), ethanol, all plastic-ware including tissue culture flasks, well plates, centrifuge tubes, stripettes, pasteur pipettes, and 1.5 ml tubes, were purchased from Fisher scientific,

Leicestershire, UK. All lab consumables were purchased from Sigma, Dorset, UK unless mentioned otherwise.

*Table 2.1 Summary of cell culture supplements used.*

Reagents	Abbr. / storage temperature	Cell line	Suppliers
Dulbecco's modified eagle's medium	DMEM, 2-8 °C	1321N1	Lonza, Slough, UK
Eagle's minimum essential medium	EMEM, 2-8°C	U87MG, SVGp12	Lonza, Slough, UK
Endothelial basal media	EBM-2, 2-8°C	hCMEC/D3	Lonza,, Slough, UK
Endothelial Growth Media-2 Single quotes	EGM-2, -20°C	HBMEC, hCMEC/D3	Lonza,, Slough, UK
Pericyte cell medium	PCM, 2-8°C	HBVP	Sciencell, Buckingham, UK
Pericyte cell growth supplement	PCGS, -20 °C	HBVP	Sciencell, Buckingham , UK
Astrocyte basal media	ABM-2, 2-8°C	SC1800 (HA)	Lonza, Slough,, UK
Astrocyte Growth Media-2 Single quotes	AGM-2, -20°C	SC1800 (HA)	Lonza, Slough,, UK
Ham's F-10 medium	2-8°C	BTNW370, BTNW914	Lonza, Slough, UK
Foetal bovine serum Cat no:10082139	FBS, -20°C	1321N1, SVGp12, U87MG	Gibco, Paisley, UK
Foetal bovine serum Cat no:10100139	FBS, -20°C	BTNW370, BTNW914	Gibco, Paisley, UK
Human serum	HS, -20°C	HBMEC,hCMEC/D3 HBVP, SC1800 (HA)	Lonza Slough,, UK
L-glutamine	-20 °C	1321N1, SVGp12, U87MG	Lonza, Slough, UK
Sodium pyruvate	2-8 °C	SVGp12, U87MG	Lonza, Slough, UK
Non-essential amino acid	NEAA, 2-8 °C	SVGp12, U87MG	Lonza, Slough, UK
Hank's balanced salt solution	HBSS, 2-8 °C	All cell lines	Lonza, Slough, UK

The 1321N1 cell line was maintained in Dulbeccos's Modified Eagle's Medium (DMEM) supplemented with 10 % (v/v) foetal bovine serum (FBS) and 2 mM L-glutamine, while the U87MG and SVGp12 cell lines were maintained in Essential Minimum Eagle Medium (EMEM) supplemented with 10 % (v/v) FBS, 2 mM L-glutamine, 1 mM sodium pyruvate and 1 % (v/v) non-essential amino acids (NEAA). All the cell lines were cultured in 75 cm<sup>2</sup> tissue culture treated flasks and maintained in a 37 °C humidified incubator supplied with 5 % CO<sub>2</sub> (Thermo Scientific Nunc, UK). For all the experiments, each of the immortalised cell lines were used between passages 2-18. Short-term endothelium, pericytes and astrocytes cell lines were grown in endothelial cell media, pericyte media and astrocyte media, respectively (Sciencell, UK). In addition, cell line and primary culture media was supplemented with 5 % (v/v) human serum (HS) and growth supplement (Table 2.1). The patient biopsy derived short term cultures of GBM, BTNW914 and BTNW370 were cultured in Ham's F-10 medium supplemented 10 % (v/v) FBS (Gibco, Paisley, UK).

### 2.1.3 Cryopreserving and Thawing Cells

The confluent cells were passaged as described in section 2.1.4. The pellet of cells obtained after centrifugation was resuspended in freezing medium. The freezing medium comprised of serum used in respective media (foetal bovine serum or human serum) and 10 % dimethyl sulphoxide (DMSO). Cell suspensions were stored in cryotubes in Mr. Frosty (Nalgene, UK) freezing container filled with isopropanol at -80 °C overnight. The cryovials were placed in the liquid nitrogen dewer (-190 °C) the following day. Frozen cells were rapidly thawed in a water bath at 37 °C and seeded in a 75 cm<sup>2</sup> tissue culture flask in a laminar flow cabinet, with 10 mL of growth medium for every 1 ml of defrosted cells. The growth medium was changed after 12-24 h for complete removal of the cryopreservatives.

## 2.1.4 Subculturing of Cells

Cells were passaged once 70-80 % confluency was reached. The subculturing of cells was under aseptic conditions in a laminar flow cabinet. Growth media, 0.25 mM trypsin and 0.1 M PBS, pH 7.4 were prewarmed at 37 °C in a water bath. The spent medium was aspirated from the flask and cells were washed with 0.1 M PBS, pH 7.4. The PBS was removed and 0.25 mM trypsin was added to the cells. The flask was incubated at 37 °C for 5 min and cells were examined under inverted light microscope to check for detachment of cells. Growth media appropriate for the cell line was added to the flask to neutralise the trypsin reaction in the flask. The cell suspension was then mixed using pipette to ensure homogeneity of detached cells and centrifuged at 179 x g for 5 min using a bench centrifuge (ALC, Buckinghamshire, UK). After centrifugation, the pellet of cells was retained. The cells were resuspended in 5 ml fresh growth medium and a 20 µl aliquot was retained to determine the cell count and cell viability using trypan blue stain. The cells were seeded at a density of  $5 \times 10^4$  cells/ ml in a 75 cm<sup>2</sup> flask which was incubated at 37 °C and 5 % CO<sub>2</sub> in a humidified incubator until confluent.

## 2.2 Cell Counting

From the trypsinised cell suspension, 10 µl was aliquotted in a 1 ml sterile 1.5 ml tube to which 10 µl of 0.4 % trypan blue dye was added. A newbauer's haemocytometer was used for counting cells, with those excluding trypan blue counted as viable. The cells were counted under the inverted light microscope at 10 X magnification (Leica DMIL, Milton Keynes, UK). The number of viable cells in the centre grid (1 mm<sup>2</sup>) of each chamber was counted, an average from five chambers was calculated and this number was multiplied with the

haemocytometer factor  $1 \times 10^4$ . The cell count was then corrected for dilution factors to obtain the number of cells per 1 ml of suspension. The cells were seeded at densities of 2000 cells/200  $\mu$ l/ well in 96 microtiter plates, 20,000 cells/ ml/ well in 24 well plates and  $1 \times 10^6$  cells/ ml/ flask in 75 cm<sup>2</sup> flasks.

## 2.2.1 Spheroid Culture

A confluent flask of monolayer cells was passaged (see section 2.1.4) and seeded to grow as spheroids. The spheroids were cultivated by two methods, hanging drop and agar coated plates.

### 2.2.1.1 Hanging Drop Method

Cell suspension was diluted in media to a concentration of 3000 cells/25  $\mu$ l of cell suspension was seeded for each spheroid on the lid of a petri dish. A total of 20 spheroids were seeded per dish. The bottom of the petri dish was filled with 2 ml of respective culture media to maintain a humidified atmosphere in the dish. The lid was placed on the petri dish with the drops of cell suspension hanging upside down. The spheroids were allowed to grow for 6 days at 37 °C and 5 % CO<sub>2</sub> in a humidified incubator and the media was changed on the third day following seeding, the formed spheroids were then used for experiments.

### 2.2.1.2 Agar Coated Plates

Tissue culture plates were coated with 1 % sterile agar and left to cool one day prior to seeding cells for spheroids. Passaged cells were seeded onto the agar coated 24-well plates at a density of 3,000 cells/ well. The plates were incubated at 37 °C and 5 % CO<sub>2</sub> in a

humidified incubator for 6 days, the media was changed after 3 days on the sixth day the spheroids were used for experiments.

## 2.2.2 Growth Curves

To study the growth pattern of the immortalised cell lines 1321N1, U87MG, SVGp12, and hCMEC/D3 and short-term cell lines HBMEC, HBVP, SC1800 growth curves were established. The cells were seeded at a density of 20,000 cells/ mL/ well in a 24 well tissue culture plate at 37 °C and 5 % CO<sub>2</sub> in a humidified incubator. Each day the cells in the wells were trypsinised and were stained with 0.4 % trypan blue dye and counted using a haemocytometer (refer to Section 2.2). For every time point, an average cell count from three wells was calculated up to day 10 and the growth medium was changed every three days to maintain cells in a healthy environment. The experiment was performed in triplicate and cell count verses time was plotted to study growth kinetics.

## 2.3 Immunostaining of cells

### 2.3.1 Fixation of cells

The cells were seeded at a density of  $1 \times 10^4$  cells/ ml on 1 mm thick coverslips in a 24 well plate. Upon cells reaching 50 % confluence, the spent media was removed and the coverslips were washed with 0.1 M PBS three times. Cells on the coverslips were then fixed by incubation with 4 % paraformaldehyde (PFA) for 15 min at room temperature followed by washing with 0.1 M PBS three times ready for immunostaining.

### 2.3.2 Fluorescent immunostaining

The fixed cells on coverslips were washed with 0.1 M PBS, pH 7.4 three times and incubated with 0.1 M glycine for 10 min for quenching background fluorescence. Cells were washed with 0.1 M PBS, pH 7.4 five times, then permeabilised by incubating with 0.1 % triton X-100 for 10 min at room temperature, followed by washing with 0.1 M PBS, pH 7.4 five times. Cells were blocked by incubating with 10 % goat serum for 1 h, followed by three washes with 0.1 M PBS, pH 7.4. Cells were then incubated with respective dilutions of primary antibody (Table 2.2) for 1 h at room temperature and at the end of the incubation period were washed with 0.1 M PBS, pH 7.4 three times. The cells were then incubated with 1:1000 dilution of secondary antibody Alexa Fluor® 488 F(ab')<sub>2</sub> Fragment of Goat Anti-Rabbit IgG (Life technologies, UK) for 30 min in the dark. The cells were then washed with 0.1 M PBS, pH 7.4 three times and mounted on a microscope slide using with VECTASTAIN mounting media (Vector Laboratories, Peterborough, UK). The slides were incubated for 24 h in dark, before analysis, the corners of the coverslip were tacked with nail varnish to prevent the cells from drying.

*Table 2.2 List of rabbit polyclonal primary antibodies, their concentration and dilutions used for immunostaining.*

Primary antibody	Antibody dilutions in 0.1 M PBS, pH 7.4	Manufacturer
GFAP	1 : 300	Abcam, Cambridge, UK
HLA	1 : 250	Santacruz, Middlesex, UK
MDR	1 : 250	Abcam, Cambridge, UK
BCRP	1 : 200	Abcam, Cambridge, UK
Occludin	1 : 250	Abcam, Cambridge, UK
Claudin-5	1 : 250	Abcam, Cambridge, UK
Isotype Control	1 : 100	Santacruz, Middlesex, UK

### 2.3.3 3,3-Diaminobenzadine (DAB) staining

The fixed cells on coverslips were washed with 0.1 M PBS, pH 7.4 three times and incubated with 10 % horse serum for 30 min, followed by three washes with 0.1 M PBS, pH 7.4. The cells were then incubated for 10 min with 0.1 % H<sub>2</sub>O<sub>2</sub> in 0.1 M PBS, pH 7.4 to quench endogenous peroxidase activity. The cells were washed with 0.1 M PBS, pH 7.4 once and incubated with respective dilutions of primary antibody for 30 min or 24 h as outlined in Table 2.3. The cells were then washed with 0.1 M TBS, pH 7.4 three times and incubated with 1:500 dilution of biotinylated secondary antibody for 30 min. After the incubation, the cells were washed with 0.1 M TBS, pH 7.4 three times and incubated with VECTASTAIN Elite ABC Kit (Vector Laboratories, Peterborough, UK) for 30 min. The cells were then washed with 0.1 M TBS three times and stained with DAB (Vector Laboratories, UK) for 10 min at room temperature. The stained cells were washed with distilled water five times and cells were counter stained with haematoxylin. These cells were dehydrated with a series of ethanol washes (50 %, 70 % and absolute) and xylene and then mounted on a glass slide using a Distyrene Plasticizer Xylene (DPX) mount media.

*Table 2.3 List of concentrations and dilutions and incubation period of rabbit polyclonal primary antibodies used for DAB staining.*

Antibody	Dilutions	Incubation period	Manufacturer
GFAP	1 : 500	24 h	Abcam, Cambridge, UK
HLA	1 : 20	30 min	Santacruz, Middlesex, USA
MDR	1 : 250	30 min	Abcam, Cambridge, UK
BCRP	1 : 250	30 min	Abcam, Cambridge, UK
EMA	1 : 350	30 min	Abcam, Cambridge, UK
CD34	1 : 300	30 min	Abcam, Cambridge, UK
Biotinylated secondary antibody	1 : 500	30 min	Abcam, Cambridge, UK

## 2.4 Protein extraction

### 2.4.1 Protein linearity experiment

Cells were grown in five T-75 flasks and the cells were extracted from one T-75 flask each day from day 3 to day 7. The cells were lysed using RIPA buffer (see appendix) and the protein concentration was quantified using the Bradford assay (see Section 2.4). The concentration of protein content was plotted to determine its relationship with cell number.

### 2.4.2 Optimisation of protein extraction method

Cells were cultured in T-75 flasks which were harvested when the flask was confluent for protein extraction. All protein extractions were carried out on ice to avoid protein degradation and maximise the yield of the proteins. Different methods were investigated for optimisation of protein extraction. In all cases the protein concentration was quantified using the Bradford assay (see Section 2.4).

#### 2.4.2.1 Method I

The confluent flask of cells was kept on ice and medium was aspirated from the flask. The cells were washed with ice cold 0.1 M PBS, pH 7.4 to remove traces of serum and the cells were scraped from the flask using a sterile cell scraper. The scraped cells were collected in a precooled 1.5 ml tube to which 500  $\mu$ l of ice cold RIPA lysis buffer was added. The samples were agitated at 40 rpm on a shaker (VXR Vibrax, Oxfordshire, UK) for 30 min at 4 °C to facilitate membrane lysis. The samples were then spun in a microcentrifuge (Sanyo, Leicester, UK) at 11451 x g for 20 min at 4 °C. After centrifugation the supernatant, which comprised of all cellular and membrane proteins, was collected in a precooled 1.5 ml tube, ready for determination of protein concentration.

#### 2.4.2.2 Method II

The confluent flask of cells was kept on ice and medium was aspirated from the flask. Cells were trypsinised as previously described in Section 2.1.4. The cell suspension was centrifuged at 179 x g for 5 min and the pellet was resuspended in ice cold RIPA buffer, ready for assay of protein content.

#### 2.4.2.3 Method III

A similar protocol, as described in Section 2.3.2, was followed, except the cells were centrifuged at 21074 x g instead of 11451 x g to determine whether an increased protein yield can be obtained, with a higher centrifugal force.

#### 2.4.2.4 Method IV

A similar protocol, as described in Section 2.3.2 was followed except following resuspension in RIPA buffer, the cells were sonicated on ice using a probe sonicator (Sanyo, Leicester, UK) at 50 hertz for three repetitions of 30 s duration. After centrifugation, at 11451 x g for 20 min at 4 °C, the supernatant, which comprised of all cellular and membrane proteins, was assayed for protein concentration.

### 2.4.3 Polycarbonate transwell and alvetex scaffold inserts

At the end of the TEER measurements (see Section 2.9.1) the co-cultured cells were lysed for protein extraction. The inserts were washed twice with HBSS, pH 7.2 (see appendix) and then incubated with 100 µl RIPA buffer for 15 min at 4 °C. The inserts were scraped and the cells which were suspended in RIPA buffer were collected in 1.5 ml tubes. The samples were spun in a microcentrifuge (Sanyo, Leicester, UK) at 11451 x g for 20 min at 4 °C. After

centrifugation the supernatant, which comprised of all cellular and membrane proteins, was collected in precooled 1.5 ml tubes and assayed for protein content.

## 2.5 Protein quantification by Bradford assay

The Bradford assay is a protein concentration estimation assay which involves binding of coomassie brilliant blue G-250 dye to the proteins in the sample (Bradford, 1976). A set of bovine serum albumin (BSA) protein standards diluted in RIPA lysis buffer (0.1 to 2 mg/mL) were used as a reference. Samples and standards were diluted in Bradford reagent (1 in 51 dilutions) in a 96-well plate. The absorbance was read at 612 nm using a plate reader Tecan GENios Pro<sup>®</sup> (Tecan, Theale, UK). The absorbance of BSA samples were plotted against concentration of BSA and a line of best fit was determined by linear regression, to allow determination of the extracted protein concentration. Protein concentrations were then corrected for dilution factors.

## 2.6 Western blotting

Western blotting technique was used for detection of cytochrome P450 enzymes and efflux transporters protein expression in the extracted protein lysate. Western blotting involved identification of protein of interest by probing with specific antibodies after electrophoretic separation of the sample and blotting over a nitrocellulose membrane. This study involved the detection of cytochrome P450 enzymes; CYP3A4, CYP2D6, the efflux transporters; ABCB<sub>1</sub> and ABCG<sub>2</sub> and tight junction proteins; occludin and claudin-5.

## 2.6.1 Sample preparation

The 2 mg/ ml protein aliquots from cells, stored at  $-20^{\circ}\text{C}$ , were thawed and mixed with 2 x Laemmli sample loading buffer (see appendix 4) at a ratio 1:1. The 1.5 ml tubes containing sample and sample buffer were heated on a block (Techne, Staffordshire, UK) for 5 min at  $90^{\circ}\text{C}$ , to denature complex structured proteins to linear proteins. Each well of 10 % polyacrylamide gel was loaded with 10  $\mu\text{g}$  protein sample.

## 2.6.2 Gel electrophoresis

Gel electrophoresis involves separation of macromolecules on the basis of their size. The electrophoresis used in this experiment was sodium dodecyl sulphate polyacrylamide gel electrophoresis (SDS PAGE). SDS PAGE is a discontinuous electrophoresis which involves two different gels; stacking gel and resolving gel. The stacking gel stacks the sample and resolving gel separates the proteins in the sample on the basis of molecular size. A 4 % stacking gel and 10 % resolving gels were prepared as per the recipe described in appendix (4).

Firstly, the resolving gel was poured into a vertical setup and allowed to polymerise with the aid of chain initiator tetramethylethylenediamine (TEMED) in the presence of the catalyst ammonium persulphate (APS). It was covered with water to avoid contact with atmospheric oxygen that inhibits polymerisation. After the resolving gel had polymerised, the stacking gel was poured and the comb was inserted. Once the gels were set, they were placed in an electrophoresis tank and the tank was filled with 1.5 M tris glycine buffer, pH 7.4. The samples were carefully loaded in the wells and the gels were run at a constant voltage of 120 V for 2 h. Ten  $\mu\text{l}$  of prestained molecular weight ladder (New England Biolabs, UK) and 5

$\mu$ l of western blotting ladder (Invitrogen, Paisley, UK) were also loaded as a reference marker for molecular weight of the proteins. The western blotting ladder consists of 9 recombinant proteins, each of which contains an IgG binding site. The IgG binding site binds to the secondary antibody used for detection of the target protein, allowing direct visualization of the standards on the western blot. Once the samples were separated and the tracking dye reached the bottom of the gel, the power supply was disconnected and the gel was transferred onto nitrocellulose membrane.

### 2.6.3 Transfer of proteins

The gel was transferred onto a nitrocellulose membrane by the wet method, which involved the soaking of a 0.2  $\mu$ m nitrocellulose membrane (BioRad, UK), Whatmann filter paper and sponges in transfer buffer (1.5 M tris glycine buffer, pH 7.4). The sandwich of gel and nitrocellulose membrane between the filter papers was closed and placed in the transfer tank which was filled with transfer buffer. Transfer took 1 h at 90 V in an ice bath.

### 2.6.4 Visualisation of transferred proteins

To ensure the proteins had successfully transferred to the nitrocellulose membrane, the blot was stained with Ponceau S red stain at room temperature with mild shaking at 40 rpm for 10 min. Ponceau red stain is a sodium salt of diazo dye and is used for reversible detection of transferred protein on a nitrocellulose membrane. The blot was then washed with distilled water, until protein bands were visible. Once the transfer of proteins was confirmed the blot was destained by repeated washes with distilled H<sub>2</sub>O. This blot was then probed with antibodies for the protein of interest.

## 2.6.5 Probing antibodies and detection of proteins

The nitrocellulose membrane was washed with distilled H<sub>2</sub>O and incubated with blocking buffered solution (1 M tris buffer saline with 0.1% tween 20 and 5% non-fat milk), which blocked all the non-specific binding sites of the proteins, for 1 h at room temperature. After 1 h, the blot was washed with washing buffer (1 M tris buffer, pH 7.4, 0.1% tween 20) (TBST) three times for 10 min each at room temperature and incubated with the relevant primary antibody (refer to dilutions of the primary antibody used in Table 2.4), overnight at 4 °C. Following incubation, the blot was washed with TBST five times for 10 min each at room temperature to remove the unbound antibody and incubated with a secondary antibody conjugated to horseradish peroxidase (1:10000 dilution) (*Table 2.4*) for 1 h at room temperature, before washing three times with TBST.

*Table 2.4 List of concentration and dilution of rabbit polyclonal primary antibodies (Abcam, UK) and secondary antibody used for probing nitrocellulose membrane blots.*

Antibody	Antibody dilution (Antibody diluted in 0.1 M TBST, pH 7.4)
CYP 3A4	1:3500
CYP 1B1	1:3000
CYP 2E1	1:3000
CYP 2D6	1:3000
BCRP (ABCG <sub>2</sub> )	1:2000
MDR-1 (ABCB <sub>1</sub> )	1:3000
β actin (loading control)	1:5000
Occludin	1:2000
Claudin-5	1:1000
Secondary Antibody (donkey polyclonal secondary antibody to rabbit IgG/ mouse IgG)	1:10000

The blot was then rinsed with distilled H<sub>2</sub>O and the proteins were detected using an ECL plus kit (GE Healthcare, UK) as per the manufacturer's instructions. The blot was incubated with ECL solution for 5 min and imaged in a gel doc XPS (Bio Rad, Town, UK) to visualise bands of proteins of interest by chemiluminescence.

## 2.7 Activity assay for drug metabolising enzymes (CYP3A4 and CYP2D6)

The functional activity of CYP3A4 and CYP2D6 in cell lines was assayed in 96-well plates by incubation with a substrate probe for the CYP of interest and measurement of the rate of formation of fluorescent metabolite. The probe used for the CYP3A4 enzyme was 7-benzyloxy-4-trifluoromethyl- coumarin (BFC) (BD Gentest©, Oxford, UK), which formed the fluorescent metabolite 7-hydroxy-4-trifluoromethylcoumarin (HFC) (BD Gentest©, Oxford, UK). The activity of CYP2D6 was determined using 3-[2-(N, N-diethyl-N-methylammonium) ethyl]-7-methoxy-4-methylcoumarin (AMMC) (BD Gentest©, Oxford, UK), which formed the fluorescent metabolite 3-[2-(N,N-diethyl-N-methylammonium) ethyl]-7-hydroxy-4-methylcoumarin (AHMC) (BD Gentest©, Oxford, UK). All substrates and metabolite were dissolved in DMSO to give a 10 mM stock and diluted 1 in 400 to ensure final solvent concentration in the reaction well did not exceed the threshold of 0.1 %. The co-factor 10 mM NADPH (stored -80 °C) was freshly prepared in 0.1 M PBS buffer (pH 7.4) and added to the flat bottom, transparent 96-well plate containing pre-warmed (37 °C) protein sample (varied according to the protocol below), substrate (varied according to the protocol below) and 0.1 M potassium phosphate buffer, pH 7.4 (see Appendix) to initiate the enzyme

reaction. The formation of HFC was measured at excitation wavelength of 410 nm and emission wavelength of 510 nm and the formation of AHMC was measured at excitation wavelength of 390 nm and emission wavelength of 460 nm in a Tecan GENios Pro® plate reader (Tecan, Theale, UK). Measurements were made at 37 °C every 30 s for 30 min with orbital shaking for 5 sec before each reading. The plates were read from the top, and gain was optimised on the first run and was set at 35 for all subsequent runs.

### 2.7.1 Protein linearity optimisation

The positive controls, overexpressed human recombinant CYP3A4 and CYP2D6 in bacosomes (Cypex, UK) were used at various concentrations ranging from 0 to 1 mg/ml to verify the optimal protein concentration to ensure the rate of enzyme activity was linear with respect to time. The following components were added to each well of a 96-well plate and left for 5-min in the plate reader to pre-warm to 37 °C: 125 µl of 50 mM of substrate (BFC or AMMC) at a final concentration of 25 mM, 25 µl CYP2D6 or CYP3A4 bacosome at a range of final concentrations between 0 to 1 mg/ml protein and 75 µl of 0.1 M potassium phosphate (pH 7.4) to make a final reaction volume of 250 µl. To initiate the reaction, 25 µl of 10 mM NADPH stock was added to each well to give a final concentration of 1 mM. Wells were measured for formation of the fluorescent metabolite (HFC or AHMC) as described in Section 2.6.

### 2.7.2 Substrate linearity optimisation

To determine the optimum substrate concentration to ensure the measured rate of enzyme activity was in the linear range, a range of BFC or AMMC concentrations were investigated

in bactosomes, using a previously optimised protein concentration 1 mg/ ml. In a 96-well plate, 125  $\mu$ l of substrate (BFC or AMMC) ranging in concentrations, between 0  $\mu$ M and 150  $\mu$ M, were incubated with 25  $\mu$ l of 1 mg/ml protein and 75  $\mu$ l of 0.1 M potassium phosphate (pH 7.4). 10 mM NADPH stock was added in each well to give a final concentration of 1 mM and to initiate the reaction. Samples were measured for formation of the fluorescent metabolite (HFC or AHMC) as mentioned previously in Section 2.6.

### 2.7.3 Enzyme kinetic study

In a 96-well plate, cells were seeded at a density of 5000 cells/ well before being incubated at 37 °C and 5 % CO<sub>2</sub> in a humidified incubator until exponential growth was well established. Once the cells were 80 % confluent (which was predicted by the growth curve of cells), the cells were washed with 100  $\mu$ l of 0.1 M potassium phosphate buffer (pH 7.4). 125  $\mu$ l of 50  $\mu$ M substrate (BFC/ AMMC), diluted in the appropriate culture medium, was added to the wells in triplicate giving final concentration of 25  $\mu$ M. 100  $\mu$ l of 0.1 M potassium phosphate buffer (pH 7.4) was added to each well giving a final reaction volume of 250  $\mu$ l. The plate was measured for fluorescent metabolite formation every 10 min for 120 min on Tecan GENios Pro® plate reader (Tecan, Theale, UK). The negative controls included a vehicle control, cells, media or buffer and 0.1 % DMSO, substrate blank (cells and media) and enzyme blank (substrate and media). All final reaction volumes were maintained at 250  $\mu$ L, and volume differences were made up using 0.1 M potassium phosphate buffer, pH 7.4.

#### 2.7.3.1 Enzyme kinetic study in mono-, co-, tri- and alvetex cultures.

The assessment of CYP activity in different cultures was assessed by replacing the growth medium with the substrate (BFC or AMMC) dissolved in the culture medium. The co-

cultures were washed with 0.1 M potassium phosphate buffer (pH 7.4) and 25  $\mu\text{M}$  substrate (BFC or AMMC), diluted in the appropriate culture medium, and 0.1 M NADPH was added to the wells in triplicate giving a final reaction volume of 200  $\mu\text{l}$ . The plate was measured for fluorescent metabolite formation every 10 min for 120 min on the Tecan GENios Pro® plate reader (Tecan, Theale, UK).

### 2.7.3.2 Standard curve for metabolites

A standard curve of the metabolites was prepared using standard concentrations of HFC or AHMC between 0 to 40  $\mu\text{M}$ , added to 0.1 mg/ mL cellular protein to a final well volume of 200  $\mu\text{L}$  in a 96-well plate. The plate was measured for metabolite fluorescence using the Tecan GENios Pro® plate reader (Tecan, Theale, UK). The relative fluorescent units (RFU) were plotted on a XY scatter plot against metabolite concentration graph and a line of best fit was fitted using linear regression.

### 2.7.3.3 Data analyses and interpretation

The fluorescence emission readings from the kinetic experiment were converted into rate of metabolite formation per min by dividing the slope of the linear line of best fit from the kinetic plot (Section 2.6.3.1). The rate of  $\Delta\text{RFU} / \text{min}$  was converted into pmol HFC or AHMC produced per min by dividing by the slope of the line of best fit obtained for the standard curve (Section 2.6.3.2) and finally this was normalised to 1mg/ml of protein dividing by the total cell number in the model being investigated to give the final rate of enzyme activity in pmol HFC or AHMC/ min/  $10^6$  cells.. The Michaelis-Menton plot of rate of enzyme activity verses substrate concentration was plotted using GraphPad Prism™ 6.05, and the  $V_{\text{max}}$  and  $K_{\text{m}}$  were estimated for recombinant CYP2D6 and CYP3A4 in bacosomes to ensure the kinetics assay for the positive control was producing values comparable to the

literature. Thereafter, all models were compared against this control using the optimal substrate concentration of 25  $\mu\text{M}$ .

## 2.8 Activity assay for efflux transporter (ABCB<sub>1</sub> and ABCG<sub>2</sub>)

The Multidrug Resistance Direct Dye Efflux Activity Kit (Merck Millipore, Oxford, UK) was used to measure the functional activity of ABCB<sub>1</sub> and ABCG<sub>2</sub> by assaying the ability of the cell to extrude fluorescent ABCB<sub>1</sub> and ABCG<sub>2</sub> substrate dyes, 3,3'-Diethyloxacarbocyanine Iodide [DiOC<sub>2</sub>(3)] solution and rhodamine 123 solution respectively. A non-fluorescent substrate vinblastine was used as a competitive inhibitor of efflux activity of ABCB<sub>1</sub> and ABCG<sub>2</sub> transporter and DMSO was included as a vehicle control.

The cell lines were only assayed for transporter activity when in the exponential phase of growth as predicted by the growth curve of cell lines, at the time point at which with maximal protein expression was observed and when the TEER reached the maximum value (Section 2.9.1). At this point, cells were extracted from the insert by scraping from the cell culture dishes and trypsinised from different mono-, co-, tri- or alvetex culture model. The transporter, activity measurements were carried out on the cell suspension of approximately  $2.5 \times 10^5$  cells. The cells were centrifuged at 200 x g for 5 min using a microcentrifuge (Sanyo, Leicester, UK) and the supernatant was discarded. The cell pellet was resuspended to a final concentration of  $1 \times 10^6$  cells/ml in 10  $\mu\text{g/ml}$  cold DiOC<sub>2</sub>(3) or 100  $\mu\text{g/ml}$  rhodamine 123 loading buffer. Cells loaded with DiOC<sub>2</sub>(3) or rhodamine 123 and were incubated for 15 min or 2 h respectively on ice. After the incubation period, the cells were centrifuged at 200 x g for 5 min and the supernatant was discarded. The cells were resuspended in 2.5 ml cold

efflux buffer (1X RPMI-1640 and 30 % BSA and 0.1 % gentamycin) and again centrifuged at 200 x g for 5 min. At this point, the resuspended cells were distributed into different tubes for each different treatment. These tubes were centrifuged at 200 x g for 5 min, the supernatant was discarded and the cell pellet was resuspended in the following media at 1 ml per test containing  $2.5 \times 10^5$  cells:

- A. 37 °C-Warmed Efflux Buffer containing DMSO
- B. 37 °C-Warmed Efflux Buffer containing vinblastine
- C. Ice-Cold Efflux Buffer
- D. 37 °C-Warmed Efflux Buffer (sample)

Tubes A, B and D were immediately transferred to a 37 °C incubator maintained at a steady oscillation of 60 rpm whereas tube C was kept on ice at all times. The tubes were incubated for 60 min and at the end of the incubation 5 ml of cold efflux buffer was added to each tube, before being placed on ice to terminate the reaction. The tubes were then centrifuged at 200 x g for 5 min in a refrigerated centrifuge at 4 °C and the supernatant was discarded. The cells were resuspended in 1 ml per test ( $2.5 \times 10^5$  cells) cold efflux buffer and centrifuged at 200 x g for 5 min at 4 °C (ALC PK120, Buckinghamshire, UK). The supernatant was discarded and the cells were resuspended in 250 µl of cold efflux buffer. Cell suspensions were transferred into the wells of a black walled 96-well plate, thereafter samples were measured on a Tecan GENios Pro® plate reader (Tecan, Theale, UK) at an excitation wavelength of 485 nm and an emission wavelength of 530 nm. The gain was set to 45 and the plates were read from the top to determine the fluorescent dye effluxed out of the cells in 60 min. The activity was calculated as % fluorescence relative to the control and plotted.

## 2.9 Co-culture on transwell for BBB model

The cells were co-cultured on 12 mm transwell with 8  $\mu\text{m}$  pore size, polycarbonate membrane insert in 48-wells plates (Figure 2.1) (Corning, UK).

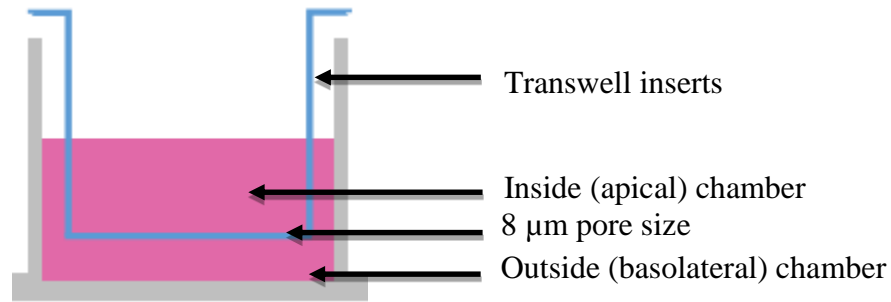


Figure 2.1 Diagrammatic representation of a transwell insert.

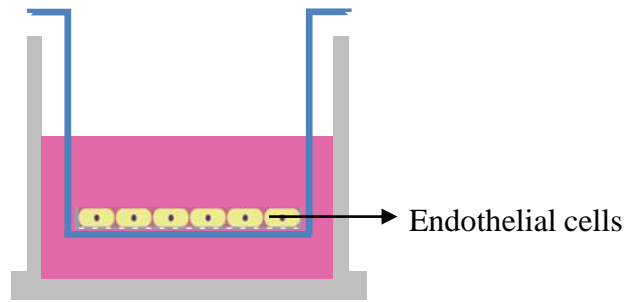
Prior to establishing the transwell models, short-term cultures were grown until day 6, to ensure cells were in the exponential phase of growth. The transwell cultures utilised the human microvascular endothelial cells (HMBEC, passage 2-7) human brain vascular pericytes (HBVP, passage 2-9) and human astrocytes (HA, passage 2-7). The short-term cultures from primary cells were used at lower passage number P2 to P15 as recommended by the supplier. The HBMEC cells were seeded at a density of 75,000 cells/ well in mono-culture and 50,000 cells/ well in co-culture and tri-culture. In co-culture, the HBVP were seeded at a density of 25000 cells/ well and the HA were seeded at a density of 25000 cells/ well. In tri-culture, the HBVP were seeded at a density of 12,500 cells/ well and the HA were seeded at a density of 12,500 cells/ well. The final cell number in each model was always the same and the ratios of the different cell components differed. The inserts were coated with 5  $\mu\text{g}$  of the extracellular matrix (ECM) glycoprotein fibronectin for 2 to 4 h and washed with HBSS, pH 7.4.

Co-cultures were defined as ‘in-contact’ if two cell populations grown together, on either side of an insert, as the pore sizes were large enough to allow physical contact between the

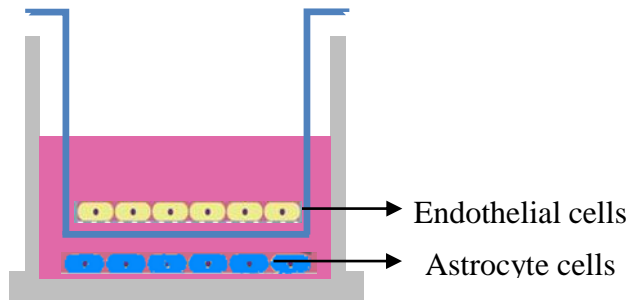
cell population. For seeding in-contact co-cultures i.e. two different cell cultures seeded on either side of the insert and the large pores of the membrane allowed physical contact between cells (refer to Figure 2.2), the inserts were inverted and seeded on the basolateral side. The inserts were incubated in an inverted position for 4 h to enable attachment of the cells, and then transferred to the culture plates and incubated for a further 48 h humidified incubator at 37 °C with 5 % CO<sub>2</sub>. After 48 h, the endothelial cells were seeded in the apical inner chamber of the insert. Co-cultures were defined as ‘out of contact’ if there was no direct physical contact, for example one cell population on the transwell insert and the other seeded on the bottom of the well in the basolateral chamber. For seeding out of contact co-cultures (refer to Figure 2.2), the cells were seeded on the bottom of the well and incubated in a humidified incubator at 37 °C with 5 % CO<sub>2</sub>. After 48 h, the endothelial cells were seeded on the apical side of the insert. All of the co-cultures were cultured in medium of respective cultures utilised, mixed at a ratio of 1:1.

For tri-cultures (refer to Figure 2.2), the cells were seeded on the basolateral side of the insert, with simultaneously seeding of cells in the bottom well, and both of them were incubated in a humidified incubator at 37 °C with 5 % CO<sub>2</sub>. After 48 h, the insert was placed in the well and the endothelial cells were seeded on the apical side of the insert. The tri-cultures were cultured in medium of respective cultures mixed in a ratio of 1:1:1. (refer to Table 2.1 for list of media). After 24 h the mono, co- and tri-cultures were measured for their trans endothelial electrical resistance (TEER) using the EVOM-2 (Merck Millipore, Oxford, UK) across five location on the insert for each of the models every day for 15 days (refer to Section 2.9). Each model was set-up in triplicate to assess intra-assay variability and every experiment was repeated three times to assess inter-assay variability. The different set up of transwell models is shown in Figure 2.2.

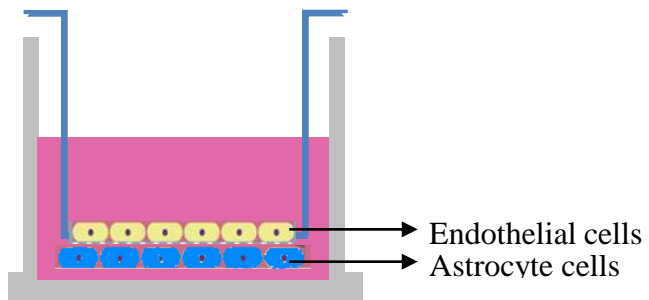
a) Monoculture of HBMEC cells



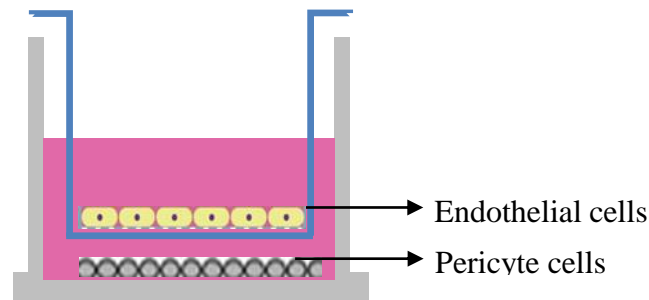
b) Co-cultures of HBMEC with HA (out of contact)



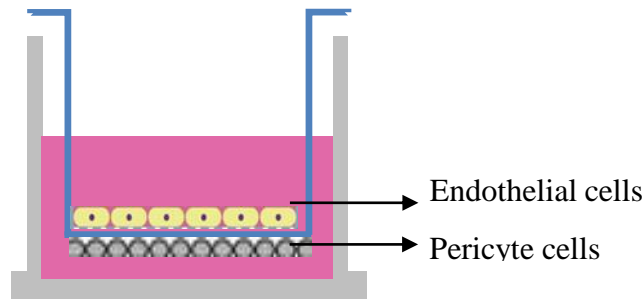
c) Co-cultures of HBMEC with HA (in contact)



d) Co-cultures of HBMEC with HBVP (out of contact)



e) Co-cultures of HBMEC with HBVP (in contact)



f) Tri-culture of HBMEC with HBVP (out of contact) and HA (in contact)

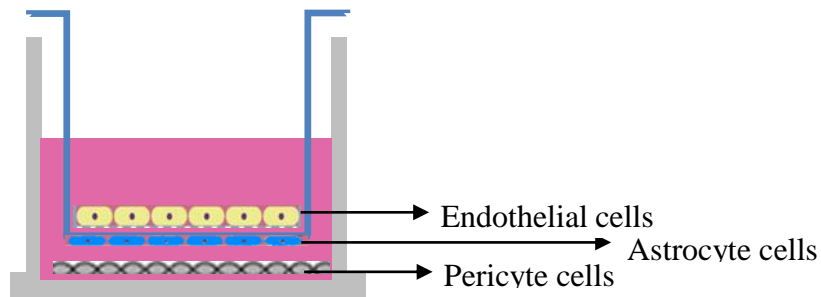


Figure 2.2 A scheme of the proposed *in vitro* BBB transwell models.

a) Monoculture of HBMEC cells b) Co-cultures of HBMEC with HA (out of contact) c) Co-cultures of HBMEC with HA (in contact) d) Co-cultures of HBMEC with HBVP (out of contact) e) Co-cultures of HBMEC with HBVP (in contact) f) Tri-culture of HBMEC with HBVP (out of contact) and HA (in contact).

### 2.9.1 Alvetex perfusion BBB model

The Alvetex perfusion model (Reinnervate, Durham, UK) comprises of a perfused plate with a peristaltic pump to maintain a shear flow of media on the cells growing in the three dimensional (3D) scaffold. The cells were seeded on a three-dimensional transwell scaffold, precoated in fibronectin, as previously described in Section 2.8; (Figure 2.2c and f), and then

transferred into a perfusion plate. The plate was connected to inlet tubing (diameter 16 mm) and outlet tubing (diameter 25 mm) which were connected to a reservoir of media containing mixtures of culture media in equal proportion. Using a peristaltic pump (Watson-Marlow, Cornwall, UK), the pressure of the shear flow was set to 20 dyne/ cm<sup>2</sup> and the flow was maintained for a period of 15 days. The shear flow was selected on the basis of literature review. The medium in the reservoir was changed every 5 days. The TEER was measured every day for a period 15 days and on the 15<sup>th</sup> day the cells from the transwell were retrieved by trypsinisation (see Section 2.3.2.2) and lysed for western blotting. The cell lysates were analysed for expression of the tight junction proteins occludin and claudin-5, efflux transporters ABCB<sub>1</sub> and ABCG<sub>2</sub> and drug metabolising enzymes CYP3A4 and CYP2D6.

### 2.9.2 Electric Cell-substrate Impedance Sensing (ECIS) for BBB model

ECIS® is a real-time, label-free, impedance-based method to study morphological changes, cell locomotion, and other behaviours directed by the cell cytoskeleton of cells grown in tissue culture (Applied Biophysics, Troy, USA). . The blood brain barrier models were set up using 8W10E+ arrays. Each well in the array was washed with 200 µl Hanks buffered salt solution pH 7.4 (HBSS) twice and incubated with 200 µl of 10 mM L-cysteine for 10 min at room temperature. The wells were washed with 200 µl HBSS and coated with 5 µg/ ml fibronectin and incubated for an hour at 37 °C. After incubation, the wells were washed with HBSS twice and the cells (endothelial cells, astrocytes and pericytes) were seeded at a density 25,000 cells/well. Cells grown up to 80% confluency in T75 flasks were passaged to seed for the ECIS. The cells were trypsinised and seeded in different culture combinations as shown in Table 2.5. The seeding density of endothelial cells in mono-culture was 75,000 cells/ well

and in the co- and tri- cultures were 50,000 cells/ well. The seeding density of astrocytes and pericytes in co-cultures was 25,000 cells/ well and in tri-cultures was 12,500 cells/ well. The ECIS machine measured the real-time changes in TEER over a period of 100 h.

*Table 2.5 The layout of the chip in the ECIS plate. E: endothelial cells, A: astrocytes, P: pericytes and ECM: extra cellular matrix.*

With ECM: fibronectin	
E	E+ A+ P
E	E+ A+ P
E + A	E+ P
E+ A	Control

### 2.9.3 Cellzscope for BBB model

Cellzscope (nanoAnalytics, Münster, Germany) measures the impedance of the co-cultures across the permeable inserts by means of electrical resistance measurements, complemented by recording the electric capacitance  $C_{cl}$ . The transwell models for Cellzscope were set up as described in Section 2.8. The transwell inserts were then moved to the 24 well array of the Cellzscope and real-time TEER readings were taken for 100 h. At the end of this time, the cells were removed from the insert, lysed using RIPA buffer and stored at -20 °C for further analysis.

## 2.10 Testing integrity of designed co-culture models

### 2.10.1 Measurement of TEER

The Millicell ERS-2 (Electrical Resistance System) is a meter and electrode system designed to reliably measure trans endothelial electrical resistance (TEER) of endothelial cells in culture. The electrode was sterilised with 70 % ethanol and air dried in the laminar hood for 15 min. The electrode was then dipped in each well, with the shorter end on the apical side of the insert and the longer end touching the base of the well. The electrode was held at 90° to the cell culture plate until the TEER value on the meter stabilised. This was repeated five times in each well to find an accurate TEER value. An increase in TEER, detected with the electronic circuit of the Millicell ERS-2 meter and its electrode, is an indication of cell monolayer health and confluence. The values obtained from the Millicell ERS-2 were used to calculate the resistance of the unit area.

$$\text{Resistance} = \text{Resistance } (\Omega) \times \text{Effective Membrane Area } (\text{cm}^2)$$

### 2.10.2 Permeability of FITC dextran

The mono-, co- and tri-culture models were set up and permeability was assessed using 1 mg/ ml FITC-dextran (mol wt. 10,000) prepared in media. The media from the apical side of the transwell insert was removed and media containing FITC-dextran was introduced in the culture set up (Figure 2.3).

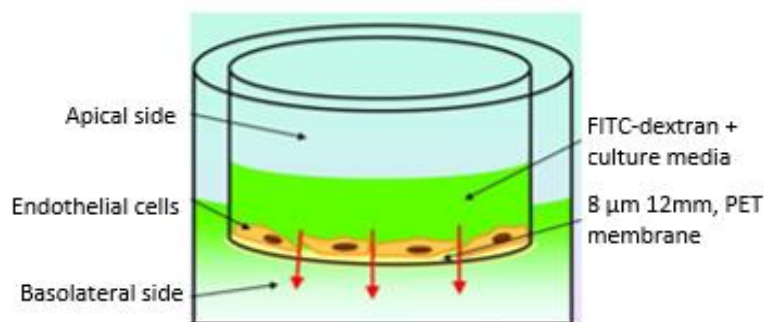


Figure 2.3 Diagrammatic representation of transwell insert used for permeability assay.

The fluorescent tagged dextran was seeded on apical side and the media was samples on the basolateral side to measure the Papp of the model.

The co-cultures were incubated in standard tissue culture conditions and at different time intervals (1 h, 2 h, 3 h,) the media from the basolateral side of the transwell insert was sampled. The fluorescence of the sampled media was read at excitation wavelength 492 nm and emission wavelength 518 nm on a Tecan GENios Pro® plate reader with the gain set at 55 (Tecan, Theale, UK). The apparent permeability of each model was calculated using the formula (Borges-Walmsley *et al.*, 2003)

$$P_{app} = \frac{1}{A \times C_0} \times \frac{dQ}{dt}$$

where, A = surface area of the polycarbonate membrane (cm<sup>2</sup>)  
 C<sub>0</sub> = concentration of the FITC-dextran on the apical side (μg/ml)  
 dQ/dt = the amount of sodium fluorescein passing across the cell layer in a defined time period (1 h, 2 h, 3 h)

### 2.10.3 Permeability of nanoparticles (NPs) across the BBB models

Various *in vitro* BBB models were tested for barrier function and permeability by addition of a short DNA oligonucleotide glioma selective aptamer, (prepared in house by C. L. Lawrence, L. Shaw and J.E. Alder) or nanoparticles (NPs) synthesised in house by Prof Kamalinder Singh and Dr Ka-Wai Wan. The lipid NPs were loaded with docetaxel, curcumin

or asiatic acid. The docetaxel loaded NPs were also tagged with rhodamine123 and transferrin ligand.

### 2.10.3.1 Toxicity screening

Prior to testing the paracellular permeability of aptamers and NPs across the tri-culture BBB model, the potential effect on cell proliferation and viability of the aptamer and NPs was determined by measuring the viability of endothelial cell lines following incubation with different concentration of aptamers, NPs and Evans Blue dye (control) all diluted in media using the CellTiter 96® AQueous One Solution Cell Proliferation Assay 3-(4,5-Dimethylthiazol-2-yl)-5-(3-Carboxymethoxyphenyl)-2-(4-sulfophenyl)-2H-tetrazolium, inner salt assay (MTS assay).

Table 2.6 List of NPs, aptamer and Evans blue concentration used for toxicity screening.

Molecules	Concentration of drug loaded in NP or aptamer		
Docetaxel loaded lipid nanoparticle with ligand transferrin	3.3 µg/ml	0.33 µg/ml	0.033 µg/ml
Docetaxel loaded lipid nanoparticle	3.3 µg/ml	0.33 µg/ml	0.033 µg/ml
Curcumin loaded lipid nanoparticle	2.87 µg/ml	0.287 µg/ml	0.0287 µg/ml
Empty lipid nanoparticle	1.2 µg/ml	0.12 µg/ml	0.012 µg/ml
Asiatic acid loaded lipid nanoparticle	1.2 µg/ml	0.12 µg/ml	0.012 µg/ml
SA43 Aptamer	100 nM	10 nM	1 nM
Evans Blue	33.3 µg/ml	3.33 µg/ml	0.333 µg/ml

The cell lines were trypsinised and seeded in 96-well microtitre plates at a density of 20,000 cells/ well. The aptamer and NPs were prepared at varying concentrations and added to the cells as detailed in Table 2.6. Cells were incubated at 37 °C, 5 % CO<sub>2</sub> in a humidified incubator for 5 days, with an MTS assay performed in triplicate on day 0, 2, 3 and 5 to determine the anti-proliferative effects of the aptamer and NPs. On the day of the assay the

MTS was thawed on ice and 40  $\mu$ l of MTS assay was added to the required wells, and the plate was incubated at 37 °C, 5 % CO<sub>2</sub> in a humidified incubator for 4 h. The plate was read for the absorbance at 492 nm wavelength on a Tecan GENios Pro® plate reader (Tecan, Theale, UK). The cell survival was calculated using the formula;

$$\text{Cell survival (\%)} = \frac{\text{Absorbance of treated cells} \times 100}{\text{Absorbance of vehicle control group (untreated cells + solvent)}}$$

### 2.10.3.2 Cellular uptake study

Cellular uptake was assessed in tri culture model previously described in Section 2.9. The inserts were incubated and checked for their TEER values using EVOM each day, until they reached a peak and plateaued. On day 6, when the TEER values peaked, tri-culture barrier was incubated with Evans Blue Dye (EBD) to determine if the barrier formed is intact. The aptamer, NPs and control was used aptamer or NPs were introduced to the well and time dependent TEER measurements were taken. The TEER values were measured at 0.25 h, 0.5 h, 1 h, 1.5 h, 2 h, 4 h, 6 h, 8 h and 24 h. The concentration of NPs used for the cellular uptake studies were selected on the basis of their IC<sub>50</sub> values calculated from the MTS assay (Table 2.7). The concentration of aptamer was determined by studying the minimum detection limit of aptamer on the glioma cells (unpublished data) and concentration of the control Evans Blue Dye was adapted from book (Yuan and Rigor, 2011).

Table 2.7 List of NPs and their concentrations used for the cellular uptake studies.

Nanoparticles	Concentration
Docetaxel loaded lipid nanoparticle with ligand transferrin tagged with rhodamine	0.33 µg/ml
Docetaxel loaded lipid nanoparticle tagged with rhodamine	0.33 µg/ml
Curcumin loaded lipid nanoparticle	0.287 µg/ml
Empty lipid nanoparticle	0.12 µg/ml
Asiatic acid loaded lipid nanoparticle	0.12 µg/ml
SA43 Aptamer	10 nM
Evans Blue	3.33 µg/ml

### 2.10.3.3 Co-localisation study

Endothelial cells were seeded on coverslips at a density of 20,000 cells/ coverslip. Following attachment of the cells to the coverslip, the media in the wells was changed. The aptamer and NPs at the concentration mentioned in Table 2.7 were dissolved in the culture medium and added the mono-culture. After 24 h, the endothelial cells were fixed as described in section 2.3.1 and immunostained as described in section 2.3.2.

## 2.11 Brain tumour barrier

The tri-culture model was set up, as described in Section 2.9, and short term cultures derived from patient biopsies of glioma, BTNW914 and BTNW370 were introduced to the barrier. The short term cultures were grown separately to spheroids by culturing on agar plates as described in Section 2.2.1.2. The spheroids were introduced in the basolateral side of the insert above the pericyte monolayer (Figure 2.4) of the insert.

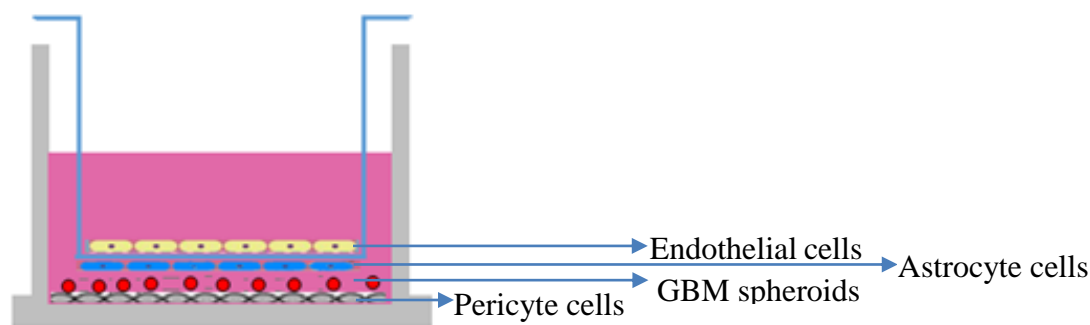


Figure 2.4 Diagrammatic representation of brain tumour barrier

A Tri-culture of HBMEC with HBVP (out of contact) and HA (in contact) and GBM spheroids laid over the pericytes. B Tri-culture of HBMEC with HBVP (out of contact) and HA (in contact) and GBM spheroids laid over the endothelial cells.

### 2.11.1 TEER measurement

The brain tumour model was studied for its TEER measurement for 10 days. The media was changed every three days of the BTB model.

### 2.11.2 Permeability of NPs tested in BTB model.

The NPs were also incubated in tri-culture GBM models with and without inhibitor for efflux transporters. Two  $\mu\text{M}$  of vinblastine was used as the efflux transporter inhibitor. After 0.5 h, 1 h, 1.5 h, 2 h, 2.5 h and 3 h, at each time point the fluorescence of the spheroids were washed with 0.1 M PBS, pH 7.4 three times. The spheroids were sampled in 96 well plate and read under the plate reader for their fluorescence at excitation wavelength of 511 nm and emission wavelength of 534 nm. The gain was set to 45 and the plates were read from the top to determine the fluorescence of the NPs. The activity was calculated as % fluorescence relative to the stock concentration of the NPs and then plotted. The following concentrations were used as described in Table 2.8.

Table 2.8 Concentration of NPs used in the BTB model permeability studies.

Nanoparticles	Concentration
Docetaxel loaded lipid nanoparticle with ligand transferrin tagged with rhodamine	0.33 µg/ml
Docetaxel loaded lipid nanoparticle tagged with rhodamine	0.33 µg/ml
Curcumin loaded lipid nanoparticle	0.287 µg/ml

## 2.12 Statistical Analyses

All data were expressed as mean values  $\pm$  standard deviation (mean  $\pm$  SD) with  $n = 3$  of triplicate experiments. Statistical analysis was carried out using the one way ANOVA with Bonferroni post-test analyses was performed. Probability values of  $p < 0.05$  were considered statistically significant.

# CHAPTER 3

# **3. Characterisation of continuous and primary cell lines.**

## **3.1 Introduction**

Cell culture is a readily accessible tool for scientific research which includes testing new drug therapies and studying mechanism of diseases (Capes-Davis *et al.*, 2010). Ensuring the cell lines used in experiments have a defined origin and are routinely screened for possible contamination is an essential criteria for researchers (Higgins *et al.*, 2010). More recently, in some publications, the generation of erroneous and misleading results has been identified and was found to be due to cellular cross-contamination, misidentified cell lines, and the use of cultures at high-passage levels (Healey, 2010; Kaplan and Hukku, 1998), hence, initial characterisation of the cultures was a prerequisite for this research.

The aim of this chapter was to characterise the cell lines for origin and cell type (both human and glial) and to determine the exponential growth phase prior to use in downstream experiments. The cell lines comprised of human glioma 1321N1 and U87MG and human glial SVGp12, patient derived short term glioma cultures, including BTNW914 and BTNW370 and short-term cultures derived from primary tissue, including human brain microvascular endothelial cell lines (HBMEC), human brain vascular pericytes (HBVP) and human cerebral astrocytes (HA).

## 3.2 Results

### 3.2.1 Growth kinetics and morphology of continuous cell lines

Growth curves were established to study the kinetics of cell line growth, namely to determine the duration of the initial lag phase, to estimate population doubling time during exponential growth, and finally the point of plateau phase where the cells became confluent and the growth rate slowed down.

The glioma cell lines U87MG (Figure 3.1A) and 1321N1 (Figure 3.1B) showed exponential growth from day 3 to day 6 and from day 2 to day 8, respectively. The non-cancerous cell line SVGp12 (Figure 3.1C) and hCMEC/D3 (Figure 3.1D) showed an exponential growth phase from day 2 to day 6 and from day 2 to day 5. When comparing the growth characteristics of all cells, U87MG had a doubling time of 30.2 h whereas 1321N1 had the longest exponential phase and the highest cell count at the end of the experiment on day 10 and a doubling time of 24.6 h. SVGp12 grew the slowest with a doubling time of 35.7 h, and had the smallest mean cell count at day 10. hCMEC/D3 grew the fastest with a doubling time of 20.4 h, and had the smallest mean cell count at day 10

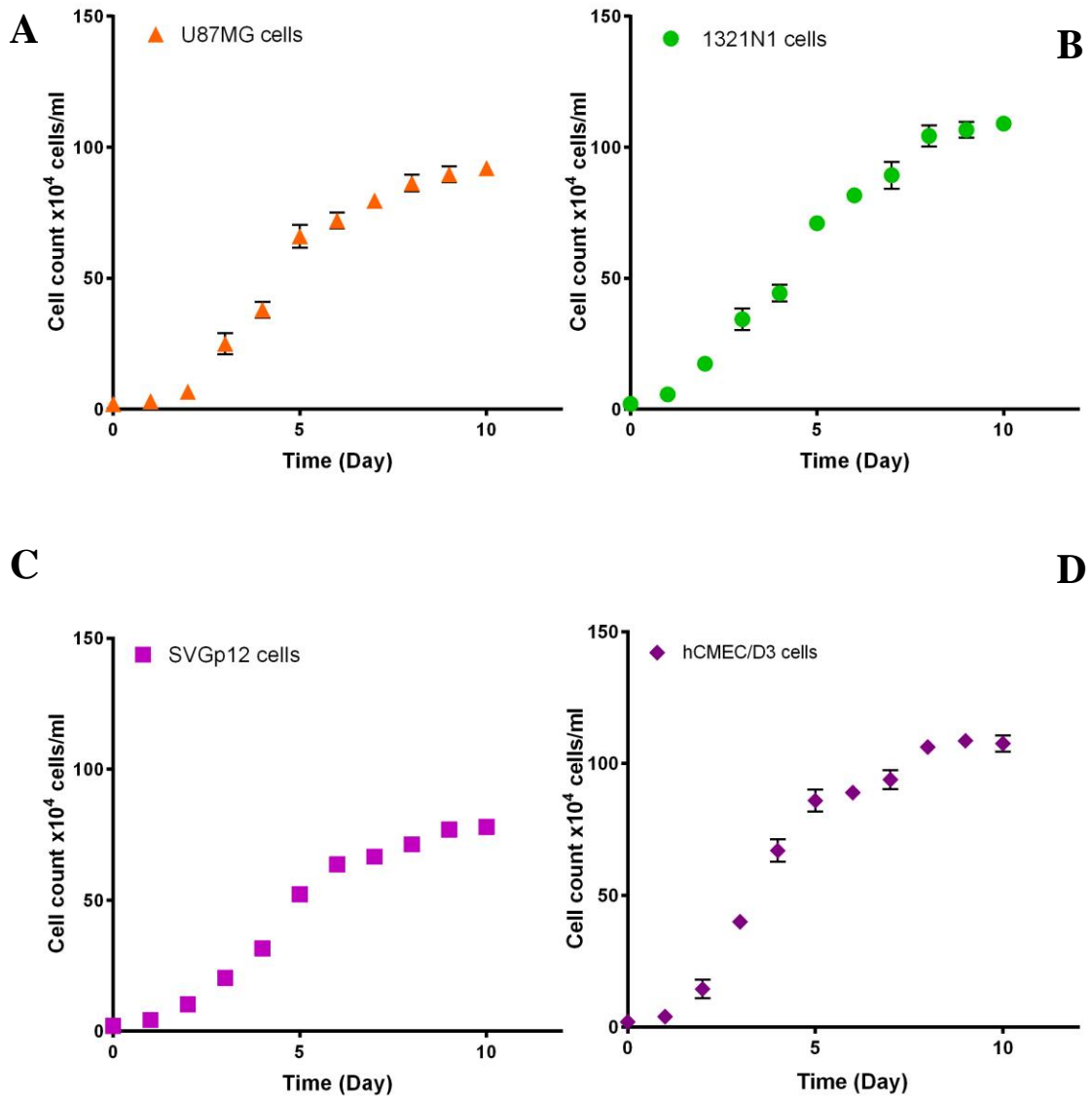


Figure 3.1 Growth analysis of human cell lines.

**A.** U87MG, grade IV glioma cell line. **B.** 1321N1, grade II glioma cell line. **C.** SVGp12, non-cancerous foetal glial cell line. **D.** hCMEC/D3, endothelial cell line. The data points are means of three replicates ( $n=3$ ) and the error bars represent  $\pm$  standard deviation ( $\pm$ SD) of three inter-experimental repeats. The exponential phase is reached on the day 3 for the U87MG, day 2 for the 1321N1, day 2 for the SVGp12 and on day 2 for hCMEC/D3 cell lines. The plateau phase is reached from the day 6 for the U87MG cell line, day 8 for the 1321N1 cell line, day 6 for SVGp12 and on day 5 for hCMEC/D3 cell lines.

The morphology of U87MG, 1321N1 and SVGp12 was observed under a light microscope during the study of growth patterns at 10 X magnification. As seen in Figure 3.1, on day 3 the adherent cell lines showed elongated cell processes (Figure 3.2A).

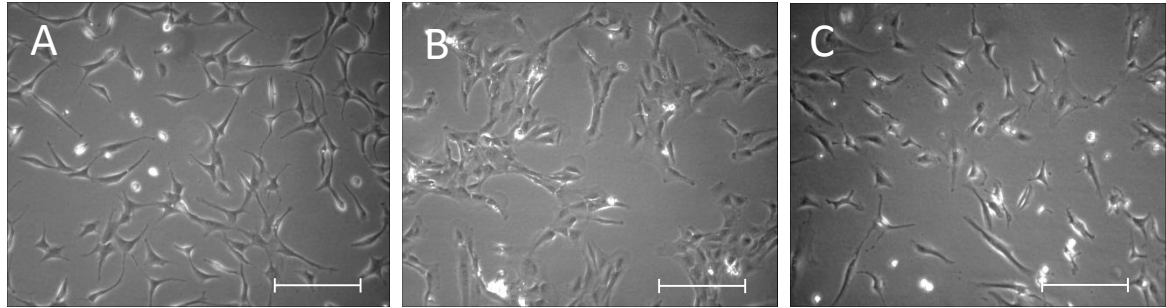


Figure 3.2 Light microscopy images of cells on day 3 of growth.

**A** U87MG, grade IV glioblastoma cell line. **B** 1321N1, grade II glioma cell line. **C** SVGp12, foetal glial astrocyte cell line. The scale bar represents 20  $\mu\text{m}$ .

### 3.2.2 Growth kinetics and morphology of short-term cultures

Growth characteristics of short-term cultures derived from primary tissue (HBMEC, HBVP and HA) were studied in cells with a passage number between P2 to P10. The HBMEC showed exponential growth between day 3 and day 6 (Figure 3.3A) and had plateaued by day 9. The HBVP showed an exponential growth phase from day 2 to day 6 (Figure 3.3B). The HA showed exponential growth between day 3 to day 7 (Figure 3.3C). A comparison of all short-term cultures together (Figure 3.3D) showed that endothelial cells and astrocytes had similar growth kinetics with a doubling time of 51.7 h and 52.3 h respectively, whereas pericytes showed the fastest growth and highest cell number at day 10, with a doubling time of 24.6 h. A growth kinetic experiment was conducted for the BTNW short-term glioma cultures, however it was not possible to continue the experiment as growth was so slow, and slowed down further with increase in passage number this estimated to be a doubling time of 9 days.

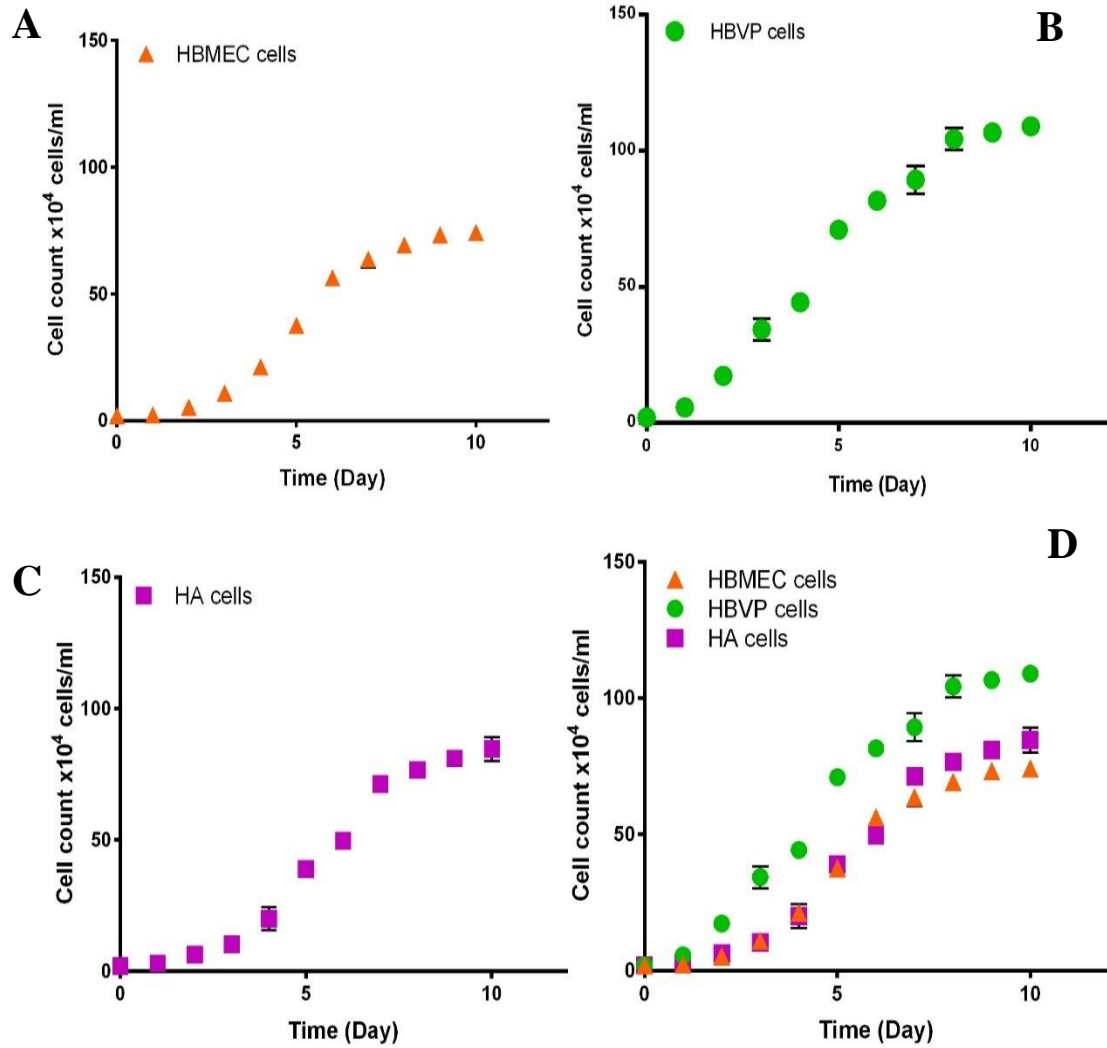


Figure 3.3 Growth analysis of primary cultures.

**A.** HBMEC, human brain microvascular endothelial cells. **B.** HBVP, human brain vascular pericytes. **C.** HA, Human astrocyte. **D.** Merge of growth curves of all the human primary cultures. The exponential phase is reached on the day 3 for the HBMEC, day 2 for the HBVP, and on the day 3 for the HA cell lines while the plateau phase is reached from the day 7 for the HBMEC cell line, day 7 for the HBVP cell line and day 7 for HA cell lines. The data points are means of three replicates ( $n=3$ ) and the error bars represent  $\pm$  standard deviation ( $\pm$ SD) of three inter experimental repeats.

As seen in Figure 3.3A, on day 5 the endothelial cells HBMEC showed closely opposed cobblestone or spindle shaped morphology. The astrocytes HA showed fibroblastic morphology with many elongated processes arising from each cell (Figure 3.4B). The pericytes HBVP were observed as thin cells with elongated processes rising from each cell (Figure 3.4C).

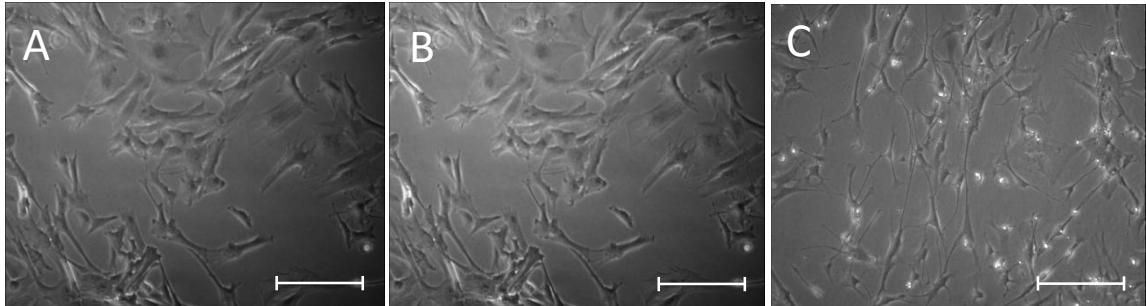


Figure 3.4 Light microscopy images of cells on day 5 of the exponential phase of growth.

**A.** Human brain microvascular endothelial cells (HBMEC). **B.** Human astrocyte (HA) **C.** Human brain vascular pericyte cells (HBVP). The scale bar represents 50  $\mu\text{m}$ .

### 3.2.3 Characterisation by immunocytochemistry

#### 3.2.3.1 Characterisation of cell lines

The cell lines, U87MG, 1321N1 and SVGp12 were characterised using a panel of antibodies raised against human leukocyte antigen (HLA) and glial fibrillary acidic protein (GFAP) to confirm expression of antigens specific for cells of glial and human origin. All cell lines expressed GFAP and HLA (Figure 3.5), thus characterising the cells as glial and human origin. An isotype control was used as a negative control since it has no specificity for a target cell yet retains all the non-specific characteristics of the antibodies (Howat *et al.*, 2014). GFAP staining was found to be located in the cytoplasm as seen in Figure 3.5 (A, E & I). HLA staining was found to be cytoplasmic Figure 3.5 (B, F & J).

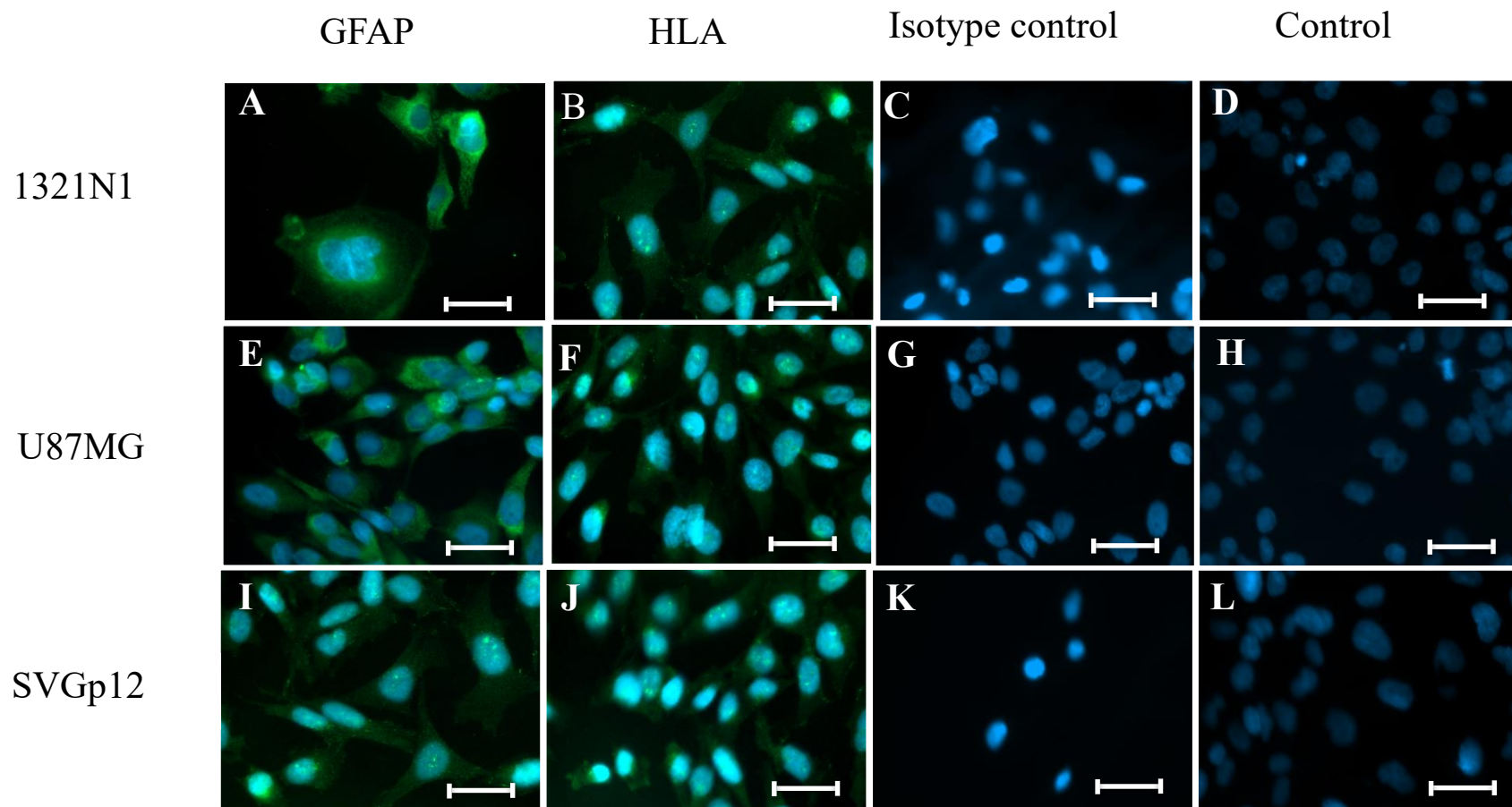


Figure 3.5 Fluorescence staining of cell lines for GFAP and HLA.

**A-D.** 1321N1 cell lines, **E-H.** U87MG cell line and **I-L.** SVGp12 cell line. All cell lines expressed GFAP (green) (A, E, and I) and HLA (green) (B, F and J) The isotype control was a rabbit IgG primary antibody (C, H, and L) and a no antibody control was also used (D, H and L). All cells were counterstained with the nuclear fluorescent dye DAPI (blue). The scale bar represents 50  $\mu\text{m}$ .

### 3.2.3.2 Characterisation of short term cultures

In this study the heterogeneous short term cultures derived from glioma patients were characterised to determine the predominant cell population. The patient derived short term cultures were defined as low passage between P2 to P4, mid-passage between P5 to P8 and high passage between P9 to P13. GFAP was used as a marker for glial cells, CD44 as a marker for endothelial cells and epithelial membrane antigen (EMA) as a marker for meningioma. EMA was included as a negative control for the purpose of confirming the diagnosis of the BTNW cultures as being glioma and not meningioma. All characterisation was done using a biotinylated secondary antibody detected by DAB staining and all cells were counter stained by haematoxylin and eosin.

The BTNW914 culture at passage 3 showed a heterogeneous cell population and expressed both GFAP and CD44, but not EMA (Figure 3.6 A-E). At mid passage 7, the cells showed dark brown staining for GFAP, indicating a high level of expression and faint brown stain for CD44, whereas no staining was observed for EMA (Figure 3.6 F-J). At passage 12, the cells showed faint staining for GFAP and no staining for both CD44 and EMA (Figure 3.6 K-O). The cells did not show any staining in the isotype or no antibody control at any of the passages.

The BTNW370 at passage 3 showed expression of GFAP, very faint staining for CD44, but no staining for EMA indicating that the cells show characteristics of glial cells and endothelial cell marker but no expression for meningioma cell marker (Figure 3.7 A-E). At passage 7 the cells showed dark brown staining for GFAP and no staining for CD44 or EMA (Figure 3.7 F-J). The BTNW370 short term culture showed a loss of expression endothelial

cell marker from low passage 3 to mid passage 7. At passage 12, the cells showed faint staining for GFAP and no staining for both CD44 and EMA (Figure 3.7 K-O).

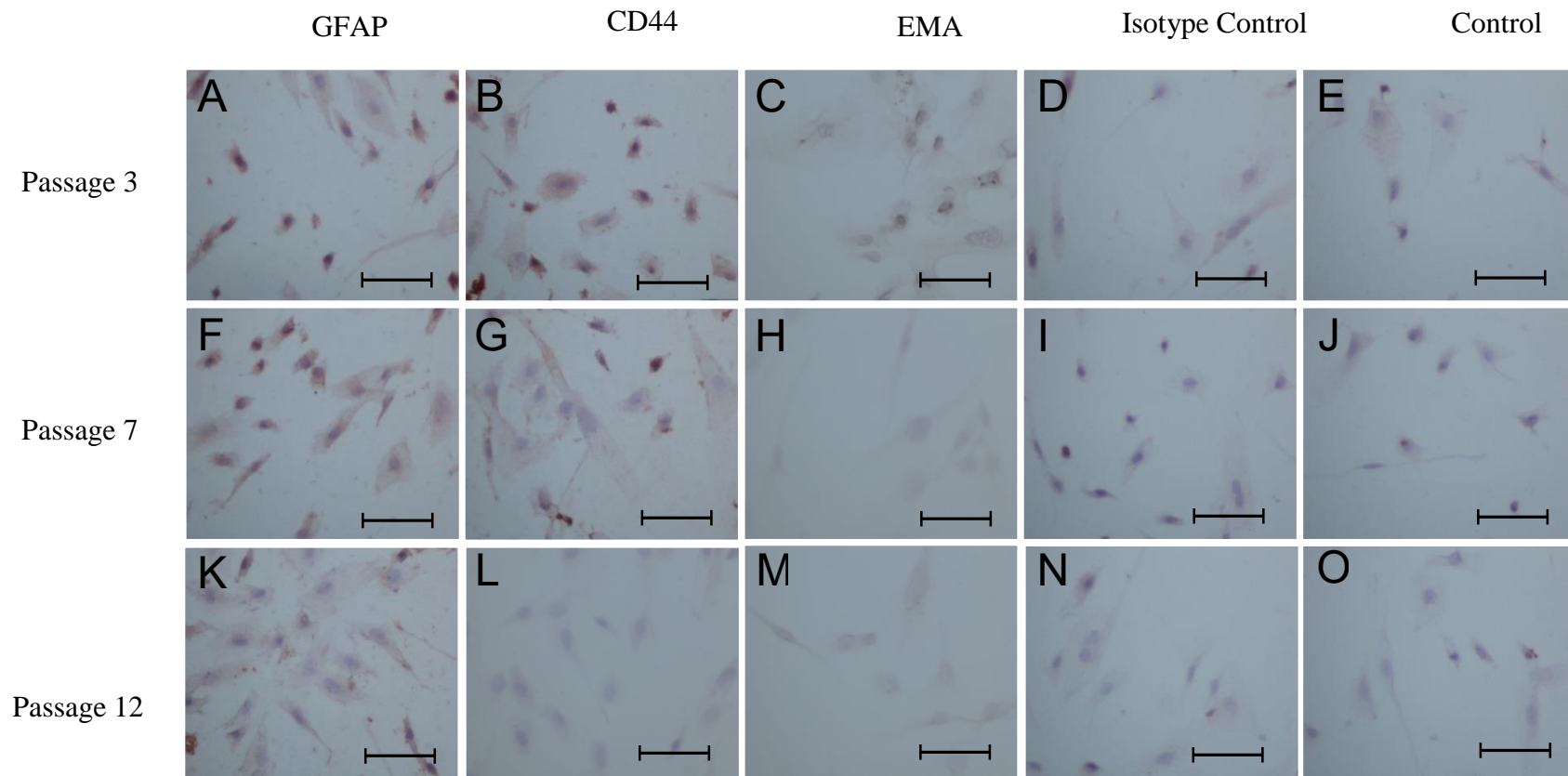


Figure 3.6 DAB staining of patient derived short term culture BTNW914.

Cells stained with GFAP, EMA and CD44 at early passage (P3) (A-E), mid passage (P7) (F to J) and late passage number (P12) (K to O). The isotype control was a rabbit IgG primary antibody (D, I, and N) and a no antibody control stain (E, J and O). All cells were counterstained with haematoxylin eosin. The expression of GFAP (A, F & K) and CD44 (B, G & L) decreases with increase in passage number the highest expression was seen at low passage (A & B respectively). The cells did not show expression of EMA (C, H & M). The scale bar represents 50  $\mu$ m.

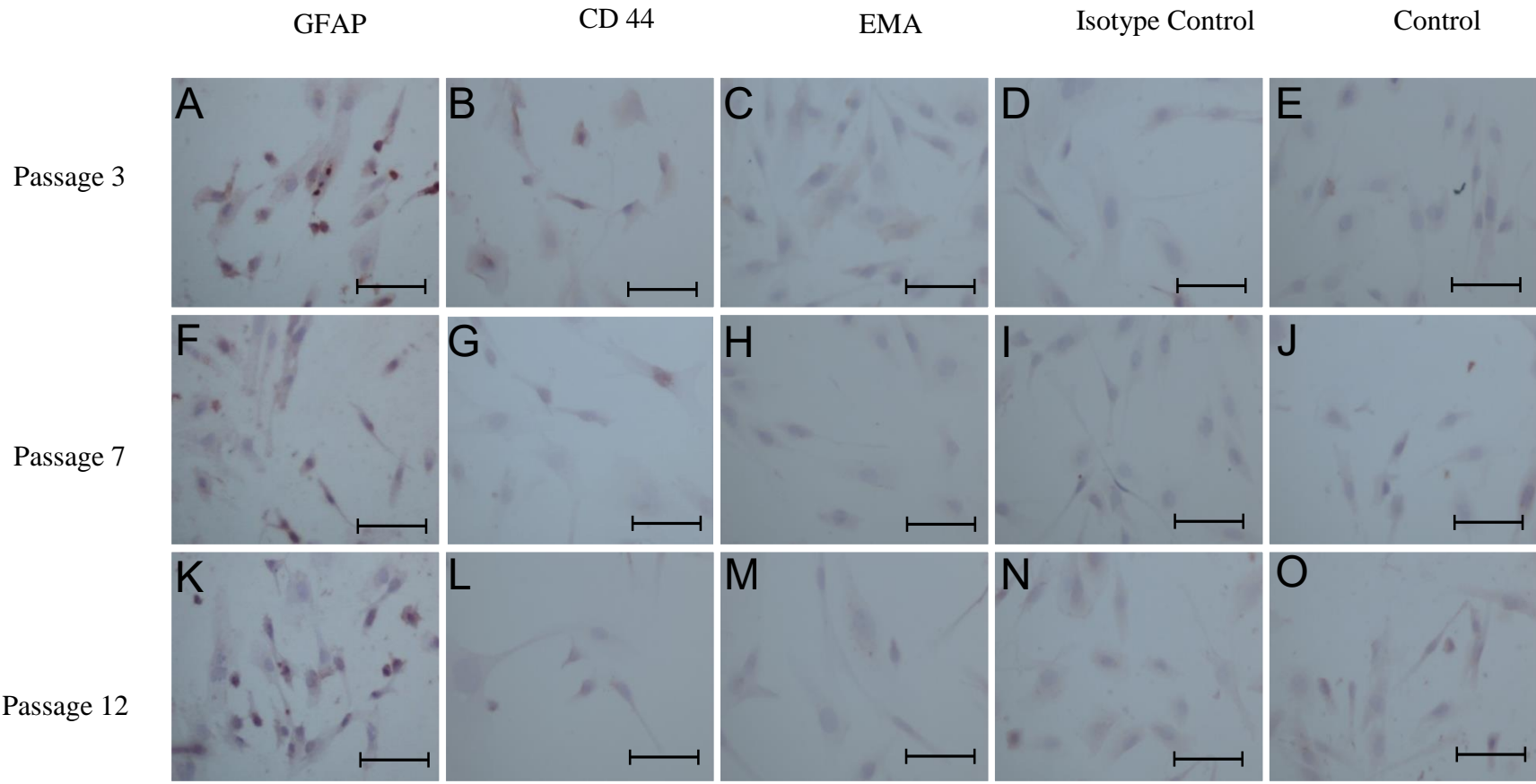


Figure 3.7 DAB staining of patient derived short term culture BTNW370.

Cells stained with GFAP, EMA and CD44 at early passage (P3) (A-E), mid passage (P7) (F to J) and late passage number (P12) (K to O). The isotype control was a rabbit IgG primary antibody (D, I, and N) and a no antibody control stain (E, J and O). All cells were counterstained with haematoxylin eosin. The expression of GFAP (A, F & K) decreases with increase in passage number the highest expression was seen at low passage (A). The cells did not show expression of CD44 (B, G & L) EMA (C, H & M). The scale bar represents 50 µm.

### 3.3 Discussion and conclusion

The study of the growth pattern of cell lines prior to performing experiments is essential to determine various growth characteristics which contribute to the experimental planning. The growth curve provides information regarding the cell number for seeding and the time at which lag phase is reached. Typical cell growth shows three phases: 1) a lag phase, which denotes time required by the cell population to recover from subculture, attach and multiply; 2) the log phase which represents the phase in which the cell numbers begin to proliferate exponentially, and 3) a second lag phase or the plateau phase in which the cell culture becomes confluent and the growth rate slows down or stops and the curve looks like a plateau when plotted on a graph (Mather and Roberts, 1998).

The early exponential growth phase of cell was therefore selected as the optimal time point for all experiments to be conducted since protein expression and function is a key end point required to meet the aims of this thesis, as protein expression and function needs be measured in healthy dividing cells (Schauble *et al.*, 2012). Various factors such as nutrient level, attachment factors and mitogens can influence the exponential phase of growth of cells. The cells when in the plateau lag phase undergo senescence which is biological aging; a phase between cell maturity and cell death (Vulic and Kolter, 2002). The plateau phase changes the cellular, molecular structure and metabolism phenotype, therefore considering drug metabolising enzyme, transporter and tight junction protein expression and function is essential to this study, investigations in the plateau phase needed to be avoided. For all the cell lines investigated, the lag phase was complete by day 3 when seeded at  $2 \times 10^4$  cells/ ml on day 0, therefore to ensure cells were in the early exponential growth phase for experiments, they were used after 3 days, or alternatively for culture set ups that required

longer incubations times (Section 5.2), a lower seeding density was used at day 0, again to ensure experiments were conducted during the exponential phase of growth. The doubling times of commercially available cell lines were compared to the literature, and where available, were found to be in agreement with published values. U87MG and 1321N1 have previously been reported to have a doubling time of 34 h and 22 h respectively, which was in close agreement the values presented here of 30.2 h and 24.6 h (Daeke *et al.*, 2000; Kin *et al.*, 2012). For the short-term cultures, doubling times were slower compared to the immortalised cell lines, which was expected as the cell lines carry a mutation for indefinite growth, thereby avoiding senescence. For HBMEC, values were reported in the literature between 48 and 72 h, and for HA 48.9 h, which was in agreement of the values determined in this study of 51.7 h and 52.3 h. No doubling times were available for comparison for SVGp12 and pericytes.

Confirmation of cell line origin and its characteristics is imperative before using cell lines in experiments for reliability in reporting experimental results to other researchers (Lucey *et al.*, 2009). Lately, there has been an emphasis on the importance of confirming the origin and type of cultured cells used for research. Macleod *et al.*, (1999) described that 45 of 252 human cell lines (18 %) supplied by 27 of 93 originators (29 %) were contaminated with different cell types due improper culturing practice (MacLeod *et al.*, 1999; Rojas, 2011). The glial fibrillary acidic protein (GFAP), is a protein expressed by the astrocytes and is involved in the maintenance of structure and functions of the cytoskeleton (Gomes *et al.*, 1999). A number of studies have reported that the neural stem cells, astrocytes and astroglial tumours express GFAP as a major filament protein (Ignatova *et al.*, 2002; Gomes *et al.*, 1999; Jung *et al.*, 2007a), therefore, GFAP can be used as a cell marker for astrocytes and for the characterisation of continuous cell lines and short term cultures. All cells of glial origin

(U87MG, 1321N1, SVGp12, BTNW and HA) used in the current study were found to express GFAP in the cytoplasm and therefore were considered appropriate to use in the culture model. The human leukocyte antigen (HLA), is a protein expressed by cells of human origin. It is used as a marker for cells to characterise their origin species and helps in prediction of cross contamination between cell lines of different species (Braun *et al.*, 2000). All cells utilised in this thesis were found to express HLA and were therefore confirmed as species appropriate for the study. Interestingly, HLA is normally found to be expressed as a cell surface antigen, however in the cell lines, the staining appeared to be cytoplasmic.

The culturing of patient derived cells could serve as a patient-specific approach to optimise an individually-designed cancer therapy (Hass and Bertram, 2009). To utilise short-term cultures as tools for cancer research, it is essential to characterise the properties and cell type since these tumours are most likely to be heterogeneous (Rojas, 2011). For glioma short term cultures, GFAP, CD44 and EMA can be used to characterise the cell population in the culture. CD44 is a cell surface marker for endothelial cells; it modulates the proliferation and apoptosis of microvascular endothelial cells (Tsuneki and Madri, 2014). Epithelial membrane antigen (EMA) is a widely used marker to identify meningioma cells (Theaker *et al.*, 1986). EMA normally acts as a barrier to the apical surface of the membrane of epithelial cells, playing a protective and regulatory role. In low grade meningioma, the cells show overexpression of EMA which is supposed to play an important role during invasion and metastasis due to reduced cell adhesion (Langner *et al.*, 2003). Culturing cells from primary tumours for use in studying cancer cells can be difficult to establish because of the slow growing nature (Wenger *et al.*, 2004). For this reason, it is often recommended to use low passage numbers less than P10 (Esquenet *et al.*, 1997) as often at passage numbers greater than this cells become quiescent and start to dedifferentiate. The most important factor contributing to the

morphology and characteristics of the cell is the passage number (Hughes *et al.*, 2007). There is no straight method for determining the passage number or age of the adherent cells; the stocks of these cell lines which are maintained in laboratories may also differ (Esquenet *et al.*, 1997). The impact of a passage number of the cells on any given cell line is complex and dependent on several factors including the tissue and species of origin, the culture conditions, and the application for which the cells are used (Hughes *et al.*, 2007; Wenger *et al.*, 2004; Vierck and Dodson, 2000). To determine the effects of passage number on cell phenotype, the aforementioned phenotypic markers GFAP, CD44 and EMA were investigated at defined time points of low passage (P3), mid-passage (P7) and high-passage (P12).

The absence of expression of EMA in BTNW914 and BTNW370 at low, mid or high passage number indicated that the short term culture was derived from biopsy of a glioma patient and not meningioma patient. The expression of GFAP at low and mid passage number was high, compared to the expression at high passage, indicating that by passage 12, the cells were beginning to lose the glial phenotype. The expression of CD44, endothelial cell marker showed a decrease in the expression from low to high passage number. As the passage number increased, the short term culture BTNW914 showed a decrease in characteristic properties. The short term culture derived from patient biopsies showed a decrease in the expression of antigens, GFAP and HLA with increase in passage number. These results confirmed that for all future experiments the short-term patient derived glioma cultures should only be used up until P7, as after this, the cells showed reduced phenotypic expression of characteristic markers.

In summary, the characterisation confirmed the origin and type of cell to be used for the experiments. The growth patterns of the cells provided information about proliferation rate of the cells and doubling time of the cell population. The growth curves were used to determine the seeding densities of the cells in future experiments. The characterisation data confirms the suitability of the cell lines and the short term cultures to be used in the development of a physiologically relevant BBB model.

# CHAPTER 4

## 4. Characterisation of drug metabolising enzymes and transporters expression and activity.

### 4.1 Introduction

The poor prognosis of glioma is largely attributed to the lack of effective treatment regimes, and the major hurdle for treatment is the poor bioavailability of the drug at the site of the tumour. There has been an emerging understanding that poor bio-availability can be due to transporters effluxing the drug out of the cells (Begley, 2004), and the presence of drug metabolising enzymes (DMEs), which serves as a metabolic barrier decreasing bioavailability at the tumour site (Nebert *et al.*, 2013; Löscher and Potschka, 2005).

In this chapter, we studied the expression profiles of the efflux transporters, ABCB<sub>1</sub> and ABCG<sub>2</sub>, and the drug metabolising enzymes, CYP3A4 and CYP2D6, in cell lines, primary cultures and short term cultures. The aim of these experiments was to fully characterise the optimal experimental conditions required to give the highest possible protein expression and activity levels comparable to those observed *in vivo* and to determine which cell lines were most suitable to be taken forward to the next stage of BBB model validation in Chapter 5. The expression of these proteins was studied under standard and altered culturing conditions including: human serum or foetal bovine serum (FBS), culturing cells in the presence of different extracellular matrices such as fibronectin, poly-L-lysine and MaxGel and protein expression and activity profiles in cell lines, primary cultures and short term cultures.

## 4.2 Results

The expression of the efflux transporters and DMEs was assessed by extracting protein from cultured cells. Various different protein extraction protocols were used to optimise the extraction methods yielding maximum protein concentration required to study expression of proteins of interest.

### 4.2.1 Protein linearity experiment

Protein was extracted by method I from the U87MG, 1321N1 and SVGp12 cells in the exponential growth phase (day 3 to day 7), which was determined by their respective growth curves (see Section 3.2.2). The extracted protein was quantified by Bradford assay in a 96 well plate and the absorbance was read at 595 nm wavelength. The day on which the maximum protein yield was reached was selected to study the protein expression profiles in the cell lines. As seen in Figure 4.1, the concentration of protein showed a linear increase with respect to time up to day 5 in 1312N1 cell line and up to day 6 in U87MG and SVGp12 cell lines. The concentration of extracted proteins started to plateau on day 7 for all the three cell lines at concentration of 2.16 mg/ml in 1321N1, 2.06 mg/ml in U87MG and 1.51 mg/ml in SVGp12. The protein concentration and cell number showed a linear relationship (data not shown).

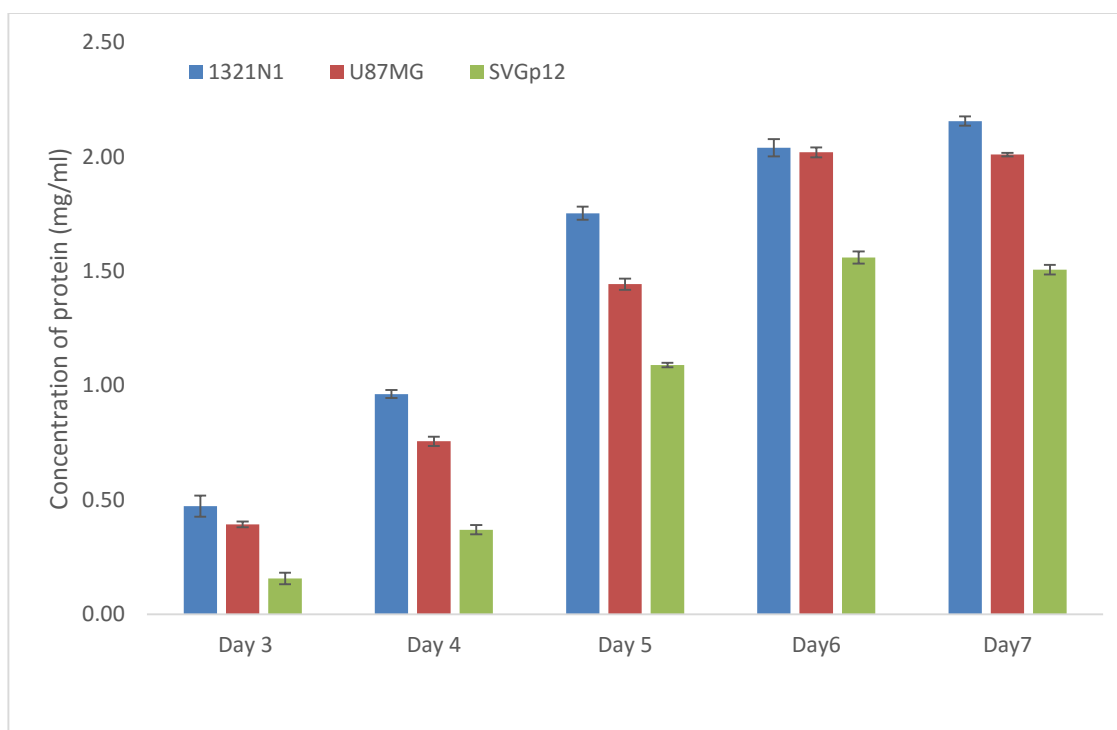


Figure 4.1 Concentration of protein extracted with respect to time in the exponential growth phase of cell lines. The data points are means of three replicates (n=3) and the error bars represent  $\pm$  standard deviation ( $\pm$ SD) of three inter repeats of an experiment.

## 4.2.2 Protein extraction method optimisation

From the previous experiment, it was concluded that cells in exponential growth phase gave the highest protein concentration. It was essential to lyse cells and to solubilise and extract protein in the intact (non-degraded) form, so that immunoreactivity was retained to study protein expression by immunoblotting. Different methods for protein extraction (see Section 2.3.2.1- 2.3.2.4) were used to maximise the protein yield. The total protein content extracted included both intracellular and surface proteins. The concentration of the protein from cell samples was extrapolated from a standard linear plot of absorbance versus known bovine serum albumin (BSA) concentration at 612 nm to determined using the Bradford assay.

The extraction of protein by Method I, which involved scraping U87MG, 1321N1 and SVGp12 cells from the flask followed by cell lysis (see Section 2.3.2.1) (Figure 4.2). The concentration of U87MG, 1321N1 and SVGp12 was 1.02 mg/ml, 1.37 mg/ml and 0.84 mg/ml respectively.

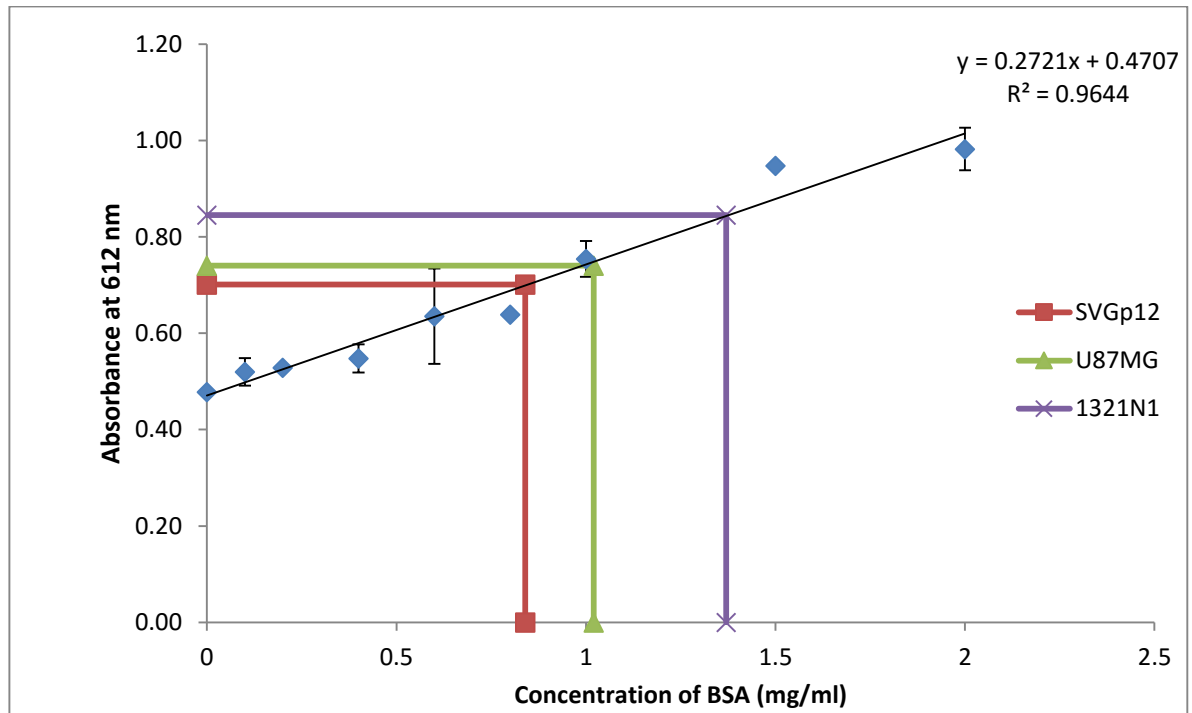


Figure 4.2 Standard linear plot of BSA (mg/mL) vs. absorbance at 612 nm.

This plot was used to calculate protein concentration after method I extraction protocol (see Section 2.3.2.1). The absorbance values were interpolated to determine the unknown protein concentration. These data points are representative of three replicates (n=3) and the error bars represent mean  $\pm$  standard deviation ( $\pm$ SD) of three inter-experimental repeats.

The extraction of protein by Method II involved trypsinising cells from the flask followed by cell lysis (see Section 2.3.2.2). As seen in Figure 4.3, the concentration of U87MG, 1321N1 and SVGp12 was 1.06 mg/ml, 1.40 mg/ml and 0.704 mg/ml respectively.

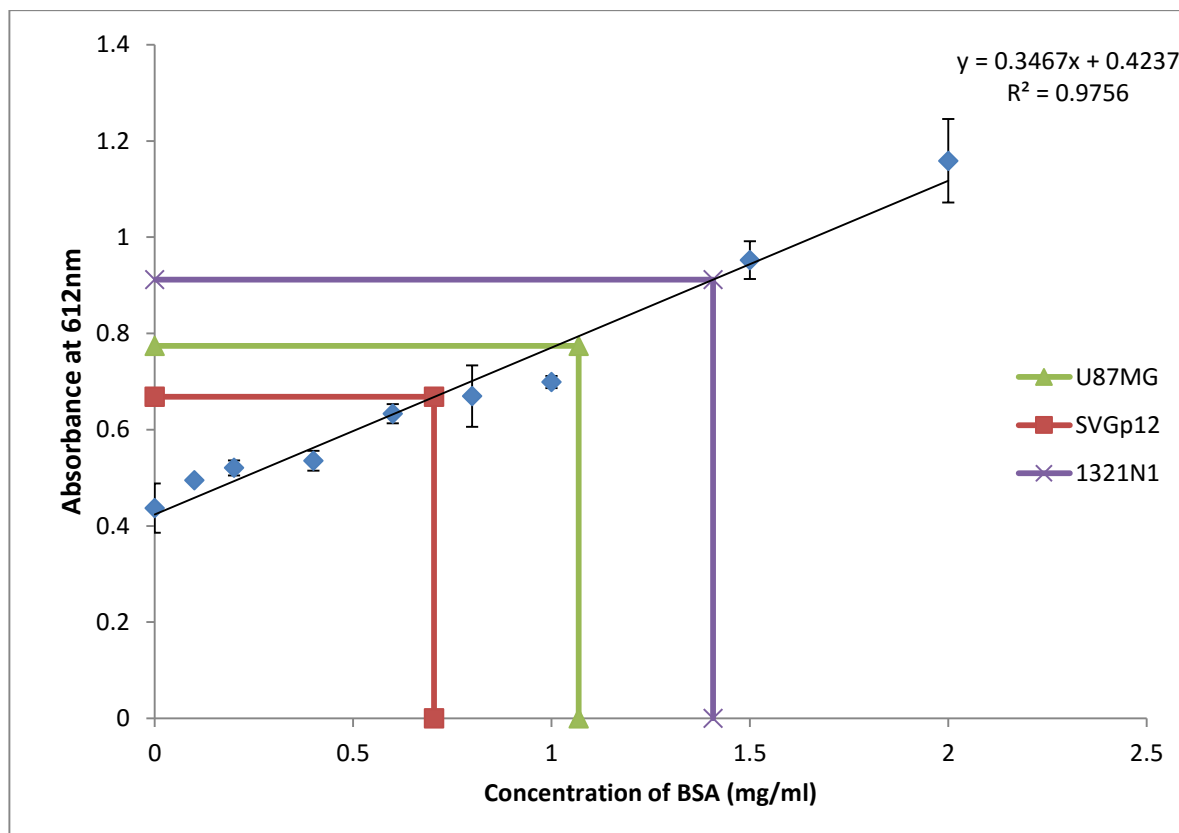


Figure 4.3 Standard linear plot of BSA (mg/mL) vs. absorbance at 612 nm.

This plot was used to calculate protein concentration after method II extraction protocol (see Section 2.3.2.2). The absorbance values were interpolated to determine the unknown protein concentration. These data points are representative of three replicates (n=3) and the error bars represent mean  $\pm$  standard deviation ( $\pm$ SD) of three inter-experimental repeats.

The extraction of protein by Method III involved spinning U87MG, 1321N1 and SVGP12 cells at a lower speed following lysis using RIPA buffer (see Section 2.3.2.3). As seen in Figure 4.4, the concentration of U87MG, 1321N1 and SVGP12 was 0.83 mg/ml, 0.67 mg/ml and 0.40 mg/ml respectively.

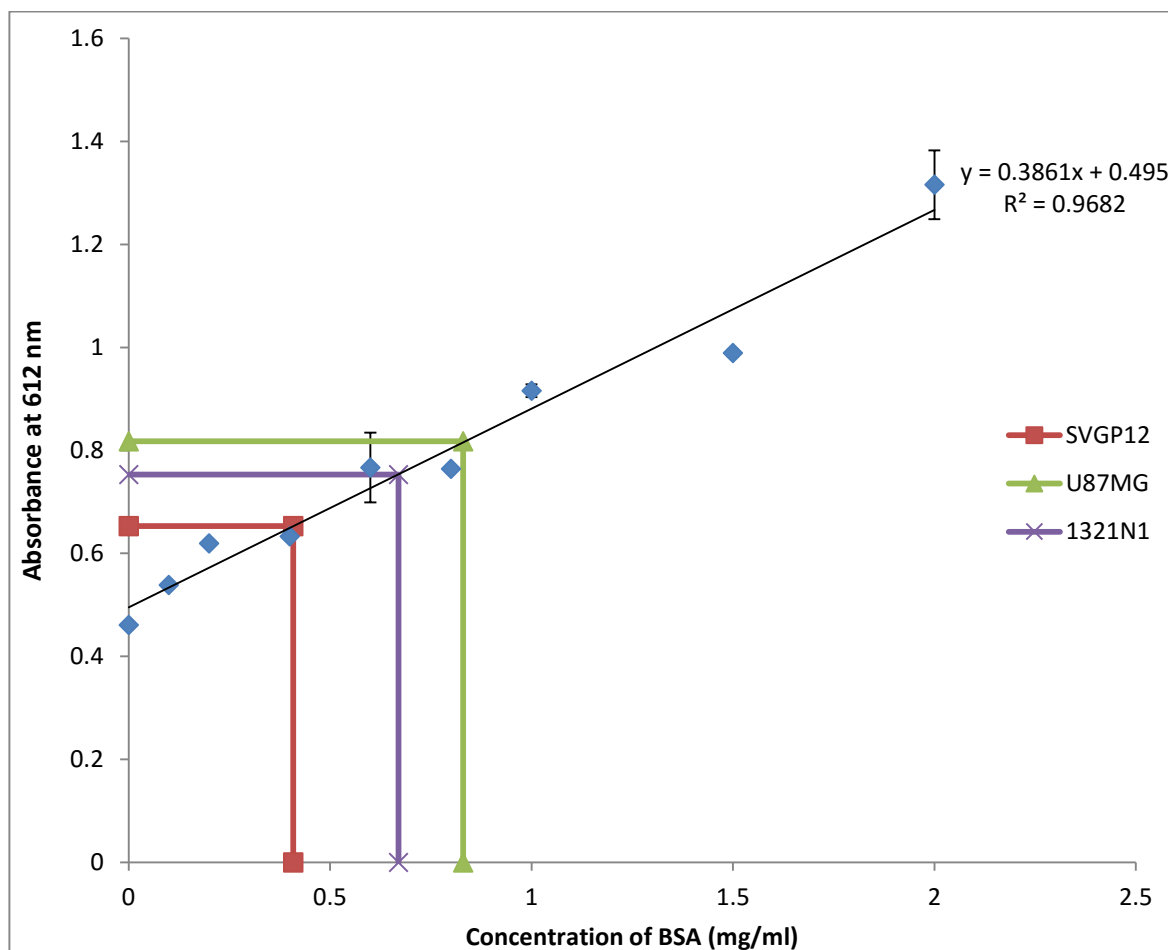


Figure 4.4 Standard linear plot of BSA (mg/mL) vs. absorbance at 612 nm.

This plot was used to calculate protein concentration after method III extraction protocol (see Section 2.3.2.3). The absorbance values were interpolated to determine the unknown protein concentration. These data points are representative of three replicates (n=3) and the error bars represent mean  $\pm$  standard deviation ( $\pm$ SD) of three inter-experimental repeats.

The extraction of protein by Method IV involved sonication of U87MG, 1321N1 and SVGp12 cells to facilitate lysis (see Section 2.3.2.4). As seen in Figure 4.5, the concentration of U87MG, 1321N1 and SVGp12 was 0.45 mg/ml, 0.27 mg/ml and 0.4 mg/ml respectively.

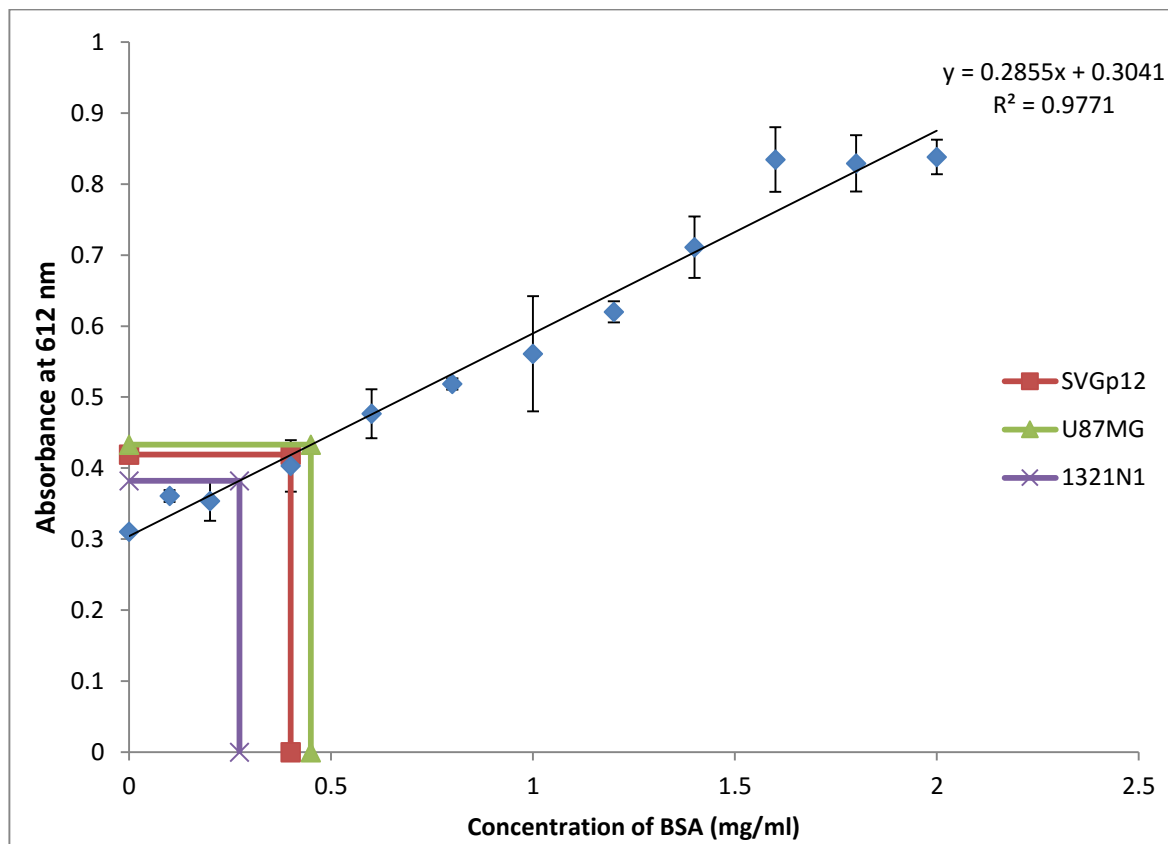


Figure 4.5 Standard linear plot of BSA (mg/mL) vs. absorbance at 612 nm.

This plot was used to calculate protein concentration after method IV extraction protocol (see Section 2.3.2.4). The absorbance values were interpolated to determine the unknown protein concentration. These data points are representative of three replicates ( $n=3$ ) and the error bars represent mean  $\pm$  standard deviation ( $\pm$ SD) of three inter-experimental repeats.

A summary of highest protein yielded from each protocol is shown in Table 4.1. SVGp12 and 1321N1 showed maximum yields of protein of 0.84 mg/ml and 1.37 mg/ml respectively using method I for extraction, which involves scraping of cells from culture dishes. U87MG showed maximum recovery of protein of 1.4 mg/ml for method II which involved trypsinising cells from culture dishes and showed concentration of 1.37 mg/ml with method I (scraping cells). Method III and method IV both showed low concentration of protein, hence, it was concluded that method I yields the optimal yield of protein most cells and was therefore used for all the subsequent experiments. Method I was preferable to method II because it involved scraping cells on ice which minimised protein degradation.

*Table 4.1 Summary of the protein concentration of cell lines using different extraction protocol.*

Protocol used		Method I	Method II	Method III	Method IV
Protein extracted (mg/ml)	U87MG	1.02	1.06	0.83	0.45
	1321N1	1.37	1.4	0.67	0.27
	SVGp12	0.84	0.70	0.4	0.43

The optimised extraction protocol method I was also used to extract proteins from all short term cultures derived from primary cells.

## 4.2.3 Protein expression profile for different cell lines

### 4.2.3.1 Protein expression profile in standard tissue culture conditions

The extracted proteins were studied for the expression of the drug metabolising enzymes, CYP3A4 and CYP2D6, and the efflux transporters, ABCB<sub>1</sub> and ABCG<sub>2</sub>. Protein was extracted from cancerous cell line (U87MG, 1321N1), glial cells (SVGp12, HA), endothelial cells (hCMEC/D3, HBMEC), pericytes (HBVP) and patient derived short term cultures (BTNW914 and BTNW370), grown in T75 flasks as a monolayer. All the Western blots shown in this Chapter were normalised by quantifying the protein concentration by Bradford assay and loading each well with an equal amount of protein. In addition, the expression of  $\beta$ -actin was used as the loading control for all Westerns by normalising densitometry measurements for proteins of interest relative to  $\beta$ -actin. All of the densitometry results from Western immunoblots were compared relative to per cent expression of CYP in the bacosomes or relative to per cent expression of rat liver lysate (RLL) for the transporter. Bacosomes were used as the positive control as they contain overexpressed human cytochrome P450 gene in a bacterial membrane. All positive controls were defined as 100 % and expression was shown relative to this.

As seen in Figure 4.6, all the cultures showed the expression of the CYP3A4. The highest expression confirmed by densitometry analysis was seen in HBMEC short-term cultures (106 %) and the lowest expression was observed for SVGp12 (9 %), and the short term glioma cultures BTNW914 (22 %) and BTNW370 (19 %) (Figure 4.7). In the immortalised cell lines, the highest expression was shown by the 1321N1 cell line (64 %).

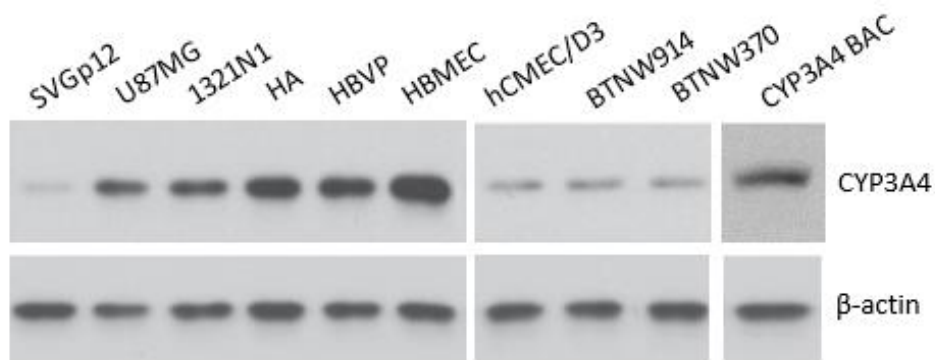


Figure 4.6 Western blots showing expression of CYP3A4 (57 kDa).

Expression was studied in immortalised cell lines and short term cultures.  $\beta$ -actin was used as the loading control. Each well was loaded with 20  $\mu$ g of protein.

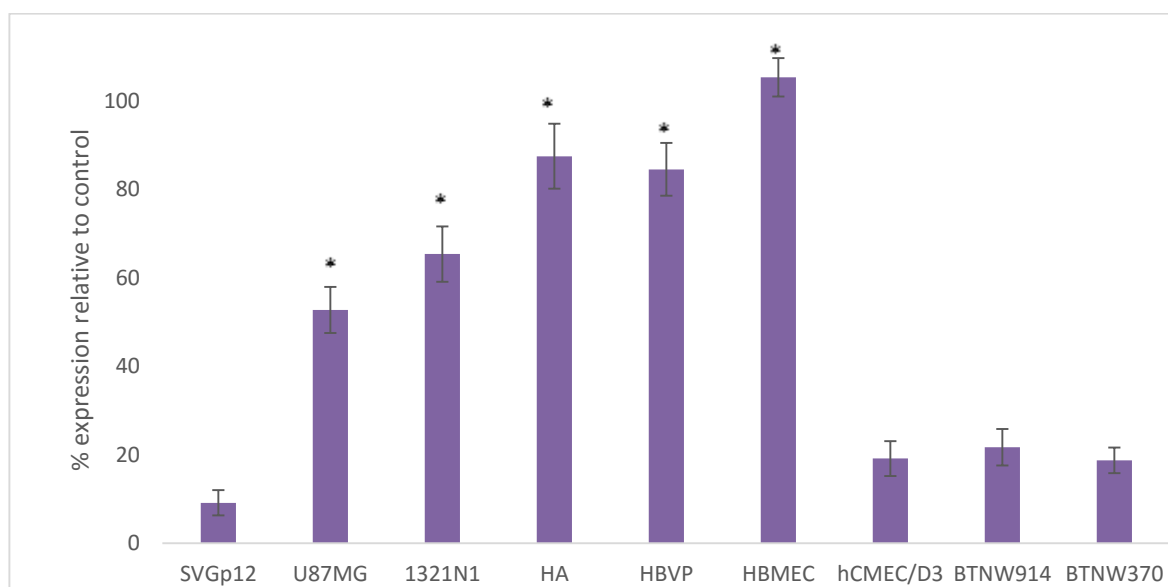


Figure 4.7 Densitometry analysis of the blots showing expression of CYP3A4.

The data is plotted per cent relative to the expression of the enzyme in positive control human CYP3A4 bacosomes. These data points are representative of three replicates (n=3) and the error bars represent mean  $\pm$  standard deviation ( $\pm$ SD) of three inter-experimental repeats. \*  $p < 0.05$  was considered to be statistically significant.

The expression of CYP2D6 enzyme in all of the different immortalised and short term cultures (Figure 4.8) was determined by Western blot. All of the results were reported relative to per cent expression of rat liver lysate (RLL) (defined as 100 %). All the cultures showed expression of the CYP2D6. The highest expression was seen in HBMEC primary cultures (117 %) and the lowest expression was observed in SVGp12 (16 %) and the, short term cultures BTNW914 (59 %) and BTNW370 (61 %). From the cell lines, the highest expression was shown by the 1321N1 cell line (56 %) (Figure 4.9).

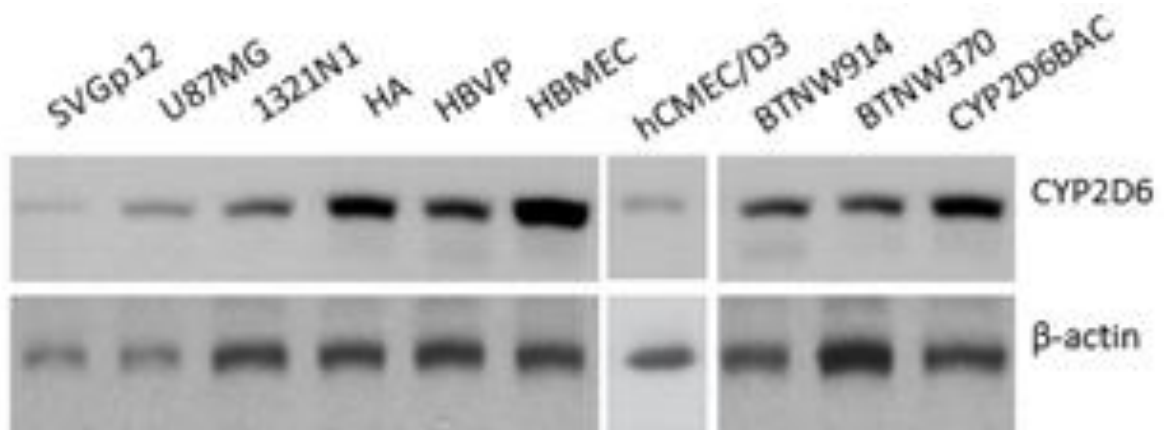


Figure 4.8 Western blots showing expression of CYP2D6 (57 kDa).

Expression was studied in immortalised cell lines and short term cultures. β-actin was used as the loading control. Each well was loaded with 20 μg of protein.

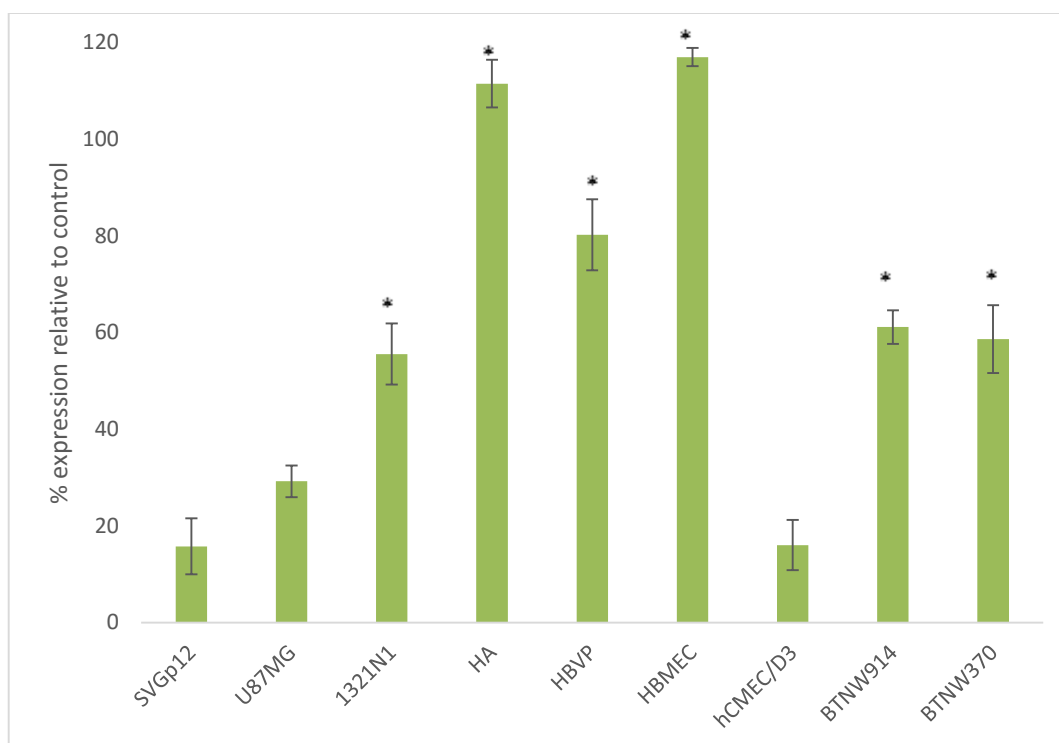


Figure 4.9 Densitometry analysis of the blots showing expression of CYP2D6.

The data is plotted per cent relative to the expression of the positive control CYP2D6 in bacosomes. These data points are representative of three replicates (n=3) and the error bars represent mean  $\pm$  standard deviation ( $\pm$ SD) of three inter-experimental repeats. \*  $p < 0.05$  was considered to be statistically significant.

The expression of ABCB<sub>1</sub> efflux transporters in all immortalised and short term cultures (Figure 4.10) was determined by Western immunoblotting and expression was semi-quantified by densitometry. All of the results were reported relative to per cent expression of rat liver lysate (RLL) (defined as 100 %) which was used as the positive control since the liver shows high expression of the ABCB<sub>1</sub> efflux transporter. All of the cultures showed expression of the ABCB<sub>1</sub> transporter. The highest expression, confirmed by densitometry, was seen in HBMEC primary cultures (98 %) and the lowest expression was observed in short term cultures BTNW914 (21 %) and BTNW370 (18 %) and the immortalised cell line 1321N1 (17 %). From the cell lines, the highest expression was shown by the foetal glial astrocytes SVGp12 (64 %) (Figure 4.11).

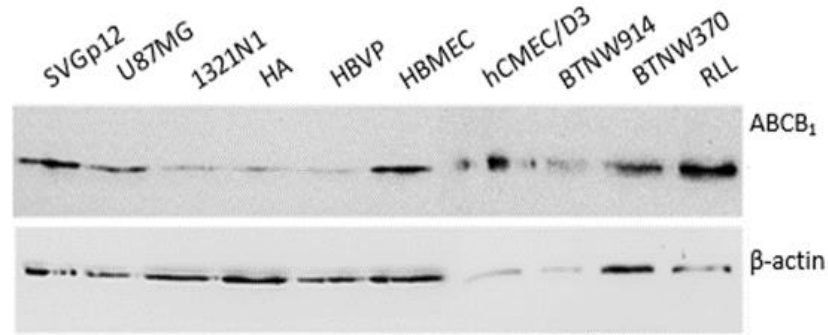


Figure 4.10 Western blots showing expression of ABCB<sub>1</sub> efflux transporter (170 kDa). Expression was studied in immortalised cell lines and short term cultures relative to the positive control rat liver lysate (RLL). β-actin was used as the loading control. Each well was loaded with 20 μg of protein.

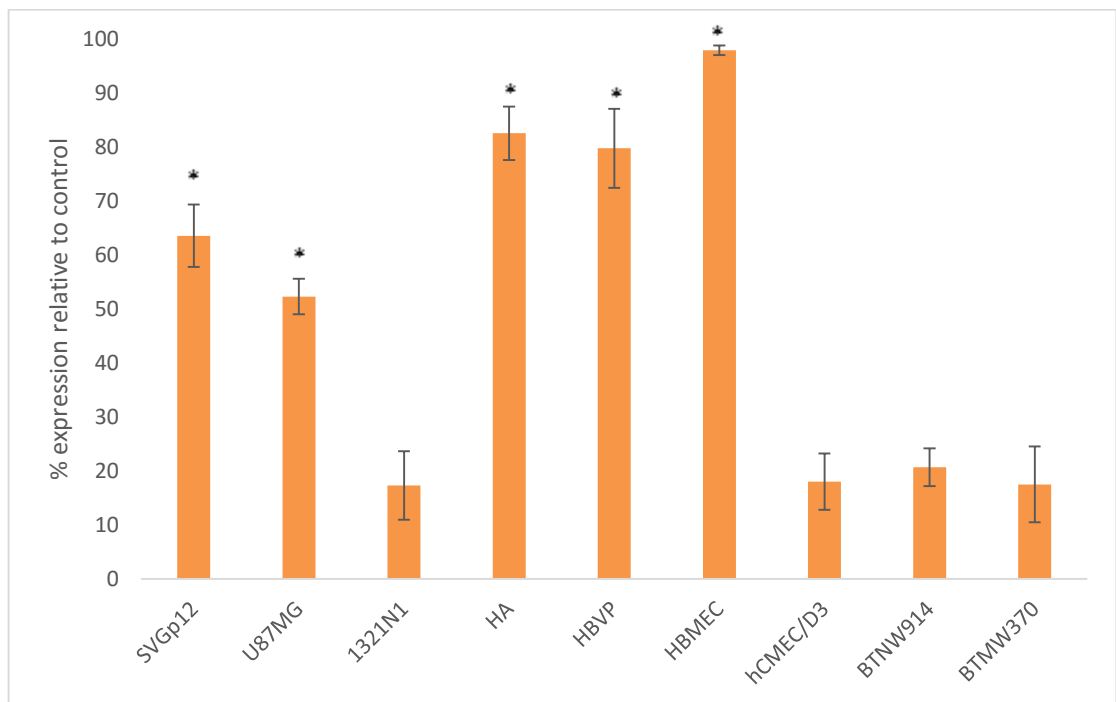


Figure 4.11 Densitometry analysis of the blots showing semi-quantitation of the ABCB<sub>1</sub> efflux transporter. The data is plotted per cent relative to the expression of the transporter in rat liver lysate. These data points are representative of three replicates (n=3) and the error bars represent mean ± standard deviation (±SD) of three inter-experimental repeats \* p < 0.05 was considered to be statistically significant.

The expression of ABCG<sub>2</sub> efflux transporter in immortalised and short term cultures (Figure 4.12) was determined by Western blot. The RLL was used the positive control since the liver shows high expression of the ABCG<sub>2</sub> efflux transporter. All the cultures showed expression of the ABCG<sub>2</sub> transporters. The highest expression from the mean of three gels, confirmed by densitometry analysis, was seen in HBMEC primary cultures (81 %) and the lowest expression was seen in the hCMEC/D3 cell line (38 %). For the cell lines, the highest expression was shown by U87MG (57 %) (Figure 4.13).

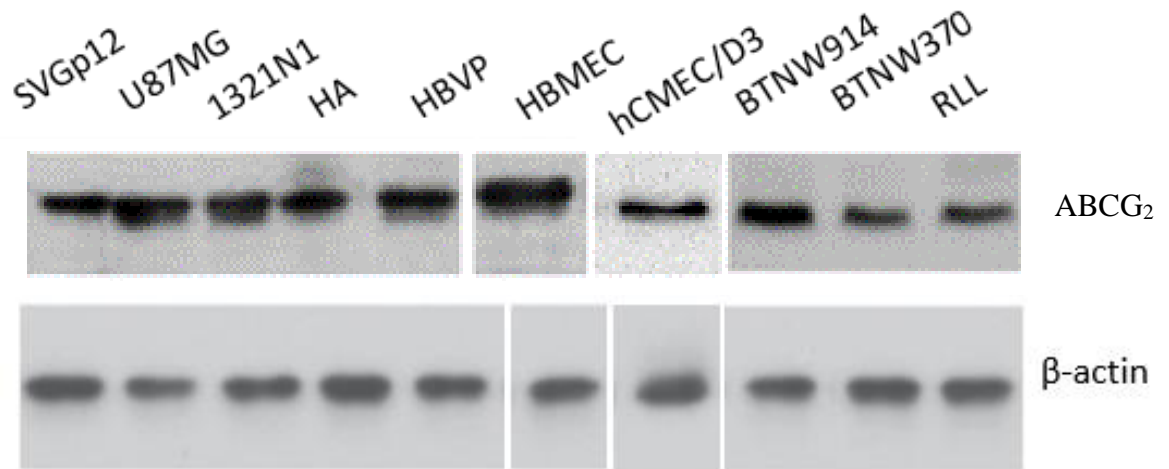


Figure 4.12 Western blots showing expression of ABCG<sub>2</sub> efflux transporter (72 kDa).

Expression was studied in immortalised cell lines, and short term cultures relative to the positive control rat liver lysate (RLL). Each well was loaded with 20 µg of protein.

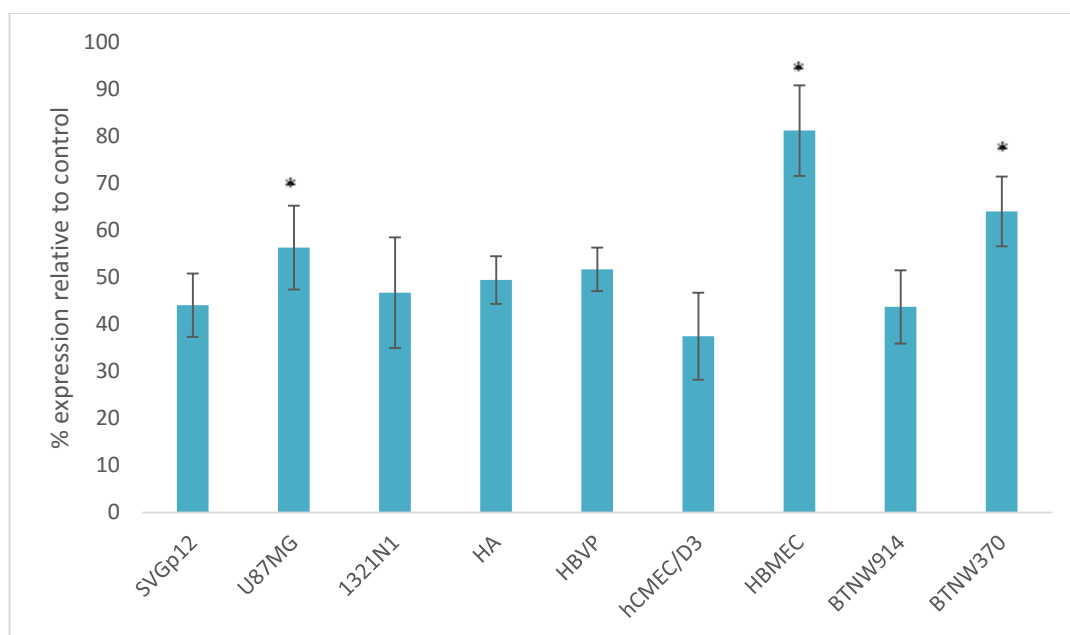


Figure 4.13 Densitometry analysis of the blots showing expression of ABCG<sub>2</sub> efflux transporter.

The data is plotted as per cent relative to the expression of the enzyme in rat liver lysate control. These data points are representative of three replicates (n=3) and the error bars represent mean  $\pm$  standard deviation ( $\pm$ SD) of three inter-experimental repeats \*  $p < 0.05$  was considered to be statistically significant.

In summary, the expression of efflux transporters; ABCB<sub>1</sub> and ABCG<sub>2</sub> and DMEs; CYP3A4 and CYP2D6 were determined by Western blot in cell lines and short term cultures. The short-term cultures that were to be used to construct the *in vitro* BBB; HBMEC, HBVP and HA showed higher expression of ABCB<sub>1</sub>, ABCG<sub>2</sub> and CYP3A4, CYP2D6 compared to the immortalised endothelial cell line hCMEC/D3 and the immortalised glial cell line SVGp12. When comparing the immortalised glioma cell lines (1321N1 and U87MG) to the short-term patient derived glioma cell lines, the results were not as clear. CYP3A4 expression was higher in the immortalised glioma cell lines compared to short-term cultures, whereas CYP2D6 and ABCB<sub>1</sub> was higher in short-term glioma cultures compared to the immortalised cell lines. There was no significant difference between cultures for ABCG<sub>2</sub>.

#### 4.2.3.2 Effect of altered culture condition on protein expression profile.

The HA, HBVP and HBMEC short-term cultures showed high expression of the efflux transporters; ABCB<sub>1</sub> and ABCG<sub>2</sub> and DMEs; CYP3A4 and CYP2D6 (Section 4.2.3.1), they were therefore taken forward to the next stage of the study, to determine whether altering experimental condition could enhance the protein expression further. In standard experimental conditions the short-term cultures were grown in 10 % FBS without ECM. The altered experimental conditions involved culture in 5 % HS without ECM, and in the presence of ECM; MaxGel, poly-L-lysine or fibronectin. These optimised conditions were then used to develop the *in vitro* BBB model. This data laid the foundation of developing a physiologically relevant model. All data was plotted as per cent protein expression relative to expression in standard culturing conditions, which was set at 100 %.

As seen in Figure 4.14, the cells cultured in human serum, compared to cells grown under standard conditions, showed little difference in the expression of ABCG<sub>2</sub>, CYP3A4 and CYP2D6. The expression was quantified by densitometry to confirm this. The cells cultured in fibronectin showed the highest expression of both efflux transporters; ABCB<sub>1</sub> and ABCG<sub>2</sub> and DMEs; CYP3A4 and CYP2D6.

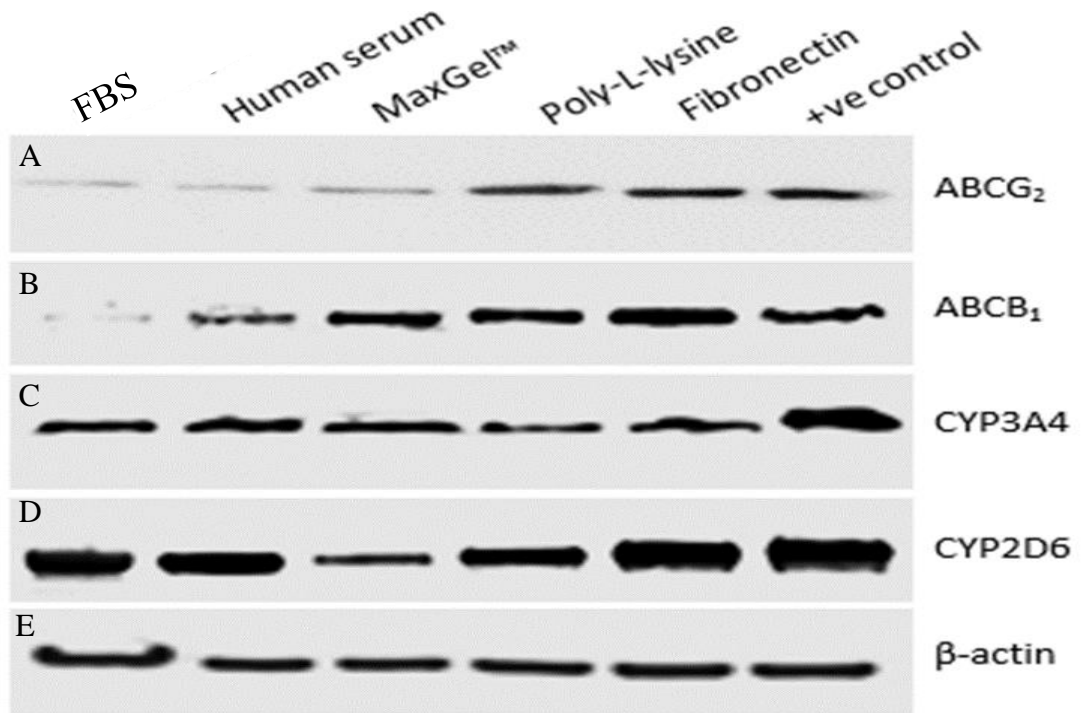


Figure 4.14 Expression of the efflux transporters and drug metabolising enzymes in HA (human astrocyte) in different culturing conditions.

**A.** Expression of ABCB<sub>1</sub> efflux transporter. **B.** Expression of ABCG<sub>2</sub> efflux transporter. **C** Expression of CYP3A4 enzyme. **D.** Expression of CYP2D6 enzyme. **E.** Expression of β-actin in all the models, β-actin was used as the loading control. Each well was loaded with 10 μg of protein.

As seen in Figure 4.15A, the expression of ABCG<sub>2</sub> was semi-quantified by densitometry. Cells cultured in the presence of fibronectin showed the highest ABCG<sub>2</sub> expression, an increase to 867% compared to the standard culture conditions whereas poly-L-lysine and MaxGel™ showed an expression of 796 % and 209 %, respectively. The cells, cultured in human serum, increased the expression of ABCG<sub>2</sub> transporter to 187 % compared to expression in standard culturing condition. As seen in Figure 4.15 B, the expression of ABCB<sub>1</sub> increased to 715 % when cultured on fibronectin, compared to the standard culturing conditions. The other ECM, poly-L-lysine or MaxGel™, showed an increase of 510 % and 508 % respectively. The cells cultured in human serum showed an increase to 270 % in the expression of ABCB<sub>1</sub> when compared to expression in standard culturing condition.

As seen in Figure 4.15 C, the expression of CYP3A4 was highest when the cells were cultured in fibronectin, and the lowest when the cells were cultured in poly-L-lysine. The expression of CYP3A4 increased to 114 % in fibronectin and 109 % in MaxGel™ and decreased to 73 % in poly-L-lysine when compared to expression in standard culturing condition. When the cells were grown in human serum, the expression of CYP3A4 showed a slight increase to 104 % when compared to cells cultured in FBS. As seen in Figure 4.15 D, the CYP2D6 enzyme expression was highest when the cells were cultured with fibronectin. The expression increased to 124% in fibronectin and 111 % in poly-L-lysine. The expression of CYP3A4 showed a decrease to 57 % in cells which were cultured with MaxGel™ as the ECM. The CYP3A4 expression increased to 115 % when the cells were grown on to human serum.

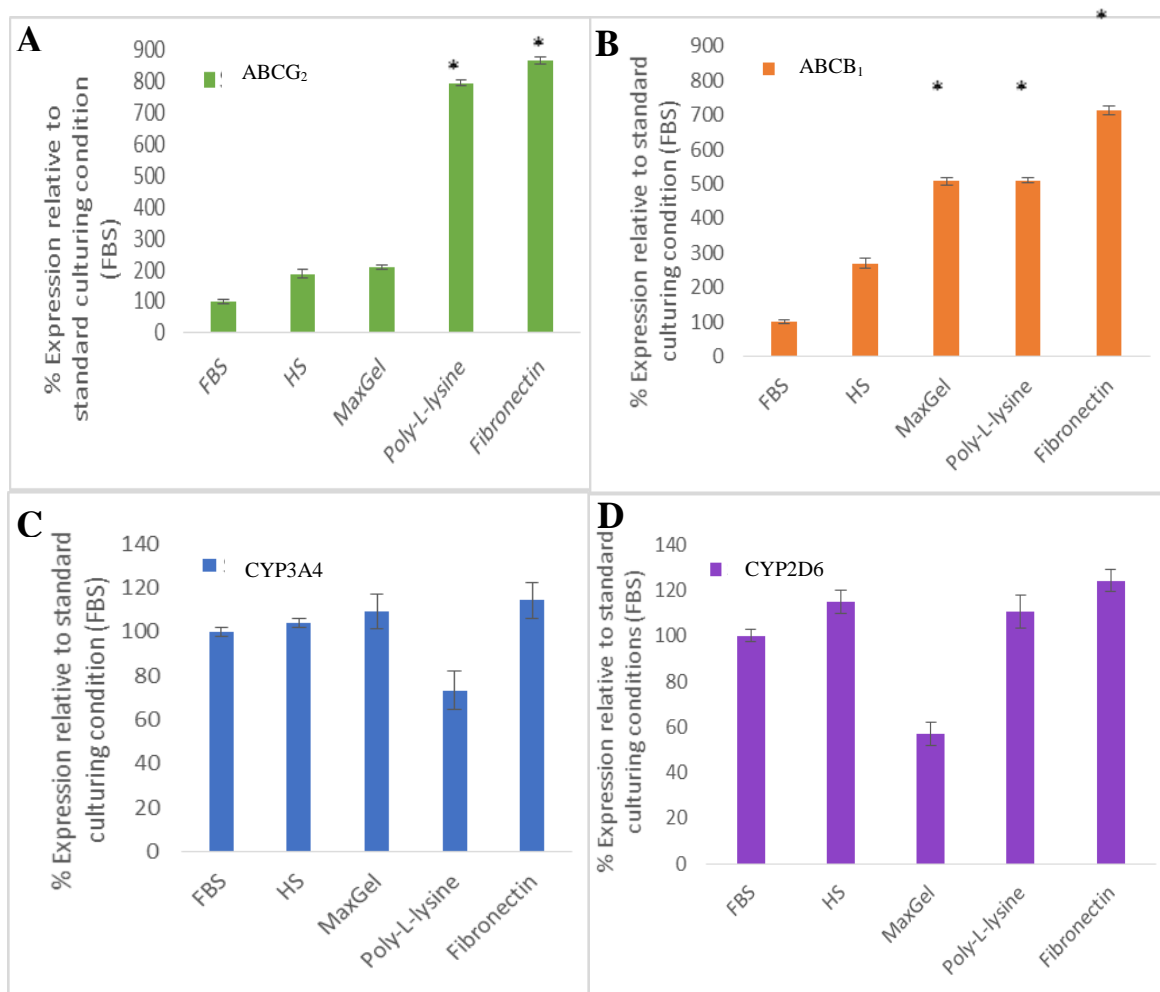


Figure 4.15 Densitometry analysis of the blots showing expression of efflux transporters and DMEs in HA cells. **A.** Expression of ABCG<sub>2</sub>, **B.** Expression of ABCB<sub>1</sub>, **C.** Expression of CYP3A4 and **D.** Expression of CYP2D6. The data is plotted as per cent relative to the expression of proteins in standard culturing conditions (10 % FBS and no ECM). The error bars represent mean  $\pm$  standard deviation ( $\pm$ SD) of three measurements of each band. \*  $p < 0.05$  was considered to be statistically significant.

As seen in Figure 4.17, expression of efflux transporters; ABCB<sub>1</sub> and ABCG<sub>2</sub> and DMEs; CYP3A4 and CYP2D6 in HBVP were assessed in various culturing conditions. The HBVP cultured in human serum compared to cells grown in standard culturing conditions (10 % FBS, no ECM) did not show a significant difference in the protein expression. The pericytes cultured in fibronectin showed the highest expression of both efflux transporters and DMEs. This is explained in details with the densitometry analysis which is expressed as per cent expression relative to standard culturing conditions (Figure 4.16).

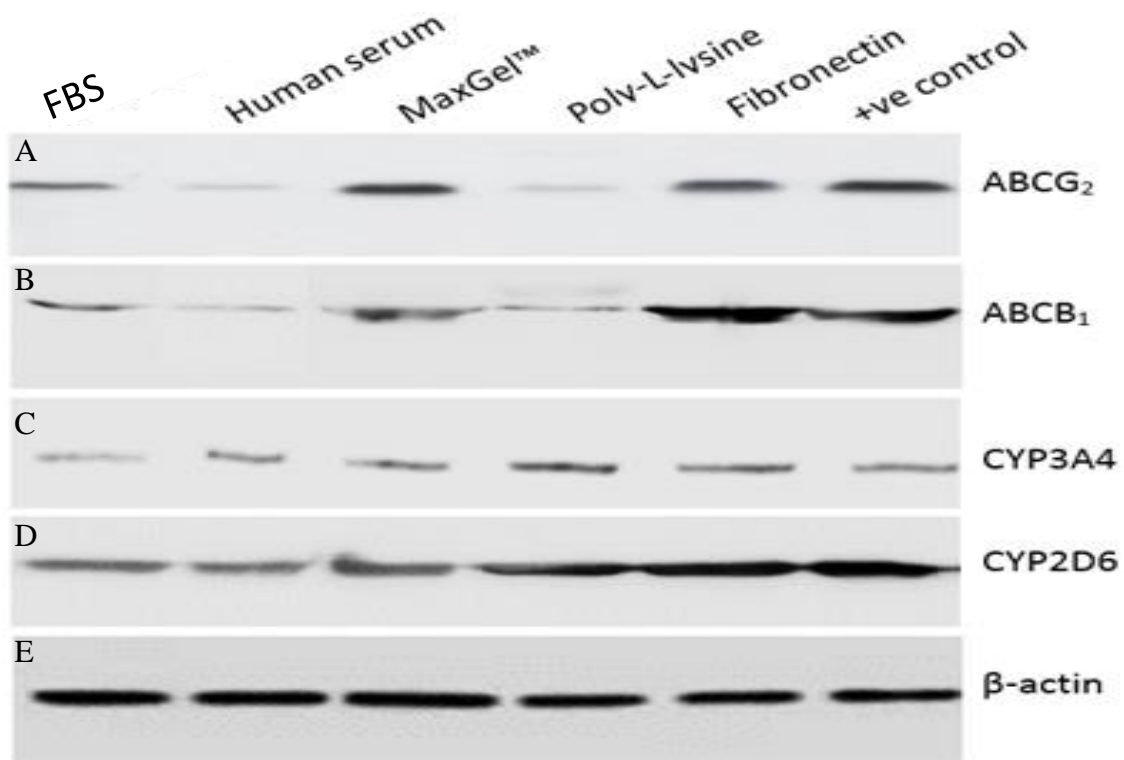


Figure 4.16 Expression of the efflux transporters and drug metabolising enzymes in HBVP (pericyte cells) in various culturing conditions.

**A.** Expression of ABCB<sub>1</sub> efflux transporter. **B.** Expression of ABCG<sub>2</sub> efflux transporter. **C.** Expression of CYP3A4 enzyme. **D.** Expression of CYP2D6 enzyme. **E.** Expression of β-actin in all the models, β-actin was used as the loading control. Each well was loaded with 10 μg of protein.

The protein expression was semi quantified by densitometry, the expression of ABCG<sub>2</sub> was highest when the cells were cultured in the presence of fibronectin. As seen in Figure 4.17 A, the expression increased to 281% when compared to the standard culturing conditions. MaxGel™ showed an increase to 257 % and poly-L-lysine showed a decrease in expression to 67 % in comparison to standard culturing conditions. The cells grown in human serum showed a decrease in the expression of ABCG<sub>2</sub> to 52 %. As seen in Figure 4.17 B, the expression of ABCB<sub>1</sub> was highest in cells cultured in the presence of fibronectin. The cells grown in fibronectin showed an increase to 194 % compared to the other ECM which showed an increase in expression to 222 % in MaxGel and a decrease in expression to 24 % in poly-L-lysine. The cells, when weaned on to human serum, showed decreased expression of the ABCB<sub>1</sub> transporter to 37 %.

As seen in Figure 4.17 C, the CYP3A4 enzyme expression was highest when the cells were cultured with fibronectin as the ECM. The expression increased to 244 % in fibronectin, 218 % in poly-L-lysine and 159 % in MaxGel™. The cells were grown in human serum which resulted in no significant change in CYP3A4 expression. As seen in Figure 4.17 D, the expression of CYP2D6 was highest when the cells were cultured in fibronectin and the lowest was when the cells were cultured in poly-L-lysine. The expression of CYP2D6 increased to 386 % in fibronectin, 210 % in MaxGel™ and 305 % in poly-L-lysine. When the cells were grown in human serum, the expression of CYP3A4 increased to 150 %, compared to cells cultured in FBS.

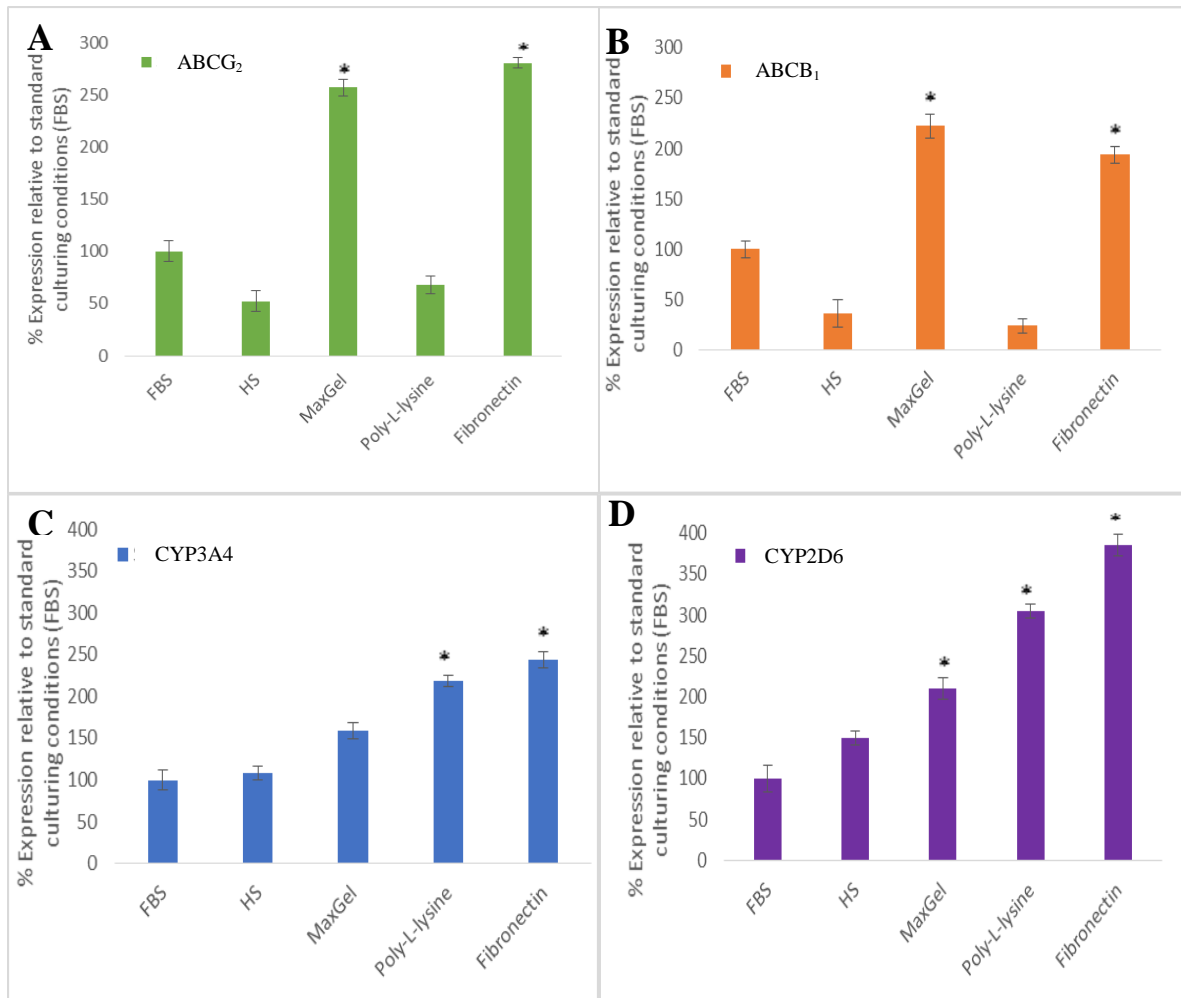


Figure 4.17 Densitometry analysis of the blots showing expression of efflux transporters and DMEs in HBVP cells.

**A.** Expression of ABCG<sub>2</sub>, **B.** Expression of ABCB<sub>1</sub>, **C.** Expression of CYP3A4 and **D.** Expression of CYP2D6. The data is plotted per cent relative to the expression of proteins in standard culturing conditions 10 % FBS and no ECM. The error bars represent mean  $\pm$  standard deviation ( $\pm$ SD) of three measurements of each band. \*  $p < 0.05$  was considered to be statistically significant.

As seen in Figure 4.18, expression of efflux transporters; ABCB<sub>1</sub> and ABCG<sub>2</sub> and DMEs; CYP3A4 and CYP2D6 in HBMEC were assessed in various culturing conditions. The cells cultured in human serum as compared to standard culturing conditions did not show significant difference in the protein expression. The cells cultured in fibronectin showed the highest expression of both efflux transporters; ABCB<sub>1</sub> and ABCG<sub>2</sub> and DMEs; CYP3A4 and CYP2D6. This is explained in detail with the densitometry analysis (Figure 4.19).

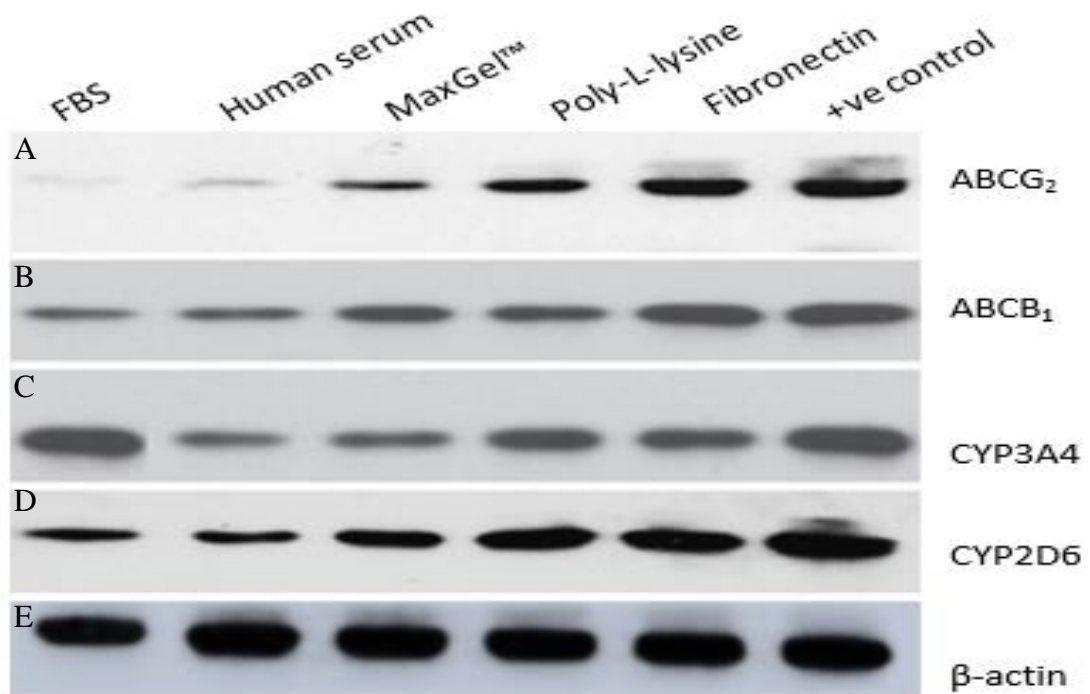


Figure 4.18 Expression of the efflux transporters and drug metabolising enzymes in HBMEC (endothelial cell) primary culture in various culturing conditions.

**A.** Expression of ABCB<sub>1</sub> efflux transporter. **B.** Expression of ABCG<sub>2</sub> efflux transporter. **C.** Expression of CYP3A4 enzyme. **D.** Expression of CYP2D6 enzyme. **E.**, β-actin was used as the loading control. Each well was loaded with 10 µg of protein.

As seen in Figure 4.19 A, the expression of ABCG<sub>2</sub> increased to 245 % in the presence of fibronectin, when compared to the standard culturing conditions. The other ECM used also showed an increase in expression, MaxGel™ to 186 % and poly-L-lysine to 212 % compared to control. The cells grown in human serum showed an increase in the expression of ABCG<sub>2</sub> to 147 %. As seen in Figure 4.19 B, the expression of ABCB<sub>1</sub> was highest in cells cultured in the presence of fibronectin, (288 %) when compared to the other ECM which showed an increase to 181 % in MaxGel™ and a decrease in expression to 161 % in poly-L-lysine. The cells grown in human serum showed an increase the expression of the ABCB<sub>1</sub> transporter to 130 %, compared to the control.

As seen in Figure 4.19 C, the expression of CYP3A4 was highest when the cells were cultured in fibronectin as the ECM. The expression of CYP3A4 increased to 123 % in fibronectin, and showed a decrease to 75 % in MaxGel and 89 % in poly-L-lysine. When the cells were weaned on to human serum, the expression of CYP3A4 decreased to 57 % compared to cells cultured in FBS. As seen in Figure 4.19 D, the CYP2D6 enzyme expression was highest when the cells were culture with fibronectin as the ECM. The expression increased to 327 % in fibronectin, 260% in poly-L-lysine and 188 % in MaxGel. The cells weaned on to human serum showed an increase the expression of CYP2D6 to 141 % when compared to control.

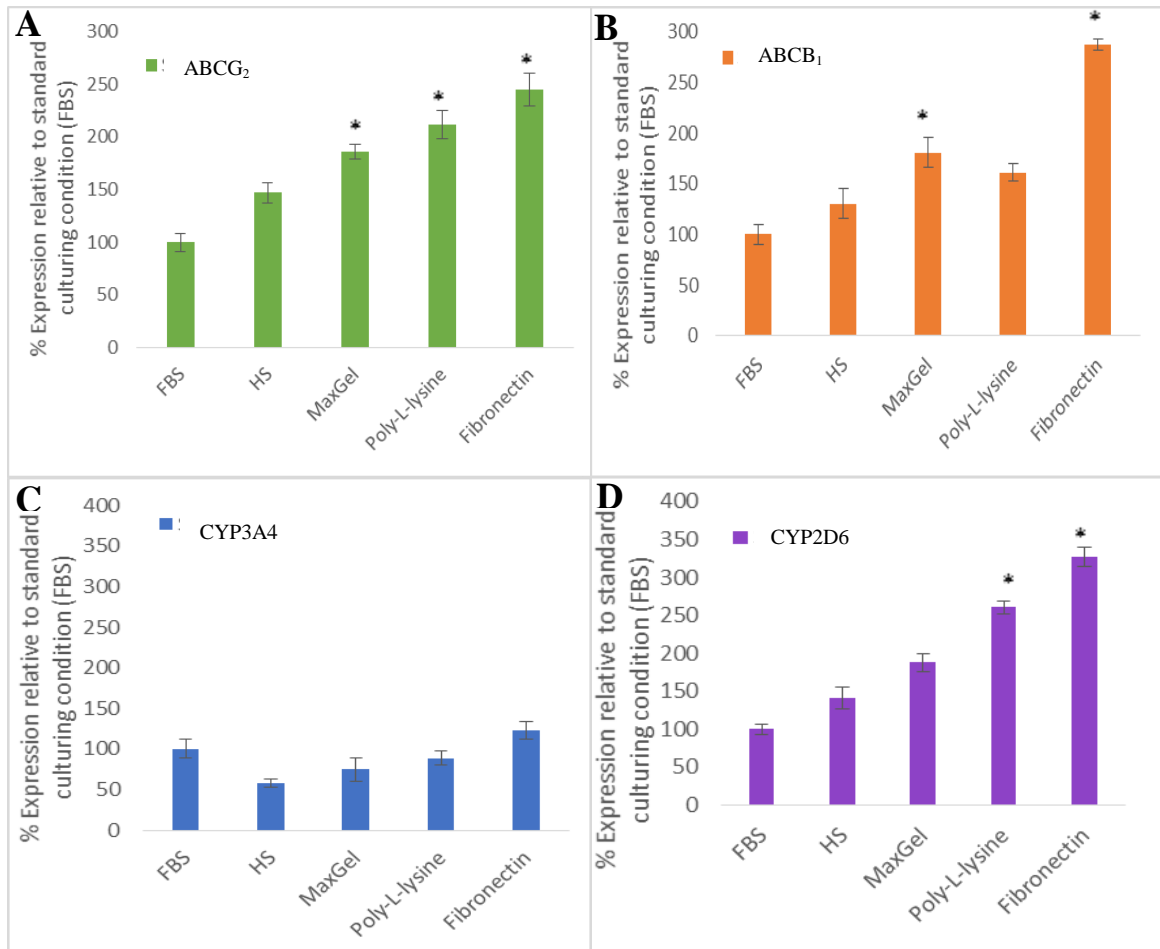


Figure 4.19 Densitometry analysis of the blots showing expression of efflux transporters and DMEs in HBMEC cells.

**A.** Expression of ABCG<sub>2</sub>, **B.** Expression of ABCB<sub>1</sub>, **C.** Expression of CYP3A4 and **D.** Expression of CYP2D6. The data is plotted per cent relative to the expression of proteins in standard culturing conditions i.e. FBS. The error bars represent mean  $\pm$  standard deviation ( $\pm$ SD) of the three measurements of each band. \*  $p < 0.05$  was considered to be statistically significant.

The various culturing conditions were performed to maximise the expression of efflux transporters; ABCB<sub>1</sub> and ABCG<sub>2</sub> and DMEs; CYP3A4 and CYP2D6 in primary cultures HA, HBVP and HBMEC. As seen in Table 4.2, the short-term cultures showed an increase in the expression of efflux transporters; ABCB<sub>1</sub> and ABCG<sub>2</sub> and DMEs; CYP3A4 and CYP2D6 when cultured in fibronectin as the ECM. HS was also chosen as the serum for cells to be cultured in. Fibronectin and HS would be adapted in to the developing the *in vitro* BBB model to enhance expression of these proteins. It was also essential to determine if the culturing had an effect on the activity of the efflux transporters; ABCB<sub>1</sub> and ABCG<sub>2</sub> and DMEs; CYP3A4 and CYP2D6, which was further studied.

Table 4.2 Summary of the % expression of different protein relative to standard culturing conditions.

Primary culture	Protein	Standard Culturing Condition	Altered culturing conditions (% relative to standard culturing conditions)			
		FBS	HS	MaxGel	Poly-L-lysine	Fibronectin
HA	ABCG <sub>2</sub>	100	259.49	508.09	510.11	714.26
	ABCB <sub>1</sub>	100	186.61	208.77	795.47	866.86
	CYP3A4	100	103.91	100.11	73.25	714.26
	CYP2D6	100	115.06	56.70	110.5	124.07
HBVP	ABCG <sub>2</sub>	100	52.38	257.14	67.95	280.52
	ABCB <sub>1</sub>	100	3.55	222.12	24.08	193.76
	CYP3A4	100	108.11	158.96	218.44	243.61
	CYP2D6	100	149.54	210.12	304.63	385.55
HBMEC	ABCG <sub>2</sub>	100	146.71	186.97	211.83	244.59
	ABCB <sub>1</sub>	100	130.52	180.93	161.05	287.37
	CYP3A4	100	57.33	74.85	88.82	122.47
	CYP2D6	100	141.26	187.75	250.23	327.15

## 4.2.4 Activity levels of efflux transporters

Most of the drugs given for the treatment of glioma such as etoposide, doxorubicin, and vinblastine, which permeate through the BBB, are actively effluxed by transporters. This leads to poor bio-availability of drugs at the tumour site, therefore it is essential to evaluate not only the expression but also the activity of the efflux transporters. After determining the expression of protein levels of the efflux transporters, activity levels were also studied in standard tissue culture conditions of 10 % FBS, no ECM and then compared to altered culturing conditions 5 % HS or the three different types of ECM to determine if the activity could be maximised.

### 4.2.4.1 Activity of efflux transporters in standard tissue culture conditions.

The cell lines, primary cultures and short term cultures were assessed for the activity of the efflux transporters, ABCB<sub>1</sub> and ABCG<sub>2</sub>, using an efflux assay kit. The cells were loaded with fluorescent substrate dyes and incubated at 37 °C. The cells were washed and measured for fluorescence after 60 min to determine the concentration of dye extruded from the cell. The control comprised of cells loaded with the dye incubated at 4 °C, the activity of efflux transporters is inhibited at 4 °C. Approximately 2.5 x 10<sup>5</sup> cells were used each test to assess the activity of ABCB<sub>1</sub> and ABCG<sub>2</sub>. The values obtained were RFU of the substrate dye not effluxed out from the cell. The inverse of that was calculated and was plotted % relative to control, which did not show any fluorescence since the efflux transporters were inhibited.

As seen from Figure 4.20 A, the highest activity of ABCB<sub>1</sub> transporter was 56.6 % in HBMEC cells, the other primary cultures HA and HBVP showed similar activity level compared to HBMEC. The cell lines showed lower activity when compared to short term

cultures. The lowest activity recorded was 9.4 % in SVGp12 cells. The short term cultures BTNW370 and BTNW914 showed relative efflux activity of 22.3 % and 17.2 % respectively. The endothelial cell line hCMEC/D3 showed activity levels of 36.8 % which was low in comparison to the short-term endothelial culture HBMEC showing 56.69 % activity. The activity of ABCB<sub>1</sub> was higher in short-term cultures HBVP and HA, compared to the cell lines and this was comparable to the expression of ABCB<sub>1</sub> studied in Section 4.2.3.1.

Activity of ABCG<sub>2</sub> transporter was observed as seen in Figure 4.20 B, the highest activity of ABCG<sub>2</sub> was 56.72 % in the HBMEC short-term culture. HBMEC and HA. The cell lines and the short term cultures showed similar activity levels of ABCG<sub>2</sub> transporter. The lowest efflux activity of 18.1 % was observed in the SVGp12 cell line. The activity levels were high in primary cultures; HBMEC, HA and HBVP which were used to develop the *in vitro* BBB model.

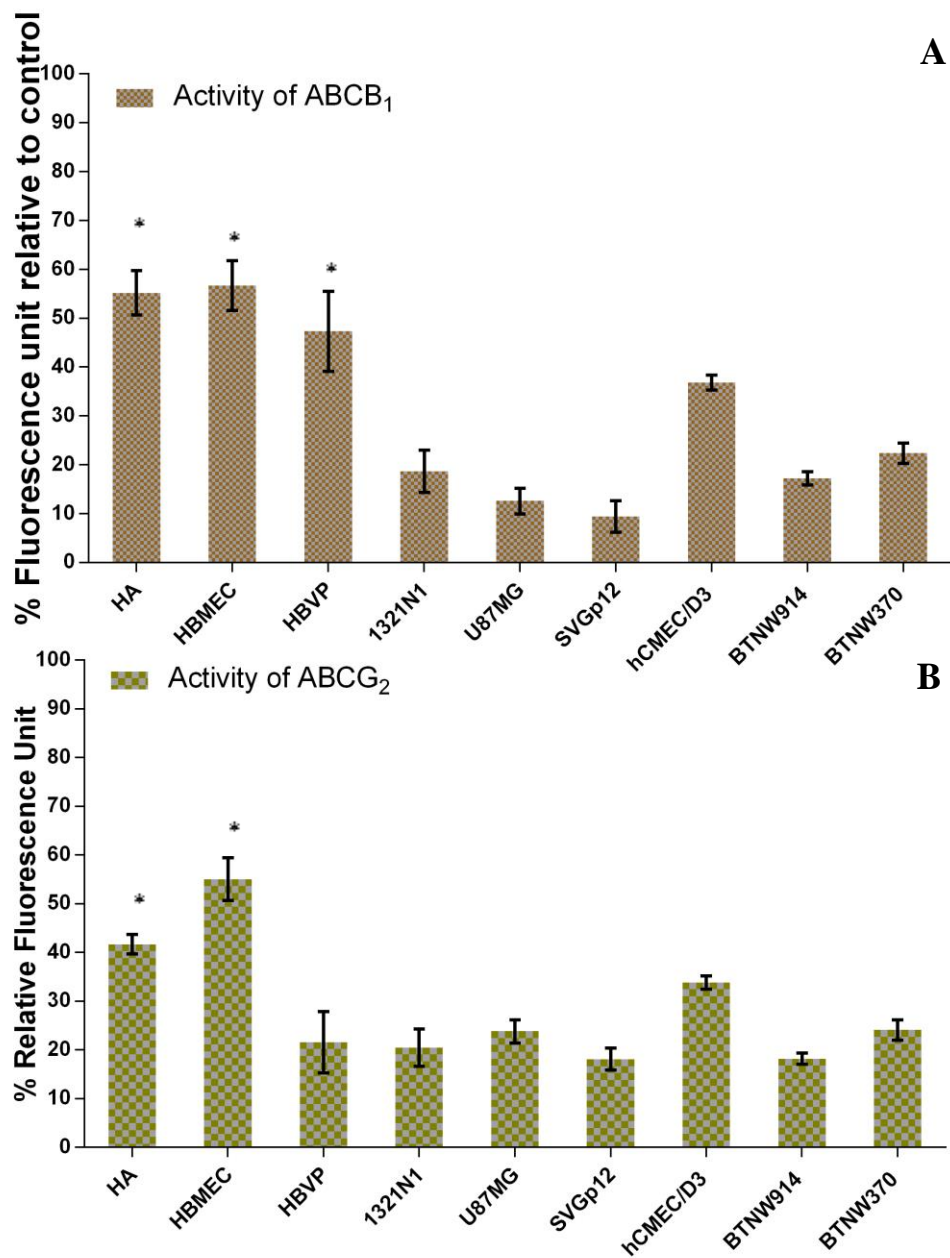


Figure 4.20 Activity of efflux transporters in different cells.

**A:** Activity of ABCB<sub>1</sub> transporter **B:** Activity of ABCG<sub>2</sub> transporter. The graphs were plotted as percentage relative to the control which was 0 % activity of the efflux transporter. The data points are means of three replicates (n=3) and the error bars represent  $\pm$  standard deviation ( $\pm$ SD) of three inter-experimental \*  $p < 0.05$  was considered to be statistically significant.

#### 4.2.4.2 Activity of efflux transporters in altered culturing conditions

Different culturing conditions were assessed with respect to the activity of the efflux transporters; ABCB<sub>1</sub> and ABCG<sub>2</sub> and DMEs; CYP3A4 and CYP2D6. In standard culturing conditions the primary cultures were grown in 10 % FBS without ECM. The altered culturing condition included culture with 5 % HS without ECM and in the presence of ECM, MaxGel, poly-L-lysine and fibronectin.

As seen in Figure 4.21 for the U87MG cell line, the activity of ABCB<sub>1</sub> was 14.3 % when cultured in standard tissue culture conditions in a monolayer with medium supplemented with 10 % FBS relative to the control. The culturing of cells in human serum increased the activity increase to 17.6 % but not significantly. The activity of ABCB<sub>1</sub> shows a significant increase with the addition of ECM. The highest efflux activity was 30.1 %, which was observed in cells grown in fibronectin. The other extracellular matrices also showed an increase in efflux activity to 22.8 % for poly-L-lysine and 25.1 % for MaxGel™ (Figure 4.21 A).

As seen in Figure 4.21 B, the highest activity for ABCG<sub>2</sub> was seen in U87MG cells grown in fibronectin 47.2 %. Cells grown on the other matrices also showed a significant increase in efflux activity when compared to the cells grown in FBS for example poly-L-lysine helped increase efflux activity to 40.5 % activity and MaxGel™ to 38.8 %. The cells, when cultured in human serum, showed an increase in efflux activity from 24.7 % to 30.1 % (Figure 4.21 B).

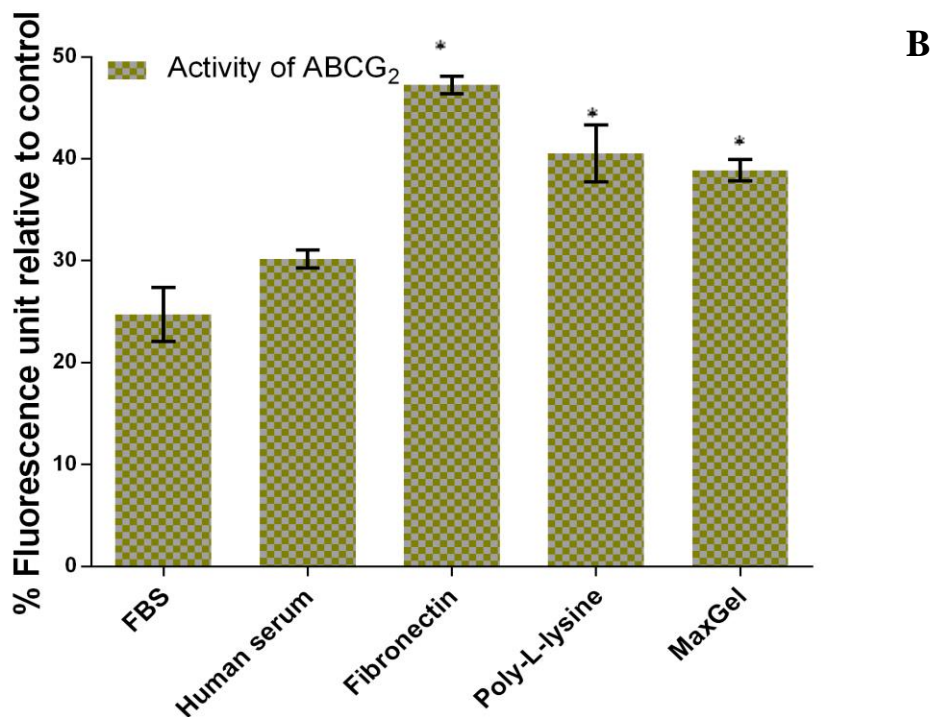
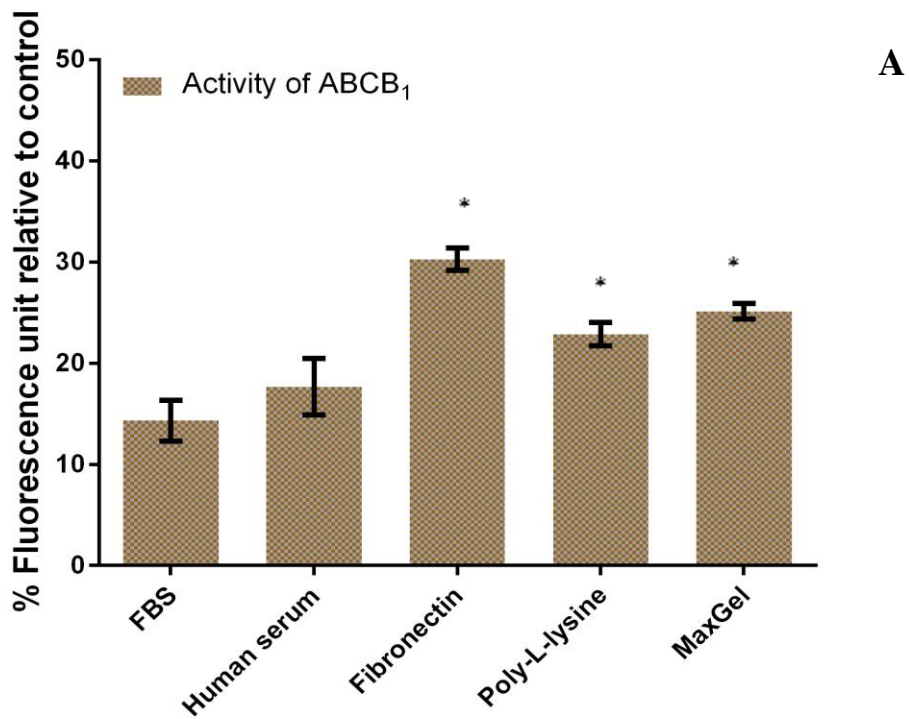


Figure 4.21 Activity of efflux transporters in U87MG cells (grade IV glioma).

**A.** Activity of ABCB<sub>1</sub> transporter **B.** Activity of ABCG<sub>2</sub> transporter. The graphs were plotted as percentage relative to the control which was 0 % activity of the efflux transporter. The data points are means of (n=2) experiments conducted in triplicate and repeated twice and the error bars represent  $\pm$  standard deviation ( $\pm$ SD) of six measurements from two experimental replicates \* p < 0.05 was considered to be statistically significant.

As seen in Figure 4.22 for the 1321N1 cell line, the activity of ABCB<sub>1</sub> was 18.2 % when cultured in standard tissue culture conditions in monolayer with medium supplemented with 10 % FBS. The culturing of cells in human serum did not significantly alter efflux activity. The activity of ABCB<sub>1</sub> showed a significant increase with the addition of ECM where in the presence of fibronectin, efflux increased to 39.6 %, in the presence of poly-L-lysine and MaxGel™ activity increased to 31.2 % and 30.2 % respectively (Figure 4.22 A).

As seen in Figure 4.22 B, the highest activity of ABCG<sub>2</sub> was 43.2 % shown by 1321N1 cells grown in fibronectin. Other matrices also showed an increase in the activity where in the presence of poly-L-lysine and MaxGel™ activity was 35.5 and 38.1 % respectively. The cells, when cultured in human serum, showed an increase in the activity of ABCG<sub>2</sub> from 22.2 % to 26.8 %, but this was not significant (Figure 4.22 B).

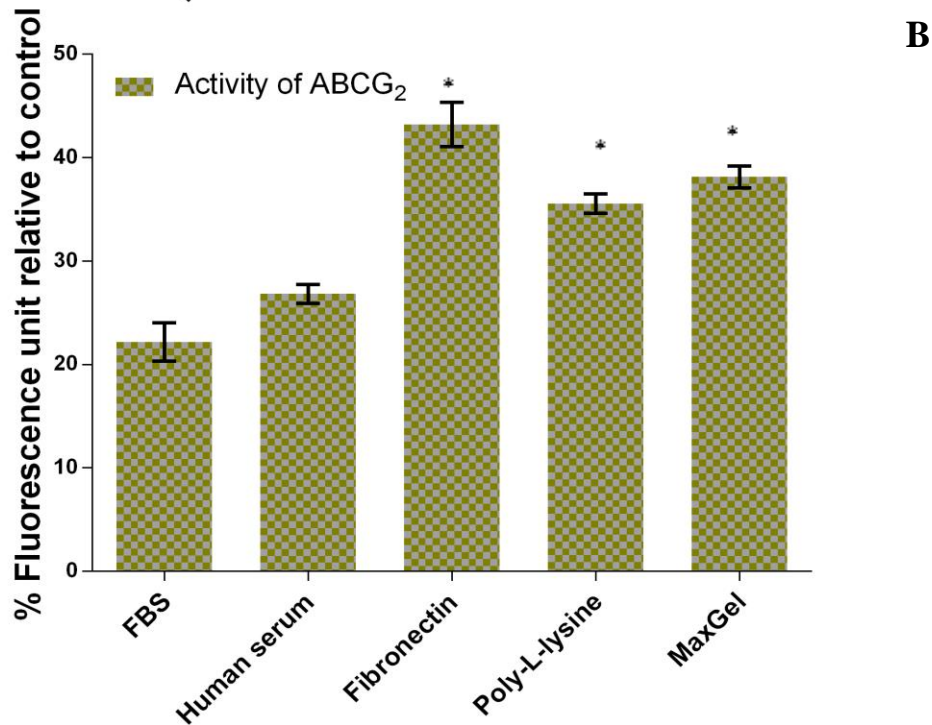
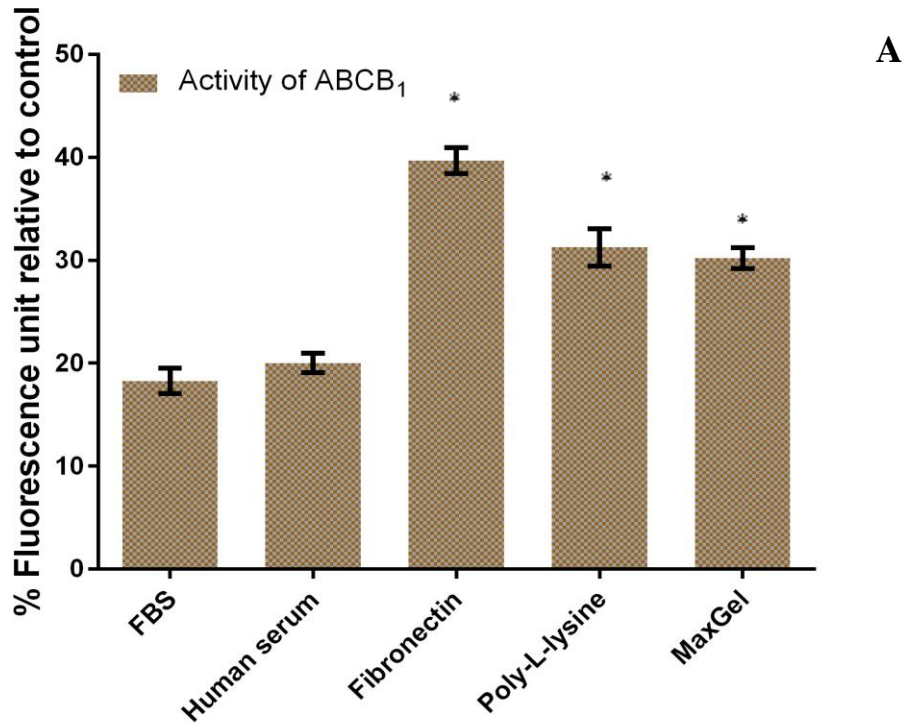


Figure 4.22 Activity of efflux transporters in 1321N1 cells (grade IV glioma).

**A.** Activity of ABCB<sub>1</sub> transporter **B.** Activity of ABCG<sub>2</sub> transporter. The graphs were plotted as percentage relative to the control which was 0 % activity of the efflux transporter. The data points are means of three replicates from two experimental repeats (n=2) and the error bars represent  $\pm$  standard deviation ( $\pm$ SD) six measurements from two experimental replicates. \* p < 0.05 was considered to be statistically significant

As seen in Figure 4.23 in the SVGp12 cell line, the activity of ABCB<sub>1</sub> was 9.2 % when cultured in standard tissue culture conditions in monolayer with medium supplemented with 10 % FBS. The culturing of cells in human serum did not significantly enhance efflux activity. The activity of ABCB<sub>1</sub> showed a significant increase with the addition of ECM in the culturing conditions. The highest activity was 22.2 % which was observed in cells grown in fibronectin. The cells in the presence of other extracellular matrices also showed an increase in the activity, to 16.1 % in the presence of poly-L-lysine and 16.7 % activity in the presence of MaxGel™ (Figure 4.23 A).

As seen in Figure 4.23 B, the highest activity of ABCG<sub>2</sub> was seen in SVGp12 cells grown in fibronectin 38.3 %. The other matrices also showed a significant increase in the activity as compared to the cells grown in FBS. Cells grown on poly-L-lysine showed 31 % efflux activity and on MaxGel™ showed 32.3 % activity. The cells when cultured in human serum showed an increase in the activity of ABCG<sub>2</sub> from 18.9 % to 23.0 % (Figure 4.23 B).

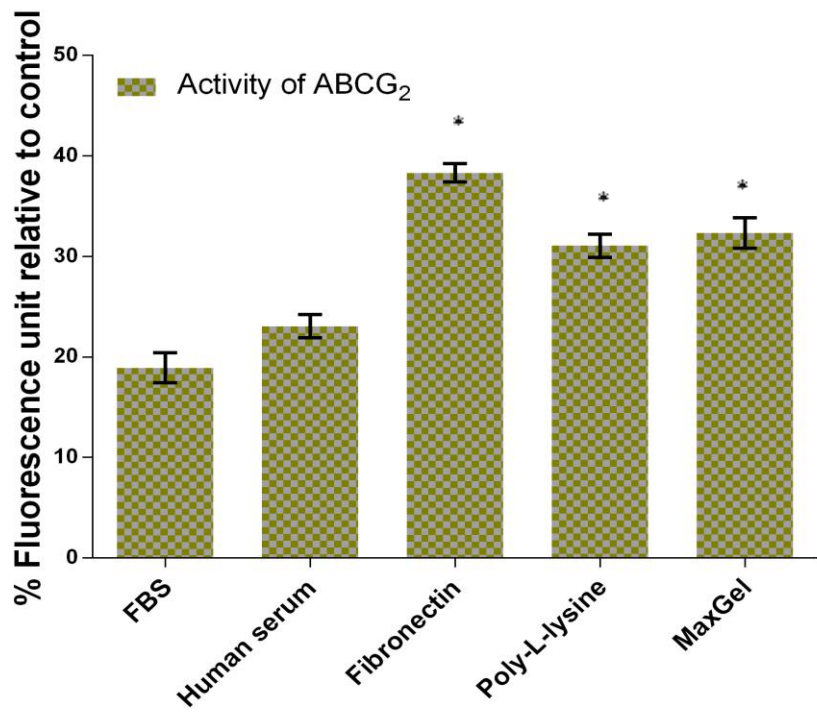
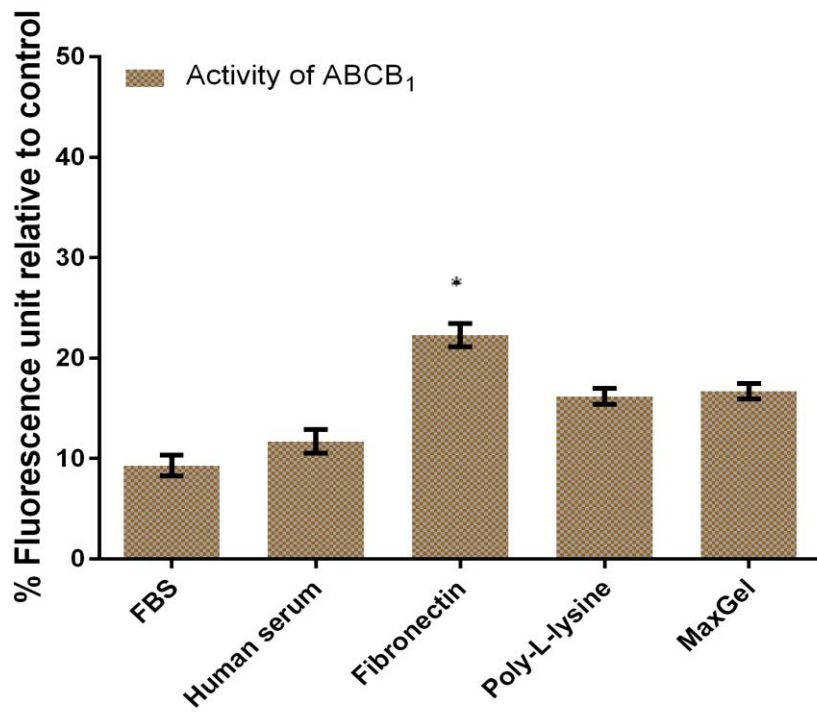


Figure 4.23 Activity of efflux transporters in SVGp12 cells (foetal glial cells)  
**A.** Activity of ABCB<sub>1</sub> transporter **B.** Activity of ABCG<sub>2</sub> transporter. The graphs were plotted as percentage relative to the control which was 0 % activity of the efflux transporter. The data points are means of three replicates from two experimental repeats and the error bars represent  $\pm$  standard deviation ( $\pm$ SD) six measurements from two experimental replicates. \*  $p < 0.05$  was considered to be statistically significant

As seen in Figure 4.24 in HBMEC short-term cultures, the activity of ABCB<sub>1</sub> was 55.7 % when cultured in standard tissue culture conditions in monolayer with medium supplemented with 10 % FBS. The culturing of cells in human serum did not make any significant change in the activity of transporter. The activity of ABCB<sub>1</sub> showed a significant increase with the addition of fibronectin in to 78.1 %. The addition of other extracellular matrices did not show much increase in the activity when compared to fibronectin. Poly-L-lysine showed an increase to 63.4 % and MaxGel™ showed 67.5 % activity of ABCB<sub>1</sub> efflux transporter (Figure 4.24 A).

As seen in Figure 4.24 B, the highest efflux activity of ABCG<sub>2</sub> was seen in HBMEC cells grown in fibronectin 82.3 %. The other matrices also showed a significant increase in the activity when compared to the cells grown in FBS, at similar activity levels; 65.3 % in the presence of poly-L-lysine and 66 % efflux activity in the presence of MaxGel™. The cells when cultured in human serum and FBS showed similar activity levels of ABCG<sub>2</sub>; 55.1 % and 55.9 % respectively (Figure 4.24 B).

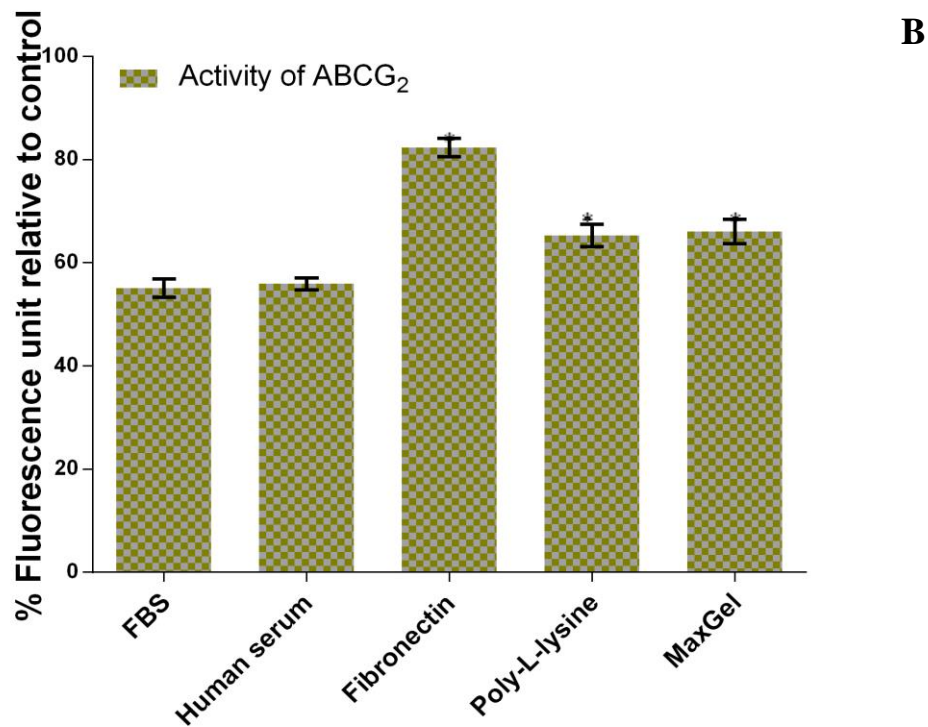
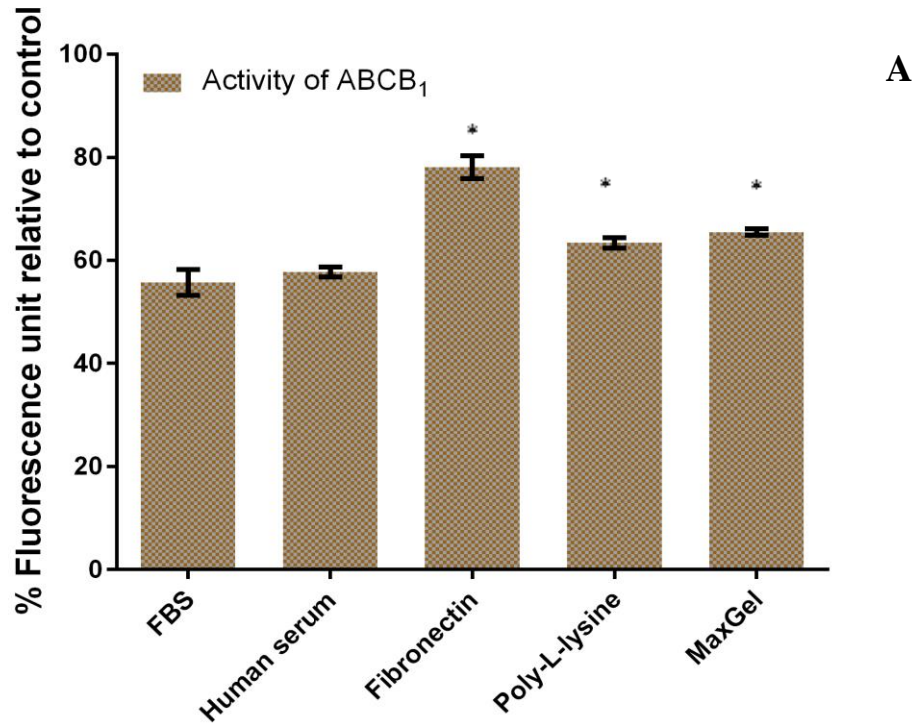


Figure 4.24 Activity of efflux transporters in HBMEC.

**A.** Activity of ABCB<sub>1</sub> transporter **B.** Activity of ABCG<sub>2</sub> transporter. The graphs were plotted as percentage relative to the control which was 0 % activity of the efflux transporter. The data points are means of three replicates from two experimental repeats and the error bars represent  $\pm$  standard deviation ( $\pm$ SD) of six measurements from two experimental replicates. \*  $p < 0.05$  was considered to be statistically significant

As seen in Figure 4.25 for the HA short-term culture, the activity of ABCB<sub>1</sub> was 56.1 % when cultured in standard tissue culture conditions in monolayer with medium supplemented with 10 % FBS. The culturing of cells in human serum did not make a significant difference in the activity of transporter. The activity of ABCB<sub>1</sub> showed a significant increase with the addition of ECM in the culturing conditions. The highest activity was 70 % which was observed in cells grown in fibronectin. In the presence of other extracellular matrices efflux activity was 64.5 % for poly-L-lysine and 63.5 % for MaxGel™ showed 63.5 % (Figure 4.25 A).

As seen in Figure 4.25 B, the highest activity of ABCG<sub>2</sub> was seen in HA cells grown in fibronectin 74.9 %. The other matrices also showed a significant increase in the activity as compared to the cells grown in FBS. Cells grown on poly-L-lysine showed 69.7 % activity and MaxGel™ showed 59.3 % activity. The cells when cultured in human serum showed an increase in the activity of ABCG<sub>2</sub> from 41.2 % to 45.8 % compared to standard conditions (Figure 4.25 B).

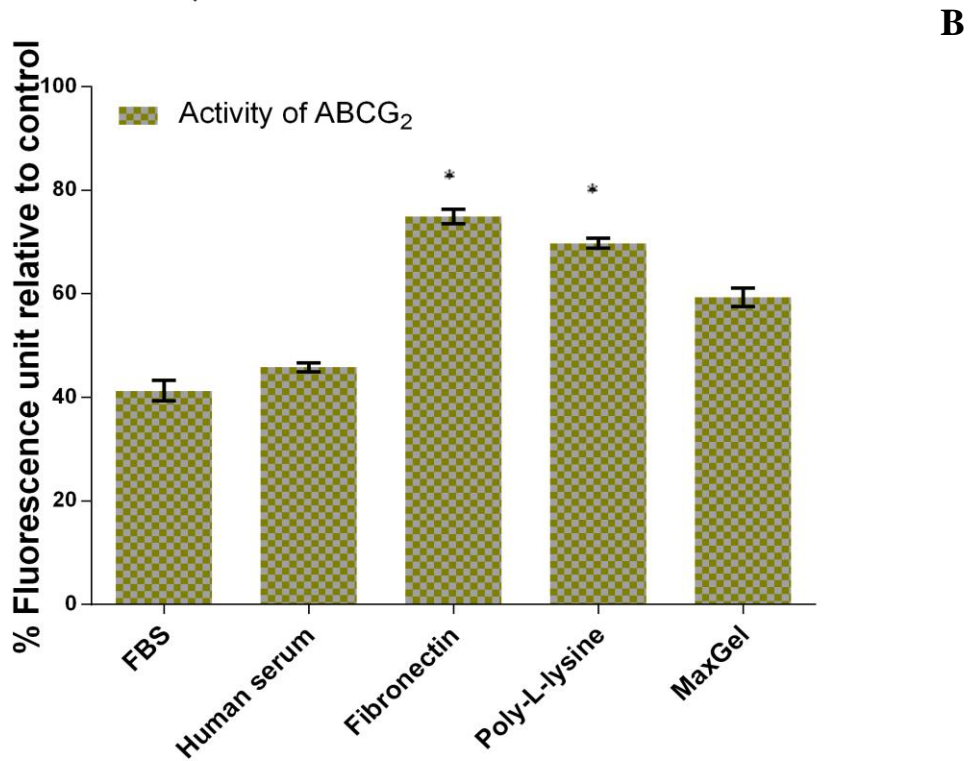
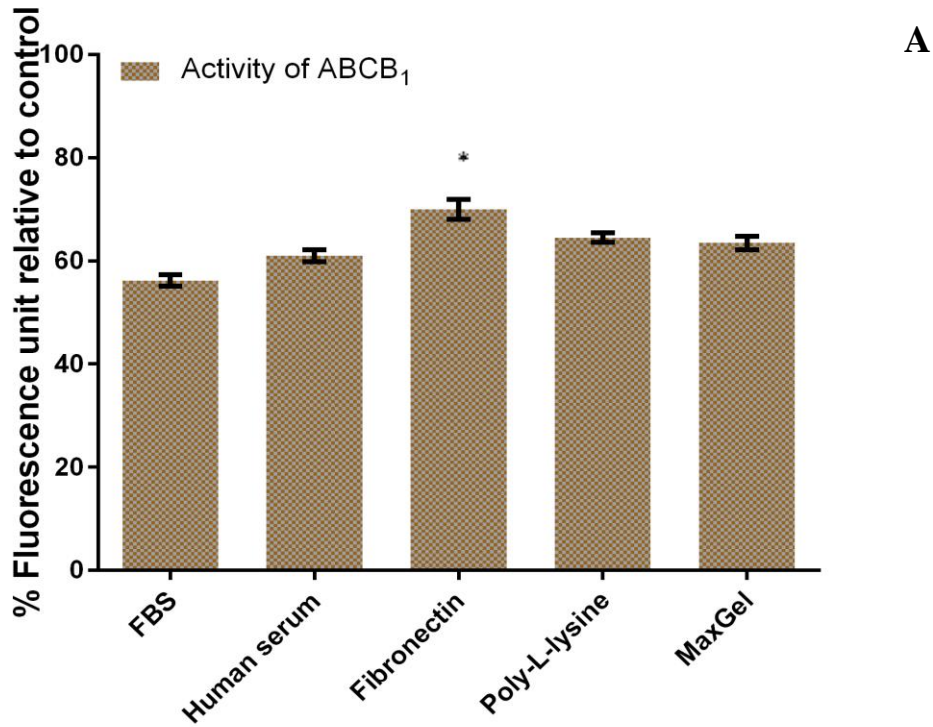


Figure 4.25 Activity of efflux transporters in HA cells.

**A.** Activity of ABCB<sub>1</sub> transporter **B.** Activity of ABCG<sub>2</sub> transporter. The graphs were plotted as percentage relative to the control which was 0 % activity of the efflux transporter. The data points are means of three replicates from two experimental repeats and the error bars represent  $\pm$  standard deviation ( $\pm$ SD) of six measurements from two experimental replicates. \*  $p < 0.05$  was considered to be statistically significant

As seen in Figure 4.26 for the HBVP cells, the activity of ABCB<sub>1</sub> was 47.3 % when cultured in standard tissue culture conditions in monolayer with medium supplemented with FBS. The culturing of cells in human serum did not make a significant difference to the efflux activity. The activity of ABCB<sub>1</sub> shows a significant increase with the addition of ECM in the culturing conditions. The highest activity was 77.1 % which was observed in cells grown in fibronectin. The other extracellular matrices also showed an increase in the activity, cells grown on poly-L-lysine showed 57.5 % and MaxGel™ showed 62.6 % activity of the ABCB<sub>1</sub> efflux transporter (Figure 4.26 A).

As seen in Figure 4.26 B, the highest activity of ABCG<sub>2</sub> was seen in HBVP cells grown in fibronectin 75.4 %. Cells grown on poly-L-lysine also showed a significant increase in the activity to 69.5 %. On the other hand MaxGel™ showed 50.6 % activity of efflux transporter which was not as high as the other extracellular matrices used. The cells, when cultured in human serum, showed a slight increase in the activity of ABCG<sub>2</sub> from 22.1 % to 26.5 %, however this was not significant (Figure 4.26 B).

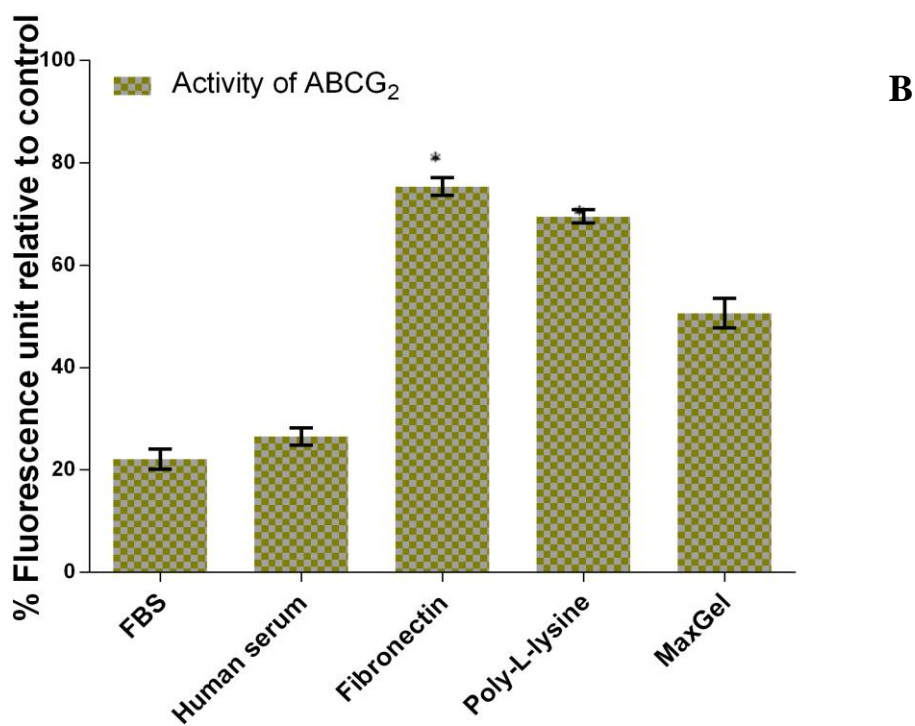
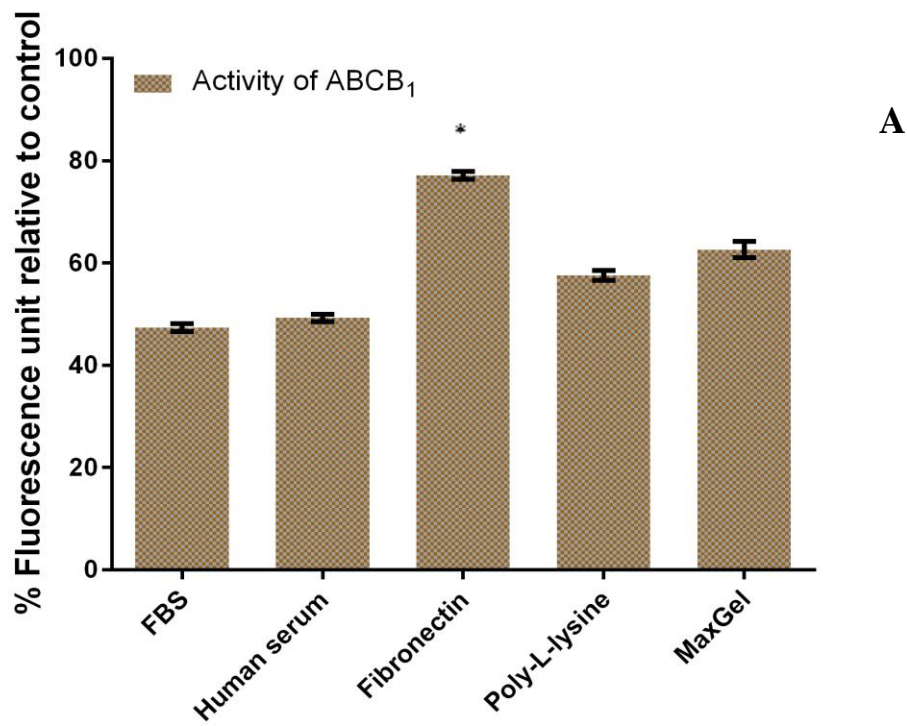


Figure 4.26 Activity of efflux transporters in HBVP cells.

**A.** Activity of ABCB<sub>1</sub> transporter **B.** Activity of ABCG<sub>2</sub> transporter. The graphs were plotted as percentage relative to the control which was 0 % activity of the efflux transporter. The data points are means of three replicates two experimental repeats and the error bars represent  $\pm$  standard deviation ( $\pm$ SD) of six measurements from two experimental replicates. \*  $p < 0.05$  was considered to be statistically significant

As seen in Figure 4.27 for the hCMEC/D3 cell line, the activity of ABCB<sub>1</sub> was 37.3 % when cultured in standard tissue culture conditions in monolayer with medium supplemented with FBS. The culturing of cells in human serum increased the activity of transporter to 40.5 % which was significant as compared to the activity by the different ECM. The activity of ABCB<sub>1</sub> shows a significant increase with the addition of ECM in the culturing conditions. The highest activity was 62.9 % which was observed in cells grown in fibronectin. The other extracellular matrices also showed an increase in the activity, cells grown on poly-L-lysine showed 53.4 % and MaxGel™ showed 50.9 % activity of ABCB<sub>1</sub> efflux transporter (Figure 4.27 A).

As seen in Figure 4.27 B, the highest activity of ABCG<sub>2</sub> was seen in hCMEC/D3 cells grown in fibronectin 60.3 %. The other matrices also showed a significant increase in the activity when compared to the cells grown in FBS. Cells grown on poly-L-lysine showed 46.5 % activity and MaxGel™ showed 49.2 % activity of efflux transporter. The cells when cultured in human serum did not show a significant increase in the activity of ABCG<sub>2</sub> (Figure 4.27 B).

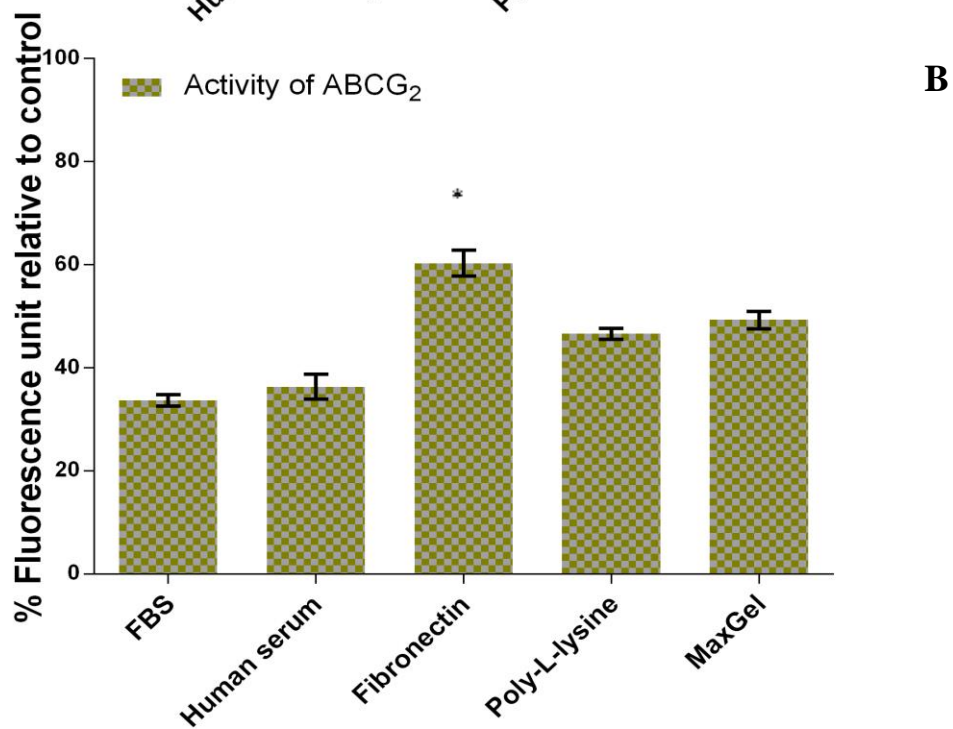
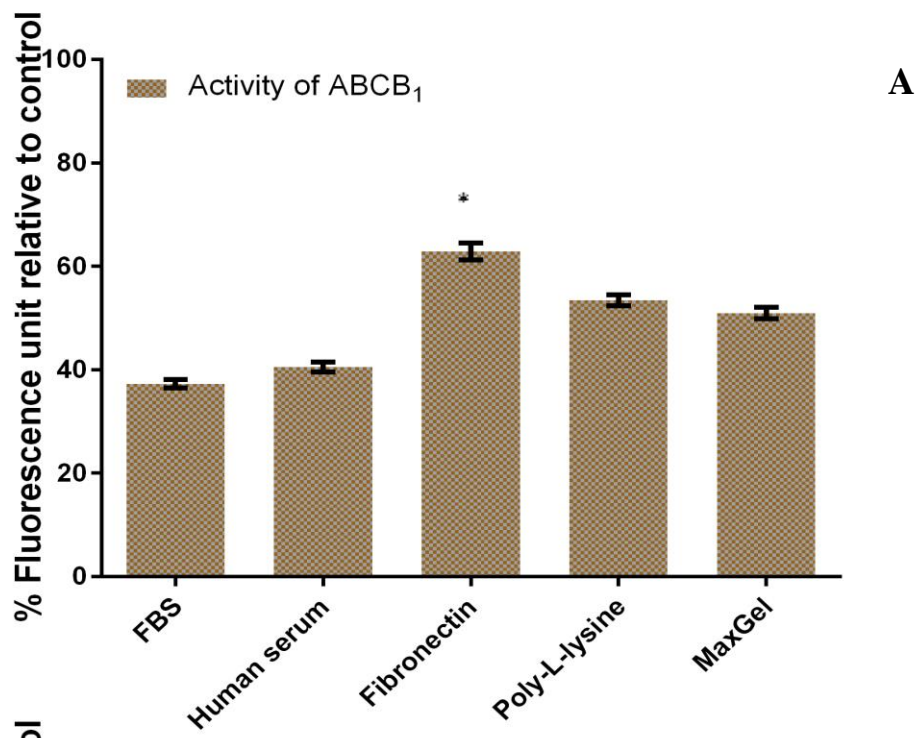


Figure 4.27 Activity of efflux transporters in hCMEC/D3 cells.

**A.** Activity of ABCB<sub>1</sub> transporter **B.** Activity of ABCG<sub>2</sub> transporter. The graphs were plotted as percentage relative to the control which was 0 % activity of the efflux transporter. The data points are means of three replicates two experimental repeats and the error bars represent  $\pm$  standard deviation ( $\pm$ SD) of three six measurements from two experimental replicates. . \*  $p < 0.05$  was considered to be statistically significant

## 4.2.5 Activity levels of drug metabolising enzymes

Certain glioma drugs which reach the tumour site are metabolised by the CYP enzymes, present at the tumour site, leading poor bio-availability of the drug. It is essential to study both expression and the activity of these enzymes in cells to be able to predict therapeutic drug concentration at the site of action. The cell lines and short term cultures were assessed for the activity of the drug metabolising enzymes CYP3A4 and CYP2D6 using fluorescent probes 7-benzyloxy-4-trifluoromethylcoumarin (BFC) and 3-[2-(N,N-diethyl-N-methylammonium)ethyl]-7-methoxy-4-methylcoumarin (AMMC) respectively, by measurement of fluorescent metabolite formation. Prior to studying the activity of enzymes, the protein and substrate concentration was optimised to ensure that kinetic measurements were in the linear region of the reaction and no component was rate limited.

### 4.2.5.1 Standard curve of metabolite

A standard curve was required to derive the concentration of metabolite produced by the CYPs of interest. A standard curve of fluorescence versus metabolite concentration for either, 7-hydroxy-4-trifluoromethylcoumarin (HFC) in Figure 4.28 or 3-[2-(N,N-diethyl-N-methylammonium) ethyl]-7-hydroxy-4-methylcoumarin (AHMC) in Figure 4.29 was plotted and the linear line of best fit was fitted. The fluorescence emission readings/ min from the kinetic experiments were converted into rate of metabolite formation per min by dividing by the slope of the linear line of best fit from standard curve as described in Section 2.6.3.2.

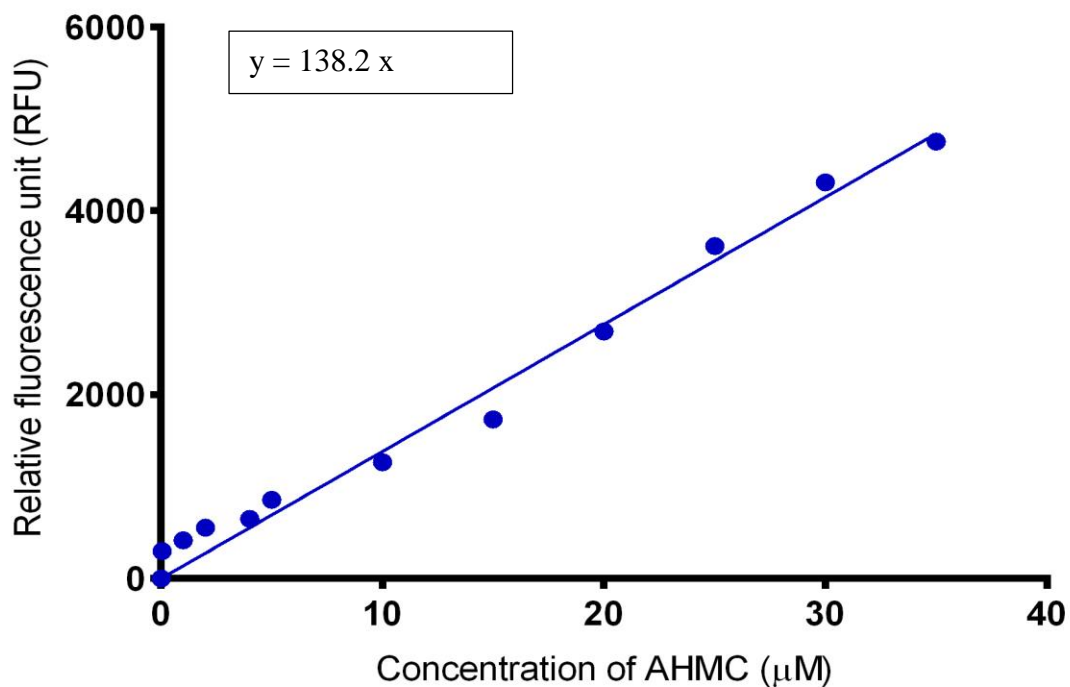


Figure 4.28 Standard plot of concentration of fluorescence *verses* AHMC metabolite concentration.

The excitation wavelength was 310 nm and emission wavelength was 410 nm. The data points are means of three replicates (n=3) and the error bars represent  $\pm$  standard deviation ( $\pm$ SD) of three inter repeats of an experiment.

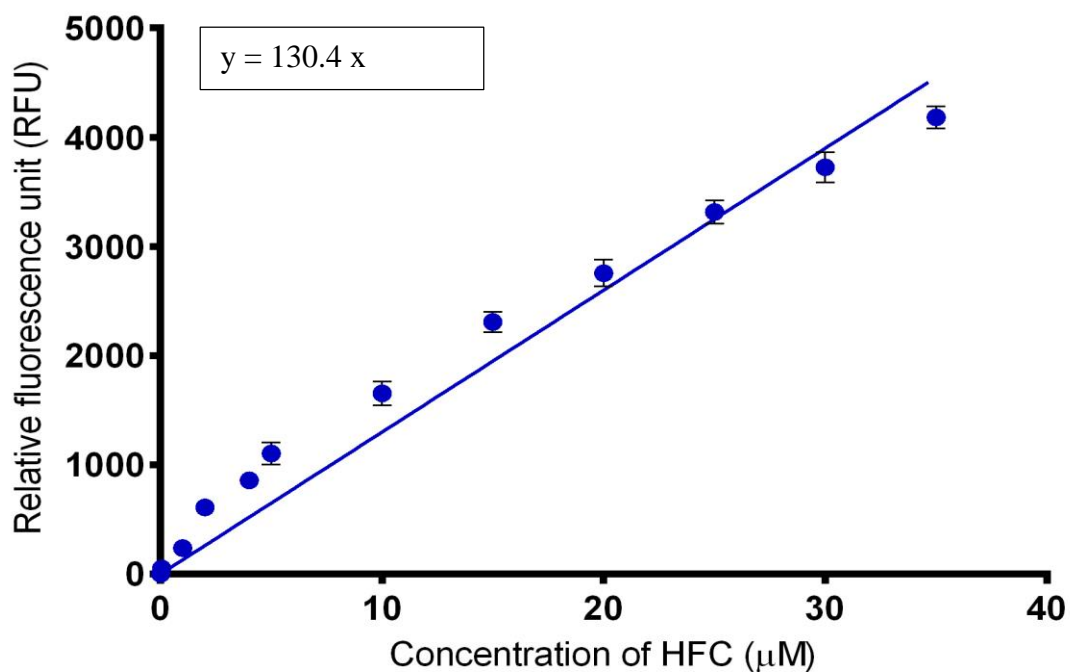


Figure 4.29 Standard plot of concentration of fluorescence *verses* metabolite HFC.

The excitation wavelength was 390 nm and emission wavelength was 460 nm. The data points are means of three replicates (n=3) and the error bars represent  $\pm$  standard deviation ( $\pm$ SD) of three inter-experimental repeats.

#### 4.2.5.2 Protein linearity optimisation

When protein concentration and hence enzyme concentration is increased, the rate of metabolite formation will increase up to a certain point until the substrate becomes rate limited, therefore the rate of metabolite formation will slow. The purpose of the next study was to characterise the linear relationship between the protein concentration and metabolism at a set substrate concentration (25  $\mu\text{M}$ ), and to determine the concentration at which linearity of metabolism was lost. A range of protein concentrations between 0.1 mg/ml to 1 mg/ml were investigated. The bacosomes were used as a protein source and the activity was measured every 30 seconds over 25 min as shown in

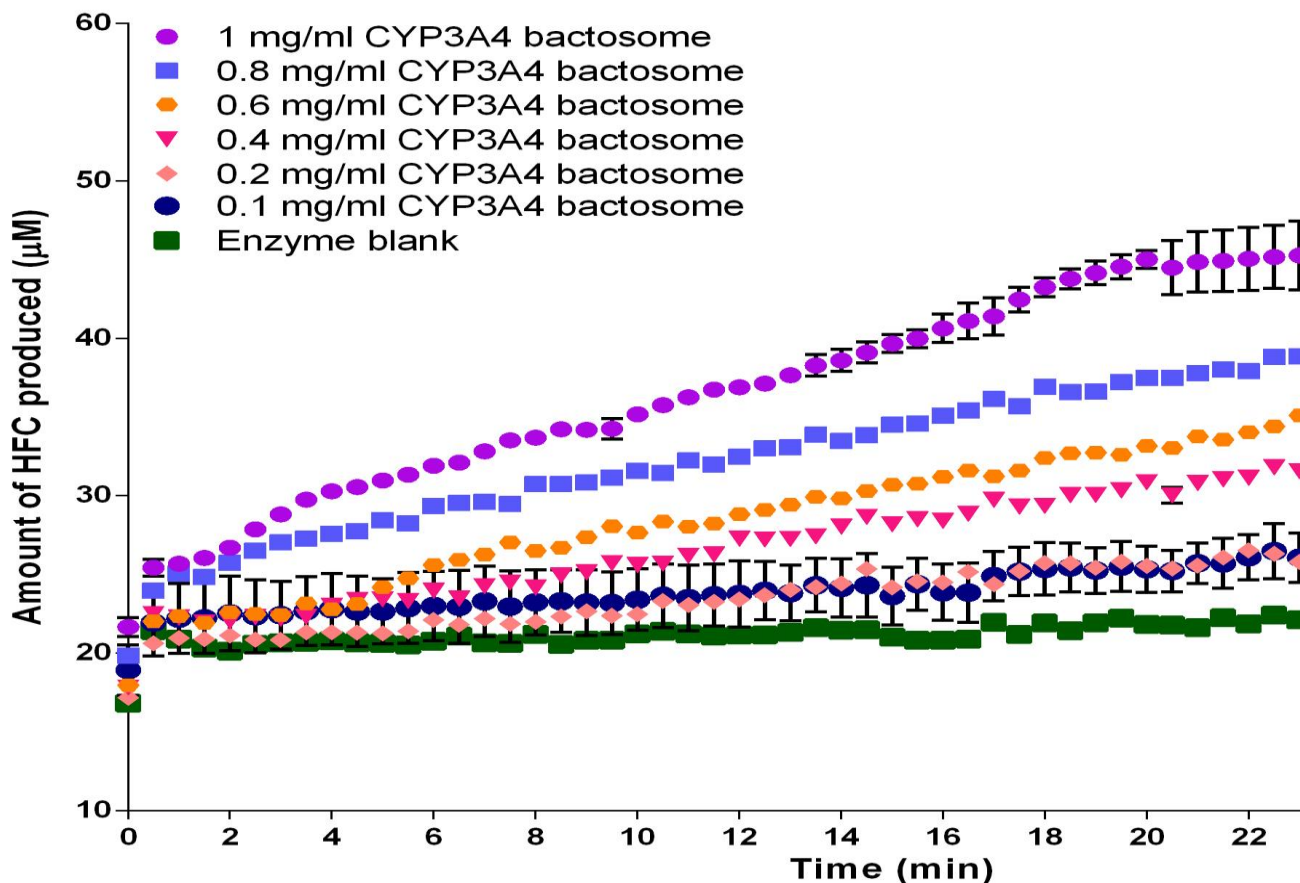


Figure 4.30 for CYP3A4 and Figure 4.31 for CYP2D6. The rate of metabolite formation was calculated with respect to bacosomes concentration as shown for CYP3A4 and CYP2D6.

The optimum protein concentration selected was 1 mg/ml for both CYP3A4 and CYP2D6, as this was within the linear region of the reaction.

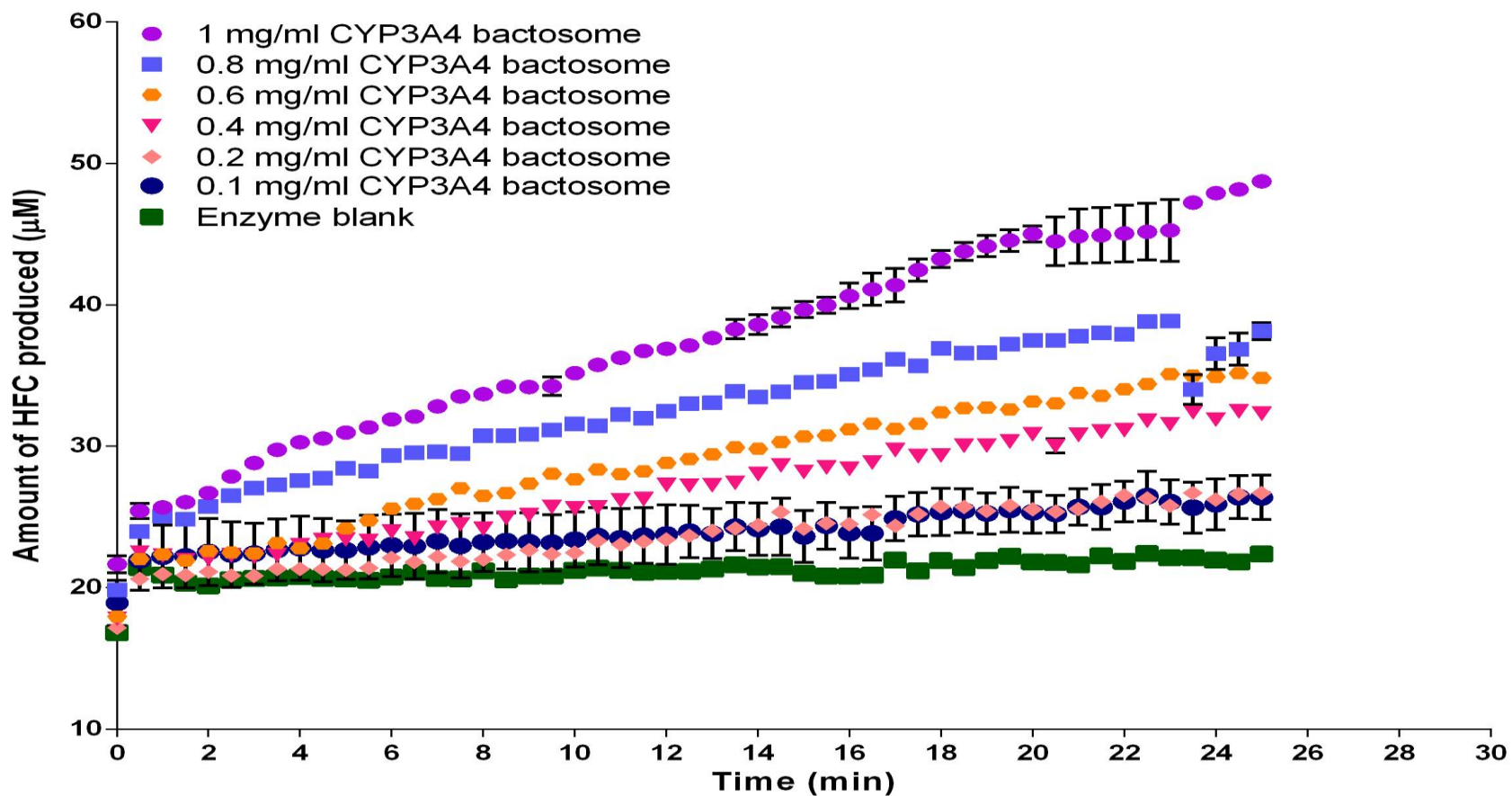


Figure 4.30 Activity of CYP3A4 metabolism of BFC to HFC at different protein concentration in bacosomes.

Fluorescent HFC metabolite formation following BFC metabolism by CYP3A4. The enzyme blank was used as the negative control. The data points are means of three replicates (n=3) and the error bars represent  $\pm$  standard deviation ( $\pm$ SD) of three inter-experimental repeats.

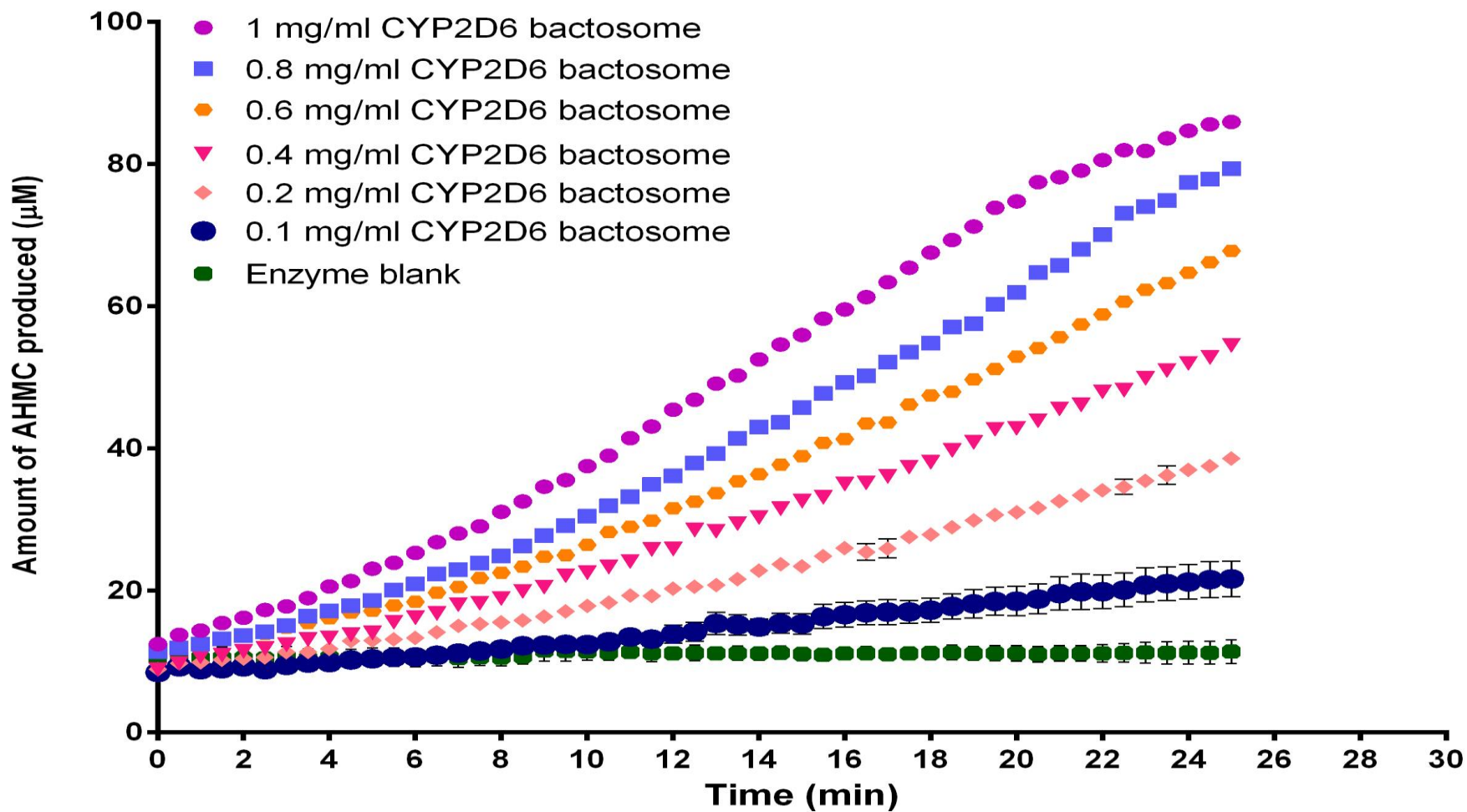


Figure 4.31 Activity of CYP2D6 metabolism of AMMC to AHMC at different protein concentrations of bacosome.

Fluorescent AHMC metabolite formation following metabolism of AMMC by CYP2D6. The enzyme blank was used as the negative control. The data points are means of three replicates (n=3) and the error bars represent  $\pm$  standard deviation ( $\pm$ SD) of three inter-experimental repeats.

### 4.2.5.3 Substrate linearity optimisation

When substrate concentration is increased, the rate of metabolite formation will increase up to a certain point until the CYP enzyme active site becomes saturated, thereafter the rate of metabolite formation will slow. A range of substrate (BFC or AMMC) concentrations between 0.1  $\mu\text{M}$  to 150  $\mu\text{M}$  was used to optimise the substrate linearity experiment. The bacosomes were used as protein source at a concentration of 1 mg/ml (optimised from the previous experiment) and the activity was measured every 30 seconds over 25 min as seen in Figure 4.32 A for CYP3A4 and Figure 4.32 B for CYP2D6. The rate of metabolite formation was calculated and plotted with respect to substrate concentration as shown for CYP3A4 and CYP2D6 in Figure 4.33A and B. It was concluded that 25  $\mu\text{M}$  of substrate concentration should be used for all the enzyme kinetic studies, as the reaction was still linear at this point.

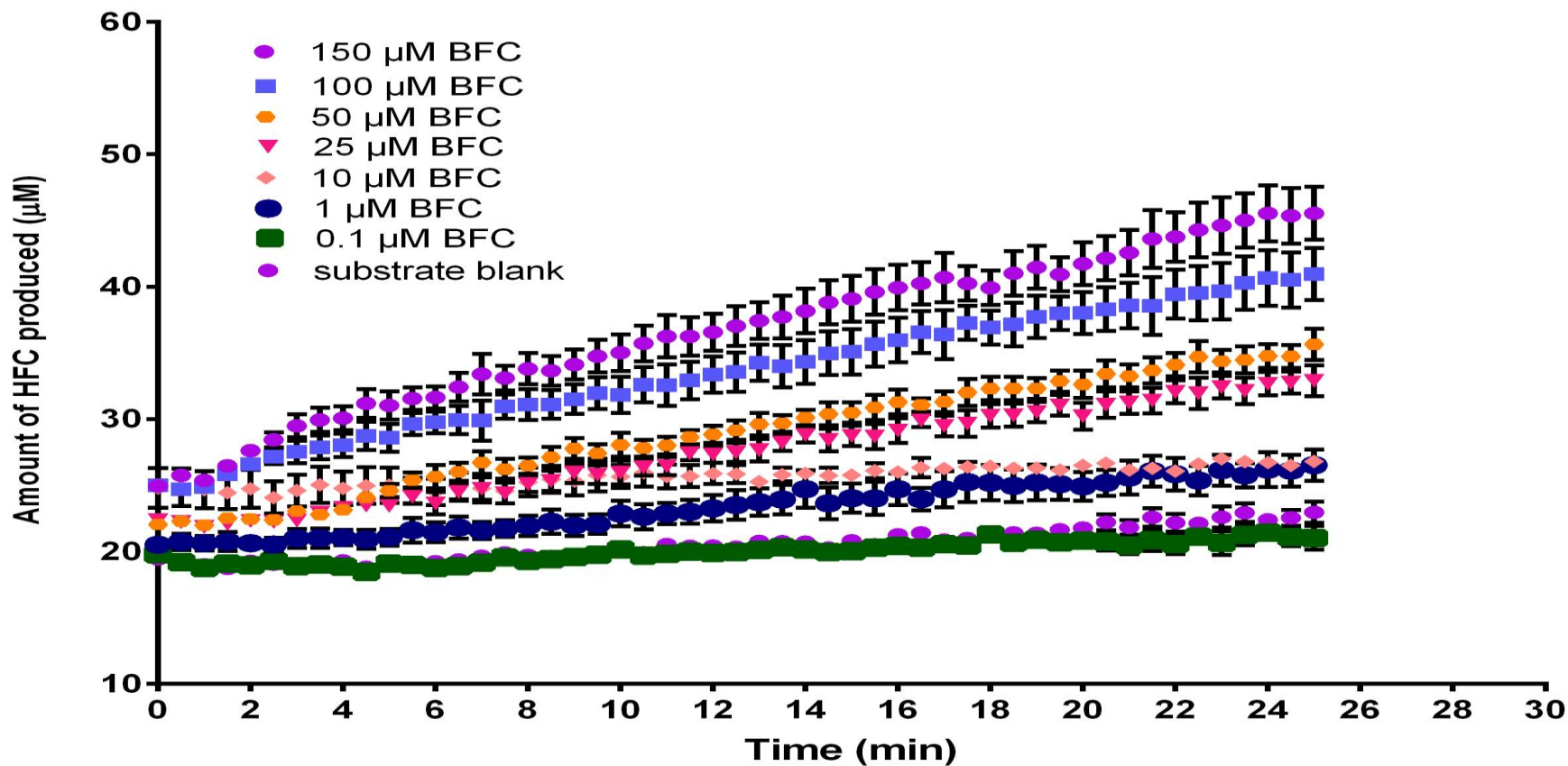


Figure 4.32 A Activity of CYP3A4 enzyme at different BFC substrate concentration with respect to time

Fluorescent HFC metabolite formation following BFC metabolism by CYP3D4. The substrate blank was used as the negative control. The data points are means of three replicates (n=3) and the error bars represent  $\pm$  standard deviation ( $\pm$ SD) of three inter-experimental repeats.

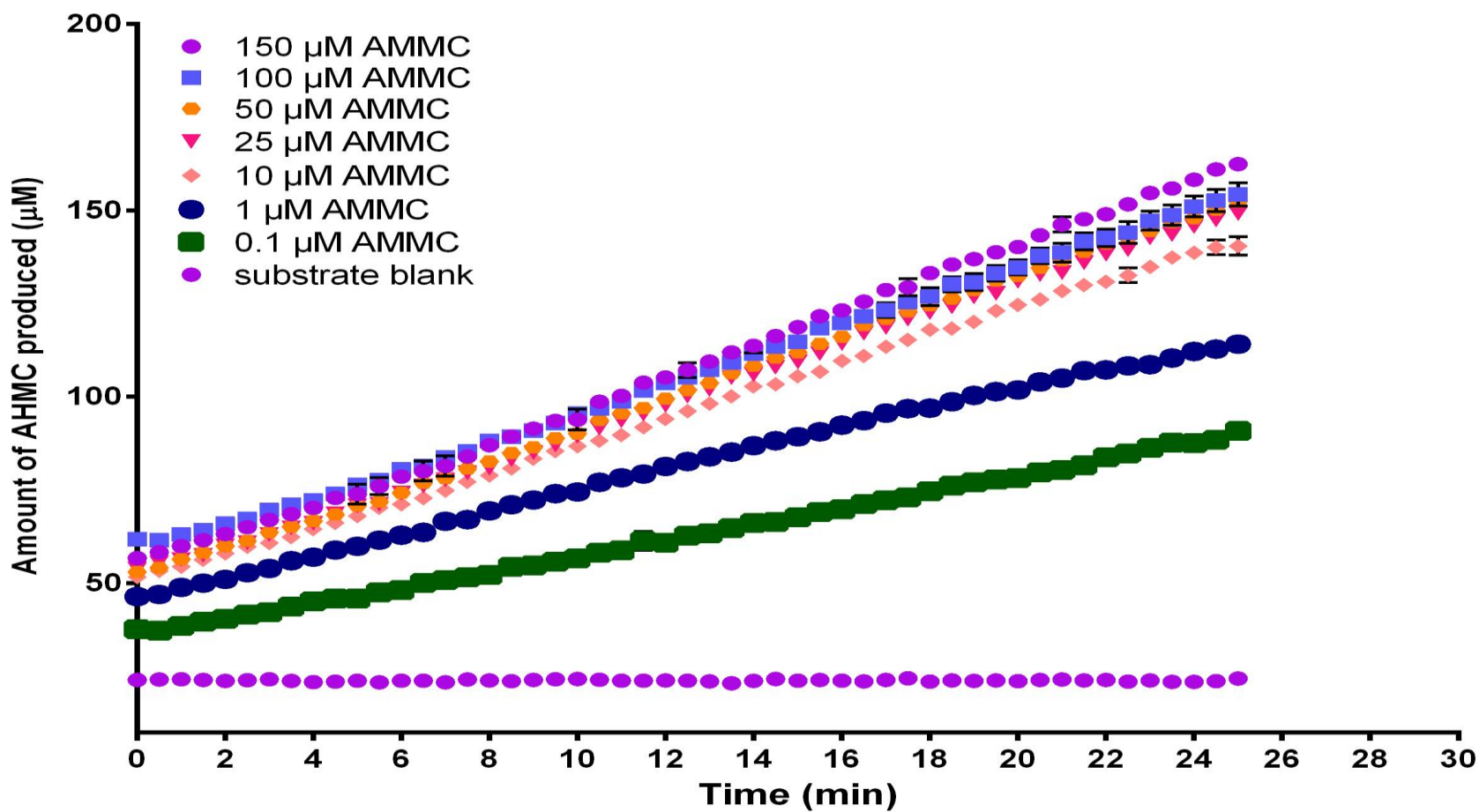


Figure 4.32 B: Activity of CYP2D6 enzyme at different AMMC substrate concentration  
 Fluorescence AHMC metabolite formation following metabolism of AMMC by CYP2D6. The substrate blank was used as the negative control. The data points are means of three replicates (n=3) and the error bars represent  $\pm$  standard deviation ( $\pm$ SD) of three inter-experimental repeats.

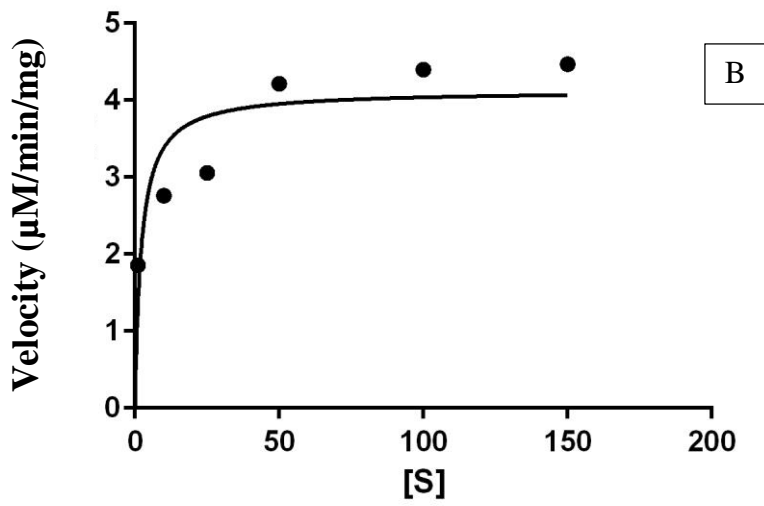
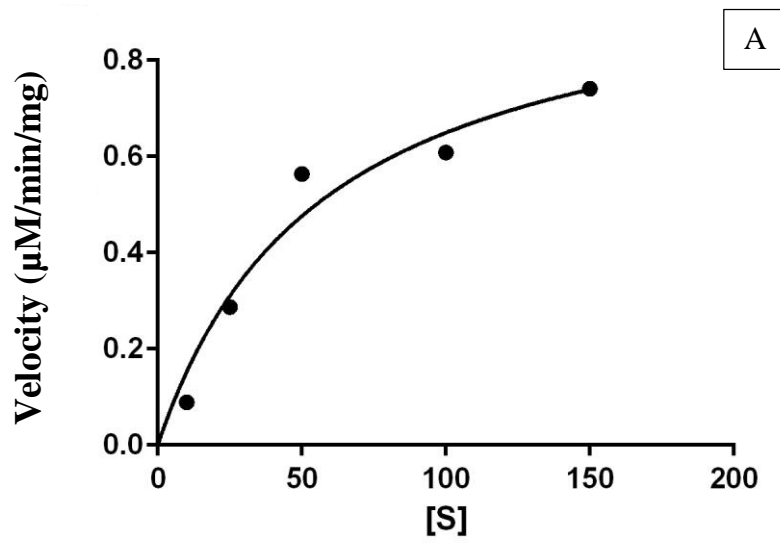


Figure 4.33 Michaelis Menton plot determining the rate of metabolism **A** CYP3A4 **B** CYP2D6

#### 4.2.5.4 CYP activity measurements in cell lines

The cell lines and short term cultures were grown in monolayer under standard conditions to an optimum cell number, yielding total protein concentration of 1 mg/ml in each well. The cells were incubated with the substrates (BFC or AMMC) at the optimum concentration of 25  $\mu$ M. The fluorescence of the metabolite (HFC/AHMC) formed in the wells was measured every 10 min up to 120 min at 37 °C [Adapted from (Donato *et al.*, 2004)]. As seen in Figure 4.34 and Figure 4.35, the fluorescent metabolite was measured and plotted against time and the rate of enzyme activity at 25  $\mu$ M substrate was determined.

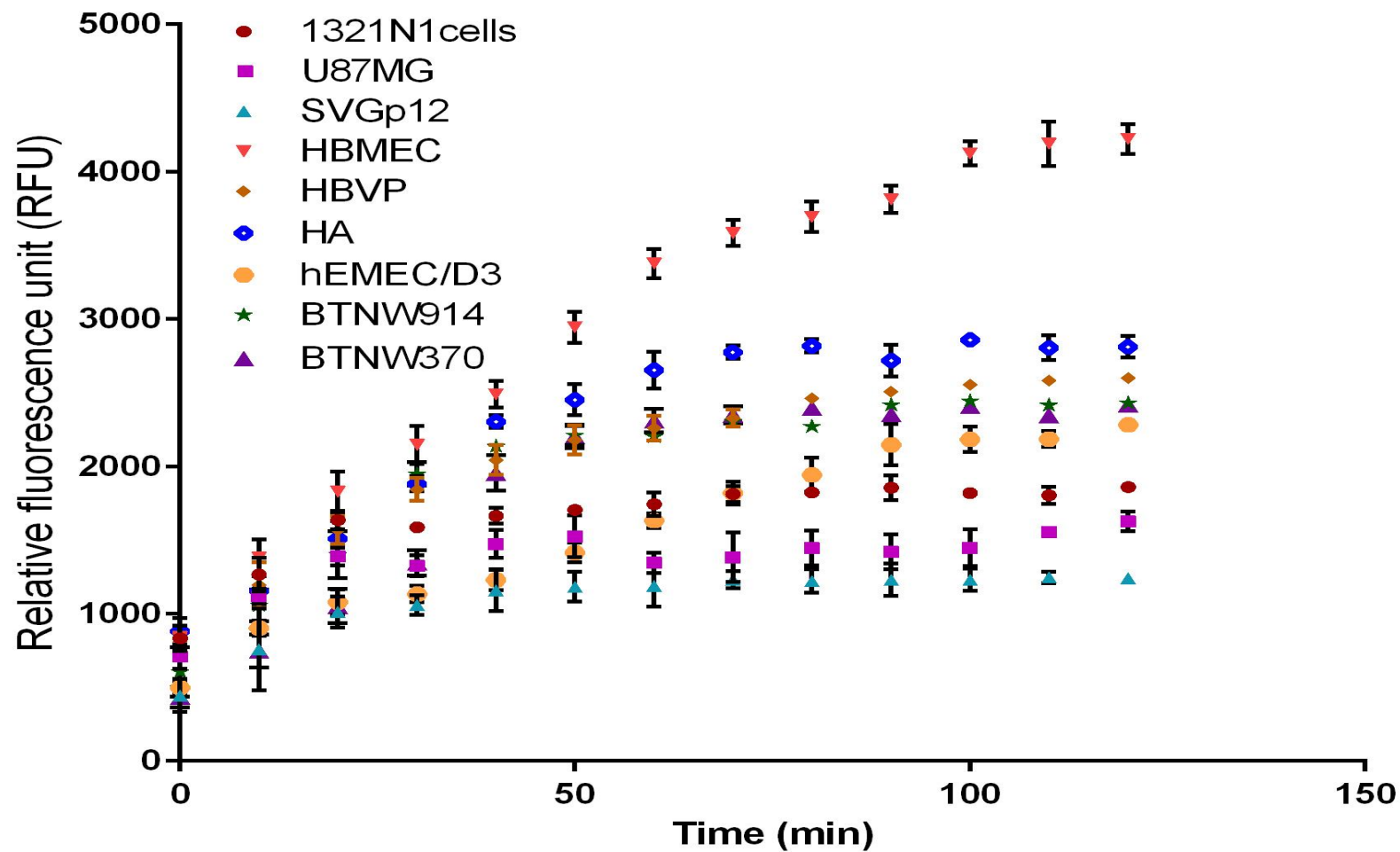


Figure 4.34 Activity CYP3A4 metabolism of 25  $\mu$ M BFC to HFC in 1 mg/ mL cell lines and short term cultures.

The metabolite HFC formation was measured at excitation wavelength 410 nm and emission wavelength 510 nm. The data points are means of three replicates (n=3) and the error bars represent  $\pm$  standard deviation ( $\pm$ SD) of three inter-experimental.

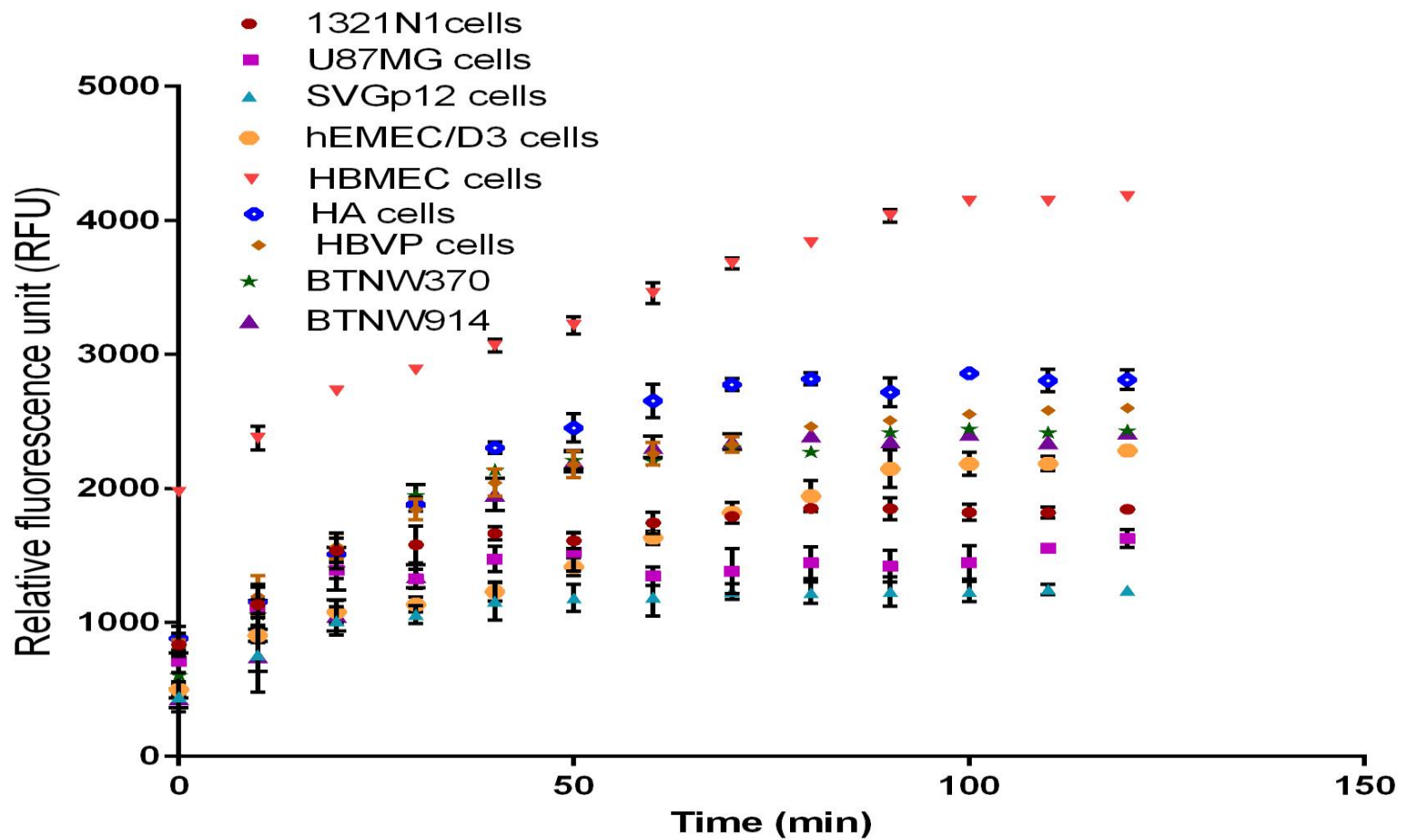
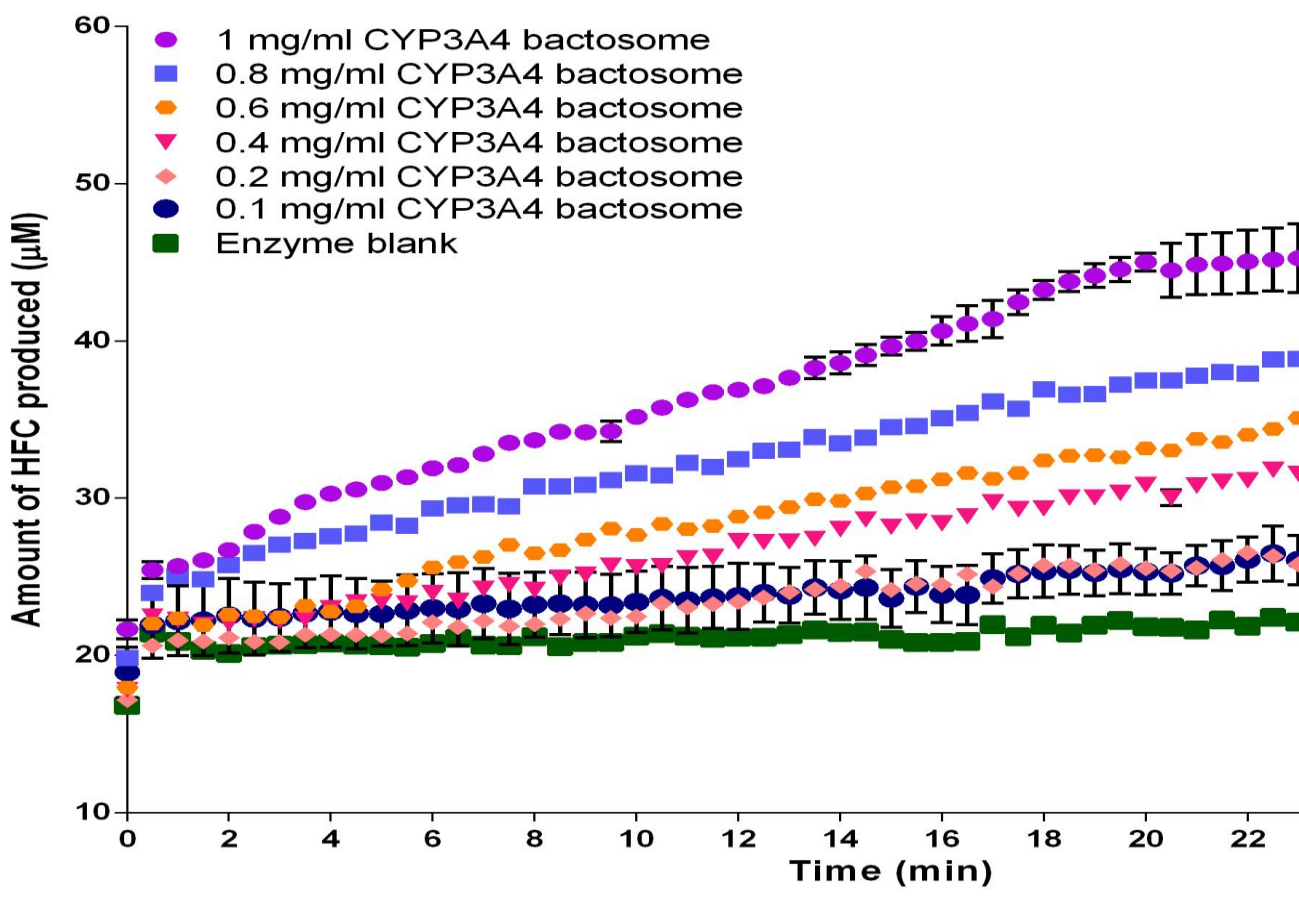


Figure 4.35 Activity CYP2D6 metabolism of 25 μM AMMC to AHMC in 1 mg/ml cell lines and short term cultures.

The metabolite AHMC formation was measured at excitation wavelength was 390 nm and emission wavelength was 460 nm. The data points are means of three replicates (n=3) and the error bars represent ± standard deviation (±SD) of three inter-experimental repeats.

After calculation of the rate of metabolism in each cell culture at 25  $\mu\text{M}$  (Table 4.3), the rate of metabolite formation was compared to relative metabolism in bacosomes at the same substrate and protein concentration (



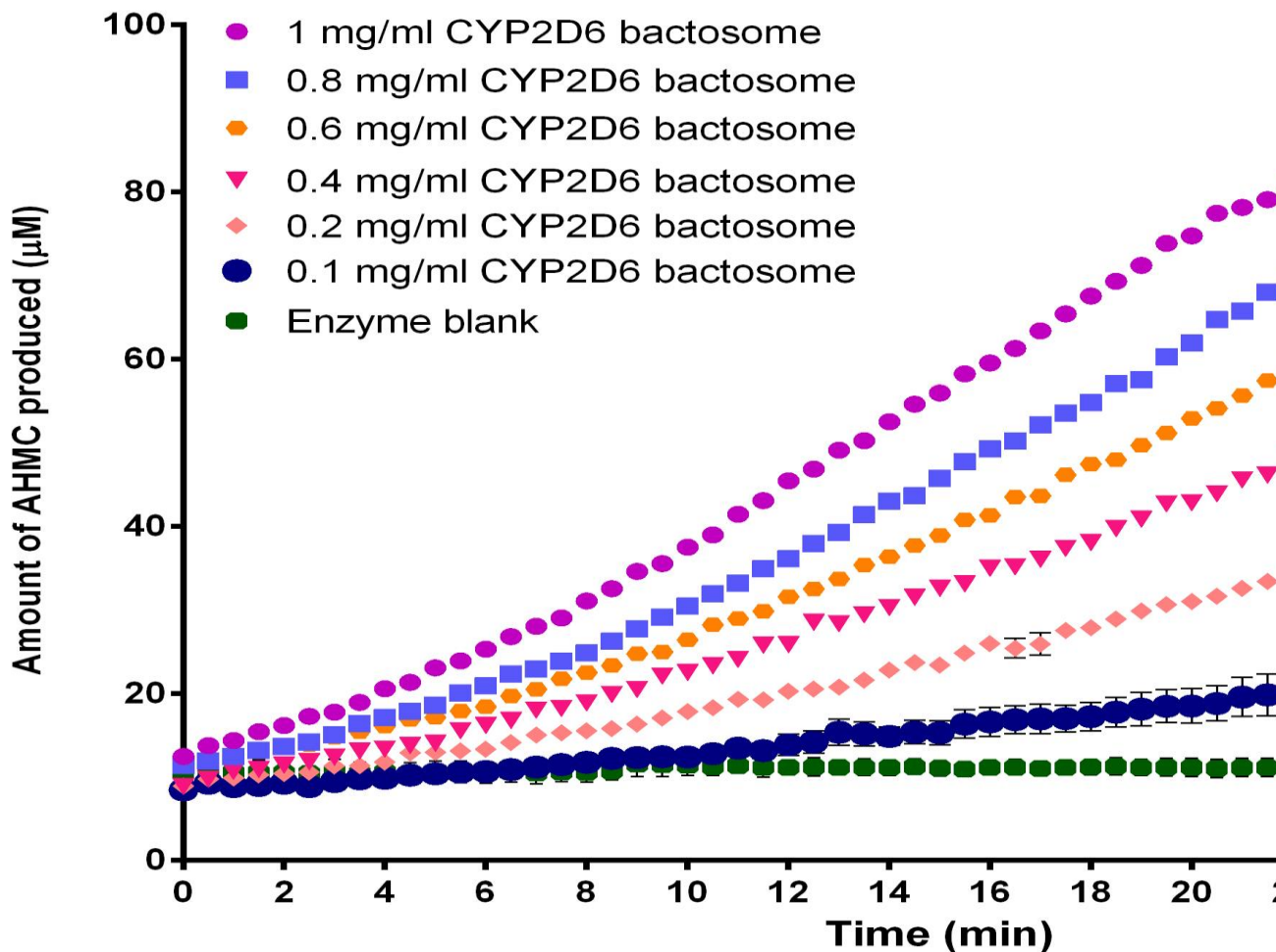


Figure 4.31).

Table 4.3 Rate of CYP3A4 and CYP2D6 enzyme at 25  $\mu\text{M}$  substrate concentration in cell lines, primary and short term cultures.

	CYP3A4	CYP2D6
Cell line/ primary cultures	Rate at 25 $\mu\text{M}$ [S] ( $\mu\text{M}$ HFC / min/ mg protein)	Rate at 25 $\mu\text{M}$ [S] ( $\mu\text{M}$ HFC / min/ mg protein)
1321N1	0.065	0.018
U87MG	0.019	0.019
SVGp12	0.017	0.016
HBMEC	0.286	0.156
HBVP	0.227	0.229

HA	0.249	0.231
hCMEC/D3	0.197	0.193
BTNW914	0.189	0.188
BTNW370	0.201	0.204

## 4.3 Discussion and conclusion

Over the last four decades, patients with glioma have shown poor prognosis when compared to patients with other cancer types such as colon cancer (Rachet *et al.*, 2009). The poor prognosis is largely due to ineffective treatment caused by poor bioavailability of the glioma therapeutics at the tumour site, which can be partly attributed to the efflux transporters and DMEs enzymes located at the site of tumour that play a crucial role in the drug disposition and metabolism (Parkinson *et al.*, 2006). In the current study, expression and activity of the efflux transporters; ABCB<sub>1</sub> and ABCG<sub>2</sub> and DMEs; CYP3A4 and CYP2D6 in glioma cell lines, short term cultures of endothelial cells, astrocytes and pericytes were determined in standard and altered tissue culturing conditions. It is well documented in hepatocyte studies that *in vitro* protein expression and activity of drug metabolising enzymes and transporters is lower than that observed *in vivo*, leading to under prediction of the extent drug metabolism (Baxter *et al.*, 2014; Galetin, 2014). To predict the drug disposition and metabolism, it is essential to use models that have expression and activity as close as possible in comparison to *in vivo* (Kuteykin-Teplyakov *et al.*, 2010). To ensure a physiologically relevant *in vitro* model is developed, experimental conditions were optimised to give the highest protein expression and activity levels.

The most critical step in protein analysis is the extraction of proteins and sample preparation (Chatterjee *et al.*, 2012), therefore the protein extraction protocol was optimised by trialling different techniques. From the Bradford assay, it was concluded that the lysing after scraping the cells from the culture dish on ice and trypsinisation of the cells both gave the highest protein yield. According to Huang *et al.*, (2010) trypsinisation of cells causes damage to the cell membrane, this could be relevant, since the current study involved looking at transmembrane transporter proteins (Huang *et al.*, 2010). To avoid, protein degradation,

scraping of cells from culture dishes was selected as the most appropriate and efficient protein extraction protocol.

There has been an extensive use of immortalised cell lines in biological experiments due to ease of use, reproducibility, faster growing properties and cheap cost. These cells are easy to maintain and can be cultured with desired properties using specific growth conditions. These cells are however prone to genotypic and phenotypic drifting which leads to the cells developing a phenotype different from the cells *in vivo* (Pan *et al.*, 2009; Stacey, 2001), resulting in misrepresentation of the tissue specific functions, leading to spurious results (Masters, 2000). The short-term cultures derived from primary cells in tissue explant, closely represent the properties of the tissue *in vivo*. These cells only grow up to a certain passage number before dedifferentiating and require specialised culturing conditions (Calatuzzolo *et al.*, 2005). The first protein expression study performed here confirmed that neither phenotypic drift or dedifferentiation had occurred as all of the CYPs and transporters were detectable in all of the cell lines used. Comparing immortalised and short-term cultures in the study here, it was found that under standard conditions short-term human astrocytes cultures and short term endothelial cells (HBMEC) had a higher expression of the CYPs and transporters compared to the immortalised counterparts SVGp12 and hCMED/D3 respectively. When comparing the glioma short term cultures (BTNW914 and BTNW370) with the immortalised glioma cell lines (U87MG and 1321N1), it was not so clear. CYP3A4 and ABCB<sub>1</sub> showed higher expression and CYP2D6 and ABCG<sub>2</sub> showed lower expression in the short-term cultures. Most of the papers have measured the expression in the form of mRNA levels. Lee *et al.*, (2007) reported the expression, localization and activity levels of efflux transporters ABCG<sub>2</sub> in brain endothelial cells of human and rat and glial cells. He observed that the expression and activity of ABCG<sub>2</sub> was higher in human endothelial cells

as compared to rat endothelial cells (Lee *et al.*, 2007). This was in unison if our findings of HBMEC (human endothelial cells) showing high expression of ABCG<sub>2</sub>. Virgintino *et al.* (2002), showed that expression of ABCB<sub>1</sub> in human endothelial cells was observed in the luminal membrane and the mRNA was detected in the cortex region (Virgintino *et al.*, 2002). There are limited reports in the literature about transporter and CYP protein expression in cells at the BBB and glioma. The expression of CYP has been described in the isolated rat brain and microvessels but as of now no data has been reported on the expression of CYP in the human BBB. Ghersi-Egea *et al.*, (1994) hypothesized that CYP enzymes are located primarily at blood-brain interfaces, where they form an enzymatic barrier. He reported the expression of CYP in isolated rat brain (Ghersi-Egea *et al.*, 1994). Dauchy *et al.* (2008), showed the activity of various different types of CYP in the microvessel of the brain.

No data was found in the literature for comparison on the expression and activity of CYP3A4, CYP2D6, ABCB<sub>1</sub> and ABCG<sub>2</sub> at the BBB *in vivo*. HBMEC, HA and HBVP showed higher expression of both the efflux transporters and the CYP enzymes compared to cell lines, thus these cells were short-listed as the component of the BBB model to be designed and were taken forward into the next study which was optimisation of experimental conditions to enhance protein expression.

When comparing protein expression in the cells grown in FBS to those grown in human serum, no significance difference was observed in any protein expression in HA, HBVP and HBMEC cultures. When ECM was added into the culture, an improvement was observed in all proteins expressed for all cell lines, most significantly and consistently for cells grown on fibronectin. The extracellular matrix (ECM), has been shown to play a complex and dynamic role in cellular functions such as structure, motility and proliferation. The addition of extracellular matrix (ECM) to the cells increased the cell adhesion and cell-cell communication (Ruoslahti, 1996). Numerous papers have attested the ability of ECM to

communicate both spatial and temporal information to the adhering cells (Rubenstein and Kaufman, 2008; Behonick and Werb, 2003; Ulrich *et al.*, 2009; Schlie-Wolter *et al.*, 2013; Ishihara *et al.*, 2008). Wolter *et al.* (2013), have shown that ECM affects cell adhesion dynamics, the formation of focal adhesion complexes, cell morphology, proliferation and intercellular communication. They also showed that when endothelial cells were cultured in fibronectin, it enhanced the cells attachment dynamics such as adhesion kinetic and force, formation of focal adhesion complexes, morphology, proliferation, and intercellular communication (Schlie-Wolter *et al.*, 2013). All the culture showed a change in the protein expression levels indicating that the culturing environment has an influence on the cell growth (Freshney, 2000).

The activity of efflux transporters in the cell lines indicated that primary cultures have a higher activity for efflux transporters as compared to cell lines. Veringa *et al.* (2013), reported the activity of ABCB<sub>1</sub> and ABCG<sub>2</sub> in glioma cultures. According to them, both the efflux transporters are functional and active at the BBB (Veringa *et al.*, 2013). It is essential to incorporate these components while designing an *in vitro* model. The activity was determined in various different culturing condition, cells cultured on fibronectin showed the highest activity. Anderson *et al.* (2002), reported the upregulated activity of ABCB<sub>1</sub> in rat endothelial cells is upregulated post radiation. No data in literature was found for comparing the activity of cells in altered culturing conditions. From the current results it was observed that the primary cells when cultured in 5 % human serum and in the presence of fibronectin as the ECM showed the highest activity for the efflux transporters ABCB<sub>1</sub> and ABCG<sub>2</sub>.

The activity of CYP3A4 and CYP2D6 was studied in all the cell lines and primary cultures. The activity was higher in primary cultures, the highest activity was observed in HBMEC primary culture. Donato *et al.* (2004), observed activity of various CYP isoforms on

hepatocytes and developed a robust activity measuring assay (Donato *et al.*, 2004). Rodriguez *et al.* (2002) reported a panel of CYP expression and activity for hepatocytes and hepatoma cell line. He also emphasised the point of loss expression or lower expression of CYP in cell lines. This supported our findings that the cell lines showed a low activity for CYP as compared to the primary culture. No data was found which utilised altered culturing conditions to increase the expression and activity to a maximal level. The data showed that the HBMEC primary culture showed the highest expression and activity for both the CYP enzymes; CYP3A4 and CYP2D6.

Despite the numerous models designed for the BBB, there has been no published BBB model having all components derived from human such as cells, ECM, serum that has been characterised for the expression and activity of CYP3A4, CYP2D6, ABCB<sub>1</sub> and ABCG<sub>2</sub>

Translating these findings here in to the design of the *in vitro* BBB model, fibronectin was chosen as the ECM to grow cells on, and short-term cultures HA, HBMEC and HBVP were chosen as the most suitable cell lines.

# CHAPTER 5

## 5. Development of the blood brain barrier model.

### 5.1 Introduction

The blood brain barrier (BBB) is a regulatory interface which restricts the transport of substances between the circulation and the central nervous system (Shawahna *et al.*, 2012). It is a complex system comprising of different cellular components such as endothelial cells, pericytes and astrocytes. Drug permeability across the BBB is an obstacle, challenging the development and success rate of neuropharmaceutical candidates (Poller *et al.*, 2008). *In vitro* models are invaluable tools for studying the BBB phenotype, signalling pathways and drug penetration into the brain. Many *in vitro* BBB models have been designed to study the underlying mechanism involved in the transport of therapeutics across the BBB. It has often been claimed that these *in vitro* models closely reflect the human BBB in terms of phenotype, restricted paracellular permeability, and functional transporters and enzymes (Lacombe *et al.*, 2011). Most *in vitro* models, however, use components from non-human species, which differ considerably in terms of intercellular tightness, active transport and metabolic activities (Chu *et al.*, 2013). These differences make it difficult to predict how a neuropharmaceutical candidate may permeate the brain and hence there is a need to develop an *in vitro* BBB model with components of human origin.

The endothelial cells form a compact layer ensheathing the blood capillaries and the presence of membrane proteins form TJs which exhibit high trans endothelial resistance. Trans-endothelial electrical resistance (TEER) is a key BBB characteristic, which provides the measurement of membrane potential, resistance and hence integrity of the BBB (Weksler *et al.*, 2013). The expression profile of efflux transporters largely determines permeability

properties and hence the study of expression profiles and functionality of efflux transporters and enzymes is an important requirement for the quality of the *in vitro* models (Wilhelm *et al.*, 2011b).

In this chapter, different co- and tri-culture models were designed and cultured mimicking the BBB *in vivo* using short term cell cultures of human origin. The designed models have been grown in different culture conditions to maximise the expression of tight junction proteins, endothelial resistance and determine the protein expression profiles of DMEs and efflux transporters. The aim of this study was to design a physiologically relevant and fully characterised BBB model that could be utilised to study the drug disposition in glioma in downstream experiments (Chapter 6).

## 5.2 Results

### 5.2.1 Validation of the TEER Instrumentation

Various co- and tri- culture models were set up as described in Section 2.8 on polycarbonate inserts to measure the TEER and expression of occludin and claudin. The first experiments were concerned with validating the EVOM instrument against the ECIS and CellZscope instruments for measuring TEER and secondly, deciding which endothelial cell line to include in the model, either the immortalised hCMEC/D3 or the short-term culture HBMEC. The immortalised endothelial cell line hCMEC/D3 was used in all validation experiments concerning TEER measurements due to ease of use.

## 5.2.1.1 TEER measurements of designed BBB models using EVOM

### 5.2.1.1.1 Assay validation for reproducibility

To assess the reproducibility of the TEER values made using the EVOM instrument, five measurements within each well were taken (Figure 5.1), to assess variability in permeability across the insert, then each culture was set up in triplicate and mean TEER taken across the three wells to give an indication of intra-assay variability (Figure 5.2). Finally, the experiment was repeated on three different occasions and the mean TEER was calculated to give an indication of inter-assay variability (Figure 5.3); which is the data reported in the results throughout the chapter.

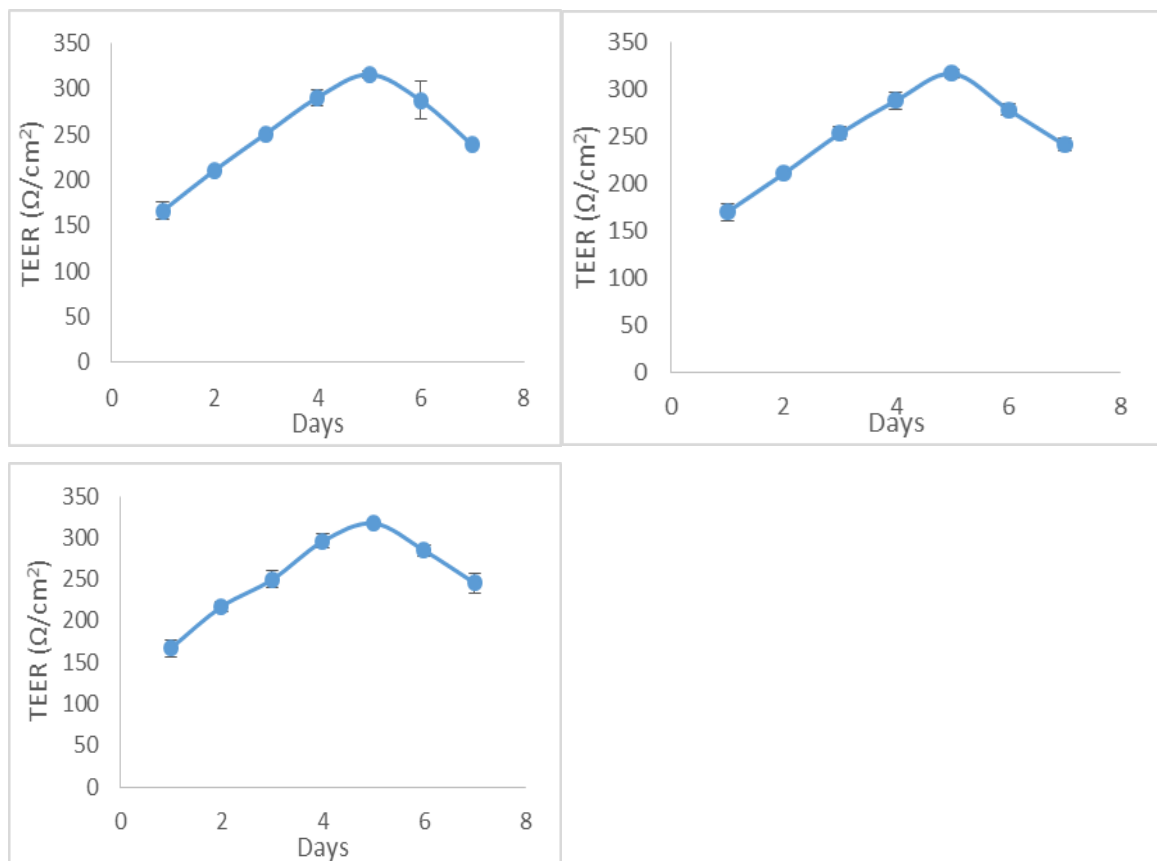


Figure 5.1 Mean of five measurements of TEER within each well

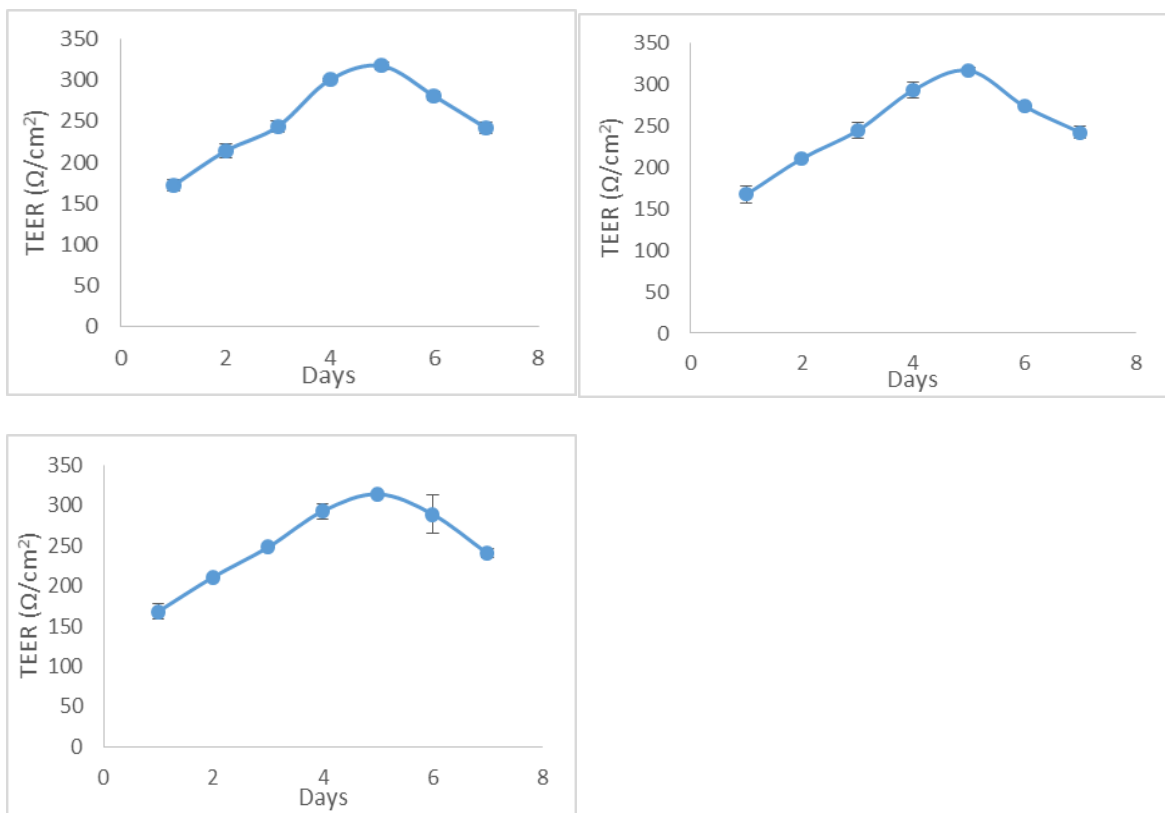


Figure 5.2 Mean of three measurements of TEER for intra-replicates of an experiment.

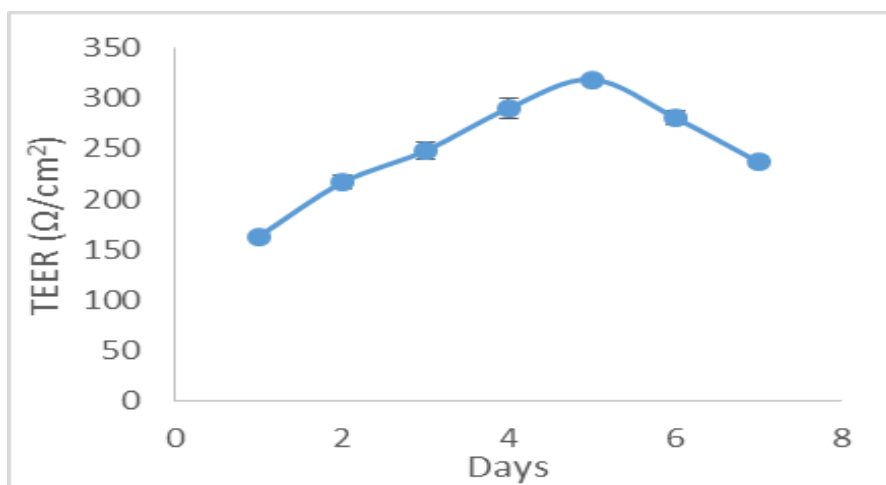


Figure 5.3 Mean of three measurements of TEER for inter-replicates of an experiment.

The hCMEC/D3 is a cell line generated from primary human brain capillary endothelial cells via a lentiviral vector system (Urich *et al.*, 2012). The mono-, co- and tri- culture models of the hCMEC/D3 human brain capillary endothelial cells with astrocytes (SC-1800) and/ or pericytes (HBVP) were analysed for TEER values over 7 consecutive days. All the models showed a steady increase in TEER values up to day 4, thereafter the tri-culture showed a decrease in the TEER values. The TEER of  $317 \Omega/\text{cm}^2$  was recorded by the hCMEC/D3 monolayer (Figure 5.4A). The co-culture of hCMEC/D3 and SC-1800 out of contact showed a peak TEER value of  $292 \Omega/\text{cm}^2$  which decreased after day 4. The co-culture of hCMEC/D3 and SC-1800 in contact showed a peak TEER value of  $326 \Omega/\text{cm}^2$  which decreased after day 5. The addition of pericytes to endothelial cell and astrocytes to form a tri-culture, increased the TEER values (Figure 5.4D and E) compared to the other models. The highest TEER recorded was  $385 \Omega/\text{cm}^2$ , which was measured in the tri-culture model of hCMEC/D3, SC1800 in contact and HBVP out of contact (Figure 5.4E).

The merged graph of the TEER values with respect to time for different co- and tri- cultures of hCMEC/D3 is shown in Figure 5.5. The co-culture of hCMEC/D3 and SC-1800 in contact and monoculture of hCMEC/D3 showed a decrease in TEER after day 5 whereas the co-culture of hCMEC/D3 and SC-1800 out of contact showed a decrease after day 4.

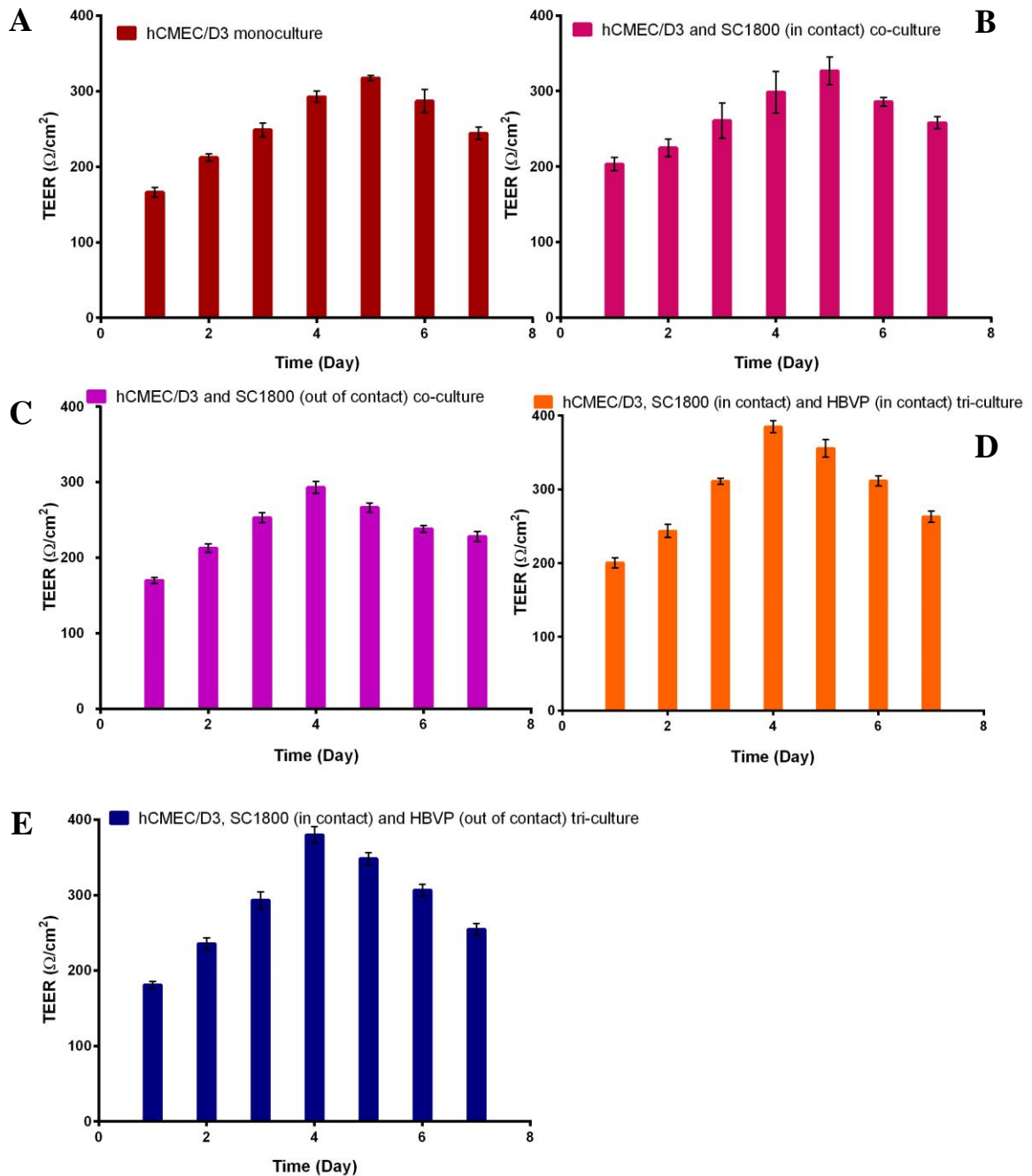


Figure 5.4 Effect of co- and tri cultivation on the induction of TEER in hCMEC/D3 monolayers of *in vitro* BBB models measured by the EVOM probe.

**A.** hCMEC/D3 monoculture. **B.** hCMEC/D3 and SC-1800 (in-contact) co-culture. **C.** hCMEC/D3 and SC1800 (out of contact) co-culture. **D.** hCMEC/D3, SC1800 (in-contact) and HBVP (in-contact) tri-culture. **E.** hCMEC/D3, SC1800 (in-contact) and HBVP (out of contact) tri-culture. TEER readings with respect to time for different culture models up to Day 7, the readings showed an increase up to day 4 and began to decline from day 4 onwards. The data points are means of three replicates ( $n=3$ ) and the error bars represent  $\pm$  standard deviation ( $\pm$ SD) of three inter-experimental repeats.

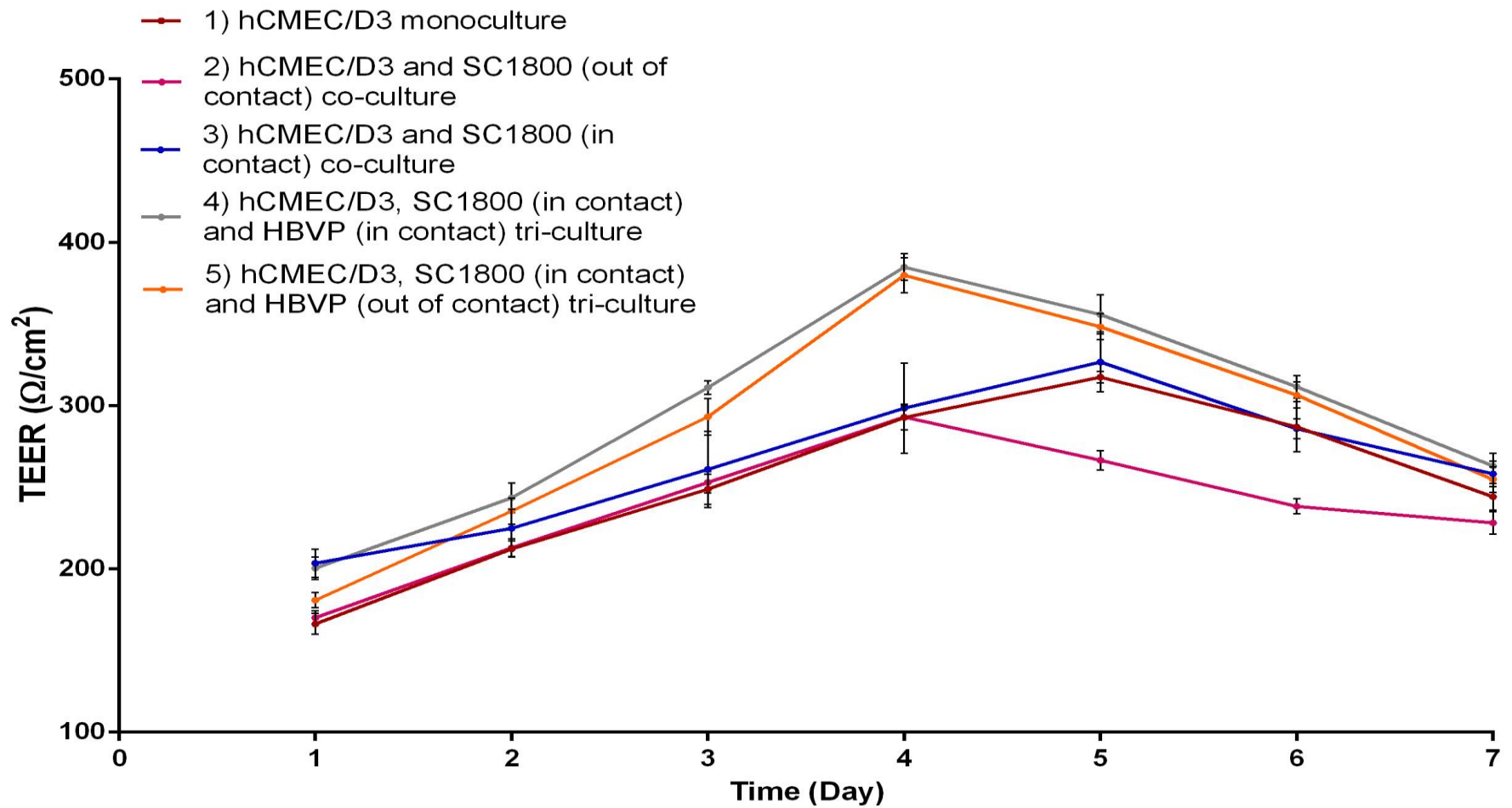


Figure 5.5 Comparison between TEER values measured by EVOM for all of the hCMEC/D3 co- and tri- culture models.

All the models showed an increase up to day 4, the tri-cultures showed a drop in the TEER values after this point, whereas other model showed a drop in TEER values after day 5. The data points are means of three replicates (n=3) and the error bars represent  $\pm$  standard deviation ( $\pm$ SD) of three inter-experimental repeats.

The models were also studied for the expression of tight junction proteins occludin and claudin-5 (Figure 5.6 A & B). All of the Western blots presented in this Chapter were normalised by quantifying the protein concentration by Bradford assay and loading each well with equal amount of protein.  $\beta$ -actin was used as the loading control, and protein expression was normalised against  $\beta$ -actin expression for densitometry analysis. The tri-culture model comprising of the hCMEC/D3, SC-1800 (in contact) and HBVP (out of contact) (Lane 5) showed the highest expression of both occludin and claudin-5 (Figure 5.6 A & B), which was also confirmed by the highest densitometry reading of 775 % for occludin and 1434 % for claudin-5 relative to the mono-culture control (Figure 5.7 A and B). All the models showed an increase in the expression of claudin-5 compared to the hCMEC/D3 mono-culture (Lane 1) suggesting that co- and tri- culturing of cells improved the level of protein expression. Whereas the expression of occludin was more variable and the expression was 52 % in the hCMEC/D3 and SC-1800 (in contact) co-culture relative to the hCMEC/D3 mono-culture control (Figure 5.6 A and B).

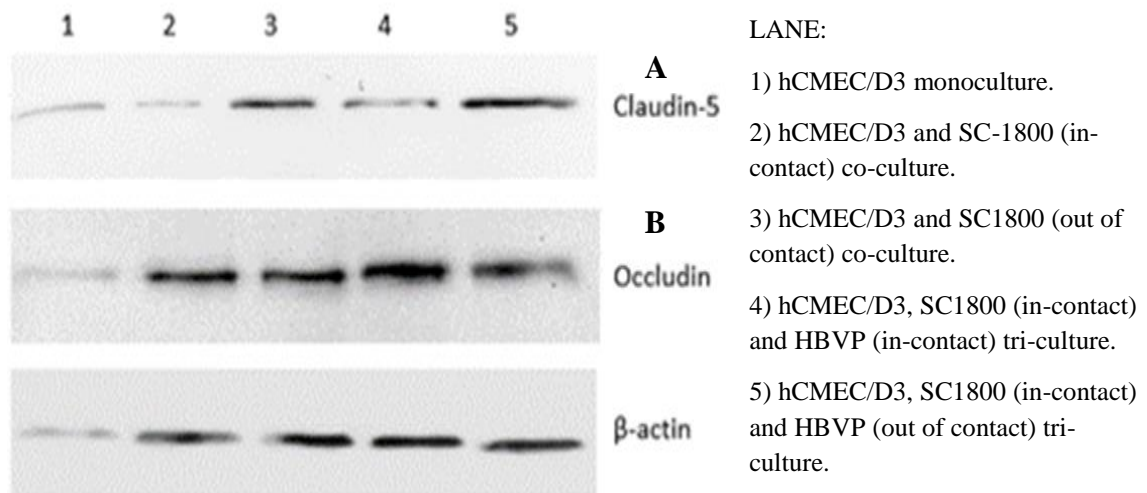


Figure 5.6 Western blots for TJs proteins expression in hCMEC/D3 mono-, co- and tri- cultures.

**A.** Western blot for claudin-5 protein (23 kDa). **B.** Western blot of for occludin protein (65 kDa). Each well was loaded with 10  $\mu$ g protein.  $\beta$ -actin protein (42 kDa) was used as the loading control.

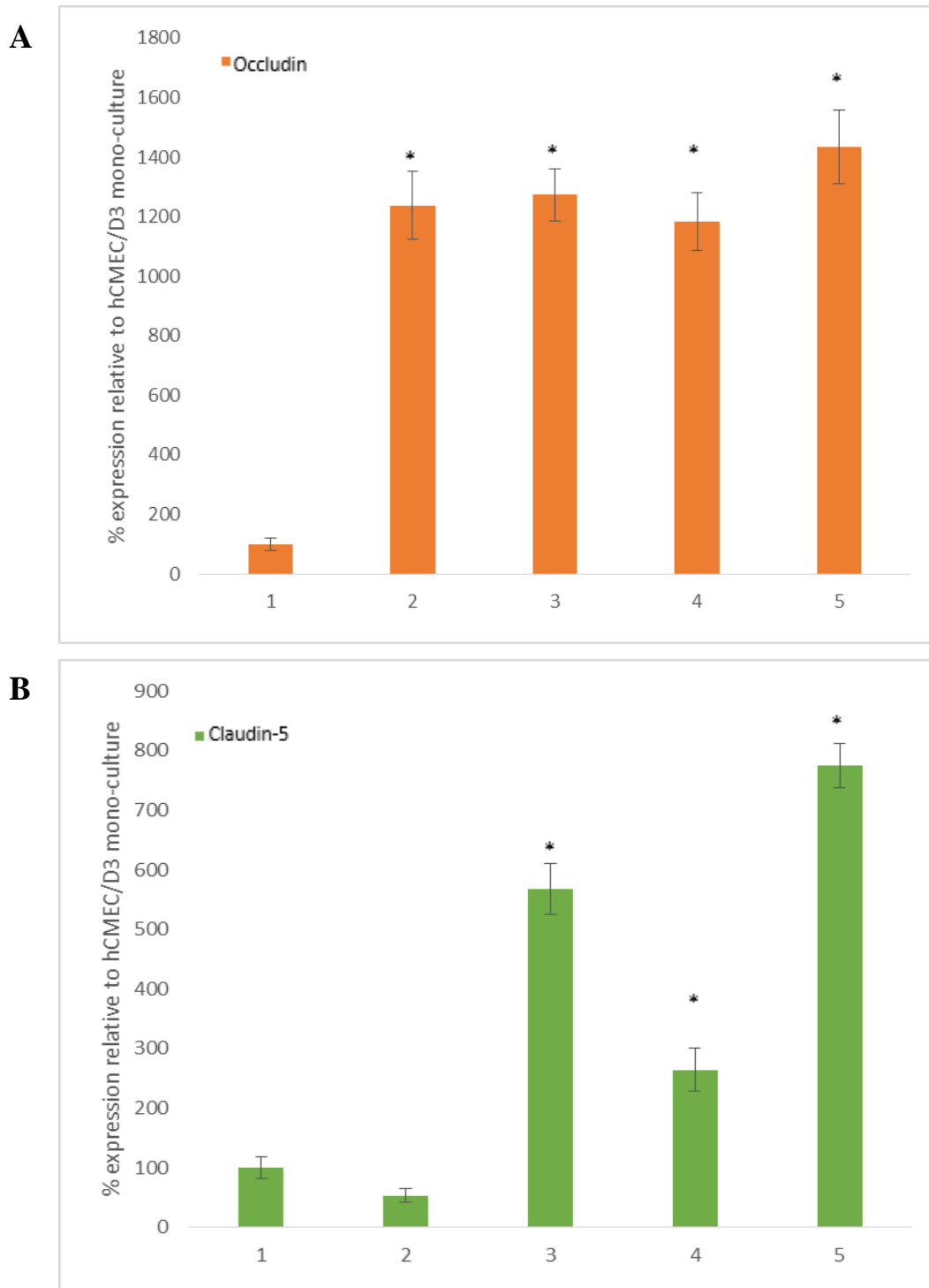


Figure 5.7 Densitometry analysis of TJs proteins expression in hCMEC/D3 mono-, co- and tri- cultures.

**A.** Densitometry for occludin expression (65 kDa). **B.** Densitometry for claudin-5 expression (23 kDa). 1) hCMEC/D3 monoculture. 2) hCMEC/D3 and SC-1800 (in-contact) co-culture. 3) hCMEC/D3 and SC1800 (out of contact) co-culture. 4) hCMEC/D3, SC1800 (in-contact) and HBVP (in-contact) tri-culture. 5) hCMEC/D3, SC1800 (in-contact) and HBVP (out of contact) tri-culture. The error bars represent  $\pm$  standard deviation ( $\pm$ SD) of three measurement of each protein band. \*  $p < 0.05$  was considered to be statistically significant.

### 5.2.1.2 TEER measurements of designed BBB models using ECIS

The ECIS instrument measured the TEER in real-time two dimensionally across cells seeded as monolayers, via an electrode at the base of the array (Section 2.8.2). In this experiment, the hCMEC/D3 was used as a representative endothelial cell line to set up co- and tri-culture models on the ECIS. The cells were seeded on the ECIS array which was coated with 5  $\mu\text{g}$  of fibronectin and the TEER reading was recorded for up to 160 h. One well on the ECIS array was kept blank which was seeded with growth medium to determine the background TEER values. The cells were supplied with their respective culture media as described in Section 2.8.

TEER values for the hCMEC/D3 monoculture were measured on the ECIS array. For this model the TEER values steadily increased before peaking at 80-100 h followed by a steady decrease in the values. The maximum value of TEER in hCMEC/D3 monoculture was 558  $\Omega/\text{cm}^2$  (Figure 5.8).

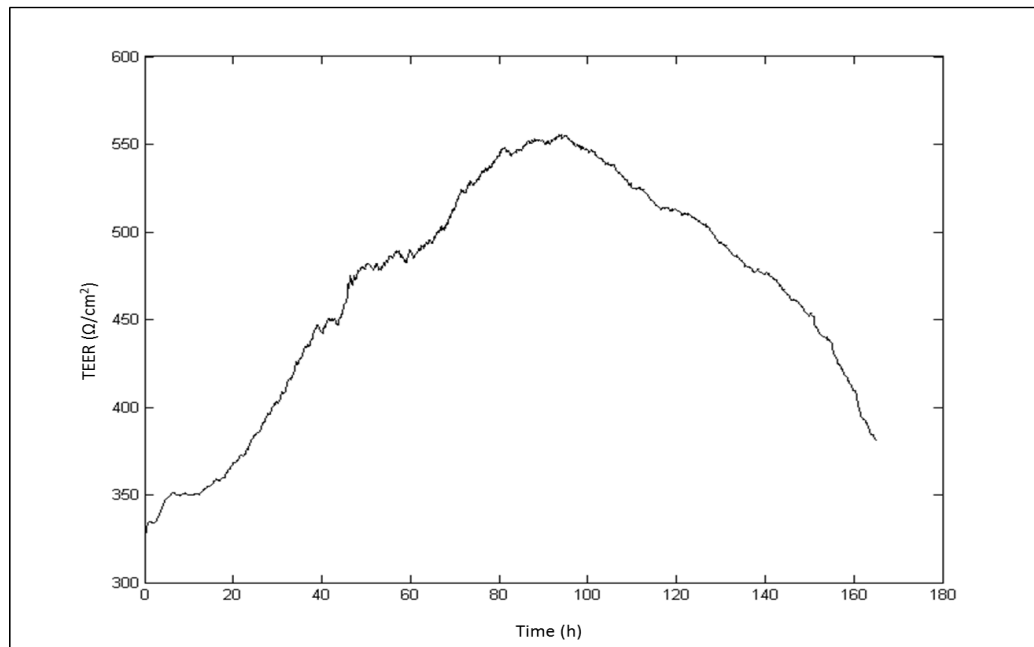


Figure 5.8 TEER measurements of endothelial (hCMEC/D3) monoculture in 2D ECIS model. The graph is an average of the data from two separate experiments.

The hCMEC/D3 cells were grown in co-cultures as a monolayer with either astrocytes (SC-1800) or pericytes (HBVP). The astrocyte co-culture showed a higher TEER compared to the pericyte co-culture. The highest TEER value for the astrocyte co-culture was  $750 \Omega/\text{cm}^2$  at 80 h, after which it dropped sharply (Figure 5.9). The highest TEER value for the pericyte co-culture was  $475 \Omega/\text{cm}^2$ , the TEER values showed a sharp decrease after 100 h (Figure 5.10).

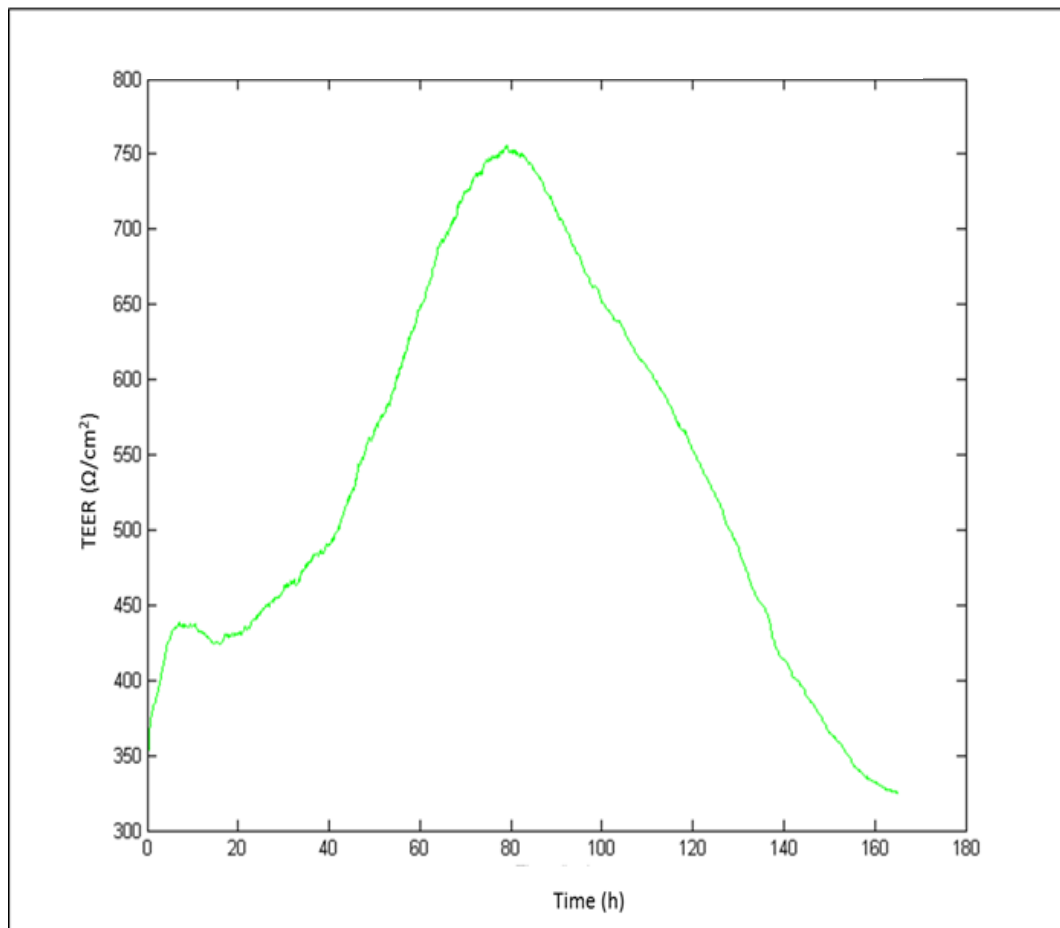


Figure 5.9 TEER measurements of endothelial cells (hCMEC/D3) and astrocytes (SC-1800) co-culture in 2D ECIS model.

The graph is an average of the data from two separate experiments.

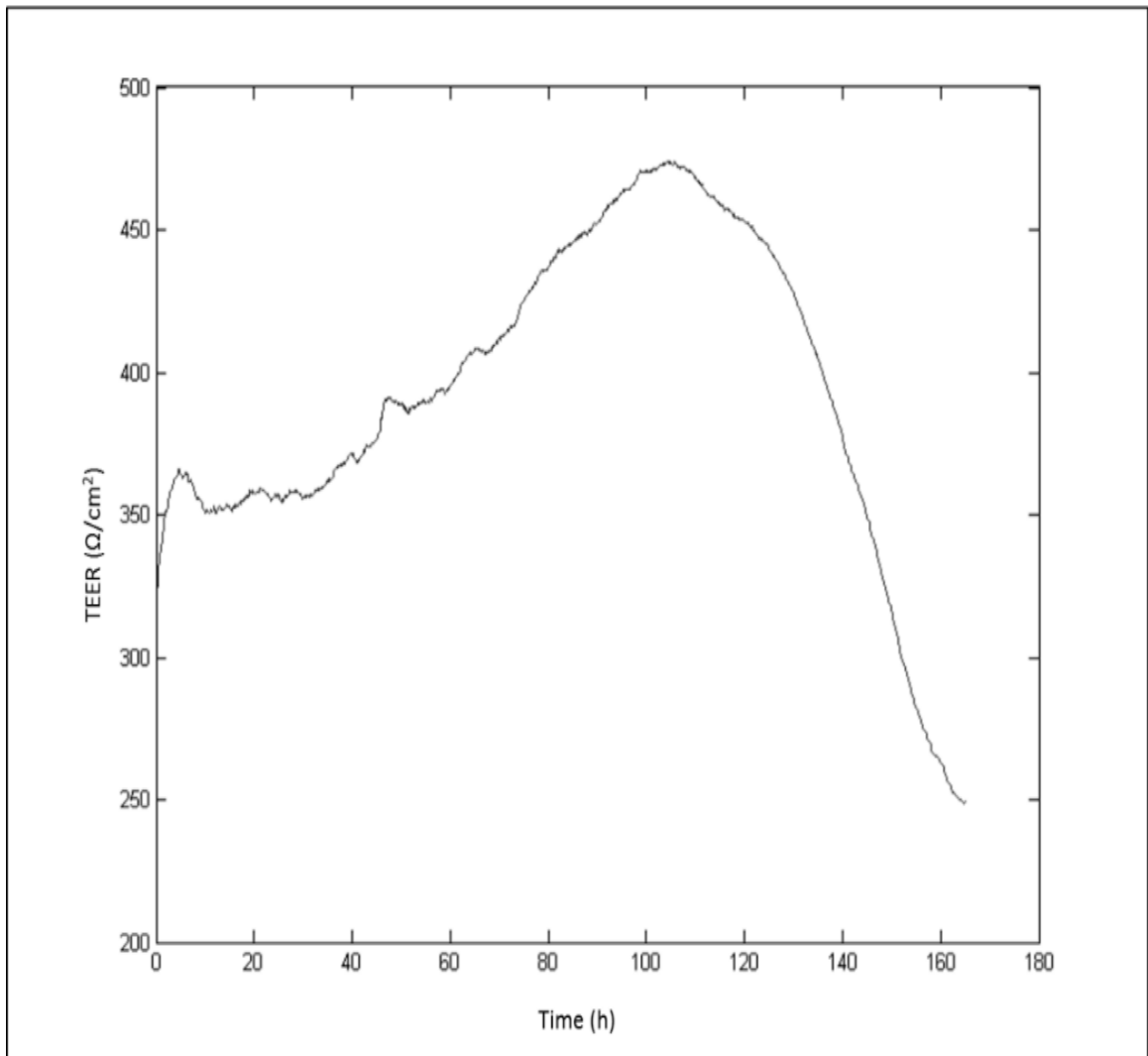


Figure 5.10 TEER measurements of endothelial cells (hCMEC/D3) and pericytes (HBVP) co-culture in 2D ECIS model. The graph is an average of the data from two separate experiments.

The TEER measurement in mono- and co-cultures on ECIS showed a similar trend to the TEER measurements obtained by the EVOM probe, where culturing two cell types together increased the TEER values. As seen in Figure 5.11, TEER values showed an increase and a small peak at  $475 \Omega/\text{cm}^2$  at 5 h followed by a drop, then a steady increase to  $760 \Omega/\text{cm}^2$ , at 80 h, after which a sharp decrease was observed.

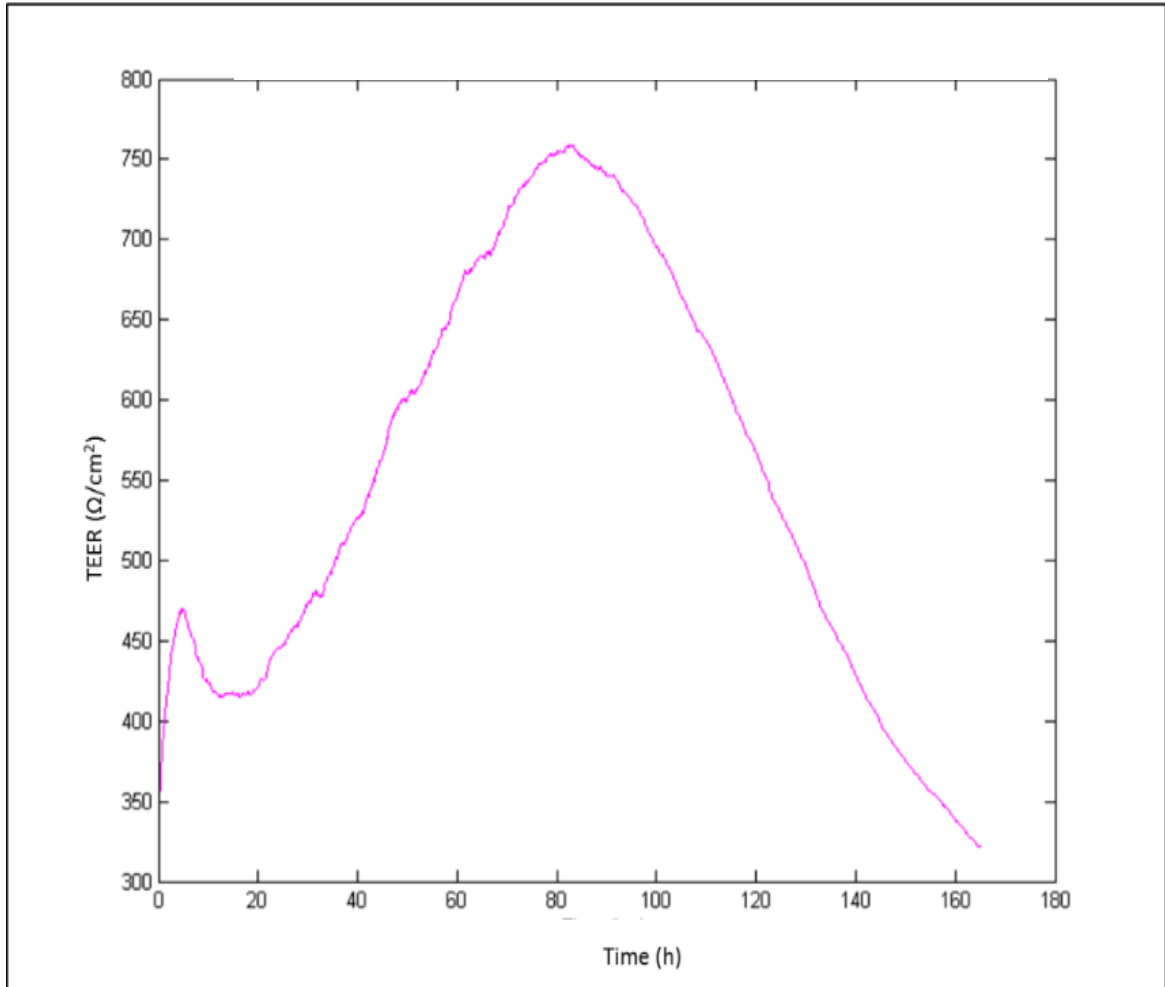


Figure 5.11 TEER measurements of endothelial cells (hCMEC/D3), astrocytes (SC1800) and pericytes (HBVP) tri-culture in 2D ECIS model.

The graph is an average of the data from two separate experiments.

The merged graph in Figure 5.12 compares the TEER values with respect to time for all the models, where the lowest TEER value of  $475 \Omega/\text{cm}^2$  was shown by the endothelial cells and pericytes co-culture. The highest values of  $760 \Omega/\text{cm}^2$  at 82 h was shown by endothelial cells, astrocyte and pericytes tri-culture. The co-culture of endothelial cells and astrocytes showed similar values to the tri-culture model, the TEER value of the co-culture was  $750 \Omega/\text{cm}^2$  at 80 h.

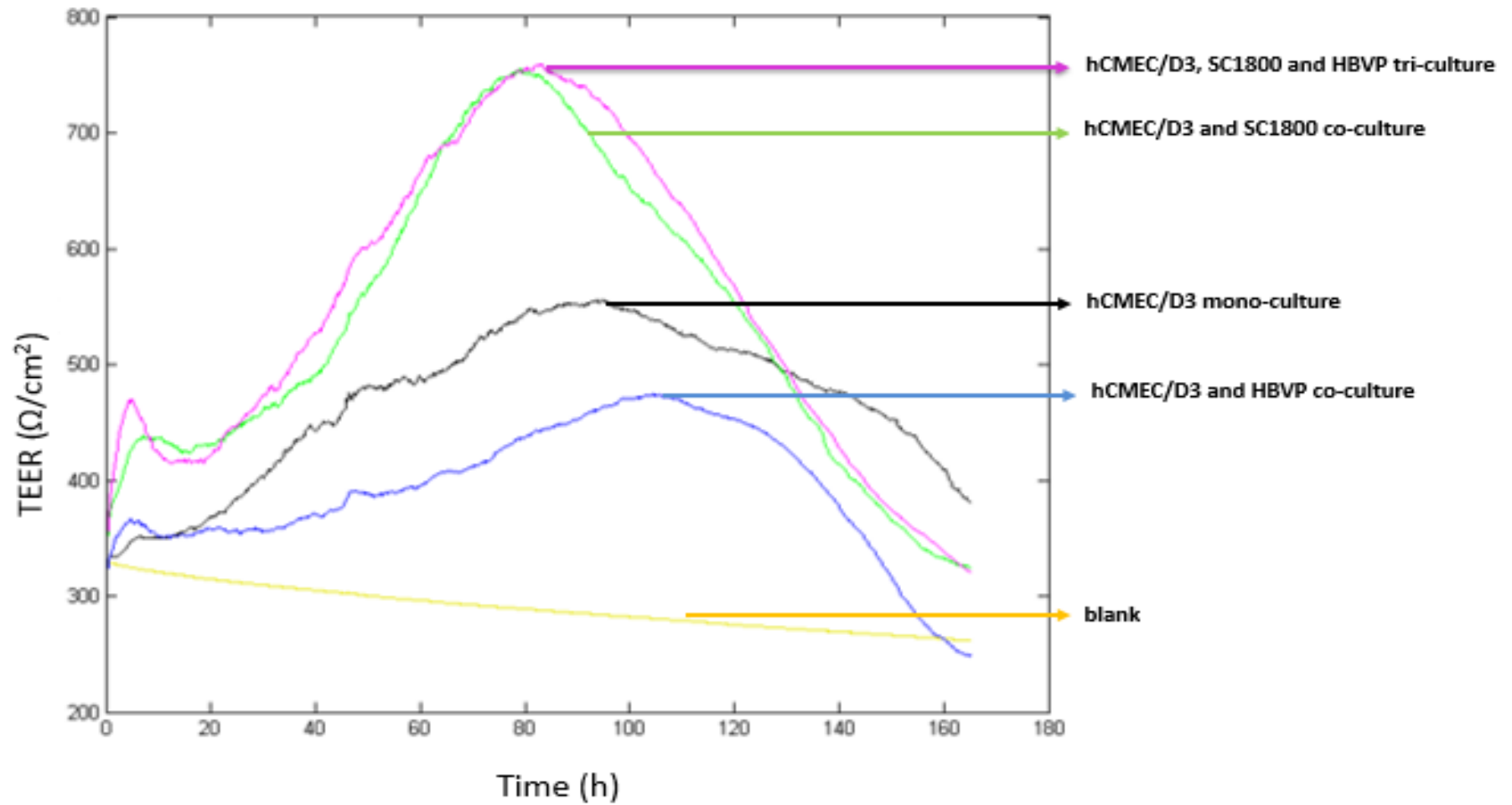


Figure 5.12 Comparison of TEER measured for co- and tri- culture 2D models set up on the ECIS array. The highest TEER values shown by the tri-culture model at 83 h. The graph is an average of the data from two separate experiments.

The models were also studied for the expression of tight junction proteins occludin and claudin-5 (Figure 5.13 A & B). The tri-culture model (Lane 4), showed the highest expression of both occludin and claudin-5, compared to all of the other models confirmed by densitometry to be 1161 % and 758 % increase relative to the hCMEC/D3 monolayer control (Figure 5.14 A & B). The co-culture of endothelial cells with astrocytes (Lane 2), showed higher expression of occludin compared to co-culture of endothelial cells with pericytes (EP) (Lane 3), confirmed by densitometry to 100 % and 52.6 %, whereas claudin was more variable and showed lower expression in the co-culture of endothelial cells with astrocytes, compared to the co-culture of pericytes (Figure 5.14 A & B) The lowest expression of occludin and claudin-5 was seen by the hCMEC/D3 mono-culture (Lane 1).

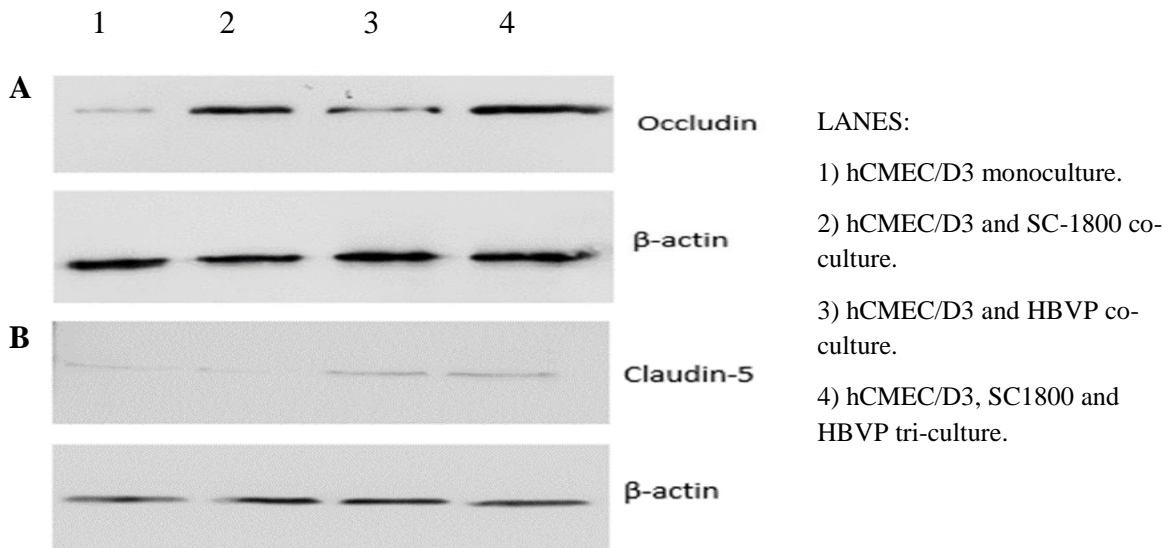


Figure 5.13 Western blots for TJs proteins expression in hCMEC/D3 mono-, co- and tri- cultures setup on the ECIS array.

**A.** Western blot of occludin protein (65 kDa) expression in different BBB models **B.** Western blot of claudin-5 protein (23 kDa) expression in different BBB models. For the Western blots, each well was loaded with 10  $\mu$ g protein.  $\beta$ -actin protein (42 kDa) was used as the loading control.

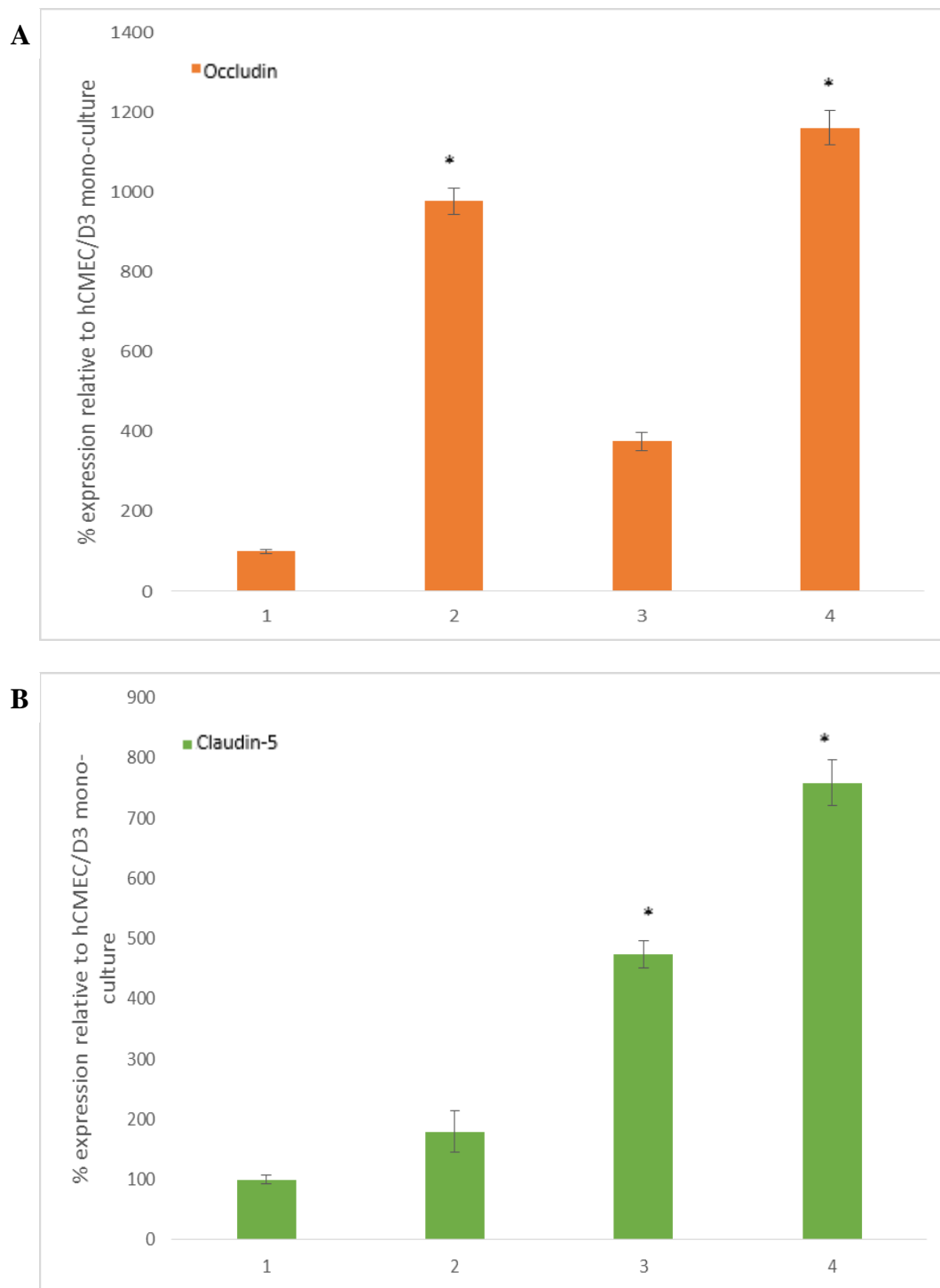


Figure 5.14 Densitometry analysis of TJs proteins expression in hCMEC/D3 mono-, co- and tri- cultures setup on the ECIS array.

**A.** Densitometry for occluding expression (65 kDa). **B.** Densitometry for claudin-5 expression (23 kDa). 1) hCMEC/D3 monoculture. 2) hCMEC/D3 and SC-1800 co-culture. 3) hCMEC/D3 and HBVP) co-culture. 4) hCMEC/D3, SC1800 and HBVP tri-culture. The error bars represent  $\pm$  standard deviation ( $\pm$ SD) of three measurements of each protein band. \*  $p < 0.05$  was considered to be statistically significant.

### 5.2.1.3 TEER measurements of BBB models using Cellzscope

The next stage was to compare the Cellzscope instrument for measuring TEER in the *in vitro* BBB models (as described in Section 2.8.3) to the EVOM probe. The Cellzscope was used to measure the TEER values of the 3D mono-, co- and tri- culture models for up to 90 h in real-time. In this measuring system an additional parameter was measured which is the capacitance of the cells. Capacitance provides additional information about the cell layer properties: in particular it is indicative of the expression of microvilli and other membrane extrusions. The cells showing low capacitance are indicative of cell attachment to the insert and integrated cell layer properties.

The hCMEC/D3 monoculture was seeded on insert and the TEER was recorded, the highest value recorded was  $7 \Omega \cdot \text{cm}^2$  at 70 h (Figure 5.15 A). The corresponding capacitance stabilises after 50 h, the cells form a compact monolayer after 50 h (Figure 5.15 B). Initially on setting up model, the mono-culture showed a high capacitance and an unstable TEER up to 40 h of measurement. The readings showed a steady increase in TEER up to 70 h which subsequently dropped after reaching the peak value.

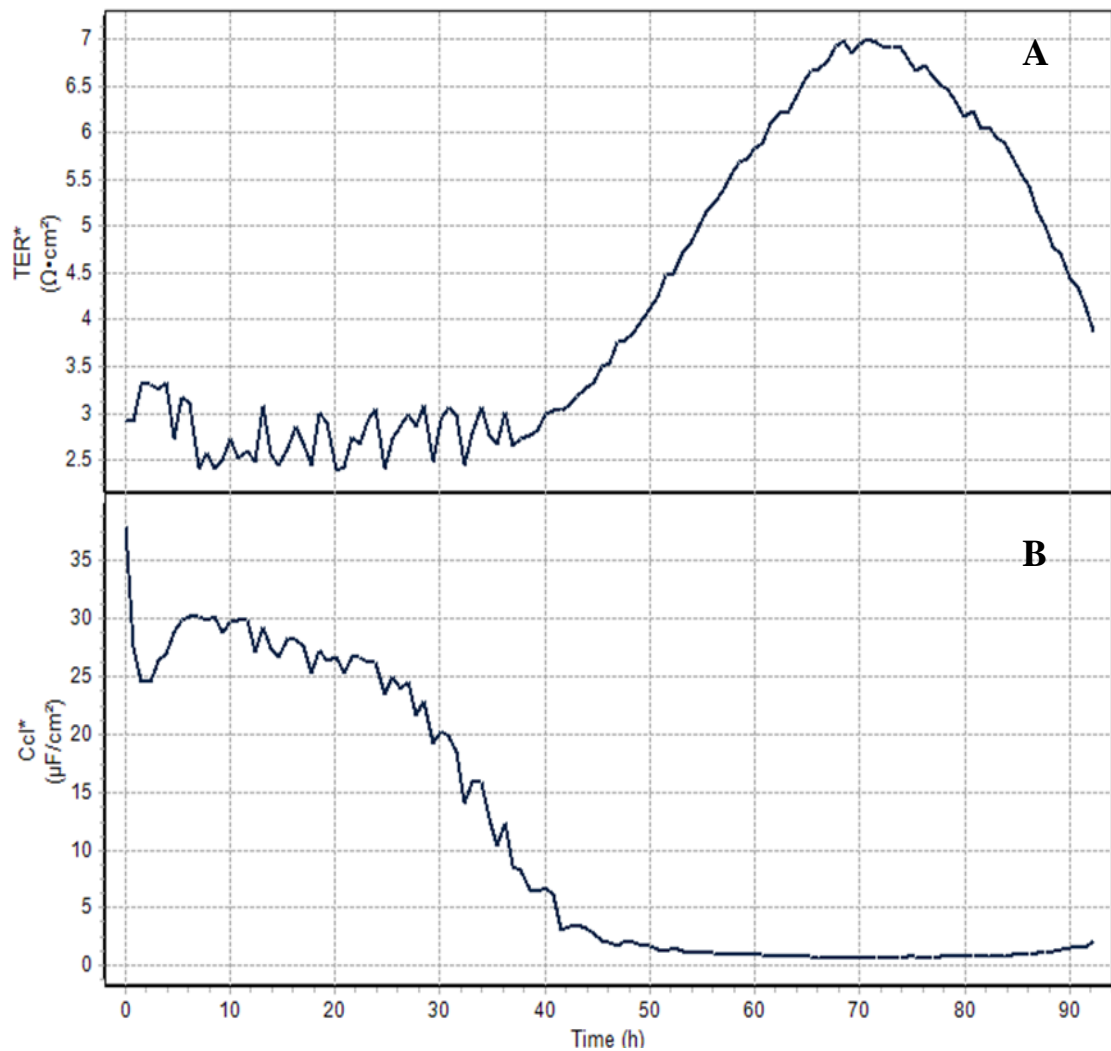


Figure 5.15 **A.** TEER measurements **B.** Capacitance of endothelial (hCMEC/D3) monoculture in 3D model. The graph is an average of data from two separate experiments.

The co-culture of endothelial cells and the astrocytes peaked at 60 h, the astrocytes in the co-culture were seeded in contact with the insert on the basolateral side. As seen in Figure 5.16, TEER values showed an increase within 5 h of seeding the cells, a small peak at  $38 \Omega \cdot \text{cm}^2$  was observed which dropped down temporarily and then TEER showed a steady increase up to 57 h. The highest value recorded was  $45 \Omega \cdot \text{cm}^2$  at 57 h (Figure 5.16 A), the corresponding capacitance value indicated that the cells formed a compact monolayer between 50 -60 h. After 60 h, the cells began to detach which was indicated by the increase in the capacitance (Figure 5.16 B).

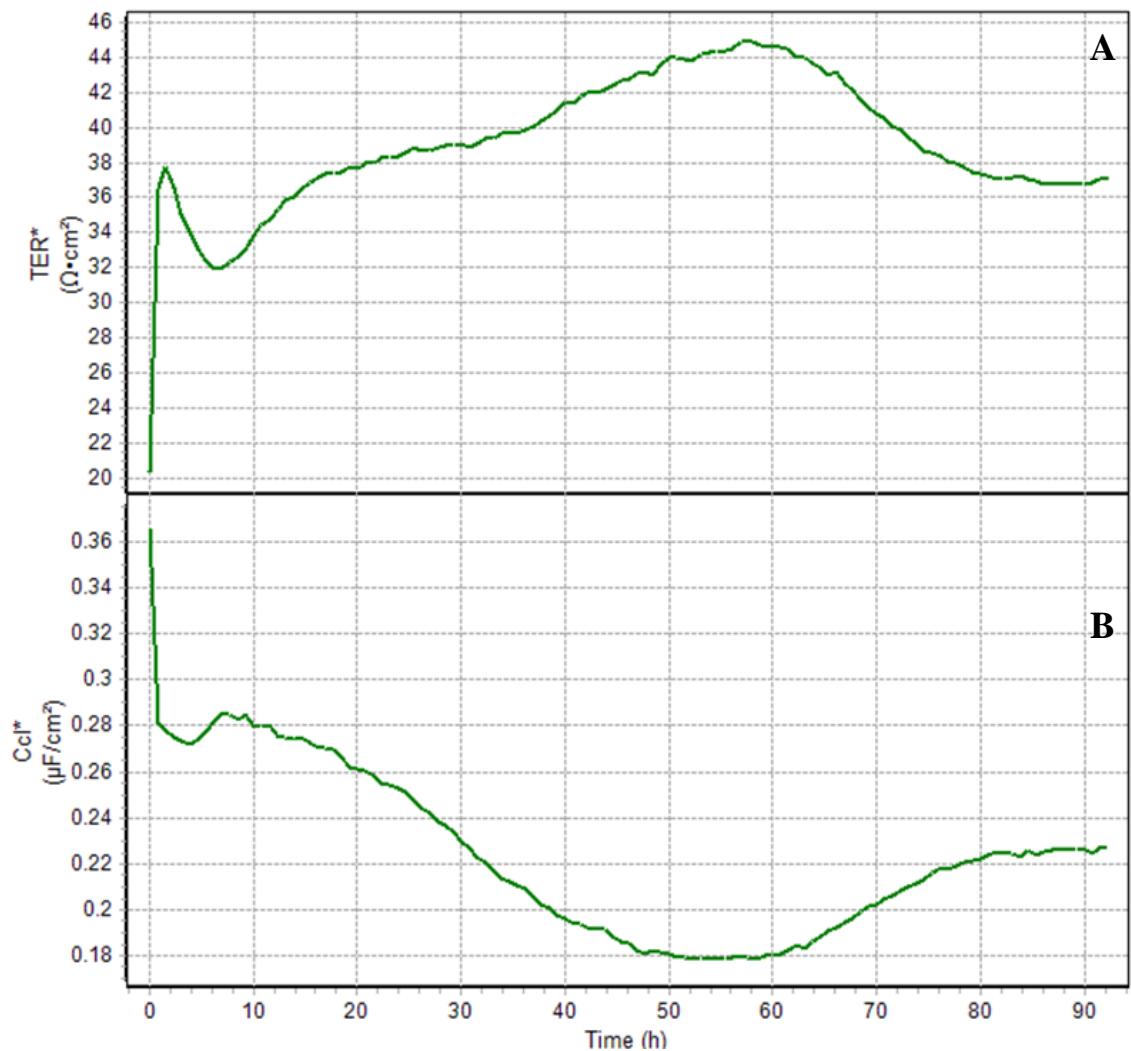


Figure 5.16 A: TEER measurements B: Capacitance of endothelial cells (hCMEC/D3) and astrocytes (SC-1800) co-culture in 3D model.

The graph is an average of data from two separate experiments.

The co-culture of endothelial cells and the pericytes peaked at 60 h, the pericytes in the co-culture were seeded in contact with the insert on the basolateral side. As seen in Figure 5.17, TEER values showed an exponential increase within 5 h of seeding the cells, a peak at  $8 \Omega \cdot \text{cm}^2$  was observed which dropped transiently and then the TEER showed a steady increase up to  $59 \Omega \cdot \text{cm}^2$ . The highest TEER value recorded was  $12.5 \Omega \cdot \text{cm}^2$  (Figure 5.17 A), the corresponding capacitance value indicated that the cells formed a compact monolayer between 50 -70 h. After 80 h, the cells begin to detach which was indicated by the increase in the capacitance (Figure 5.17 B).

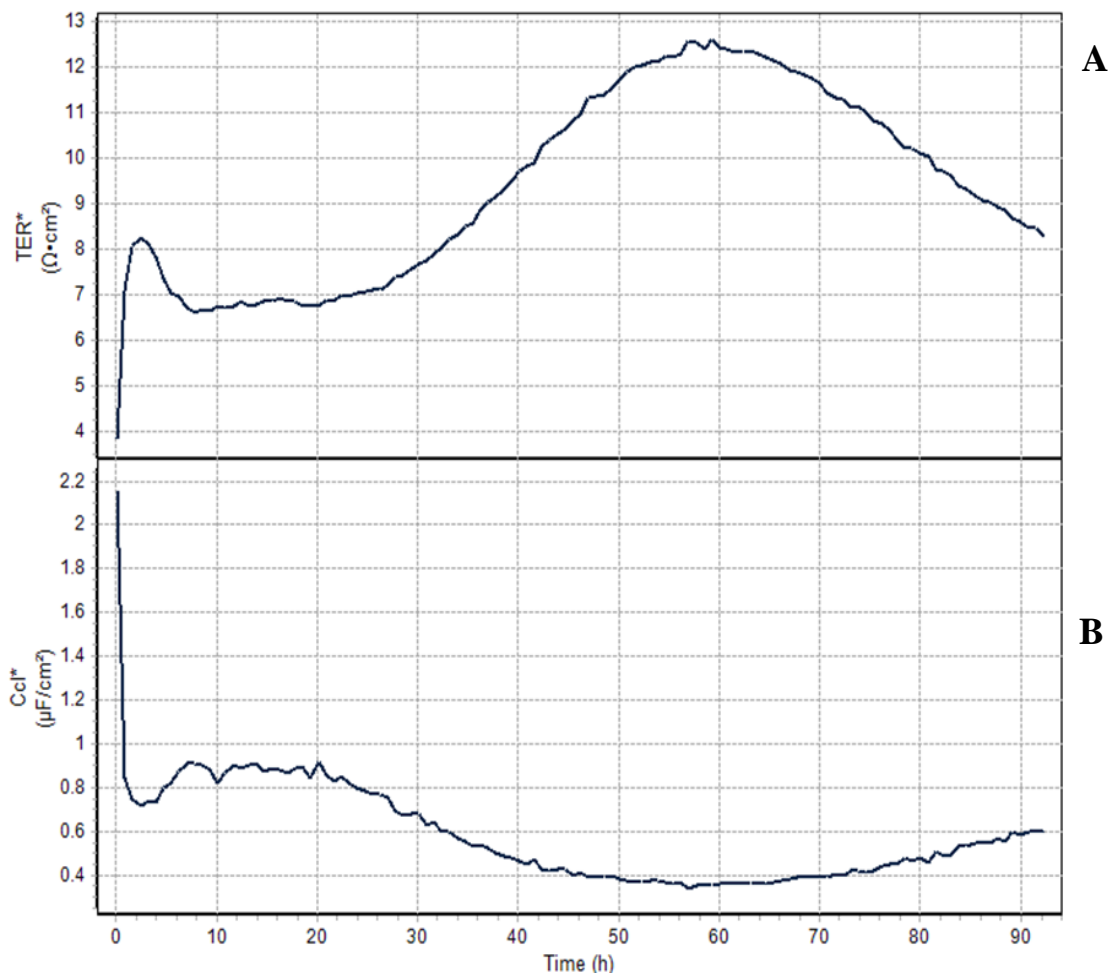


Figure 5.17 **A.** TEER measurements and **B.** Capacitance of endothelial cells (hCMEC/D3) and pericytes (HBVP) co-culture in 3D model.

The graph is an average of data from two separate experiments.

The TEER values in tri-culture of endothelial cells, astrocytes and the pericytes peaked between 65 h, the astrocytes and pericytes in the co-culture were seeded in contact of the insert on the basolateral side. As seen in Figure 5.18, TEER values showed an increase within 5 h of seeding the cells, a peak TEER at  $12 \Omega \cdot \text{cm}^2$  was observed which dropped down and then the TEER showed a steady increase up to 65 h. The highest TEER value recorded was  $22 \Omega \cdot \text{cm}^2$  (Figure 5.18 A), the corresponding capacitance value indicated that the cells formed a compact monolayer after 40 h. The cells remained in a compact monolayer, which was indicated by a stable capacitance value (Figure 5.18 B).

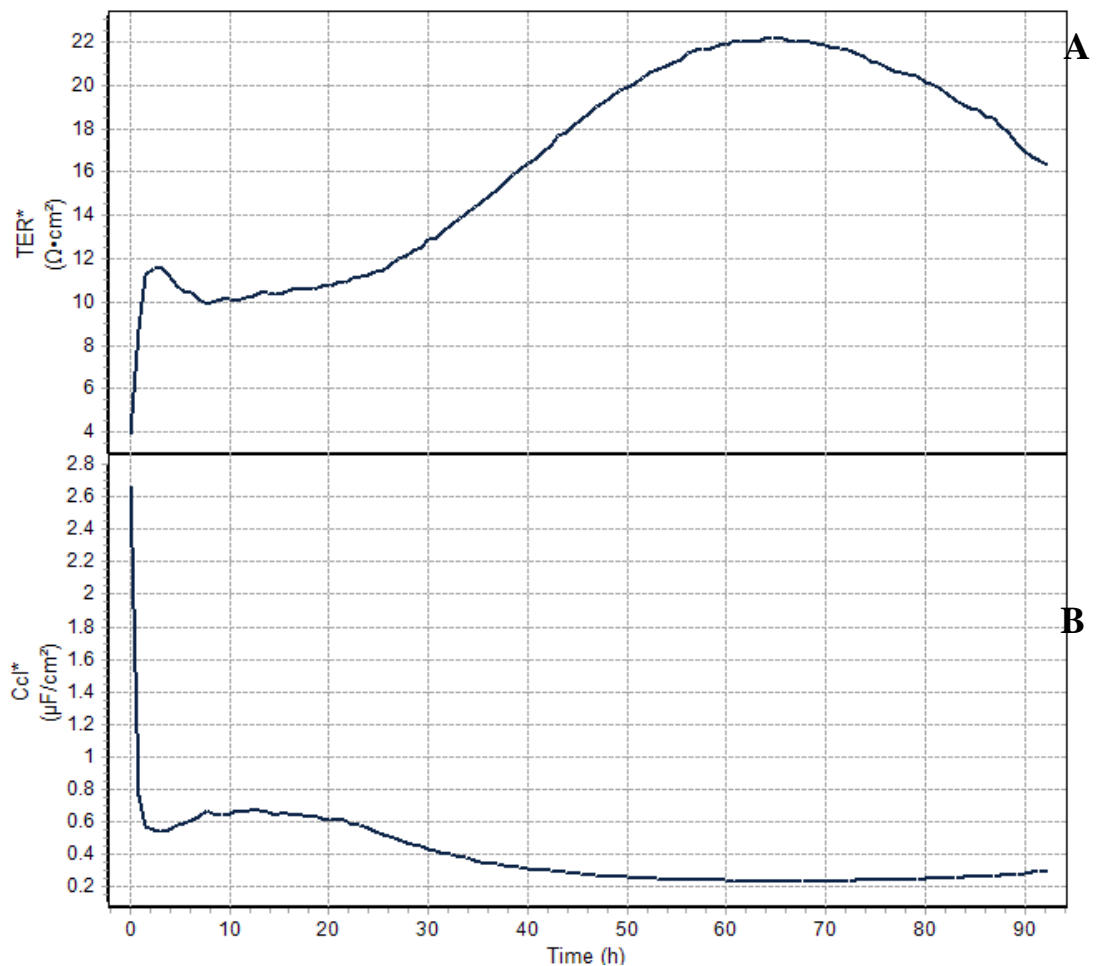


Figure 5.18 A. TEER measurements and B. Capacitance of endothelial cells (hCMEC/D3), astrocytes (SC1800) and pericytes (HBVP) tri-culture in 3D model.

The graph is an average of data from two separate experiments.

The merged graph in Figure 5.19 compared the TEER values of all the different models, where the highest TEER was shown by endothelial and astrocyte co-culture and the lowest value was shown by the endothelial mono-culture. The TEER of all the models began to decrease after 70 h. Unlike the models set up and measured using EVOM and ECIS the tri-culture model did not show the highest TEER readings. The overall TEER values given by the Cellzscope were much lower than the TEER values given by model measured using EVOM and ECIS. The tri-culture measured by Cellzscope gave a TEER of 22  $\Omega \cdot \text{cm}^2$  whereas ECIS gave 258  $\Omega/\text{cm}^2$  and EVOM gave 760  $\Omega/\text{cm}^2$ . The unit of measurement and algorithms used to calculate TEER in the three systems was different in all instruments, both ECIS and EVOM measured resistance in  $\Omega/\text{cm}^2$  whereas CellZscope measured resistance in  $\Omega \cdot \text{cm}^2$ .

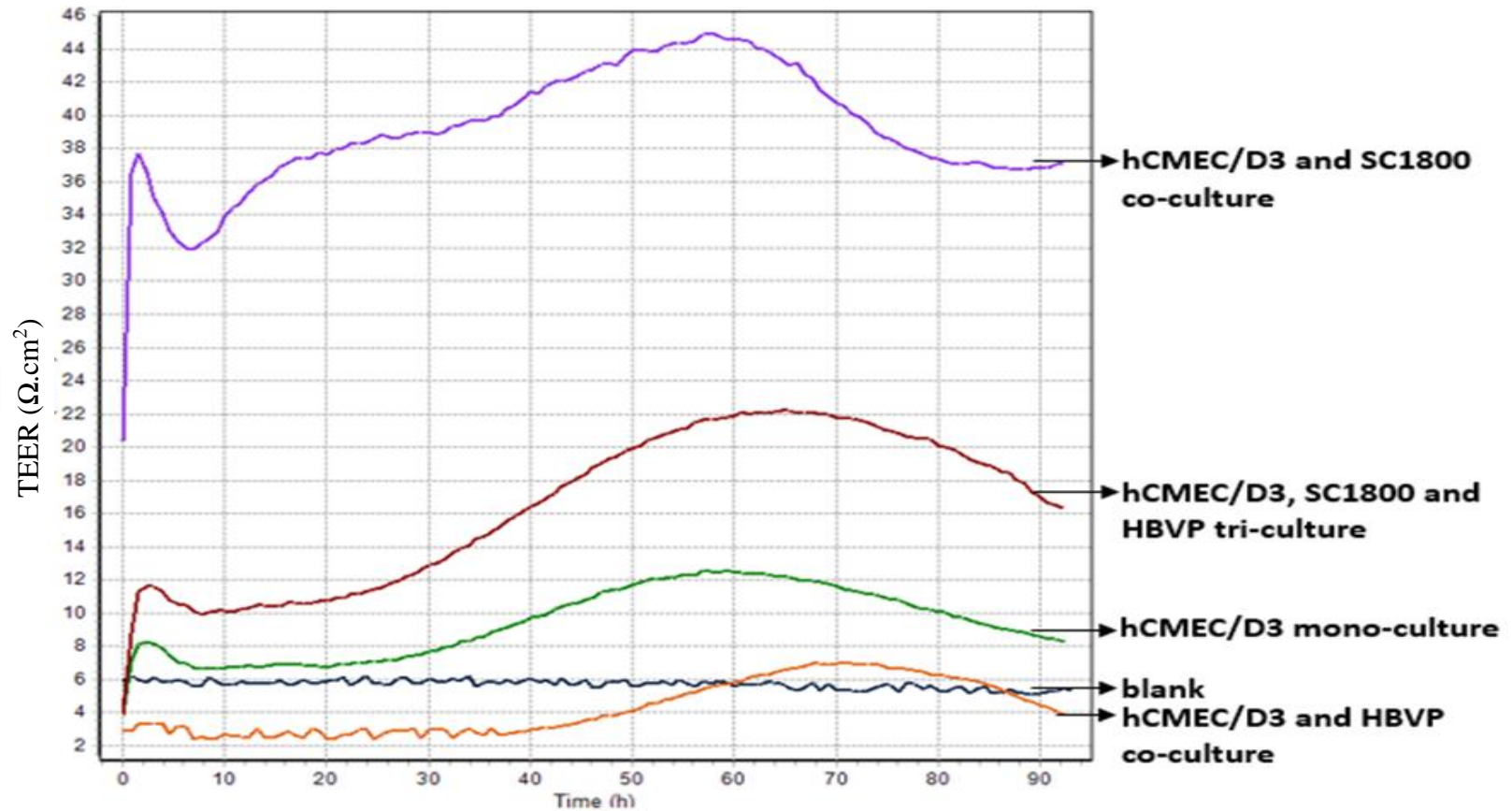


Figure 5.19 Comparison of all the TEER measurements in different co- and tri- culture 3D models set up on the Cellscope.

The highest TEER value was recorded in an EA co-culture model at 58 h. All the models showed a decrease in the TEER after 65 h. The graph is an average of data from two separate experiments.

The models were also studied for the expression of tight junction proteins occludin and claudin-5 (Figure 5.20 A & B). The tri-culture model, hCMEC/D3, SC1800 (in-contact) and HBVP (in-contact) tri-culture (Lane 4) showed the highest expression of both occludin and claudin-5 as compared to all the models, confirmed by densitometry to be an 201 % and 371 % increase relative to the hCMEC/D3 monoculture (Figure 5.21 A & B). The co-culture of astrocyte, hCMEC/D3 and SC-1800 (in-contact) (Lane 2) showed a higher expression of both occludin and claudin, confirmed by densitometry to be 146 % and 309 % respectively, which when compared to the pericyte co-culture hCMEC/D3 and HBVP (in-contact) (Lane 3) was only 78 % occludin and no expression of claudin-5 (Figure 5.21 A & B).

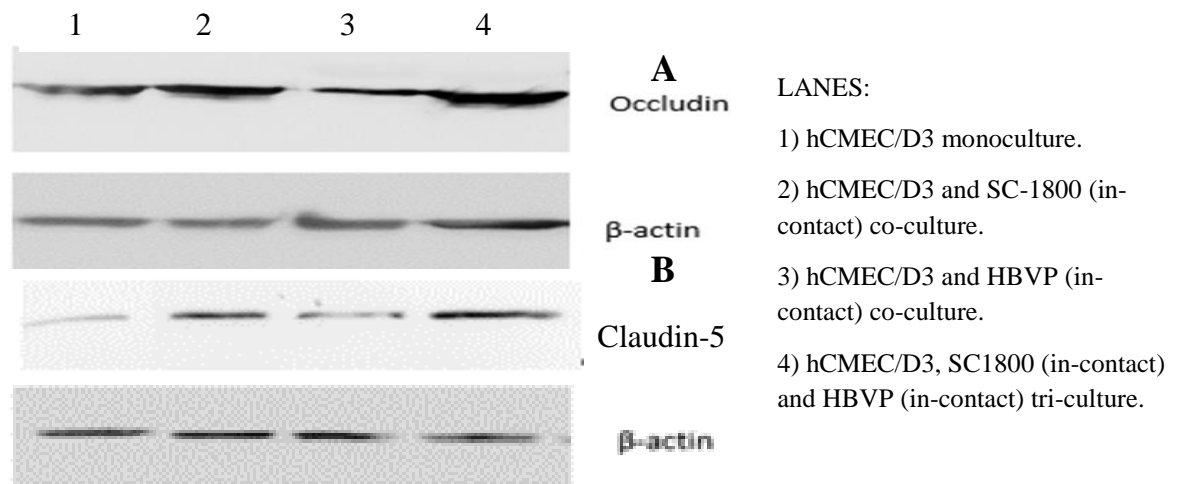


Figure 5.20 Western blots for TJs protein expression in hCMEC/D3 mono-, co- and tri- cultures set up on Cellzscope.

**A.** Western blot for occludin protein expression (65 kDa). **B.** Western blot for claudin-5 protein expression (23 kDa). Each well was loaded with 10  $\mu$ g protein.  $\beta$ -actin protein (42 kDa) was used as the loading control.

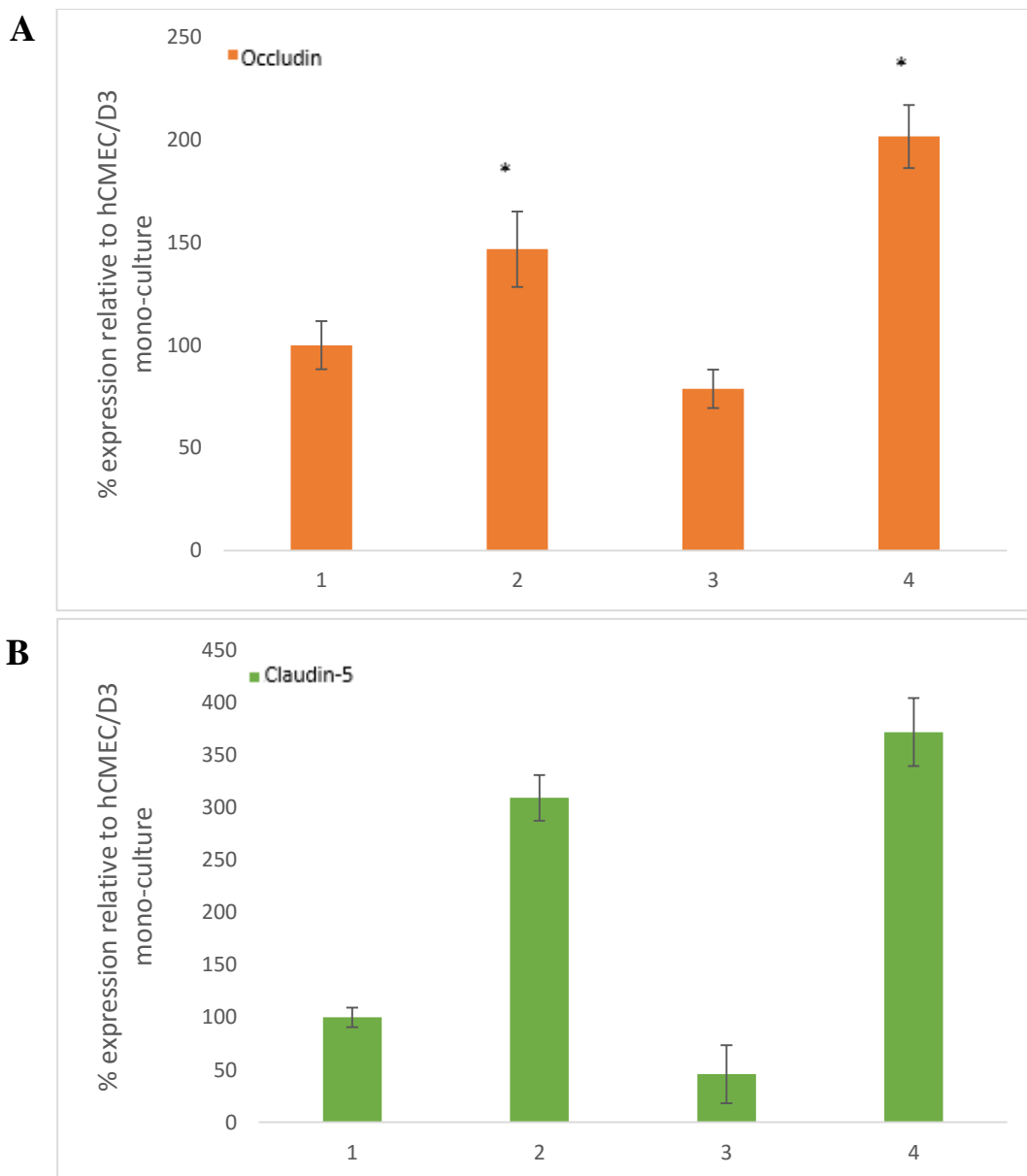


Figure 5.21 Densitometry analysis of TJ proteins expression in hCMEC/D3 mono-, co- and tri- cultures set up on Cellscope.

**A.** Densitometry for expression of occludin (65 kDa). **B.** Densitometry for expression of claudin-5 (23 kDa). 1) hCMEC/D3 monoculture. 2) hCMEC/D3 and SC-1800 (in-contact) co-culture. 3) hCMEC/D3 and HBVP (in-contact) co-culture. 4) hCMEC/D3, SC1800 (in-contact) and HBVP (in-contact) tri-culture. The error bars represent  $\pm$  standard deviation ( $\pm$ SD) of three measurements of each protein band. \*  $p < 0.05$  was considered to be statistically significant.

## 5.2.2 Optimising experimental conditions

### 5.2.2.1 Short-term endothelial cells: mono-, co- and tri- cultures

The HBMEC endothelial cells mono-, co- (with astrocytes) and tri- (with astrocytes and pericytes) culture models were assessed for TEER values over 15 consecutive days using the EVOM instrument. All of the models showed a steady increase in TEER values up to day 10 (Figure 5.22). The lowest TEER values  $100 \Omega/\text{cm}^2$  were recorded in the monolayer culture of HBMEC (Figure 5.22 A) and co-culture model comprising of HBMEC and HBVP cells out of contact (Figure 5.22 B). The models where endothelial cells were in contact with pericytes and astrocytes, continued to demonstrate increased resistance until day 13 (Figure 5.22 C & E). In models where endothelial cells were out of contact with pericytes and astrocytes (Figure 5.22 B & D), the TEER values started to fluctuate and decrease after day 10. The highest TEER value of  $258 \Omega/\text{cm}^2$  was recorded for the tri-culture comprising of the HBMEC on the insert, HBVP cells in contact with the insert and the HA cells out of contact at the bottom of the well (Figure 5.22 F).

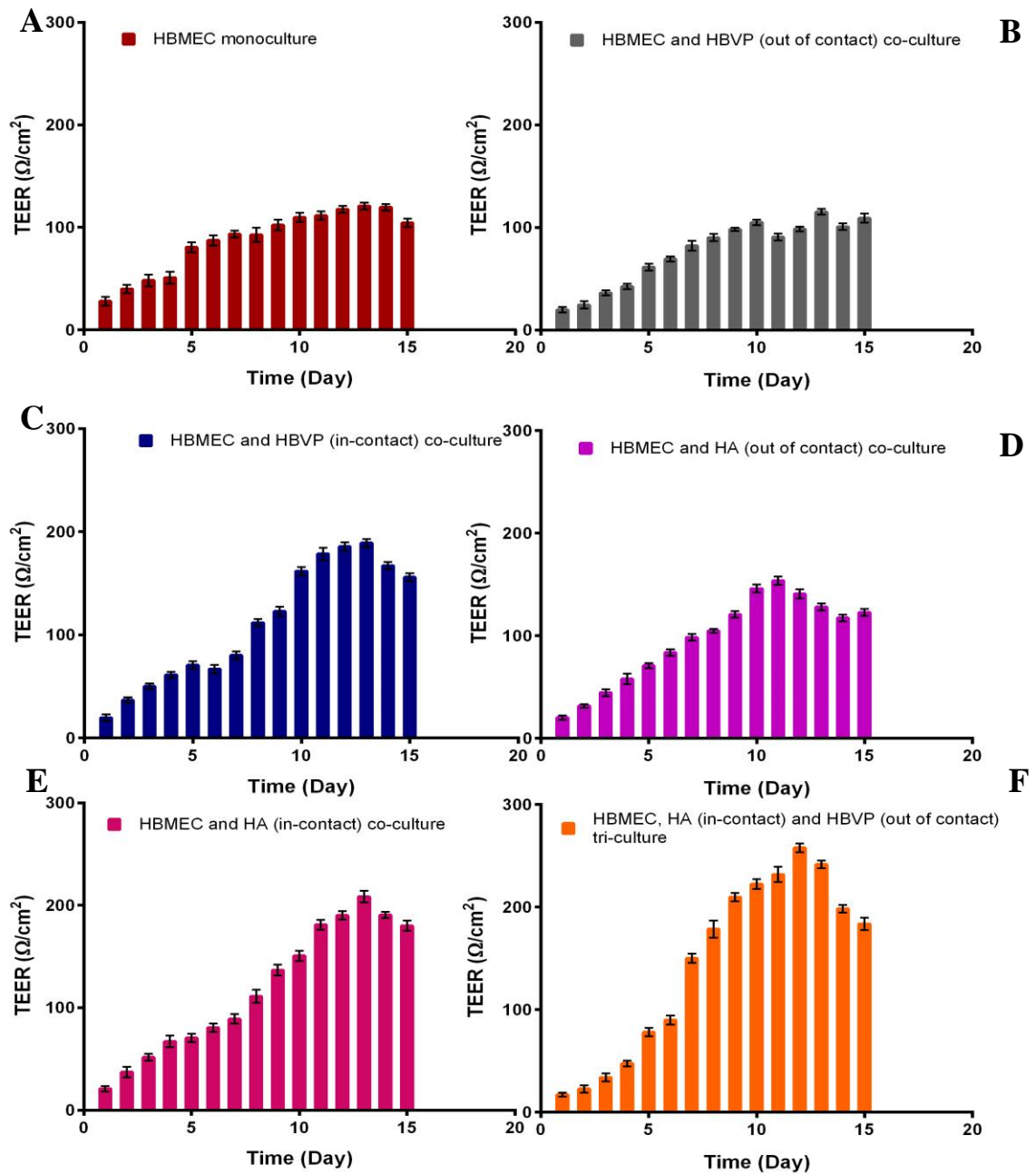


Figure 5.22 Effect of co- and tri cultivation on the induction of TEER in HBMEC monolayers of *in vitro* BBB models.

**A.** HBMEC monoculture. **B.** HBMEC and HBVP (out of contact) co-culture. **C.** HBMEC and HBVP (in-contact) co-culture. **D.** HBMEC and HA (out of contact) co-culture **E.** HBMEC and HA (in-contact) co-culture **F.** HBMEC, HA (in-contact) and HBVP (out of contact) tri-culture. TEER readings for different culture models up to Day 15. The data points are means of three experimental repeats ( $n=3$ ) and the error bars represent  $\pm$  standard deviation ( $\pm$ SD), where each experiment was conducted in triplicate and each culture was measured five times ( $n=15$ ).

The TEER readings of all the HBMEC co- and tri-models were plotted together on a line graph to compare the trend TEER values of different models with respect to time (Figure 5.23). The highest TEER was of  $258 \Omega/\text{cm}^2$  was shown by the tri-culture model having HBMEC, HA (in-contact) and HBVP (out of contact). All models showed a drop in the TEER values after day 13.

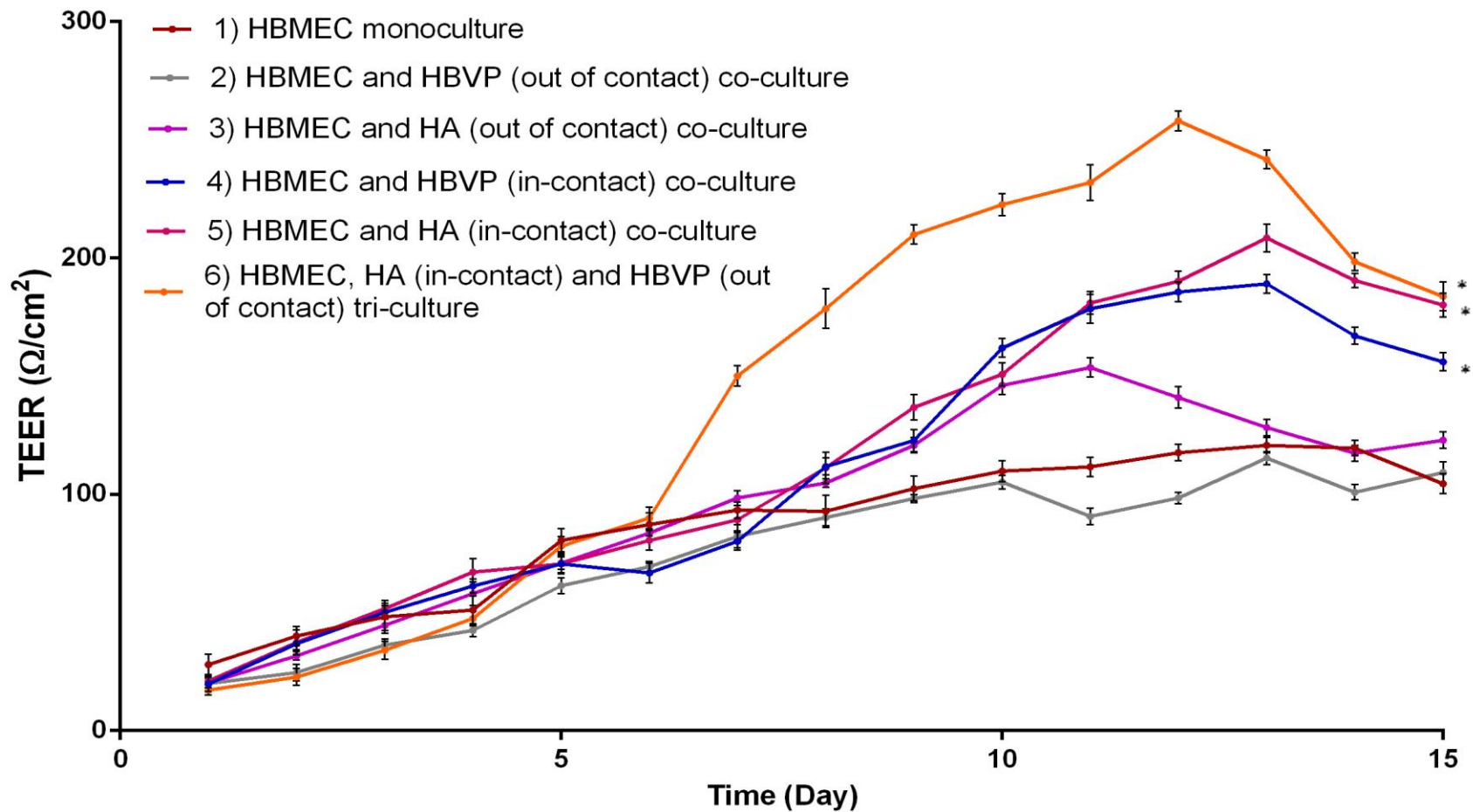


Figure 5.23 Comparison of TEER values between all the HBMEC co- and tri- culture models.

There was a steady increase in the TEER values for all models up to day 6. After day 6 the tri-culture model showed an large increase in the TEER values compared to other models. The data points are means of three experimental repeats (n=3) and the error bars represent  $\pm$  standard deviation ( $\pm$ SD), where each experiment was conducted in triplicate and each culture was measured five times (n=15). \* p < 0.05 was considered to be statistically significant.

As seen in Figure 5.24, the tri-culture model in lane 6, comprising of the HBMEC, HA (in-contact) and HBVP (out of contact) showed highest expression of both occludin and claudin-5, confirmed by densitometry as 867 % and 136 % relative to the HBMEC monoculture (Lane 1) (Figure 5.24 A & B). The co-culture of HBMEC and HBVP out of contact (Lane 2) showed the lowest expression of occludin and the HBMEC and HBVP in contact (Lane 3), had the lowest expression of claudin, confirmed by densitometry to be 93 % and 17 % respectively (Figure 5.25 A & B).

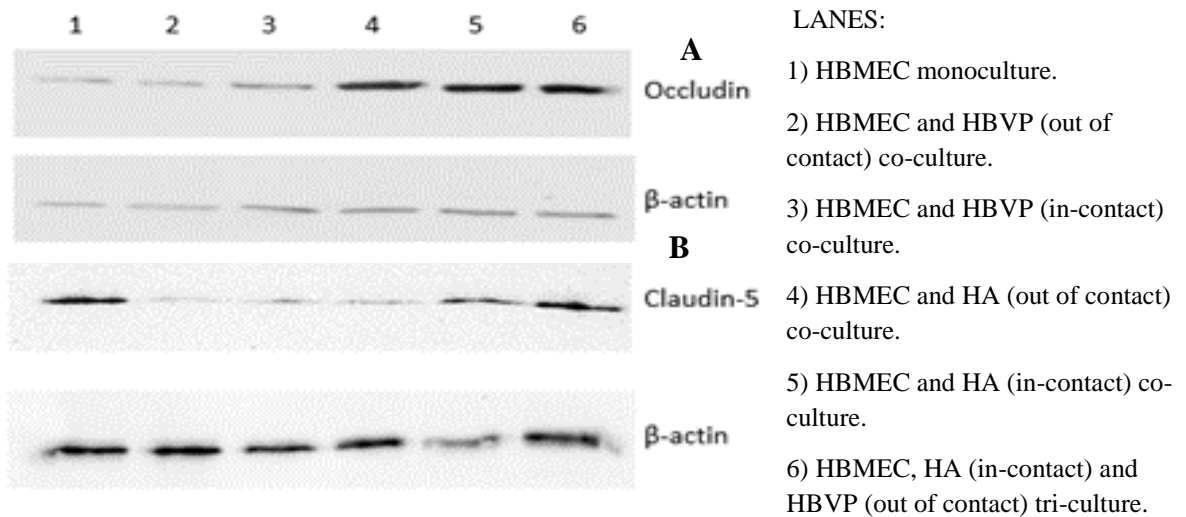


Figure 5.24 Western blots for TJs proteins expression in HBMEC mono-, co- and tri- cultures.

**A.** Western blot for occludin protein (65 kDa). **B.** Western blot for claudin-5 protein (23 kDa). Each well was loaded with 10  $\mu$ g protein.  $\beta$ -actin protein (42 kDa) was used as the loading control.

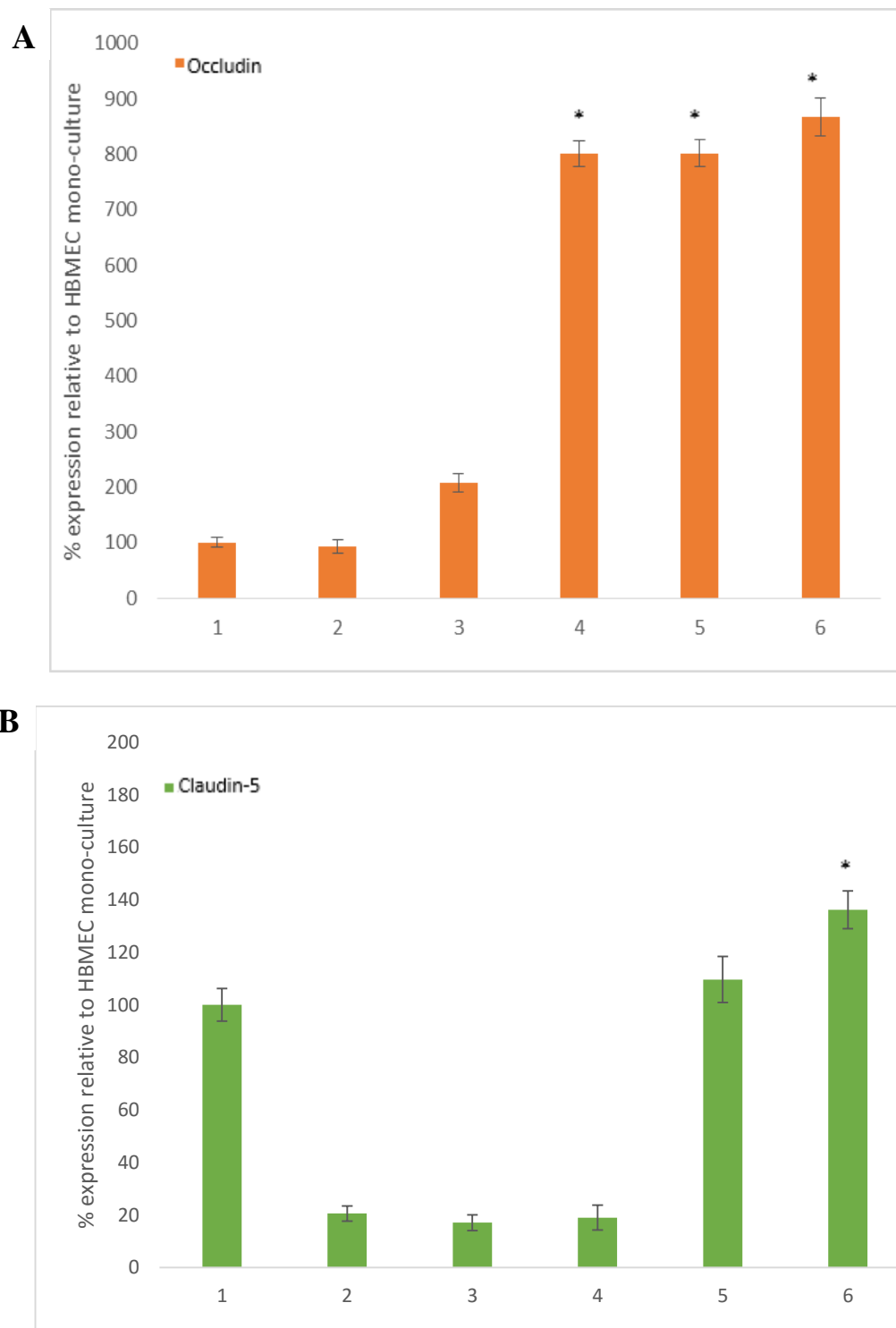


Figure 5.25 Densitometry analysis of TJ proteins expression in HBMEC mono-, co- and tri- cultures.

**A.** Densitometry analysis for occludin (65 kDa). **B.** Densitometry analysis for claudin-5 (23 kDa). 1) HBMEC monoculture. 2) HBMEC and HBVP (out of contact) co-culture. 3) HBMEC and HBVP (in-contact) co-culture. 4) HBMEC and HA (out of contact) co-culture. 5) HBMEC and HA (in-contact) co-culture. 6) HBMEC, HA (in-contact) and HBVP (out of contact) tri-culture. The error bars represent mean  $\pm$  standard deviation ( $\pm$ SD) of three measurements of each protein band quantified. \*  $p < 0.05$  was considered to be statistically significant.

### 5.2.2.2 Comparison of culture models in FBS and human serum

The main aim was to develop an *in vitro* BBB model having components of human origin to avoid any species variability. All of the cultures investigated in the thesis had been grown in human serum (HS), however to determine the effects of HS compared to foetal bovine serum (FBS) on the properties of the BBB and to allow comparison to studies in the literature, a small subset of experiments were conducted comparing the two conditions. The primary cells were weaned from FBS to human serum, in order to determine the effect of human serum on the TEER values. The co- (HBMEC and HA) and tri- culture (HBMEC, HA and pericyte) models giving the highest TEER values in Figure 5.19 were selected for the study, as the high TEER and TJ protein expression suggested that the BBB formed was intact under these conditions. TEER values were taken between day 1 to day 15 using the EVOM instrument.

All of the culture models showed a similar trend for the TEER values (Figure 5.26 A-D) and no significant difference was seen in the TEER values when the cells were cultured in FBS or human serum. The tri-culture model grown in FBS showed highest TEER value of 258  $\Omega/\text{cm}^2$  on day 12. The tri-culture model grown in human serum showed highest TEER value of 259  $\Omega/\text{cm}^2$  on day 13. A similar trend was seen with the co-culture models, the maximum TEER value of the model grown in FBS was 211  $\Omega/\text{cm}^2$  on day 12 and the model grown in human serum was 208  $\Omega/\text{cm}^2$  on day 13. .

As seen in Figure 5.27, a scatter plot comparing the TEER values with respect to time for both the models cultured in FBS and human serum showed no difference.

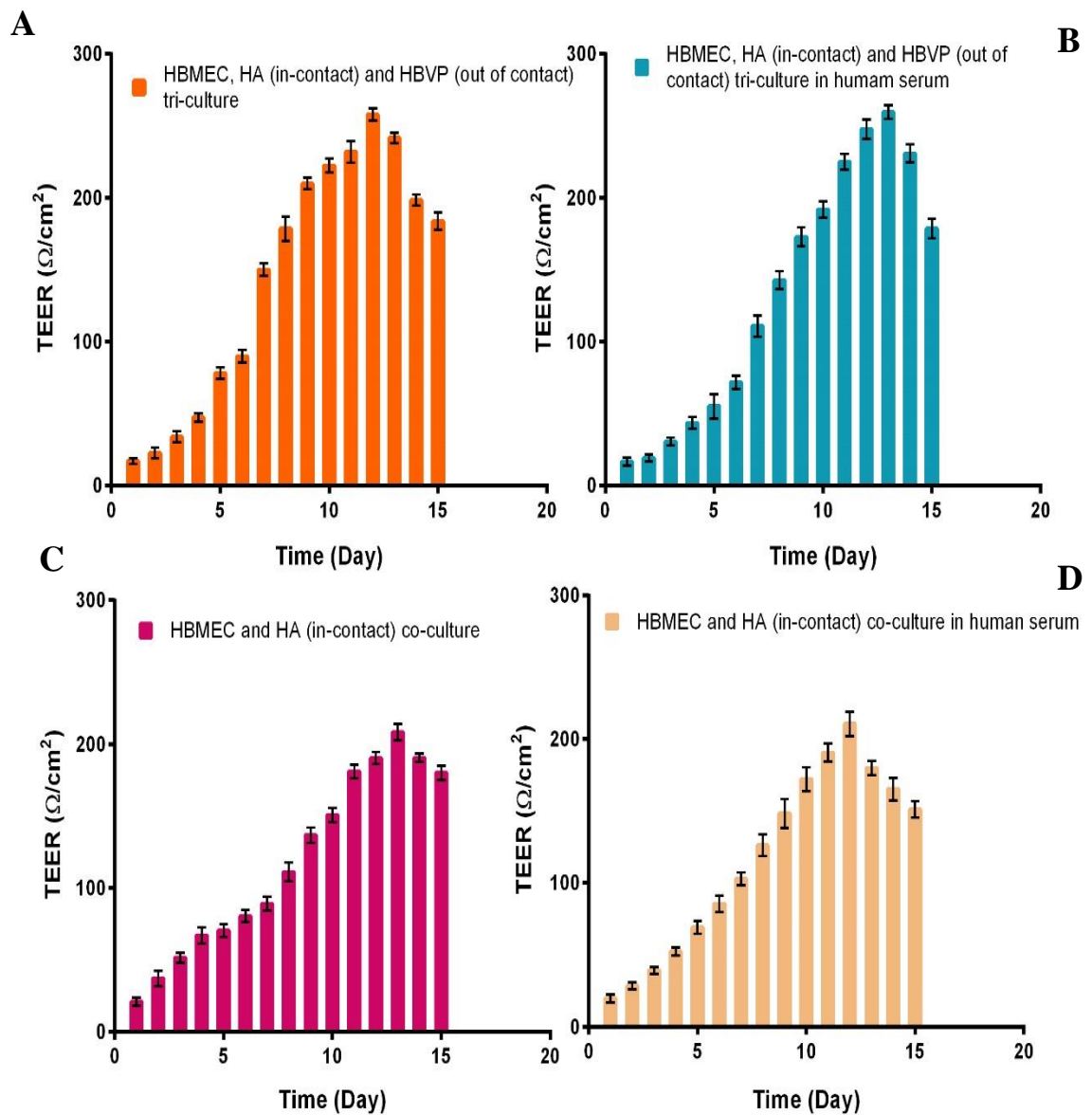


Figure 5.26 Effect of foetal calf serum and human serum on the induction of TEER in HBMEC co- and tri-culture *in vitro* BBB models.

**A.:** HBMEC, HA (in-contact) and HBVP (out of contact) tri-culture model cultured in foetal bovine serum. **B.** HBMEC, HA (in-contact) and HBVP (out of contact) tri-culture model cultured in human serum. **C.** HBMEC and HA (in-contact) co-culture model cultured in foetal bovine serum. **D.** HBMEC and HA (in-contact) co-culture model cultured in human serum. TEER readings for different culture models up to Day 15. The data points are means of three replicates ( $n=3$ ) and the error bars represent  $\pm$  standard deviation ( $\pm$ SD) of three inter-experimental replicates.

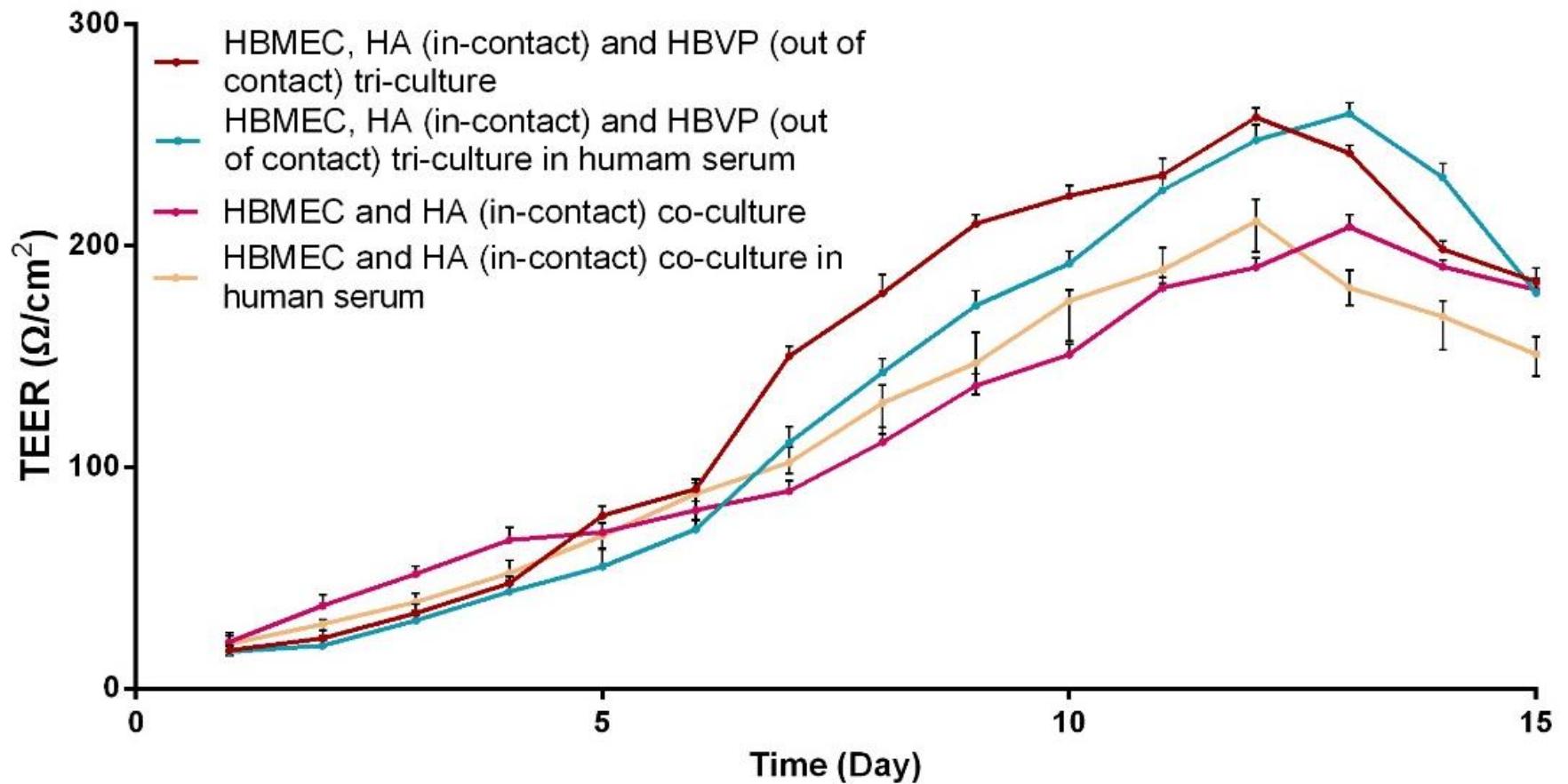


Figure 5.27 Comparison between TEER values obtained from HBMEC co- and tri-cultures of *in vitro* BBB models grown in foetal calf serum and human serum in. All models traced a similar pattern of TEER values showing no significant difference in the readings. The data points are means of three replicates (n=3) and the error bars represent  $\pm$  standard deviation ( $\pm$ SD) of three inter-experimental repeats. \* p < 0.05 was considered to be statistically significant.

The models were studied for the expression of the tight junction proteins, occludin and claudin-5 (Figure 5.28 A & B). The tight junction proteins occludin and claudin-5 showed similar expression in models grown in human serum or FBS. The expression of occludin was 225 A.U. in HBMEC, HA (in-contact) and HBVP (out of contact) tri-culture model cultured in human serum as compared to other models which gave an average value of 255 A.U. As seen in Figure 5.29 B, expression of claudin was seen to be similar in all the co-cultures and tri-culture models grown in FBS and HS. The expression of claudin-5 was 239 A.U. in HBMEC, HA (in-contact) co- culture model cultured in human serum as compared to other models which gave an average value of 248 A.U

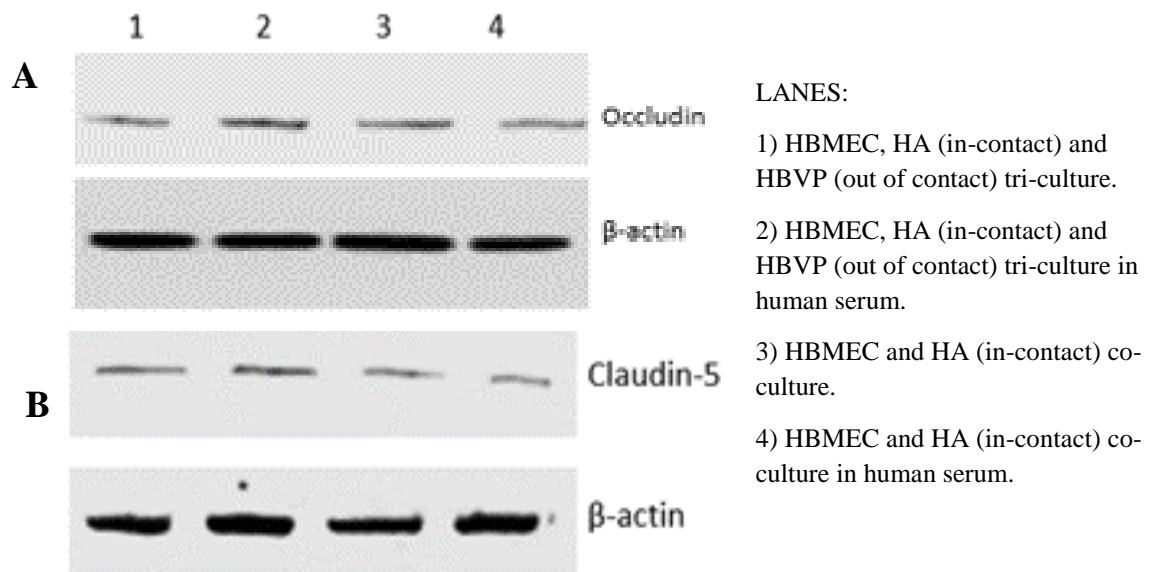


Figure 5.28 Western blots for TJs protein expression in HBMEC co- and tri-cultures of *in vitro* BBB models grown in foetal calf serum and human serum.

**A.** Western blot of different models for occludin protein (65 kDa) **B.** Western blot of different models for (claudin-5 protein (23 kDa). Each well was loaded with 10  $\mu$ g protein.  $\beta$ -actin protein (42 kDa) was used as the loading control.

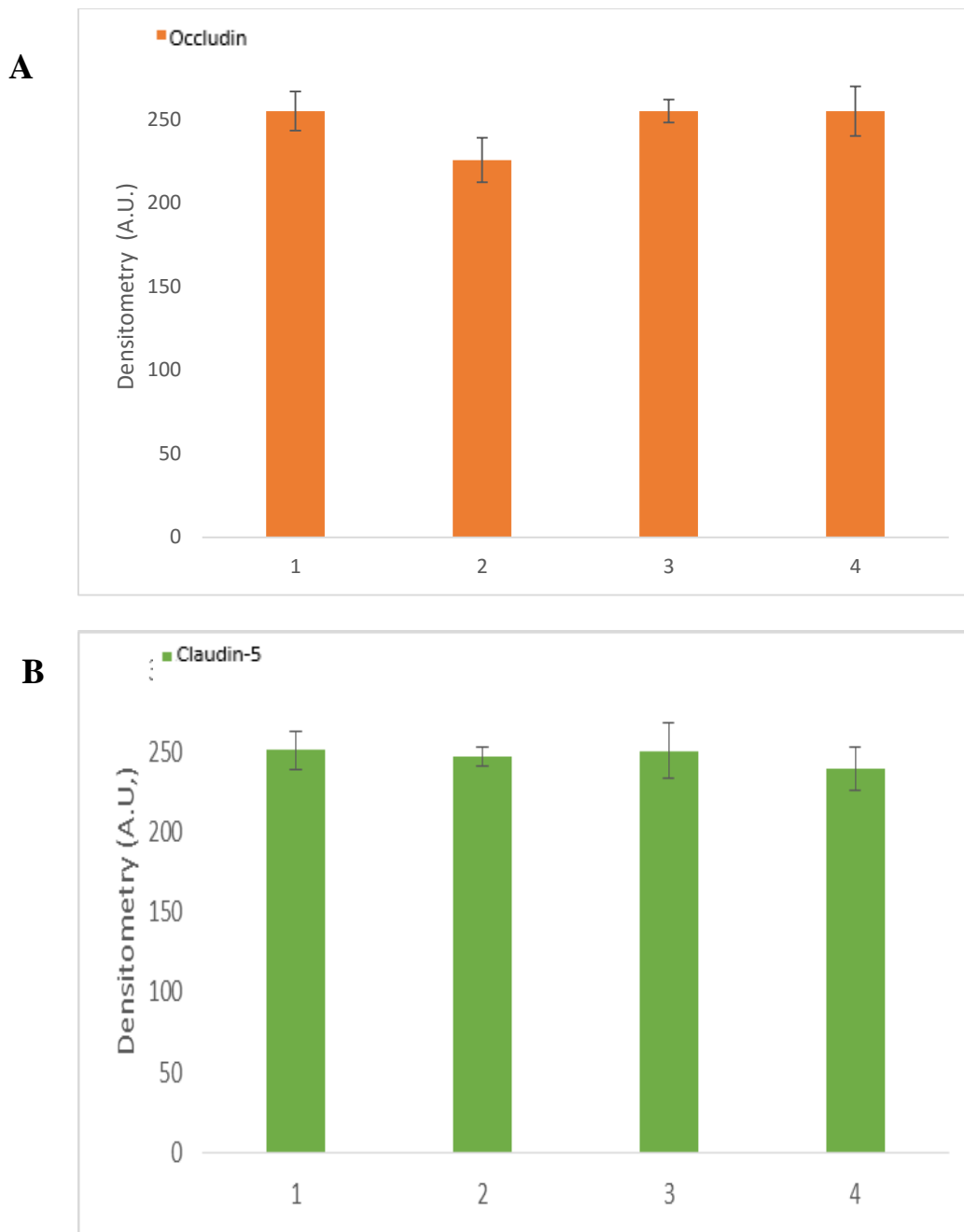


Figure 5.29 Densitometry analysis of TJs proteins expression in HBMEC co- and tri-cultures of *in vitro* BBB models grown in foetal calf serum and human serum.

**A.** Densitometry for expression of culture models for occludin (65 kDa). **B.** Densitometry for expression of culture models for claudin-5 (23 kDa). 1) HBMEC, HA (in-contact) and HBVP (out of contact) tri-culture model cultured in foetal bovine serum. 2) HBMEC, HA (in-contact) and HBVP (out of contact) tri-culture model cultured in human serum. 3) HBMEC and HA (in-contact) co-culture model cultured in foetal bovine serum. 4) HBMEC and HA (in-contact) co-culture model cultured in human serum. The error bars represent  $\pm$  standard deviation ( $\pm$ SD) of three measurement of each protein band. \*  $p < 0.05$  was considered to be statistically significant.

### 5.2.2.3 Comparison of models grown on static polycarbonate, Alvetex insert and perfused Alvetex insert.

*In vivo* the cells grow in a three dimensional environment and are under a constant shear stress (5-50 dyne/cm<sup>3</sup>) due to the surrounding blood flow. In this study, we took the culture models which gave us the highest TEER value and TJ protein expression; which was the tri-culture model and the co-culture models comprising of the endothelial cells and the astrocytes (in contact) (Section 5.2.1.1), and cultured them in a three-dimensional polycarbonate scaffold (Alvetex insert), with perfusion of media, to apply shear stress, thus trying to mimic the conditions *in vivo*.

The inserts were connected to a perfusion plate which was maintained at flow pressure of 20 dyne/cm<sup>2</sup>. These perfused models were compared to the static models also set up using the Alvetex scaffold. The perfusion of tri-culture model increased the maximum TEER value from 456  $\Omega$ /cm<sup>2</sup> to 723  $\Omega$ /cm<sup>2</sup> (Figure 5.30 A & B). The perfusion of co-culture model increased the TEER value from 421  $\Omega$ /cm<sup>2</sup> to 647  $\Omega$ /cm<sup>2</sup> (Figure 5.30 C & D). The tri-culture model, HBMEC, HA (in-contact) and HBVP (out of contact) showed a higher TEER value than the co-culture model, HBMEC and HA (in-contact) (Figure 5.30 A & C).

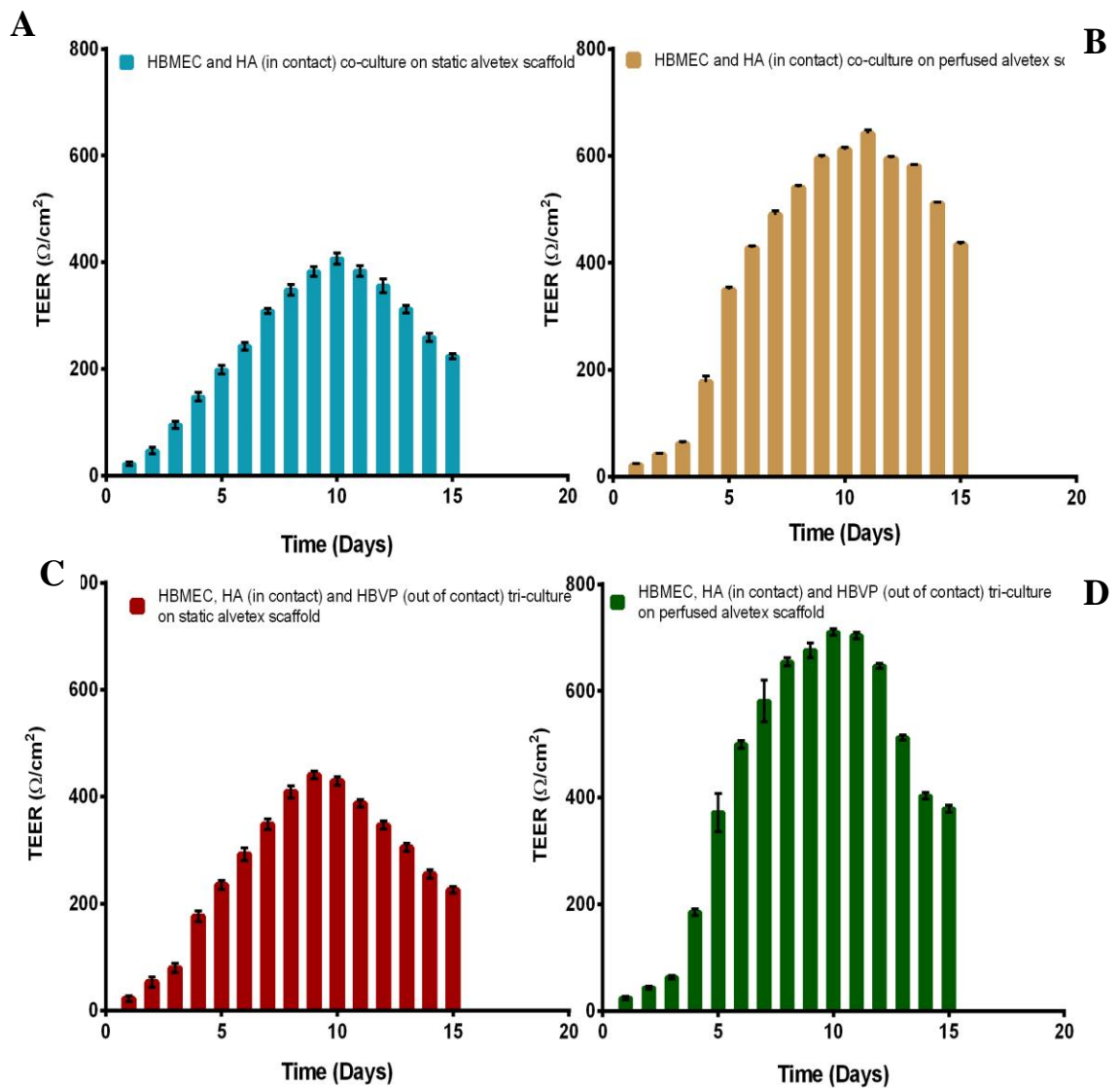


Figure 5.30 Comparison of TEER values between co- and tri-culture models of HBMEC in Alvetex scaffold with and without perfusion (sheer flow).

**A.** Co-culture of HBMEC and HA in static conditions. **B.** Co-culture of HBMEC and HA in perfused conditions **C.** Tri-culture model of HBMEC, HA and HBVP in static conditions. **D.** Tri-culture model of HBMEC, HA and HBVP in perfused conditions. The data points are means of three replicates (n=3) and the error bars represent  $\pm$  standard deviation ( $\pm$ SD) of three inter-experimental repeats.

The merged graph of the TEER values with respect to time for different co- and tri- cultures models cultured in static polycarbonate inserts, static Alvetex scaffolds and perfused Alvetex scaffolds is shown in Figure 5.31. The tri-culture and co-culture models when grown in the 3D Alvetex scaffold showed an increase in the TEER values as compared to the tri-culture on polycarbonate inserts. The Alvetex model when perfused with a flow of media showed a further increase in the TEER values. The TEER value of tri-culture model was  $258 \Omega/\text{cm}^2$  in polycarbonate insert model which increased to  $440 \Omega/\text{cm}^2$  in static alvetex insert which further increased to  $710 \Omega/\text{cm}^2$  in the perfused Alvetex inserts. It can be concluded that the cultures grown in 3D scaffolds showed a higher TEER values compared to 2D inserts. The introduction of flow by perfusing the scaffolds enhanced the TEER expression.

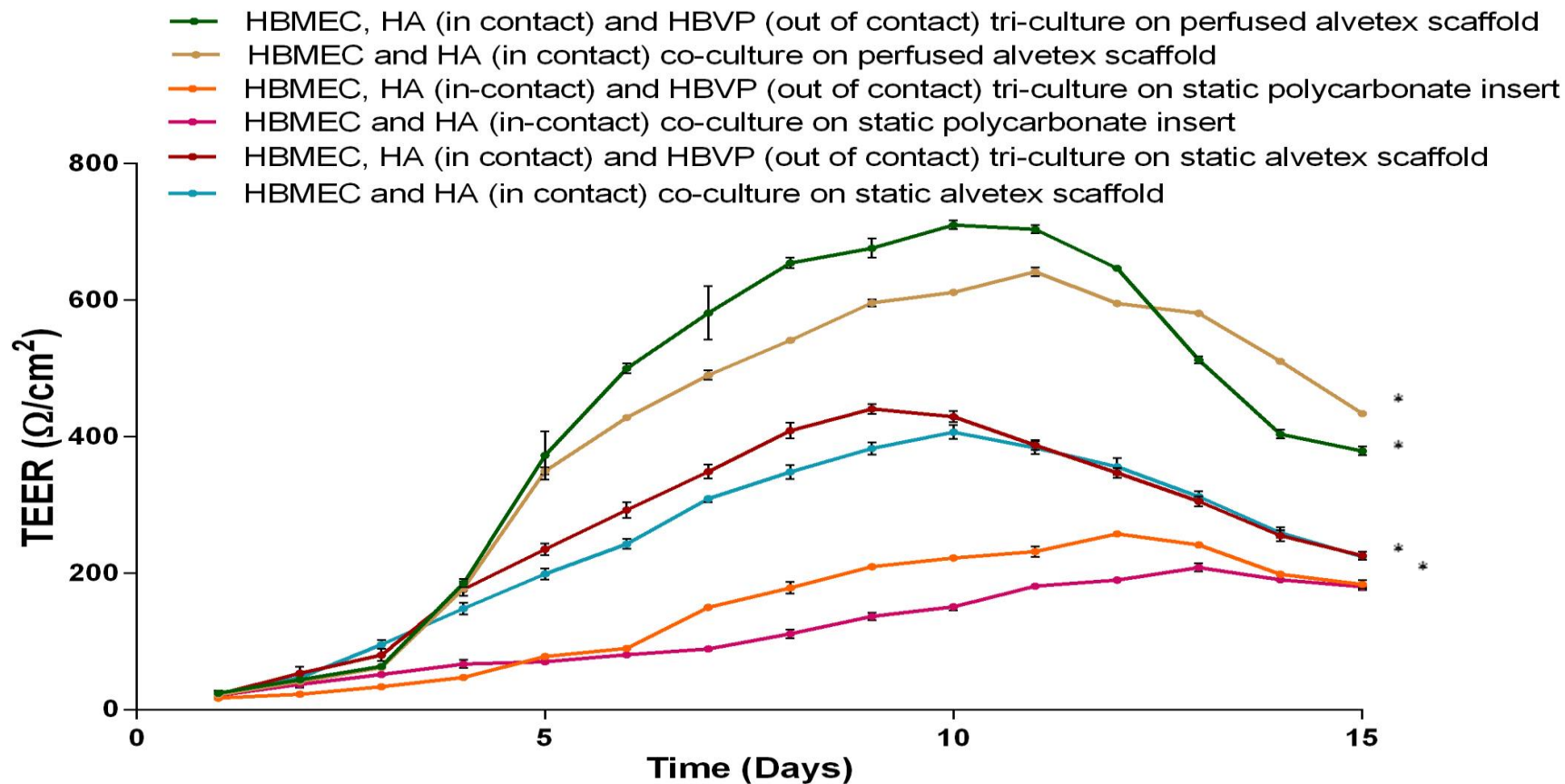


Figure 5.31 Comparison of TEER measurements in co- and tri- cultures of HBMEC with perfused alvetex scaffold, static alvetex scaffold and static polycarbonate insert of BBB models.

The data points were means of three replicates (n=3) and the error bars represent  $\pm$  standard deviation ( $\pm$ SD) of three inter-experimental repeats. \*  $p < 0.05$  was considered to be statistically significant.

The models were also studied for the expression of tight junction proteins occludin and claudin-5 (Figure 5.32 A & B). The tight junction proteins occludin and claudin-5 showed the lowest expression in co-cultures on static polycarbonate inserts (Lane 1) and highest expression in tri-cultures on perfused Alvetex inserts (Lane 6), confirmed by densitometry to be 716 % and 307 % for occludin and claudin respectively (Figure 5.33 A & B). The co-culture of HBMEC and HA (in-contact) (Lanes 1, 3 and 5) grown in different inserts showed lower expression of occludin and claudin when compared to the tri-culture HBMEC, HA (in-contact) and HBVP (out of contact) grown on different inserts (Lanes 2, 4 and 6).

- 1) HBMEC and HA (in-contact) co-culture static polycarbonate insert.
- 2) HBMEC, HA (in-contact) and HBVP (out of contact) tri-culture static polycarbonate insert.
- 3) HBMEC and HA (in-contact) co-culture on static alvetex scaffold.
- 4) HBMEC, HA (in-contact) and HBVP (out of contact) tri-culture on static alvetex scaffold.
- 5) HBMEC and HA (in-contact) co-culture on perfused alvetex scaffold.
- 6) HBMEC, HA (in-contact) and HBVP (out of contact) tri-culture on perfused alvetex scaffold.

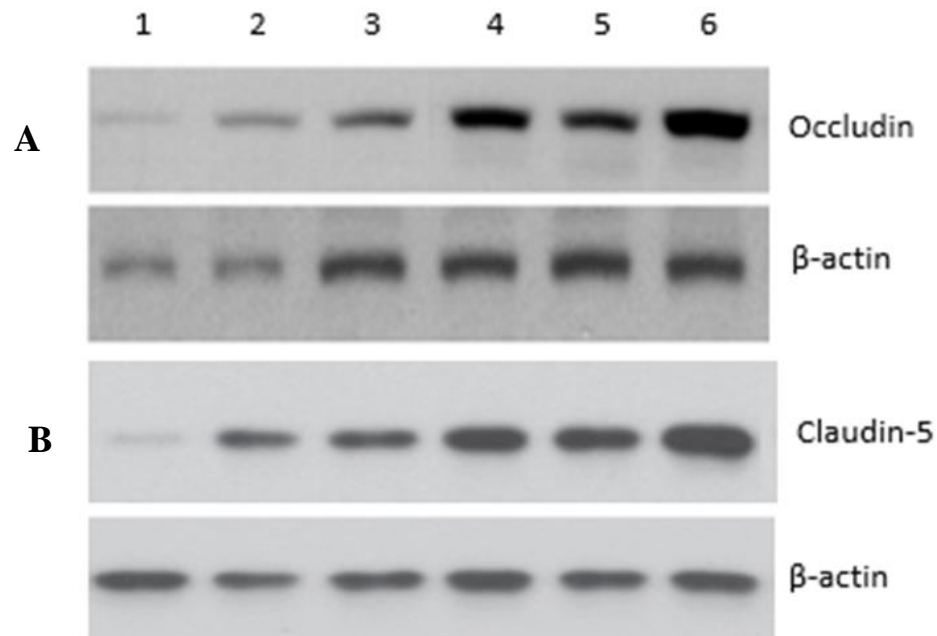


Figure 5.32 Western blots for TJs proteins expression in HBMEC tri-cultures set up on different inserts.

**A.** Western blot for claudin-5 protein (23 kDa). **B.** Western blot for occludin protein (65 kDa). Each well was loaded with 10  $\mu$ g protein.  $\beta$ -actin protein (42 kDa) was used as the loading control.

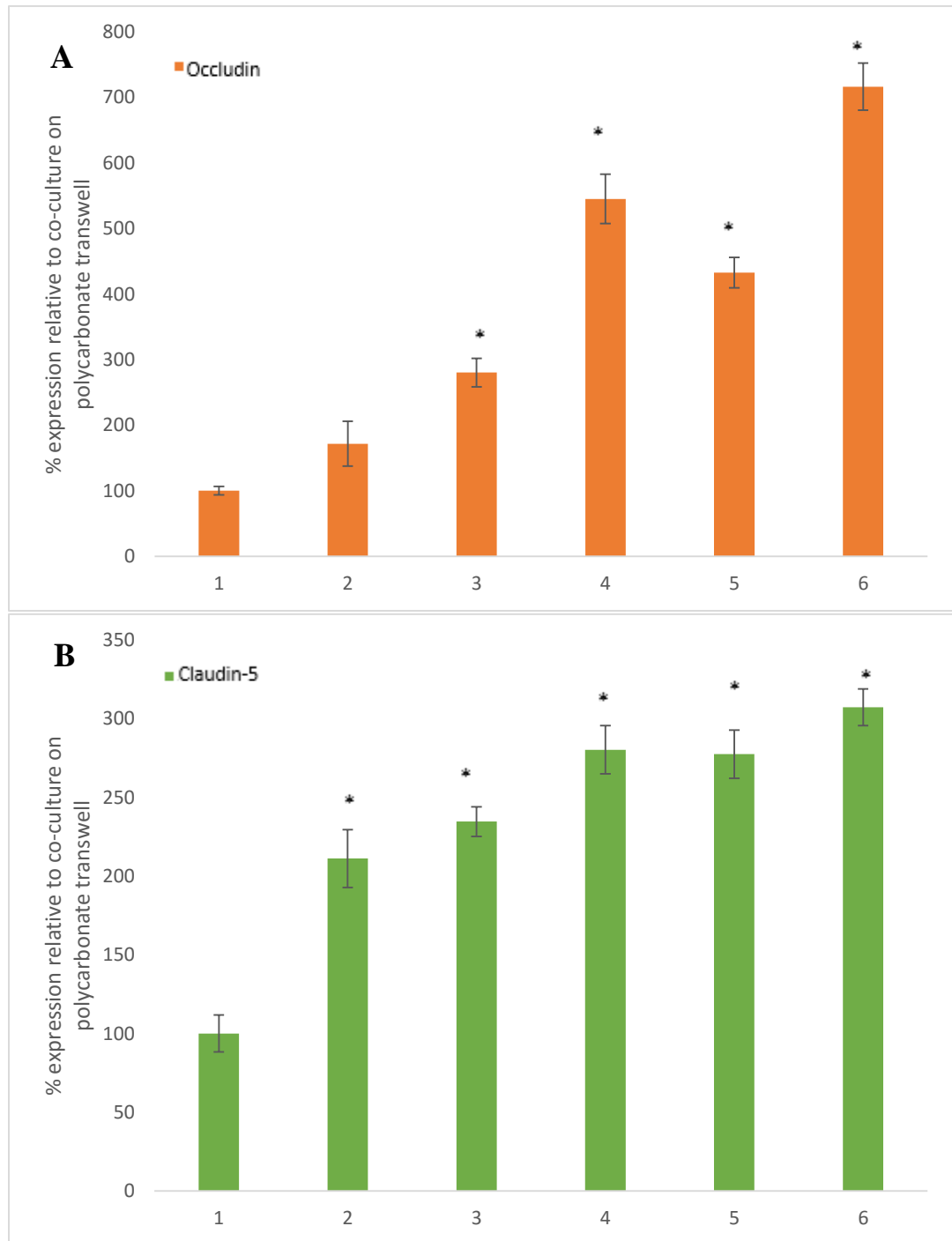


Figure 5.33 Densitometry analysis of TJs proteins expression in HBMEC tri-cultures set up on different inserts.

**A.** Densitometry for expression of occludin (65 kDa). **B.** Densitometry for claudin-5 expression (23 kDa). 1) HBMEC, HA (in-contact) co-culture on static polycarbonate insert. 2) HBMEC, HA (in-contact) and HBVP (out of contact) on tri-culture static polycarbonate insert. 3) HBMEC, HA (in-contact) co-culture on static Alvetex scaffold. 4) HBMEC, HA (in-contact) and HBVP (out of contact) tri-culture on static Alvetex scaffold. 5) HBMEC, HA (in-contact) co-culture on perfused alvetex scaffold. 6) HBMEC, HA (in-contact) and HBVP (out of contact) tri-culture on perfused Alvetex scaffold. The error bars represent  $\pm$  standard deviation ( $\pm$ SD) of three measurements of each protein band. \*  $p < 0.05$  was considered to be statistically significant.

#### 5.2.2.4 Effect of location of pericyte in co- and tri- culture models

The tri-culture of endothelial cells, astrocyte and pericyte showed a high TEER value when compared to co-culture of endothelial cells and astrocytes. In the following study cultures of endothelial cells, astrocytes and pericytes were grown in various formations with: 1) pericytes in contact with the HBMEC and HA on the insert or 2) HBMEC and HA co-cultured on the insert with pericytes out of contact or 3) HBMEC and HA co-cultured on the insert in the presence of pericyte conditioned media and all were compared to the control 4) co-culture of HBMEC and HA (in-contact). This was conducted to see if the location of the cells in the tri-culture affected the TEER values and the expression of TJs proteins and also to determine whether factors secreted into pericyte conditioned media stimulated the other cells leading to increase in TEER values.

All the three models show similar readings of TEER up to day 6, after which the tri-culture model comprising of HBMEC, HA (in-contact) and HBVP (out of contact) showed the highest TEER value of  $259 \Omega/\text{cm}^2$  on day 13 (Figure 5.34 B). The HBMEC, HA (in-contact) and HBVP (in-contact) tri-culture showed a peak TEER value of  $210 \Omega/\text{cm}^2$  on day 12 (Figure 5.34 A). The co-culture of HBMEC, HA (in-contact) grown in pericyte conditioned media showed maximum peak TEER value of  $208 \Omega/\text{cm}^2$  on day 13. As seen in Figure 5.35, showing the merge of the TEER measurements with respect to time for all models, the HBMEC and HA (in-contact) co-culture supplemented with pericyte conditioned media did not show any significant difference in the TEER values when compared to the control HBMEC and HA (in-contact). All the models showed a decline in the TEER values after day 13.

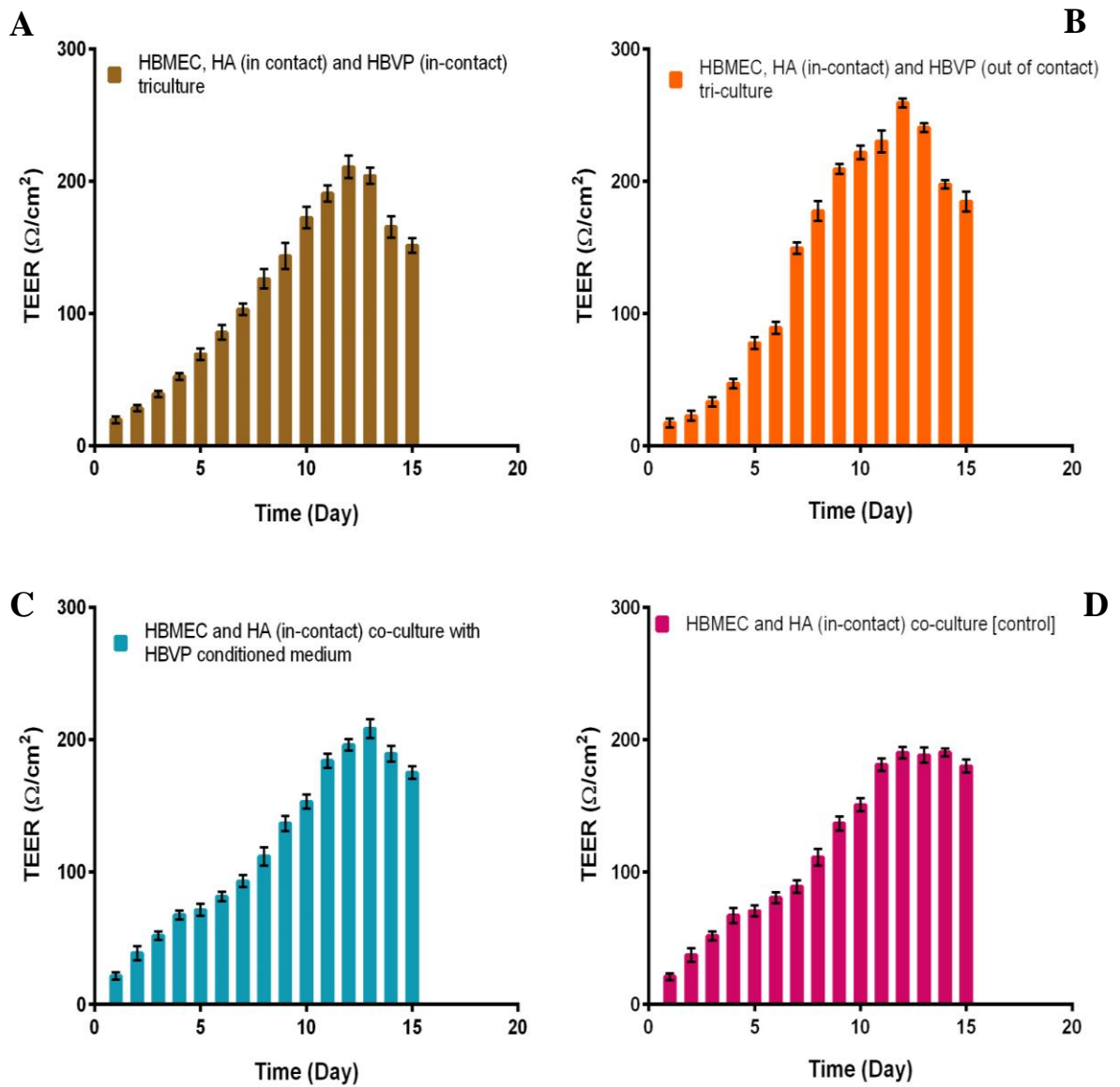


Figure 5.34 Effect of location of pericyte on the induction of TEER in tri- or co-culture *in vitro* BBB models.

**A.** HBMEC, HA (in-contact) and HBVP (in-contact) tri-culture. **B.** HBMEC, HA (in-contact) and HBVP (out of contact) tri-culture. **C.** HBMEC, HA (in-contact) co-culture with HBVP conditioned medium. **D.** HBMEC, HA (in-contact) co-culture [control]. The data points are means of three replicates ( $n=3$ ) and the error bars represent  $\pm$  standard deviation ( $\pm$ SD) of three inter-experimental repeats.

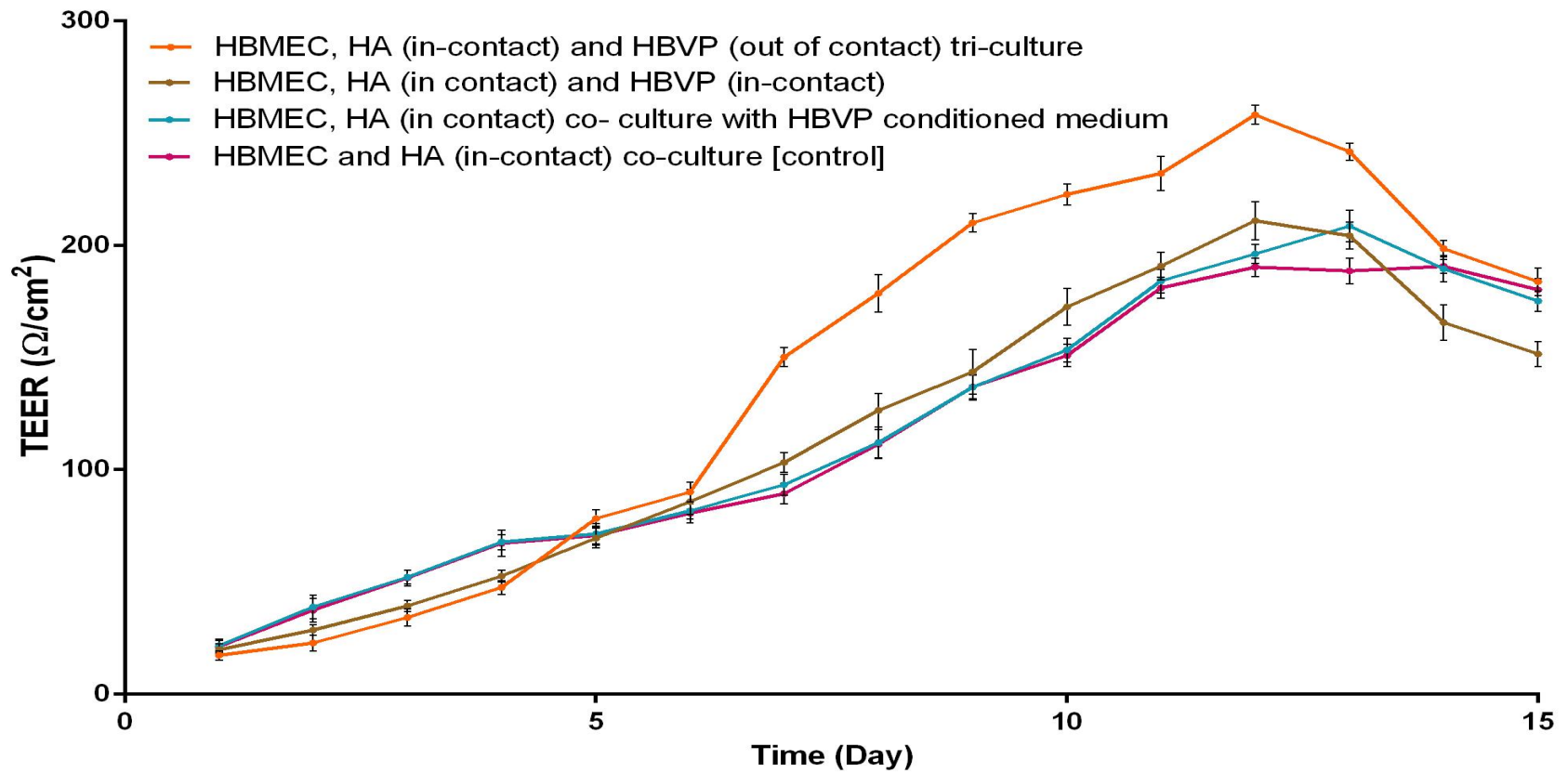


Figure 5.35 Comparison of TEER values between HBMEC and HA (in-contact) co-culture with different location of pericyte.

Tri-culture models of pericyte seeded either in or out of contact showed higher TEER values after day 6 in comparison to the control and the co-culture with pericyte conditioned medium. The data points are means of three replicates (n=3) and the error bars represent  $\pm$  standard deviation ( $\pm$ SD) of three inter-experimental repeats. \*  $p < 0.05$  was considered to be statistically significant.

The models were studied for the expression of the tight junction proteins, occludin and claudin-5 (Figure 5.36 A & B). Tri-culture models with pericytes out of contact (Lane 3) or in contact with the transwell insert (Lane 4) showed a higher expression of tight junction proteins occludin and claudin-5 when compared to co-culture with pericyte conditioned medium (Lane 2) and co-culture alone (Lane 1). Densitometry measurements confirmed these findings indicating a highest value of 169 % for occludin (Lane 4) and 136 % for claudin (Lane 4) (Figure 5.37).

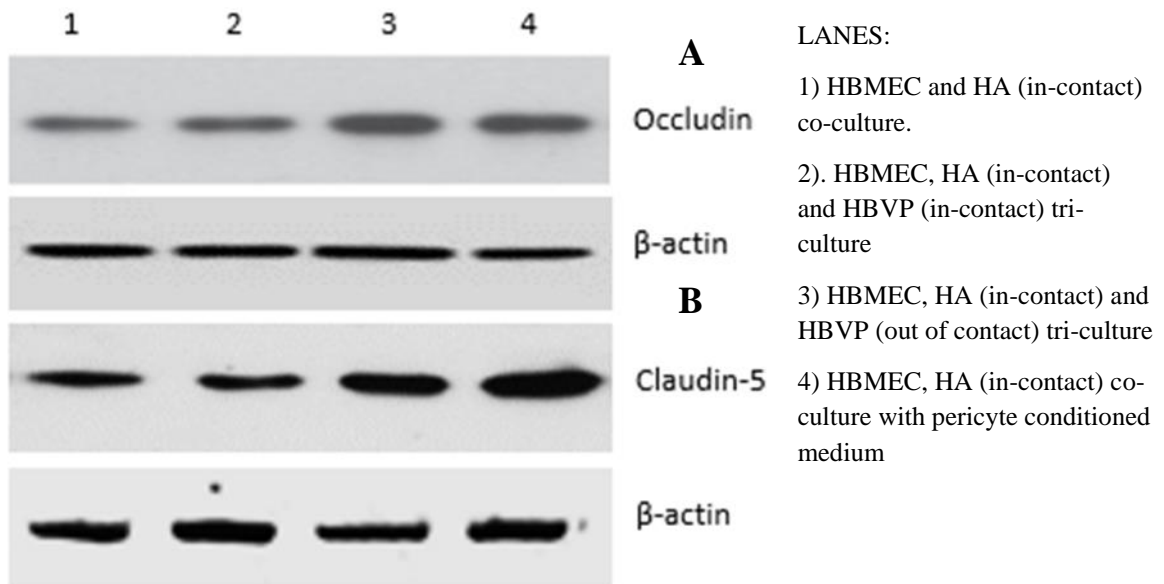


Figure 5.36 Western blots of TJs proteins expression in HBMEC co- and tri-cultures with different location of HBVP.

**A.** Western blot of different models for occludin protein (65 kDa). **B.** Western blot of different models for claudin-5 protein (23 kDa). Each well was loaded with 10 µg protein. β-actin protein (42 kDa) was used as the loading control.

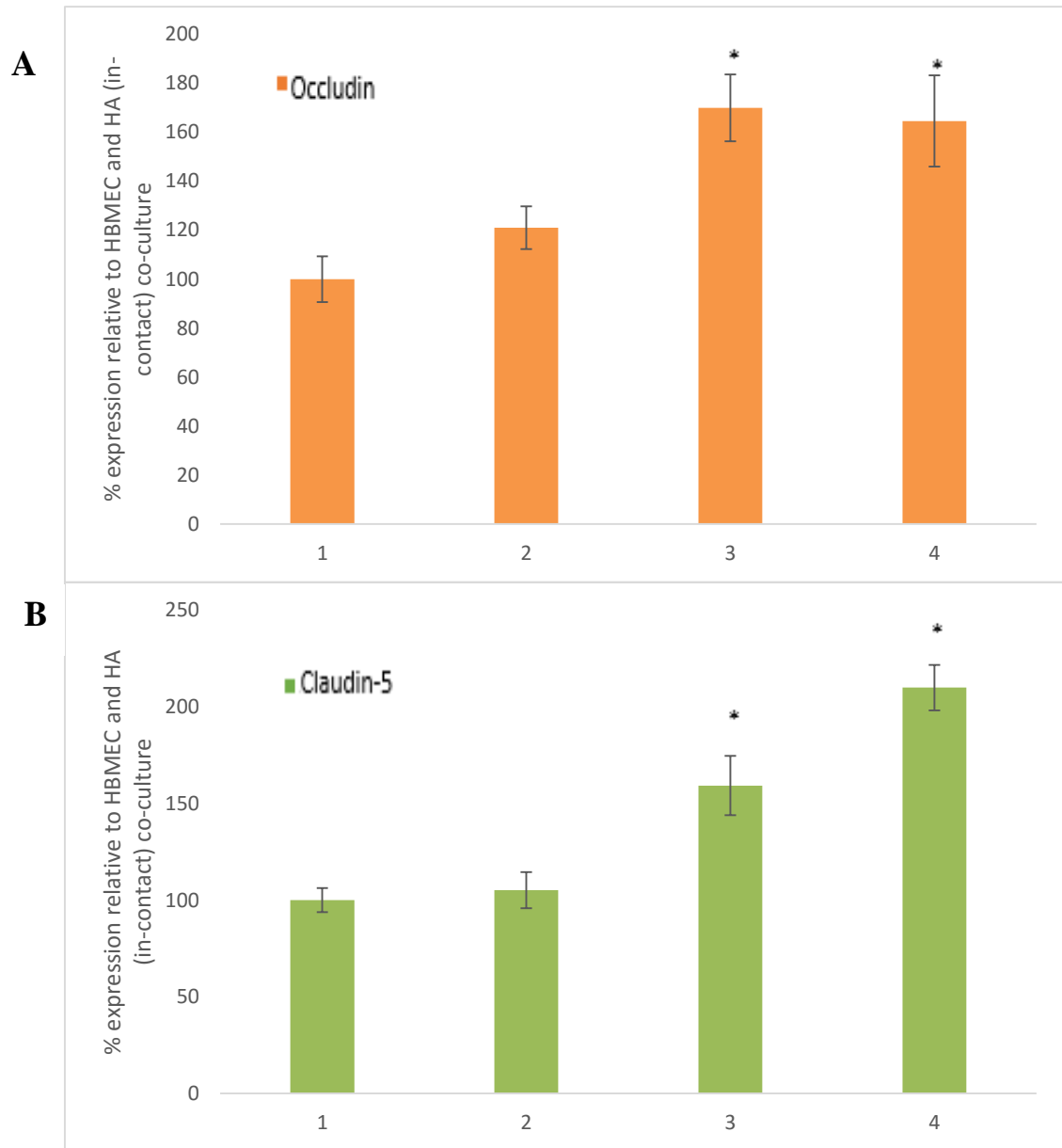


Figure 5.37 Densitometry of TJs proteins expression in HBMEC co-, tri-cultures with different location of HBVP.

**A.** Densitometry for occluding expression (65 kDa). **B.** Densitometry for claudin-5 expression (23 kDa). 1) HBMEC and HA (in-contact) co-culture. 2) HBMEC, HA (in-contact) co-culture with pericyte conditioned medium 3) HBMEC, HA (in-contact) and HBVP (out of contact) tri-culture. 4) HBMEC, HA (in-contact) and HBVP (in-contact) tri-culture. The error bars represent  $\pm$  standard deviation ( $\pm$ SD) of three measurements of each protein band. \*  $p < 0.05$  was considered to be statistically significant.

### 5.2.3 Expression and activity of proteins in designed *in vitro* BBB models.

#### 5.2.3.1 Expression and activity of efflux transporters ABCB<sub>1</sub> and ABCG<sub>2</sub> in HBMEC models

The efflux transporters located at the BBB play an important role in the disposition of drug administered for the treatment of glioma. It was therefore essential to characterise the expression and activity of the efflux transporters in designed *in vitro* BBB models to construct a physiologically relevant model. The expression and activity of efflux transporters ABCB<sub>1</sub> and ABCG<sub>2</sub> were studied in all the HBMEC mono-, co- and tri-culture BBB models.

As seen in Figure 5.38A, expression of ABCB<sub>1</sub> efflux transporter was higher in models comprising of endothelial cells and astrocytes (Lane 4 and 5) compared to all of the other models comprising of endothelial cells and pericytes (Lane 2 and 3). The tri-culture of HBMEC, HA (in-contact) and HBVP (out of contact) (Lane 6) and co-cultures of HBMEC and HA showed similar expression of ABCB<sub>1</sub> efflux transporters. The HBMEC monoculture showed the lowest expression of ABCB<sub>1</sub> transporters (Lane 1).

All models showed expression of ABCG<sub>2</sub> efflux transporters (Figure 5.38 B), the lowest expression was seen in co-culture model of HBMEC and pericyte (out of contact) (Figure 5.38 A) (Lane 2). The HBMEC mono-culture (Lane 1) showed expression higher when compared to the co-culture models (Lane 2,3,4,5), but the expression of ABCG<sub>2</sub> efflux transporter was higher in tri-culture model (Lane 6) compared to all the other designed BBB models. The expression was semi quantified by densitometry as seen in Figure 5.39 which showed similar trend of results.

LANES:

- 1) HBMEC monoculture.
- 2) HBMEC and HBVP (out of contact) co-culture.
- 3) HBMEC and HBVP (in-contact) co-culture.
- 4) HBMEC and HA (out of contact) co-culture.
- 5) HBMEC and HA (in-contact) co-culture.
- 6) HBMEC, HA (in-contact) and HBVP (out of contact) tri-culture.

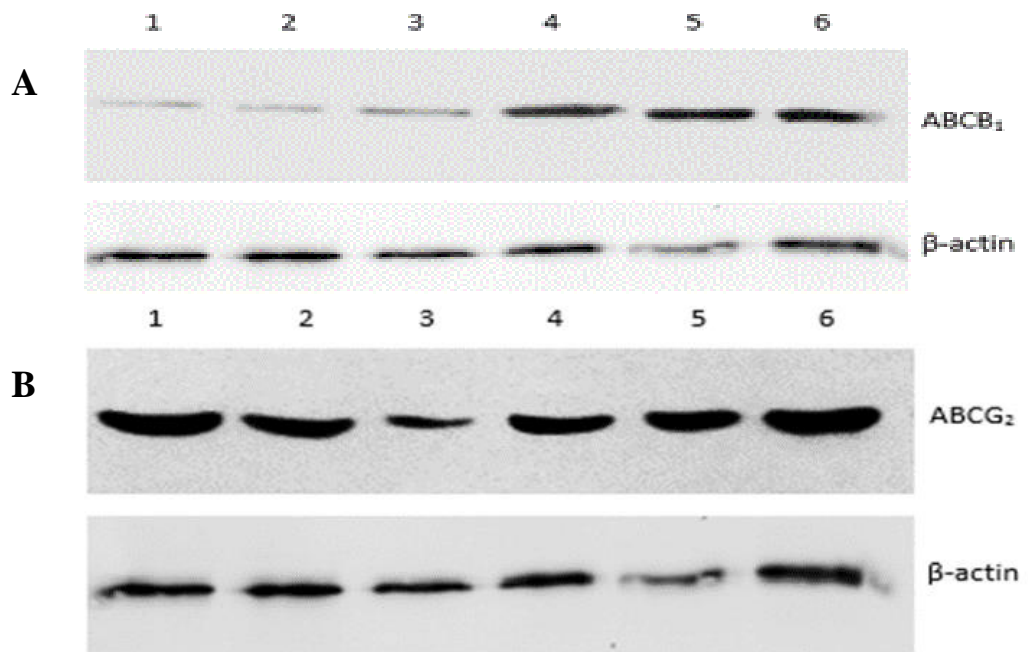


Figure 5.38 Expression of efflux transporters in different *in vitro* BBB models.

**A.** Expression of ABCB<sub>1</sub>. **B.** Expression of ABCG<sub>2</sub>. β-actin was used as the loading control. Each well was loaded with 10 μg of protein.

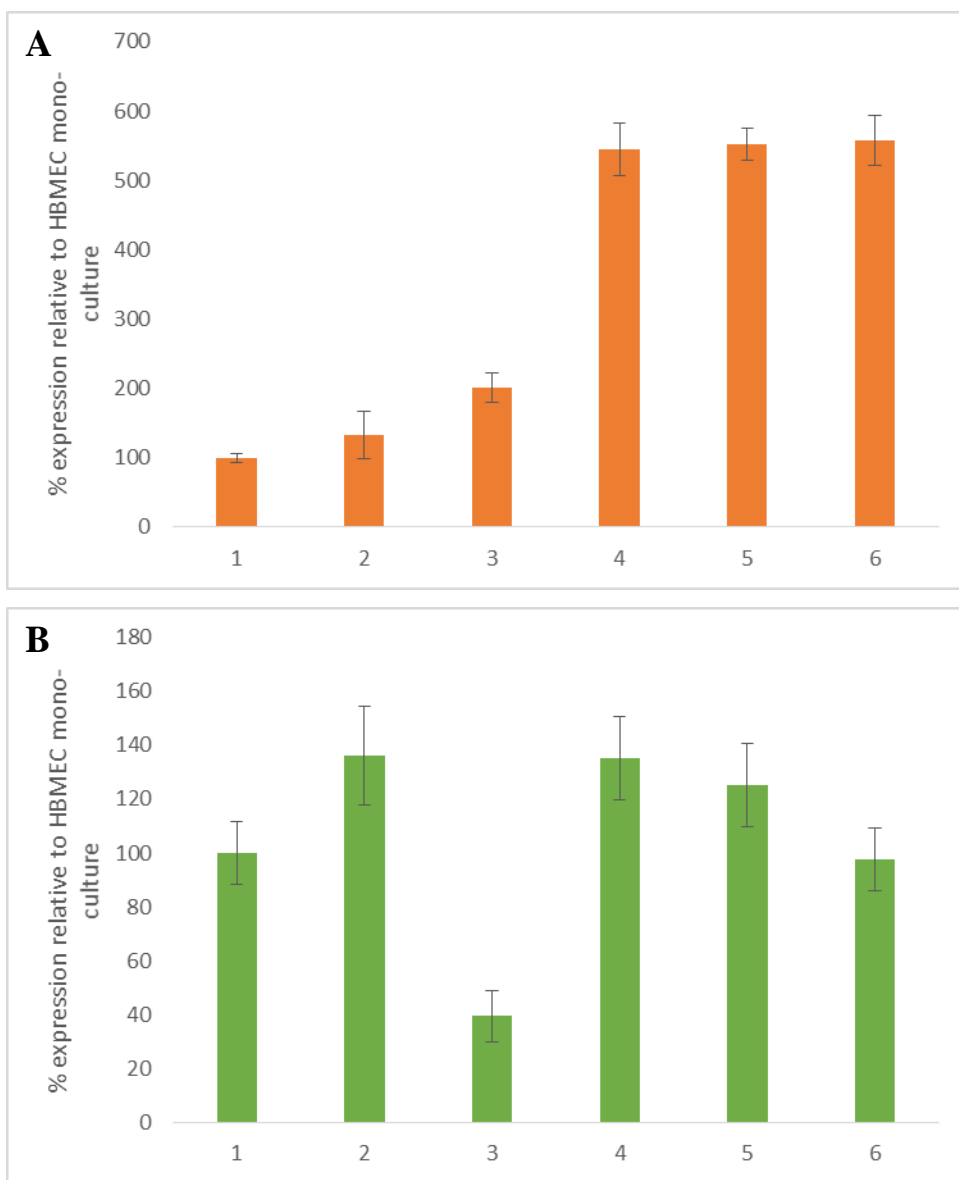


Figure 5.39 Densitometry of efflux transporters in different *in vitro* BBB models. **A.** ABCB<sub>1</sub>. **B.** ABCG<sub>2</sub>

\*  $p < 0.05$  was considered to be statistically significant

The activity of the efflux transporter ABCB<sub>1</sub> was assessed in different BBB models set up using HBMEC mono-, co-, and tri-cultures (Figure 5.40). The activity of ABCB<sub>1</sub> transporter was highest in the tri-culture model compared to all the other models. The co-cultures of astrocytes showed a similar activity in both in-contact and out of contact model which was also observed in the expression of the ABCB<sub>1</sub>. All the models showed a higher activity compared to the mono-culture suggesting co- and tri- culture enhances the activity of ABCB<sub>1</sub>. The co-culture of endothelial cells with pericytes, when grown in contact showed an increase in the activity of ABCB<sub>1</sub> compared to pericytes grown out of contact co-culture. The highest activity was shown by the tri-culture which was comparable to the expression of the ABCB<sub>1</sub>, as the tri-culture showed a high expression of ABCB<sub>1</sub>.

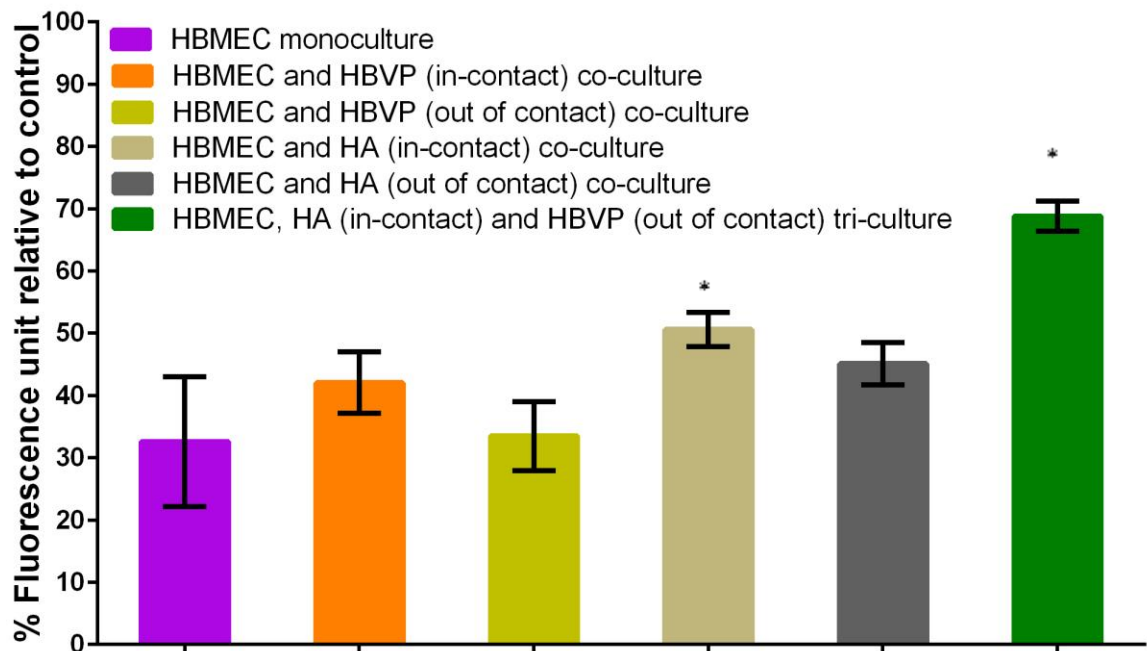


Figure 5.40 Activity of ABCB<sub>1</sub> efflux transporter in different *in vitro* BBB models.

Activity of ABCB<sub>1</sub> in the different model designed, highest activity was observed in tri-culture model HBMEC, HA (in-contact) and HBVP (out of contact). The efflux activity was measured by using substrate rhodamine123, the data was plotted relative to control. The dye loaded cells at 4 °C which inhibits the activity of the efflux transporter was the control. The data points are means of three replicates (n=3) and the error bars represent ± standard deviation (±SD) of three inter-experimental repeats. \* p < 0.05 was considered to be statistically significant

The activity of ABCG<sub>2</sub> transporter was assessed in all the different types of BBB model derived from HBMEC mono-, co- and tri-culture set-up. The highest activity of ABCG<sub>2</sub> transporter was recorded in the tri-culture model as compared to all the other models which is similar to the expression of ABCG<sub>2</sub>, where the highest expression was shown by the tri-culture model. The co-cultures of astrocytes showed a similar activity in astrocyte in-contact as compared to astrocytes grown out of contact (Figure 5.41). As seen in the activity of ABCB<sub>1</sub>, all the models showed a higher activity as compared to the mono-culture suggesting co- and tri- culture enhances the activity of the ABCG<sub>2</sub> efflux transporter. The co-culture of endothelial cells with the pericytes grown in contact also showed an increase in the activity of ABCG<sub>2</sub> compared to pericytes grown in out of contact co-culture (Figure 5.38). The co-culture of endothelial cells with the pericytes showed the lowest expression and activity of ABCG<sub>2</sub>.

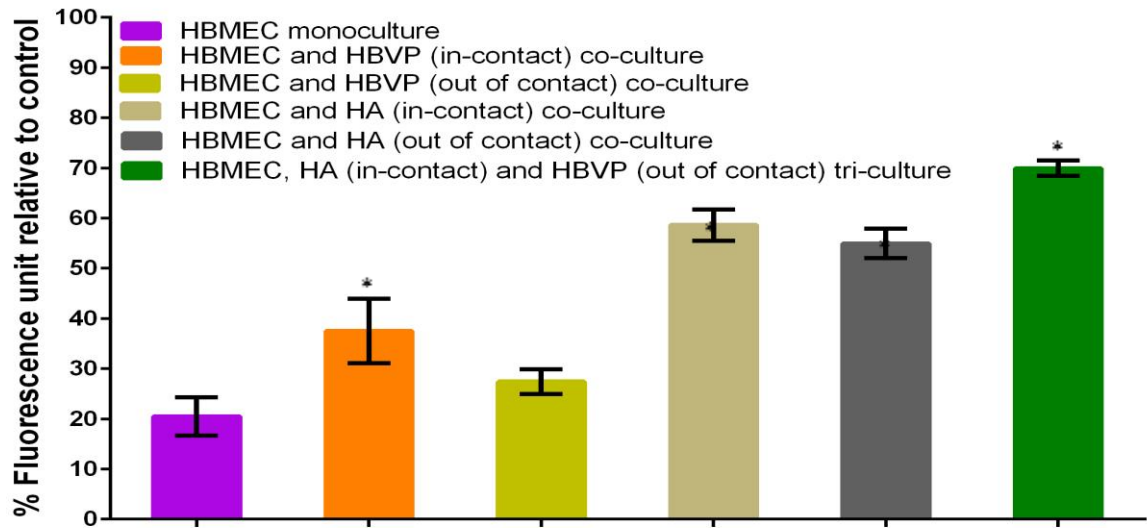


Figure 5.41 Activity of ABCG<sub>2</sub> efflux transporter in different *in vitro* BBB models.

Activity of ABCB<sub>1</sub> in the different model designed, highest activity was observed in tri-culture model HBMEC, HA (in-contact) and HBVP (out of contact). The efflux activity was measured by using substrate rhodamine123, the data was plotted relative to control. The dye loaded cells at 4 °C which inhibits the activity of the efflux transporter was the control. The data points are means of three replicates (n=3) and the error bars represent ± standard deviation (±SD) of three inter experimental repeats. \* p < 0.05 was considered to be statistically significant.

### 5.2.3.2 Expression and activity of drug metabolising enzymes CYP3A4 and CYP2D6 in HBMEC models.

The drug metabolising enzymes are responsible for the metabolism of certain drugs administered for the treatment of glioma. The metabolism leads to poor bio-availability of the drug at the tumour site. It is essential to evaluate the expression of these enzymes in the *in vitro* BBB models to construct a physiological relevant model. The expression and activity of drug metabolising enzymes CYP3A4 and CYP2D6 was studied in all the HBMEC mono-, co- and tri-culture BBB models by Western blotting.

Both astrocyte in-contact co-culture and tri-culture models both showed similar levels of expression of the CYP3A4 and CYP2D6. The lowest expression of both the enzymes was observed in the pericyte in-contact and pericyte out of contact model (Figure 5.42). CYP2D6 was lowest in HBMEC monoculture whereas CYP3A4 expression was lowest in pericyte co-culture. The CYP2D6 enzyme showed highest expression in the astrocyte co-cultures and the tri-culture. The expression of CYP3A4 was highest in the tri-culture model. This was confirmed by the densitometry analysis (Figure 5.43).

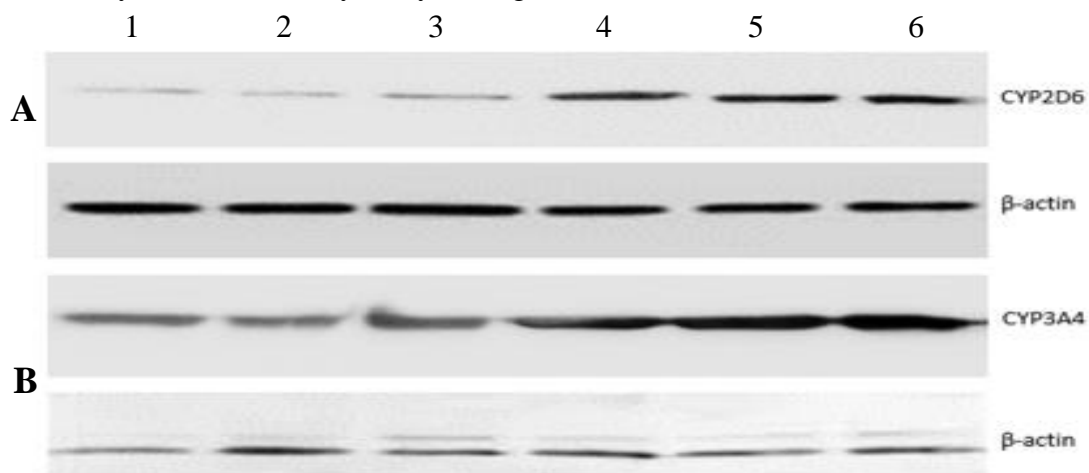


Figure 5.42 Expression of drug metabolising enzymes in different *in vitro* BBB models.

**A** Expression of CYP2D6 enzyme. **B**. Expression of CYP3A4 enzyme.  $\beta$ -actin was used as the loading control. Each well was loaded with 10  $\mu$ g of protein. 1) HBMEC monoculture. 2) HBMEC and HBVP (in-contact). 3) HBMEC and HBVP (out of contact). 4) HBMEC and HA (out of contact). 5) HBMEC and HA (in-contact). 6) HBMEC, HA (in-contact) and HBVP (out of contact).

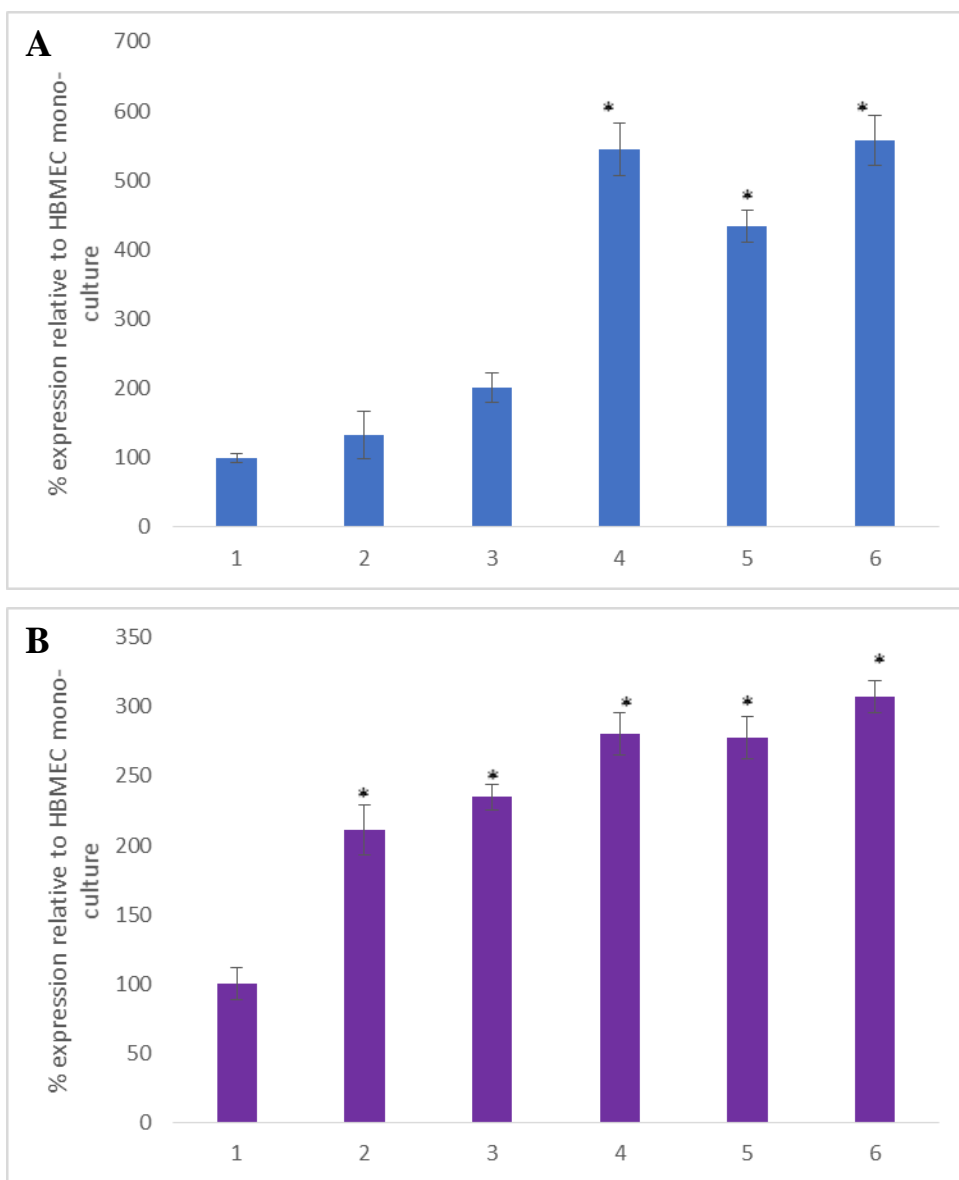


Figure 5.43 Densitometry of drug metabolising enzymes in different *in vitro* BBB models.

**A** CYP2D6 enzyme. **B.** CYP3A4 enzyme. 1) HBMEC monoculture. 2) HBMEC and HBVP (in-contact). 3) HBMEC and HBVP (out of contact). 4) HBMEC and HA (out of contact). 5) HBMEC and HA (in-contact). 6) HBMEC, HA (in-contact) and HBVP (out of contact). \*  $p < 0.05$  was considered to be statistically significant

The fluorescence metabolite formation was measured with respect to time for up to 60 min after addition of the probe substrate BFC or AMMC for CYP3A4 and CYP2D6, as seen in Figure 5.44 and Figure 5.45 respectively.

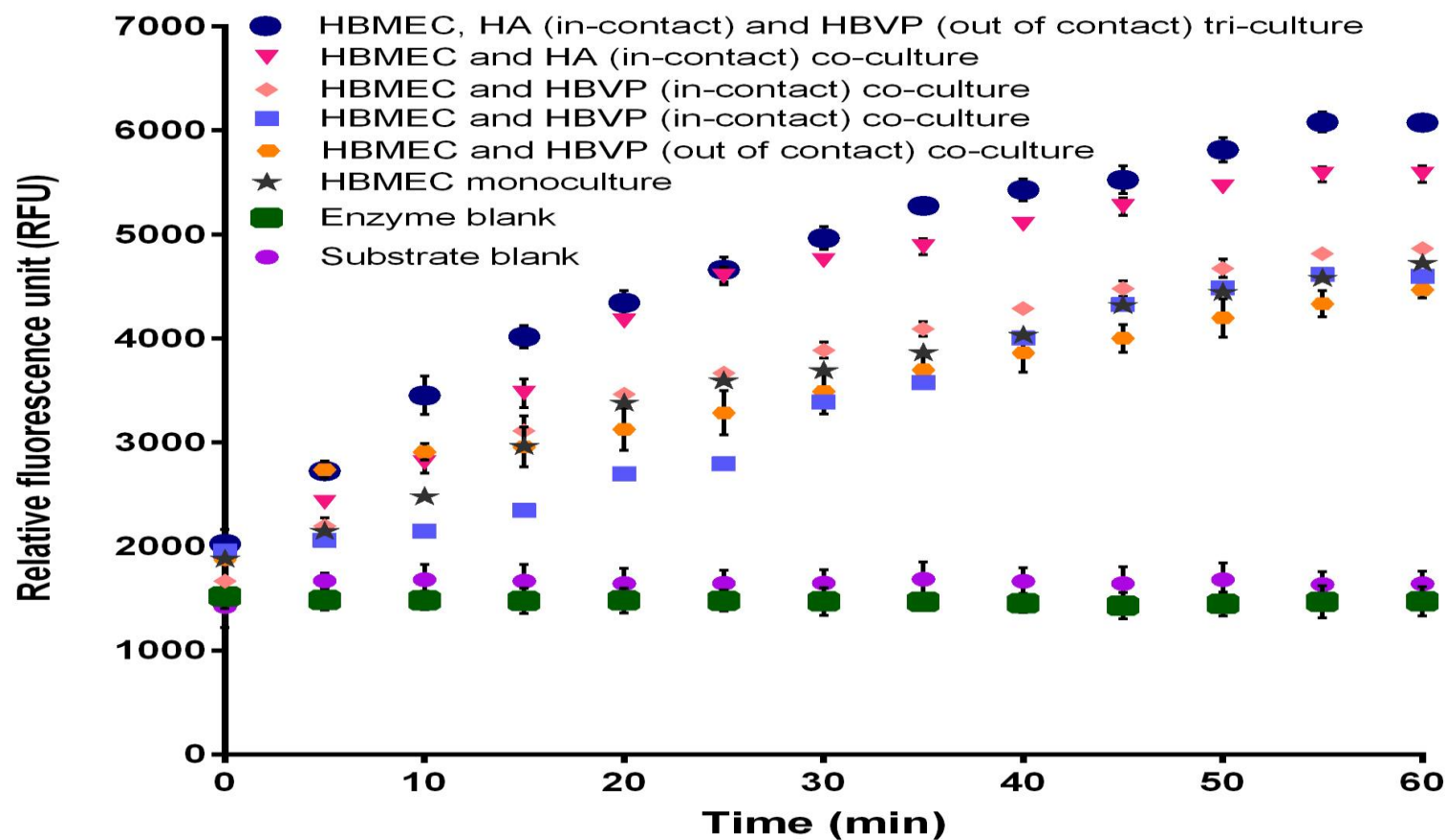


Figure 5.44 Measurement of fluorescent HFC formation by CYP3A4 with respect to time in different *in vitro* BBB models.

Fluorescent HFC metabolite formation following BFC metabolism by CYP3A4. The enzyme blank was used as the negative control. The substrate blank included the cells with buffer and NADPH. Each model had equal number of cells to measure the activity. The data points are means of three replicates (n=3) and the error bars represent  $\pm$  standard deviation ( $\pm$ SD) of three inter-experimental.

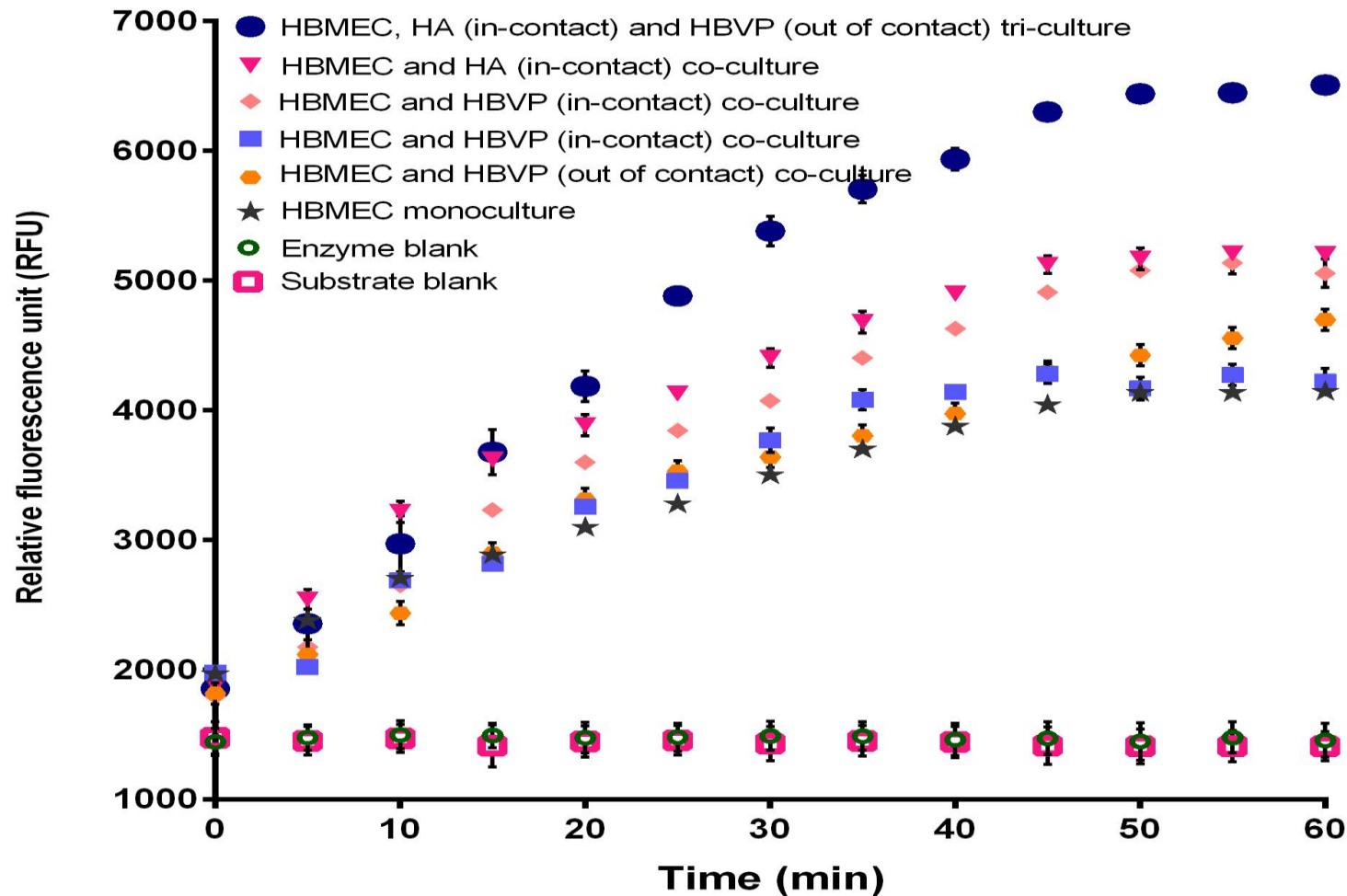


Figure 5.45 Measurement of AMHC formation by CYP2D6 in different *in vitro* BBB models.

Fluorescent AHMC metabolite formation following AMMC metabolism by CYP3A4. The enzyme blank was used as the negative control. The substrate blank included the cells with buffer and NADPH. Each model had equal number of cells to measure the activity. The data points are means of three replicates (n=3) and the error bars represent  $\pm$  standard deviation ( $\pm$ SD) of three inter-experimental repeats.

After calculation of the rate of metabolism in each model at 25  $\mu\text{M}$  of substrate concentration (Table 5.1), the rate of metabolite formation was compared to relative metabolism in bacosomes at the same substrate and protein concentration.

Table 5.1 Rate of enzyme activity at 25  $\mu\text{M}$  [S]

	CYP3A4	CYP2D6
Models	Rate at 25 $\mu\text{M}$ [S] ( $\mu\text{M}$ HFC / min/ mg protein)	Rate at 25 $\mu\text{M}$ [S] ( $\mu\text{M}$ HFC / min/ mg protein)
HBMEC monoculture.	0.365	0.359
HBMEC and HBVP (out of contact) co-culture.	0.389	0.377
HBMEC and HBVP (in-contact) co-culture.	0.419	0.416
HBMEC and HA (out of contact) co-culture.	0.434	0.421
HBMEC and HA (in-contact) co-culture.	0.459	0.437
HBMEC, HA (in-contact) and HBVP (out of contact) tri-culture.	0.483	0.479

#### 5.2.4 Comparison of expression and activity of proteins between Alvetex perfusion and transwell tri-culture model

The main aim of the project was to develop a 3D BBB model, therefore it was essential to study the efflux transporters and DMEs components of the BBB in the Alvetex scaffolds. Previous TEER data had shown that models grown on a 3D scaffold formed a stronger barrier (Figure 5.31) compared to 2D transwell insert models. Also, expression and activity levels of efflux transporters and DMEs was highest in tri-cultures compared to the other models,

therefore expression and activity of transporters and DMEs in the Alvetex scaffold was only compared against the most successful models to date.

#### 5.2.4.1 Expression and activity of efflux transporters ABCB<sub>1</sub> and ABCG<sub>2</sub>.

The expression and activity of the Alvetex perfusion model for efflux transporters ABCB<sub>1</sub> and ABCG<sub>2</sub> was compared with the transwell tri-culture model. Western blots were undertaken to assess the expression of efflux transporters in the tri-culture transwell and tri-culture Alvetex models. As seen in Figure 5.41 A & B, Alvetex perfusion model showed a higher expression of both the efflux transporters compared to the transwell tri-culture model. The expression of ABCG<sub>2</sub> was higher than ABCB<sub>1</sub> in both the Alvetex perfused model and the transwell tri-culture model.  $\beta$ -actin was used to normalise the data and to confirm that each well was loaded with equal amount of protein. These results can be confirmed by densitometry analysis (Figure 5.46 C and D)

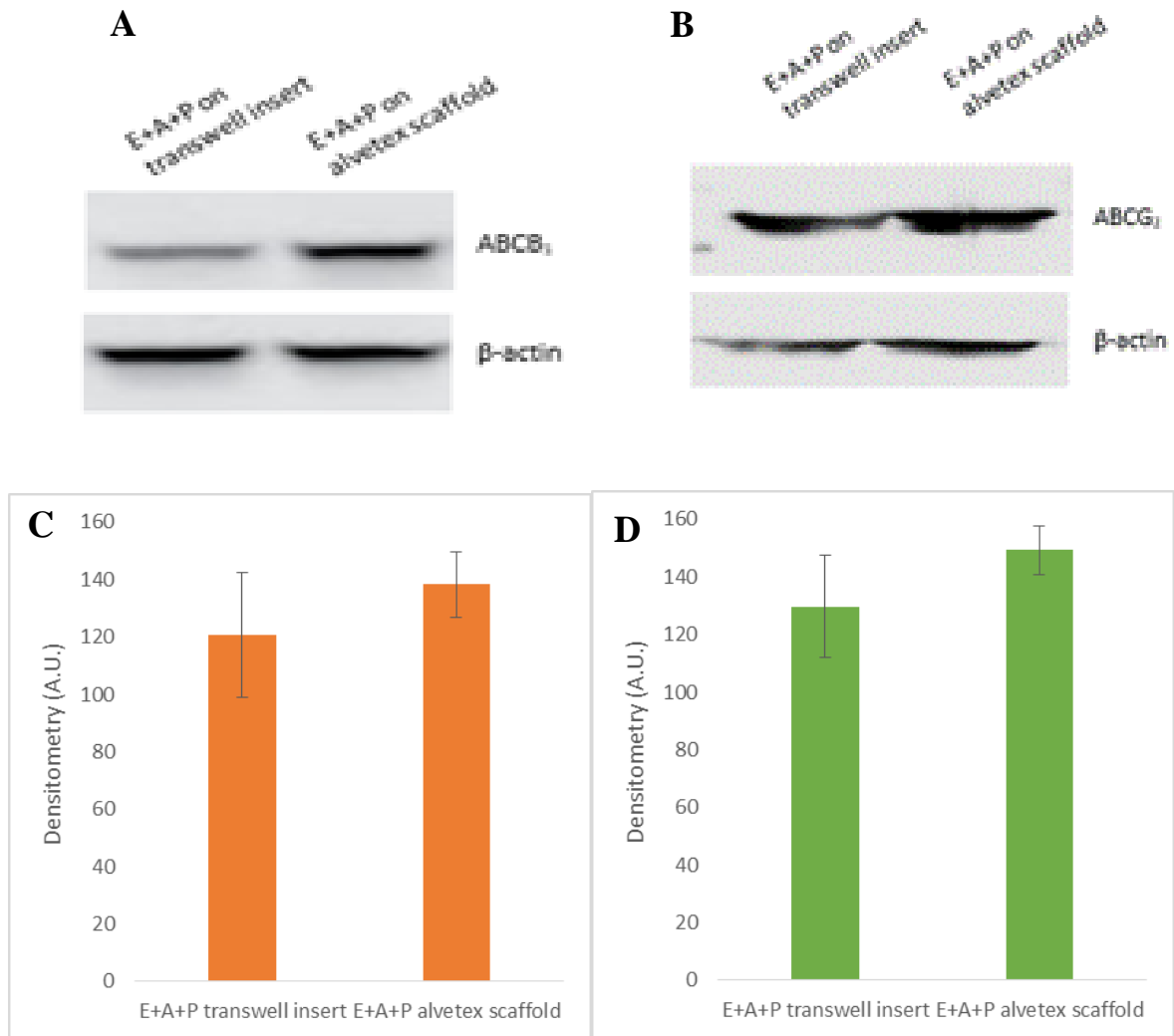


Figure 5.46 Expression and activity of efflux transporter in both tri-culture *in vitro* BBB models.

**A.** Expression of ABCB<sub>1</sub> transporter. **B.** Expression of ABCG<sub>2</sub> transporter. β-actin was used as the loading control. Each well was loaded with 10 μg of protein. **C.** Densitometry of ABCB<sub>1</sub> transporter. **D.** Densitometry of ABCG<sub>2</sub> transporter. The data points are means of three replicates (n=3) and the error bars represent ± standard deviation (±SD) of three inter-experimental repeats.

As seen in Figure 5.47, the activity of efflux transporter ABCB<sub>1</sub> did not show significant higher activity in Alvetex perfusion model when compared to transwell tri-culture model, whereas the activity of ABCG<sub>2</sub> transporter showed significantly higher activity compared to the transwell tri-culture model.

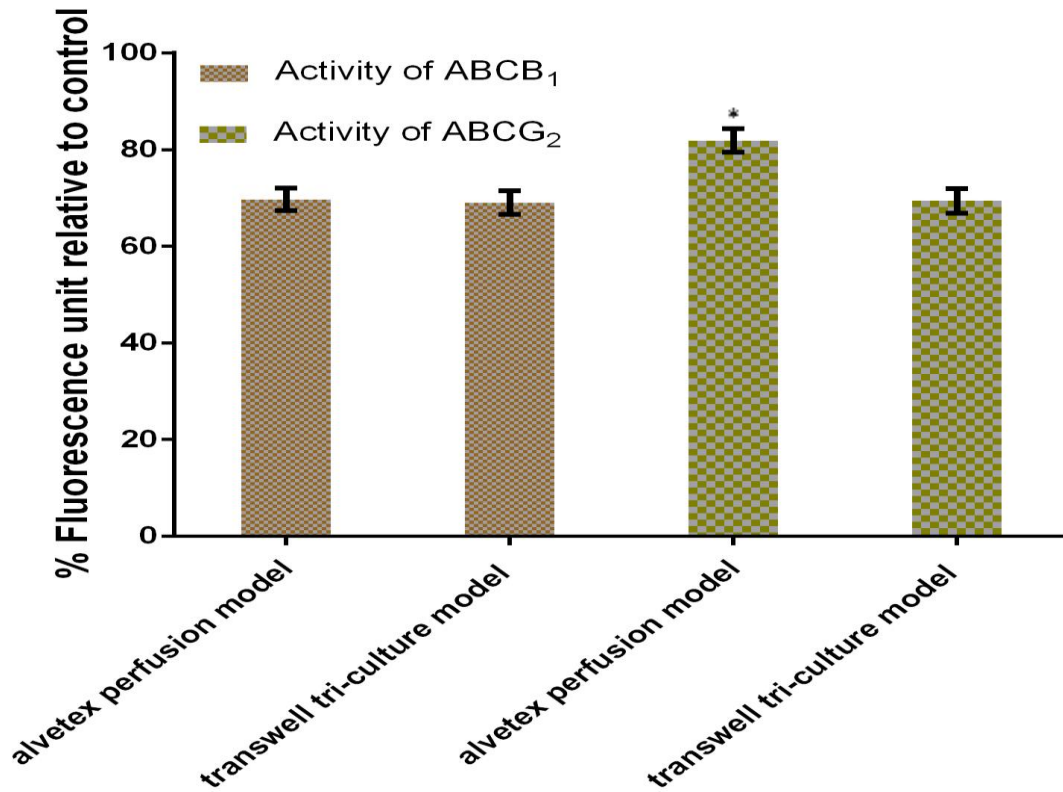


Figure 5.47 Activity of ABCB<sub>1</sub> and ABCG<sub>2</sub> in the different designed tri-culture models.

The data points are means of three replicates (n=3) and the error bars represent  $\pm$  standard deviation ( $\pm$ SD) of three inter-experimental repeats.

#### 5.2.4.2 Expression and activity of drug metabolising enzymes CYP3A4 and CYP2D6.

The expression and activity of the Alvetex perfusion model for drug metabolising enzymes CYP3A4 and CYP2D6 was compared with the transwell tri-culture model. The tri-culture model showed high TEER and high activity compared to all the designed *in vitro* BBB model. The Western blots were undertaken to assess the proteins levels of the drug metabolising enzymes in both the tri-culture set ups.

As seen in Figure 5.48 A & B, the alvetex perfusion model showed a higher expression of both the drug metabolising enzymes CYP3A4 and CYP2D6 compared to the transwell tri-culture model.  $\beta$ - actin was used to normalise the data and to confirm that each well was loaded with equal amount of protein. The densitometry showed the higher expression of CYP3A4 in alvetex tri-culture was 158.27 A.U. as compared to 93.68 A.U in transwell tri-culture. The densitometry showed the higher expression of CYP2D6 in alvetex tri-culture was 138.68 A.U. as compared to 63.68 A.U in transwell tri-culture (Figure 5.48 C & D).

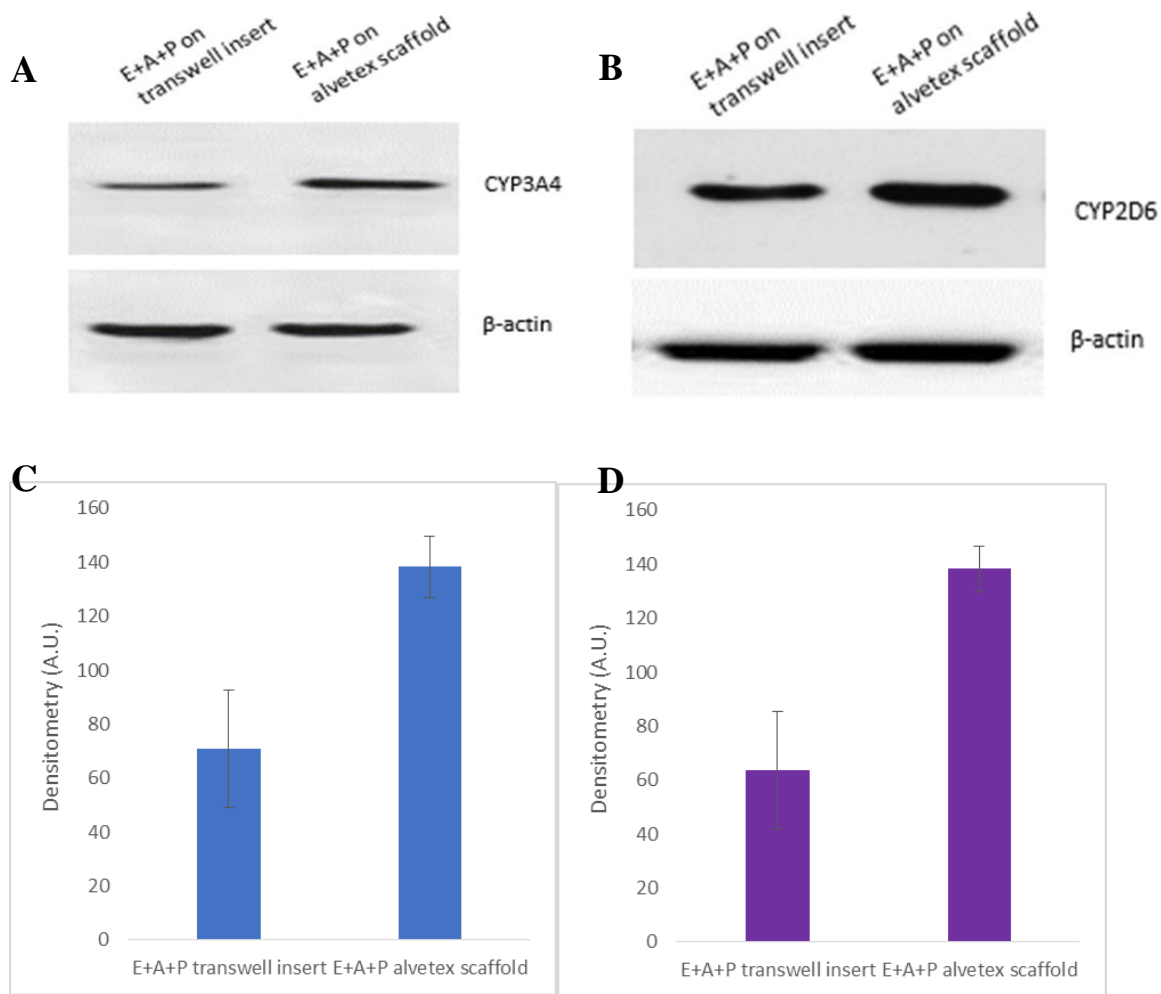


Figure 5.48 Expression and activity of drug metabolising enzyme in both tri-culture *in vitro* BBB models.

**A.** Expression of CYP3A4 enzyme. **B.** Expression of CYP2D6 enzyme.  $\beta$ -actin was used as the loading control. Each well was loaded with 10  $\mu$ g of protein. **C.** Densitometry of CYP3A4 enzyme. **D.** Densitometry of CYP2D6 enzyme. The data points are means of three replicates ( $n=3$ ) and the error bars represent  $\pm$  standard deviation ( $\pm$ SD) of three inter experimental repeats

The models were studied for the activity levels of the drug metabolising enzymes (Figure 5.49). The 25  $\mu$ M fluorescent metabolite was incubated with the fluorescence was read up to 60 min. The fluorescence of cultures and was measured, the alvetex scaffold showed a higher fluorescence of the metabolite formed as compared to the tri-culture model on transwell insert. The data was used to calculate the rate of enzyme at 25  $\mu$ M of substrate concentration.

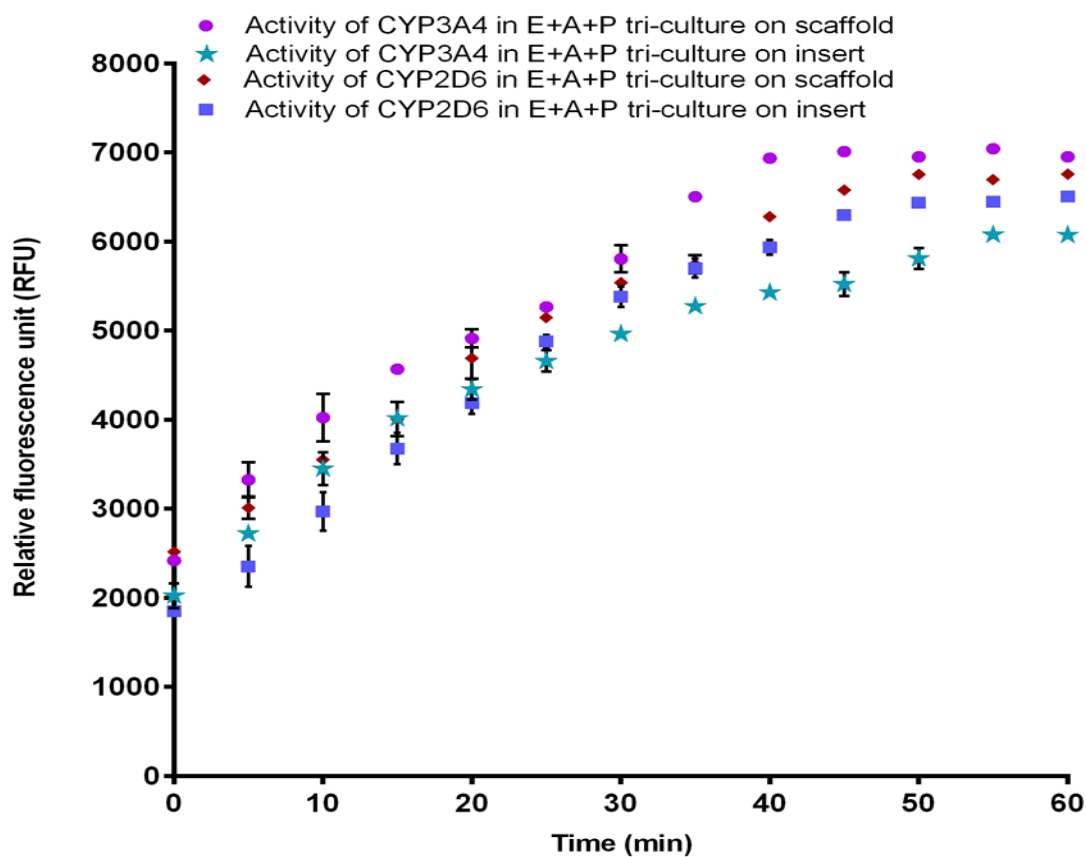


Figure 5.49 Activity of CYP3A4 and CYP2D6 in the different designed tri-culture models.

The data points are means of three replicates (n=3) and the error bars represent  $\pm$  standard deviation ( $\pm$ SD) of three inter experimental repeats.

After calculation of the rate of metabolism in each model at 25  $\mu$ M of substrate concentration (Table 5.2) the rate of metabolite formation was compared to relative metabolism in bacosomes at the same substrate and protein concentration.

Table 5.2 Rate of enzyme activity at 25  $\mu$ M [S]

	CYP3A4	CYP2D6
Models	Rate at 25 $\mu$ M [S] ( $\mu$ M HFC / min/1mg/ml protein)	Rate at 25 $\mu$ M [S] ( $\mu$ M HFC / min/1mg/ml protein)
Tri-culture in tranwell insert	0.483	0.479
Tri-culture on alvetex insert	0.621	0.598

## 5.3 Discussion and conclusion

The BBB is a highly organised interface, as such *in vivo* complexity is difficult to attain *in vitro*. There has been an on-going search for an *in vitro* BBB model which is simple, reproducible and closely mimics the *in vivo* barrier both functionally and anatomically (Gaillard *et al.*, 2001). The *in vitro* model in comparison to *in vivo* will need to have high throughput capacity, low cost, help in identification of early signs of cell toxicity and reduce the number of animal usage. As yet, no simple *in vitro* model has been able to mimic the functional abilities of BBB *in vivo* (Obermeier *et al.*, 2013). Each *in vitro* model should be optimised and characterised for a well-defined purpose (Bicker *et al.*, 2014; Erben *et al.*, 1995). For the purpose of predicting drug disposition when treating CNS disease such as glioma, it is essential, that the *in vitro* BBB model possesses relevant characteristics, such as the full complement of drug metabolising enzymes and transporters and a functional barrier. To date, no BBB model has been adopted by the pharmaceutical industry as the “gold standard”, which makes the development of a reliable model an important task (Patabendige *et al.*, 2013). Until then, it has been proposed that combined approaches should be applied for the development of a BBB model which can be used to rationalise and optimise the evaluation of drug penetration in CNS drug delivery (Lundquist and Renftel, 2002; Shawahna *et al.*, 2012). The aim of this chapter was therefore to 1) study functional integrity of the BBB using TEER measurements and detection of TJ proteins, 2) measure expression and activity of key transporters and DMEs important for glioma drug disposition, utilising a range of different mono-, co- and tri-culture systems, in different experimental conditions (serum, 2D, 3D, cell conformation (in or out of contact with the insert) static, perfusion) as well as reviewing different instruments for TEER determination.

Reproducibility of TEER measurements across the insert were checked, and confirmed to have a coefficient of variance (CV) value of  $< 15\%$ , which was considered to be acceptable (Li and Chow, 2005). Initial problems caused due to un-uniform monolayer of cells due to clusters of cells forming on the insert were overcome by optimising the cell seeding density and optimising the concentration extracellular matrix (data not shown), and this was supported by reproducibly measurements observed across the insert. Thereafter the intra-assay (triplicate measurements across three models on one plate) and inter experimental repeats (different plates set up on three separate occasions) gave CV values  $< 15\%$  confirming good reproducibility of TEER measurements by EVOM.

The EVOM instrument for TEER measurements was also validated against two other instruments. Firstly, for the 2D ECIS array, the cells were seeded on top of each other in layers and the resistance was measured at the base of the set up. A disadvantage of the ECIS, is that the array does not have compartments to perform any permeability assays or screening for novel compounds, unlike the EVOM probe which can be used across transwell inserts/scaffolds. The advantage of using the ECIS was that it gave a real time measurement of the TEER, unlike the EVOM probe that measured TEER at discrete time points. Interestingly, a small peak was observed in all cultures at 5 h, which was attributed to cell adherence. Such details were lost with the EVOM probe which only provided TEER measurements every 24 h. Although the model was a two dimensional measurement of resistance, the pattern of TEER with respect to time in ECIS was comparable to the pattern observed by EVOM in the hCMEC/D3 mono-, and tri- cultures, where the highest reading TEER was seen in the tri-culture followed by co-culture at approximately 3.5 days, compared to the EVOM that showed a TEER peak at 4 days in the tri-culture model. Semi-quantitation of Western blots for occludin and claudin supported the TEER measurements, also indicating the highest

expression in the tri-culture and lowest expression in the monoculture matched the highest and lowest TEER values. .

The designed *in vitro* BBB models were set up on transwell inserts and measured using Cellzscope. The advantage of using Cellzscope was that it measured TEER in real time and did not require the manual insertion of probe which might disrupt the barrier forming cells (Benson *et al.*, 2013). The values of the TEER were very low when compared to the TEER values measured using the EVOM. The TEER was also measured in  $\Omega\cdot\text{cm}^2$  as opposed to  $\Omega/\text{cm}^2$  in the other two measuring systems (EVOM, ECIS). Due to lack of information from the company about the algorithm used to calculate the Cellzscope TEER, a direct comparison of values to EVOM was not possible, The tri-culture model measured by Cellzscope gave a peak TEER of  $22 \Omega\cdot\text{cm}^2$  and co-culture gave a TEER of  $45 \Omega\cdot\text{cm}^2$  at 2.4-2.7 days, however the TEER data was not supported by Western blot densitometry analysis, which revealed lowest occludin and claudin expression in the same co-culture model. Again, a small peak was observed at 5 h in all models, which also coincided with a decrease in capacitance, so was again attributed to cell adherence.

The most important characteristic of an *in vitro* BBB model is a high TEER value (Wilhelm *et al.*, 2011b). When comparing all three instruments for measuring TEER, and subtracting the background blanks from EVOM (already done), ECIS and CellZscope (data not shown), EVOM gave the highest TEER values. In addition, the EVOM model appeared to maintain a barrier for longer, whereas TEER declined quickly in the ECIS and Cellzscope models. EVOM and ECIS were thought to give reliable TEER values, as these were supported by the Western blot analysis of TJ protein expression, however, Cellzscope was deemed unreliable. It was decided the EVOM probe should be used so transwell and 3D models could be

measured, however it was highlighted that a disadvantage of the EVOM was a lack of real-time TEER measurements.

The next validation step was to compare the immortalised human endothelial cell line (hCMEC/D3) against the short-term human endothelial cell line (HCMEC). In the current study, different co- and tri- cultures were set up using two different endothelial cell lines, The cell lines both showed an increase in the TEER values in co- and tri- cultures compared to their monocultures. The hCMEC/d3 in tri-culture showed the highest peak TEER of 385  $\Omega/\text{cm}^2$  at day 4, whereas the HBMEC in tri-culture had a lower TEER at 258  $\Omega/\text{cm}^2$ . Both of the cell lines in tri-culture showed the highest TJ protein expression compared to the other models. The developed BBB model required a steady plateau phase in the TEER values which can be used to test the permeability of novel therapeutics, including NPs. The co- and tri-cultures of immortalised hCMEC/D3 did not establish a steady plateau phase, whereas the model designed using short-term HBMEC cell cultures did. In the literature it was reported that best results are obtained with models based on primary endothelial cells; the major limitation of the models using immortalised endothelial cell lines was the relatively high paracellular permeability (Roux and Couraud, 2005). A model with high paracellular permeability cannot to be used for screening of novel drugs or NPs, therefore, the model cannot be used commercially and defeats the purpose of designing an *in vitro* BBB model. The HBMEC primary culture are highly purified version of brain cells and were found to have unmatched value for basic and translational research (Naik and Cucullo, 2012). The complex TJs between these endothelial cells are primarily responsible for the barrier function and provide a high electrical resistance of about 2000  $\Omega/\text{cm}^2$  *in vivo* (Crone and Olesen, 1982). It is known that complexity of TJs is higher in brain capillaries than in other vessels, their development and regulation is highly complex but they form an essential component

for maintaining a healthy micro environment in the CNS (Lai and Kuo, 2005). Compared to the *in vivo* TEER values, the *in vitro* model was still a long way off achieving physiologically relevant resistance. Taking, the results and literature into consideration, the short-term HBMEC cultures were chosen as the most suitable for the model.

Cells harvested from human origin are frequently utilised for the development and optimisation of *in vitro* BBB models. These primary cultures provide the closest phenotypic resemblance to the cells *in vivo* (Lundquist and Renftel, 2002), it therefore follows that all components in the culture such as serum and ECM should also be of human origin, however this is often not the case. One of the aims here was to ensure that all the components used to develop the BBB model were kept similar to *in vivo* as possible. A small study was conducted where cells that had been initially cultured in 10 % foetal bovine serum (FBS) were weaned on to 5 % human serum. Interestingly, there was no significant difference in the TEER values or expression of TJs proteins occludin and claudin-5 in cells of the model grown in (FBS) or human serum. Serum is added to culture media to promote cell proliferation and maintain *in vivo* like conditions. Harvey *et al.* (2002), suggested that the serum inhibits the formation of TJs and lowering the level of serum in culture promotes formations TJs and tightens the barrier. Serum has many components that could affect tight junctions, including proteins, lipids, hormones, and growth factors. Chang *et al.*, (1997) showed that the clotting factors present in the serum do not affect the TJs by measuring the TEER. They suggested that the growth factors such as fibroblast growth factors, vascular endothelial growth factor, and hepatocyte growth factor-scatter factor are likely to have a role in causing a gradual decline in the TEER caused by decrease in TJs formation (Chang *et al.*, 1997). Since the presence of 5 % serum did not appear to inhibit barrier formation it was decided to continue using serum of human origin to avoid any inter-species variability (Harvey *et al.*, 2002).

The final part of the model validation involved investigations of various cell confirmations (mono-, di- and tri-) in or out of contact with the insert (2D) or scaffold (3D) and static or perfused environments. It has been demonstrated by several groups that co- and tri-cultivation of pericytes and/or astrocytes with endothelial cells show an increase in the TEER resistance when compared to the mono-cultivation of endothelial cells (Hatherell *et al.*, 2011; Nakagawa *et al.*, 2007a; Deli *et al.*, 2005). Nakagawa *et al.*, describes that co-culture of pericytes with endothelial cells gave a high TEER value of 388  $\Omega/\text{cm}^2$  using EVOM and low permeability (Nakagawa *et al.*, 2007a; Nakagawa *et al.*, 2009b). On the other hand, Hatherell *et al.* (2011), showed that the co-culture of endothelial cells with the astrocytes seeded on the basolateral side of the insert gave a high TEER value of 240  $\Omega/\text{cm}^2$  using EVOM. The presence of astrocytes and/or pericytes elevates the TEER values. In the data reported here, the co-cultures of endothelial cells and astrocytes/ or pericytes both showed a higher TEER value when compared to endothelial mono-culture. This supported the findings of Goldstein *et al.* (2008), who stated that the co-culturing of endothelial cells with astrocytes/ pericytes increased the complexity and formation of the TJs (Goldstein, 1988). Comparing the two co-culture models of astrocytes and endothelial cells in the study here, the in-contact model showed a higher TEER value when compared to out of contact model. The astrocytes in contact with the endothelial cells were separated by a 8  $\mu\text{m}$  membrane, the short lived factors secreted by astrocytes are able to penetrate the 8  $\mu\text{m}$  barrier which helped modulate the BBB properties by improving cell-cell signalling resulting in an increase in the TEER (Cohen-Kashi Malina *et al.*, 2009; Abbott *et al.*, 2006b). It is also known that these astrocyte derived soluble factors secreted in the culture medium are responsible for the induction of the BBB phenotype on the endothelial cells (Rubin *et al.*, 1991; Haseloff *et al.*, 2005). The 8  $\mu\text{m}$  pore size of the polycarbonate membrane used restricts the migration of astrocytes across the surface of the insert, but does not restrict the astrocytic foot processes. These astrocyte foot

processes penetrate through the pore of the filter and interact with the endothelial cells seeded which leads to tightening of the barrier (Patabendige *et al.*, 2013). The synergistic effect of the cell-cell interaction leads to induction of the BBB properties thus explaining the higher TEER values observed with the tri-culture model (Nakagawa *et al.*, 2007a). Thus, the presence of both pericytes and astrocytes enhances the tight junction formation and increases the tightness of the barrier as seen in the study here and confirmed in the literature (Nakagawa *et al.*, 2009a).

The endothelial cells hold a unique position among biomechanically responsive cells *in vivo*, these cells are subjected to interaction with other cells and are relatively under high shear stress due to constant blood flow which gives the BBB its integrity and function. Consequently, endothelial cells are an important component of models to study the effect of shear stress on cell function (Shawahna *et al.*, 2012; Davies, 1989). Siddharthan *et al.*, have described a model in which the endothelial cells are co-cultured with astrocytes and subjected to flow. Cells subjected to shear stress or flow show an increased expression of the tight junction proteins occludin and claudin and decreased permeability when compared to cells in static cultivation (Siddharthan *et al.*, 2007).

Similar results were observed when the co- and tri- cultures in this study, cultures that were grown on a perfused Alvetex scaffold gave the highest TEER values. The initial TEER values of the models were similar, after day 3 the model with shear stress showed an increase in the TEER. The highest value of TEER in a perfused model was  $710 \Omega/\text{cm}^2$  whereas the highest TEER value of a static model was  $250 \Omega/\text{cm}^2$ . Cucullo *et al.* (2008), have reported similar results in his study where the dynamic model with pulsatile flow showed a TEER of  $1000 \Omega/\text{cm}^2$  and the static model showed a TEER of  $70 \Omega/\text{cm}^2$ . Several reports have suggested that application of shear stress induces morphological and functional changes in

endothelial cells (Siddharthan *et al.*, 2007; Krizanac-Bengez *et al.*, 2003; Cucullo *et al.*, 2008).

As seen in the current study, the presence of pericyte in the co-culture model of endothelial cells and astrocyte enhanced the TEER values of the models. The pericyte were cultured by three different methods, in-contact, out of contact and conditioned media. All the models showed a similar TEER pattern and expression of TJs proteins higher than the control which was the co-culture of endothelial cells and astrocytes. Pericytes are normally associated with three major roles i) CNS microvasculature-contractility ii) regulation of endothelial cell activity and iii) macrophage activity (Lai and Kuo, 2005). These roles involve participation in different cell signalling components which either interact with the pericyte or are produced by the pericyte. The cell signalling agents include neuromodulators, vasoactive peptides, metabolic factors, growth factors and cytokines. The pericyte have shown to regulate the endothelial cell growth and proliferation by secreting TGF- $\beta$ -1 (Rucker *et al.*, 2000). The TGF- $\beta$ -1 enhances the expression of contractile proteins such as actin, thus strengthening the barrier, hence explaining why conditioned media alone was enough to improve TEER (Bandopadhyay *et al.*, 2001).

To date no *in vitro* BBB model developed has been assessed for the expression and activity levels of the efflux transporters; ABCB<sub>1</sub> and ABCG<sub>2</sub> and DMEs; CYP3A4 and CYP2D6. To improve activity and expression levels it is necessary to mimic the *in vivo* microenvironment of the cells. Extensive work has been done in xenobiotic drug metabolism and disposition in *in vitro* liver models, therefore the aim was to translate this work to *in vitro* BBB models (Godoy *et al.*, 2013; Baxter *et al.*, 2014). The efflux transporters and DMEs both play a crucial role in drug disposition and metabolism in glioma. In the presence of a brain tumour, the BBB has often been reported to be compromised (On *et al.*, 2013), increasing the

possibility that chemotherapeutic agents may be able to enter the CNS, however, the efflux transporters and drug metabolising enzymes will still be functional leading to poor bio-availability of the drug. It is essential therefore, to develop therapeutics which can not only overcome the physical barrier but also the transport barrier and the metabolic barrier at the tumour site, thus enabling treatment of the tumour. In the current study the expression and activity levels of all the proposed models were studied for the efflux transporters; ABCB<sub>1</sub> and ABCG<sub>2</sub> and DMEs; CYP3A4 and CYP2D6 activity. The tri-culture model showed the highest expression and activity compared to the other designed models. As compared to mono-culture which showed 32 % activity for ABCB<sub>1</sub>, the tri-culture showed 68 % activity. The activity of ABCG<sub>2</sub> was also higher in tri-culture, 69 % as compared to the mono-culture showing 20 % activity. These expression and activity levels of the efflux transporters; ABCB<sub>1</sub> and ABCG<sub>2</sub> and DMEs; CYP3A4 and CYP2D6 established the physiologically relevant characteristic of the designed BBB model. In liver, the efflux transporters and enzymes are studied by modelling *in vitro* for the purposes of drug toxicology and safety pharmacology, making this model possibly more predictive of drug toxicity compared with existing models (Baxter *et al.*, 2014; Godoy *et al.*, 2013).

In summary, the BBB model was developed by utilising multiple cell types in optimised culture conditions giving the highest expression of efflux transporters; ABCB<sub>1</sub> and ABCG<sub>2</sub> and DMEs; CYP3A4 and CYP2D6. The model was also optimised for a high expression of TJs proteins and high TEER values. On comparison of the various models studied, the tri-culture model of astrocytes (in contact) and pericytes (out of contact) of HBMEC monoculture model gave the highest resistance and high expression of tight junction proteins, occludin and claudin-5. The modelled barrier was translated to a 3D scaffold and induced

with shear stress by perfusing the scaffold. This model was further tested by permeability assays and NPs and aptamers to assess its functionality as an *in vitro* BBB model.

# CHAPTER 6

## 6. Functionality of the tri-culture as an *in vitro* BBB model

### 6.1 Introduction

There has been an emerging need to develop short term *in vitro* models and computational tools that can predict the efficacy and toxicity of therapeutics and NPs on the body (Hanada *et al.*, 2013; Masserini, 2013). The urgent need to develop a model for screening of CNS targeted therapeutics has led to development of various *in vitro* BBB models. These models allow screening of designed novel therapeutics and delivery systems including NPs and aptamers.

The major strategy in treating the glioma is to circumvent the BBB, in recent years nanobiotechnology has been suggested as a promising strategy to overcome the BBB. It provides efficient tools for diagnosis, delivery mechanism and increases the chances of developing curative treatment for glioma. Papers have suggested improved transportation of glioma drugs such as temozolomide (Modi *et al.*, 2009) and doxorubicin (Ulbrich *et al.*, 2009) compared to conventional systemic delivery. Nanoparticles are small in size and are able to flow easily through the blood capillaries due to appropriate surface functionalisation thereby rendering NPs as biological entities (Tian *et al.*, 2012; Oberdorster *et al.*, 2009). These developing neuro-therapeutics have to be screened for their toxicity, safety and long term effect on the body (Ragnai *et al.*, 2011; Lu *et al.*, 2006). Methods for the toxicity testing of NPs are the same as the techniques used in modern drug development, however, the toxic mechanism of NPs can be more diverse than that of drug compounds (Lee *et al.*, 2009). NPs can be used to encapsulate drugs and slowly release drugs at the site which prevents the drug from being effluxed and metabolised by the enzymes. Until recently most

of the screening of the NPs has been done on two dimensional models which comprise of cells cultured in dishes, the use of 3D BBB models forms a bridge between 2D models and *in vivo* models (Masserini, 2013; Oberdorster *et al.*, 2009; Tian *et al.*, 2012).

In the study here, it has previously been shown that the tri-culture model of HBMEC, HA (in-contact) and HBVP (out of contact) and co-culture of HBMEC and HA (in-contact) constructed on polycarbonate membrane gave higher TEER values, higher expression of TJ proteins and higher expression and activity of efflux transporters (ABCB<sub>1</sub> and ABCG<sub>2</sub>) and DMEs (CYP3A4 and CYP2D6). In this chapter, the tri-culture model and co-culture model were characterised for their permeability using dextran tagged with FITC. The flux of fluorescence of FITC-dextran molecules from the apical side to the basolateral side of the insert was measured. The model showing lowest permeability and hence improved and more physiologically relevant barrier properties was then used to screen the effects of various lipid NPs and aptamers on the TEER values (measured by EVOM) of the modelled *in vitro* BBB with respect to time. Nanoparticles had been designed by Prof Singh and Dr Wan for delivery of chemotherapeutic agents (NP loaded with: docetaxel, aciatric acid or curcumin either with or without transferrin (delivery tag) or rhodamine (for fluorescent detection of the NP)) and an aptamer called SA43 had previously been shown to be an effective glioma targeting molecule (unpublished data Shraddha Aptekar, PhD thesis).

## 6.2 Results

### 6.2.1 FITC-Dextran permeability assay

The permeability of the model was tested using dextran (10,000 Da), which was tagged to FITC. The permeability was determined at 1 mg/ml of FITC-dextran which was adapted as

described in Simoneau *et al.*, 2012. The paracellular permeability of model 1), the tri-culture model [HBMEC, HA (in-contact) and HBVP (out of contact)], and model 2), the co-culture model [HBMEC and HA (in-contact)] was studied. The fluorescence of media containing FITC-dextran collected from the basolateral side of models were compared to the fluorescence of 100  $\mu$ l stock of 1 mg/ml FITC-dextran stock loaded in the apical side of the model was determined in a 96-well plate using a plate reader. The fluorescence was sampled from the apical side of the well at time 0 h, 1 h, 2 h and 3 h, for measurement of apparent permeability. As seen in Figure 6.1, the level of fluorescence increased with respect to time demonstrating flux of FITC-dextran cross the barrier. The fluorescence levels were higher in model 2, suggesting the paracellular permeability of the tri-culture model was lower than that of the co-culture model. At 1 h, the permeability of tri-culture is 7.61 % relative to the fluorescence of the FITC-dextran stock which is lower than 28.30 % shown by co-culture model. A similar trend was seen at 2 h and 3 h, the permeability shown by tri-culture was 11.69 % and 19.86 % respectively and co-culture was 35.42 % and 76.28 %.

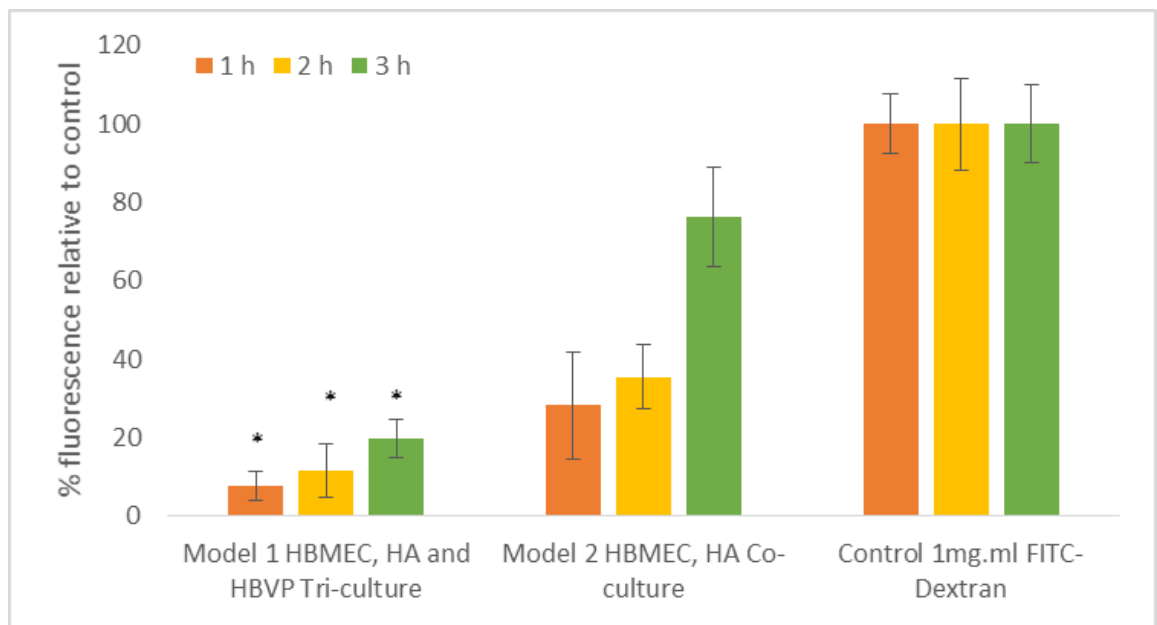


Figure 6.1: Permeability of FITC-dextran across different models at time intervals 1 h, 2 h and 3 h relative to the control of FITC-dextran stock on the apical side which was defined as 100 %. \*  $p < 0.05$  was considered to be statistically significant. The data points are means of three replicates ( $n=3$ ) and the error bars represent  $\pm$  standard deviation ( $\pm$ SD) of three inter repeats of an experiment.

### 6.2.1.1 Apparent permeability ( $P_{app}$ ) of the designed models

The linear relationship of FITC-dextran concentration versus relative fluorescence unit (RFU) was plotted to quantify concentration of FITC-dextran, to enable further calculation of the apparent permeability co-efficient  $P_{app}$  value for both models by using the formula described in Section 2.9.2.

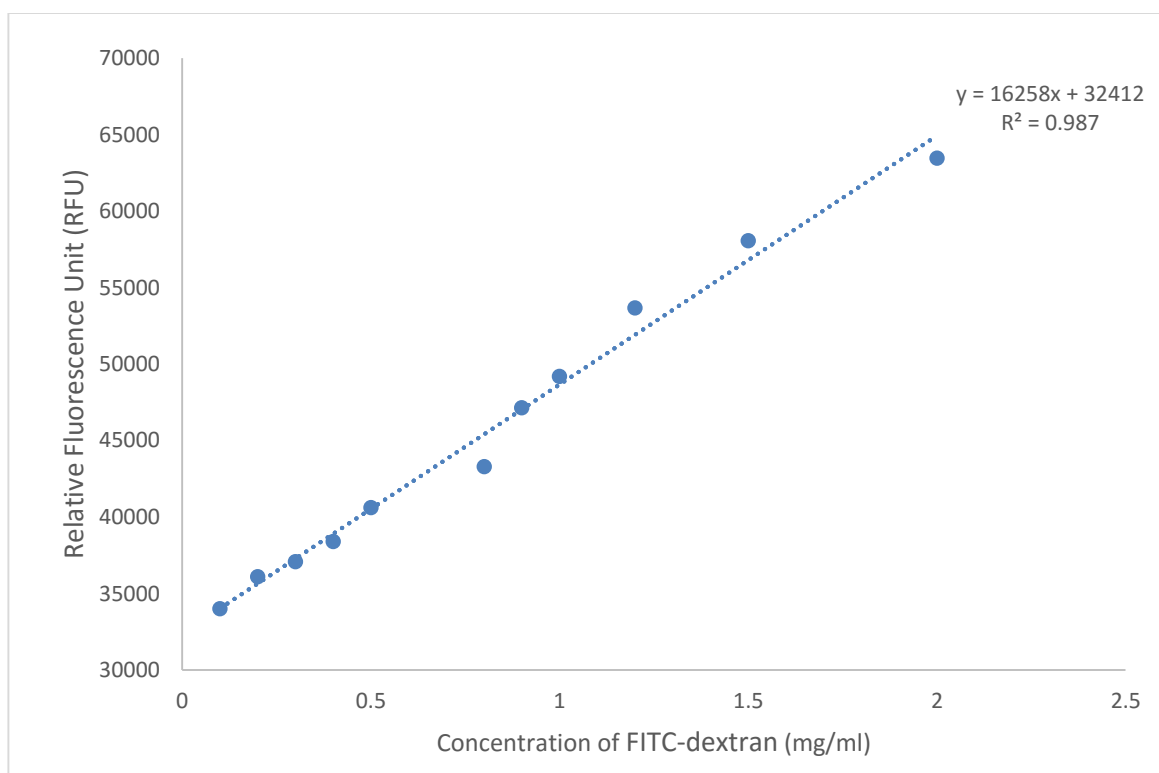


Figure 6.2: Standard plot of fluorescence *versus* concentration of FITC-dextran measured at excitation wavelength 492 nm and emission wavelength 518 nm. The data points are means of three replicates (n=3).

The  $P_{app}$  values of the *in vitro* BBB models are shown in Table 6.1 **Error! Reference source not found.** The apparent permeability of tri-culture was lower at  $6.18 \pm 1.38 \times 10^{-5} \text{ cm. min}^{-1}$  compared to  $15.08 \pm 1.40 \times 10^{-5} \text{ cm. min}^{-1}$  obtained for the co-culture model.

Table 6.1 Apparent permeability value of the *in vitro* BBB models

Model	$P_{app}$ values ( $\text{cm. min}^{-1}$ )
Tri-culture [HBMEC, HA (in-contact) and HBVP (out of contact)]	$6.18 \pm 1.35 \times 10^{-5}$
Co-culture [HBMEC and HA (in-contact)]	$15.08 \pm 1.40 \times 10^{-6}$

## 6.2.2 Screening of nanoparticles and aptamer

SA43 Aptamer and lipid nanoparticles containing docetaxel, curcumin and asiatic acid were screened on the tri-culture *in vitro* BBB model to determine their permeability across the barrier. As the NPs contained known toxic drugs and the cytotoxicity properties of the aptamer were unknown, it was necessary to determine the optimum concentration to be used in the tri-culture model by investigating the cytotoxicity of the NPs on endothelial cells. Presence of a cytotoxic response would cause a breakdown in the barrier leading to the generation of false data. Cell viability screening following exposure to aptamer and NPs was done using the MTS assay and the percentage of viable cells was determined (see Section 2.9.3).

### 6.2.2.1 Toxicity screening of nanoparticles and aptamer by MTS

The toxicity screening of the NPs determined the concentration of the NPs to be used for the cellular uptake studies. All percentage viability was expressed relative to the vehicle control for the aptamer/ NP. As seen in Figure 6.3, the percentage cell viability of docetaxel loaded lipid NPs decreased with time, showing lowest percentage of 67.04 % of viable cells on day 3 at a concentration of 0.1  $\mu\text{g/ml}$ . The docetaxel lipid nanoparticle tagged with rhodamine (Figure 6.3 A) showed similar results as compared to docetaxel lipid nanoparticle tagged with rhodamine and transferrin ligand. The transferrin ligand tagged NPs showed a decrease in per cent viable cells with time, showing 64.24 % viable cell at 72 h at a concentration of 0.1  $\mu\text{g/ml}$ . (Figure 6.3 B). The concentration of 0.1  $\mu\text{g/ml}$  was used for screening in the models

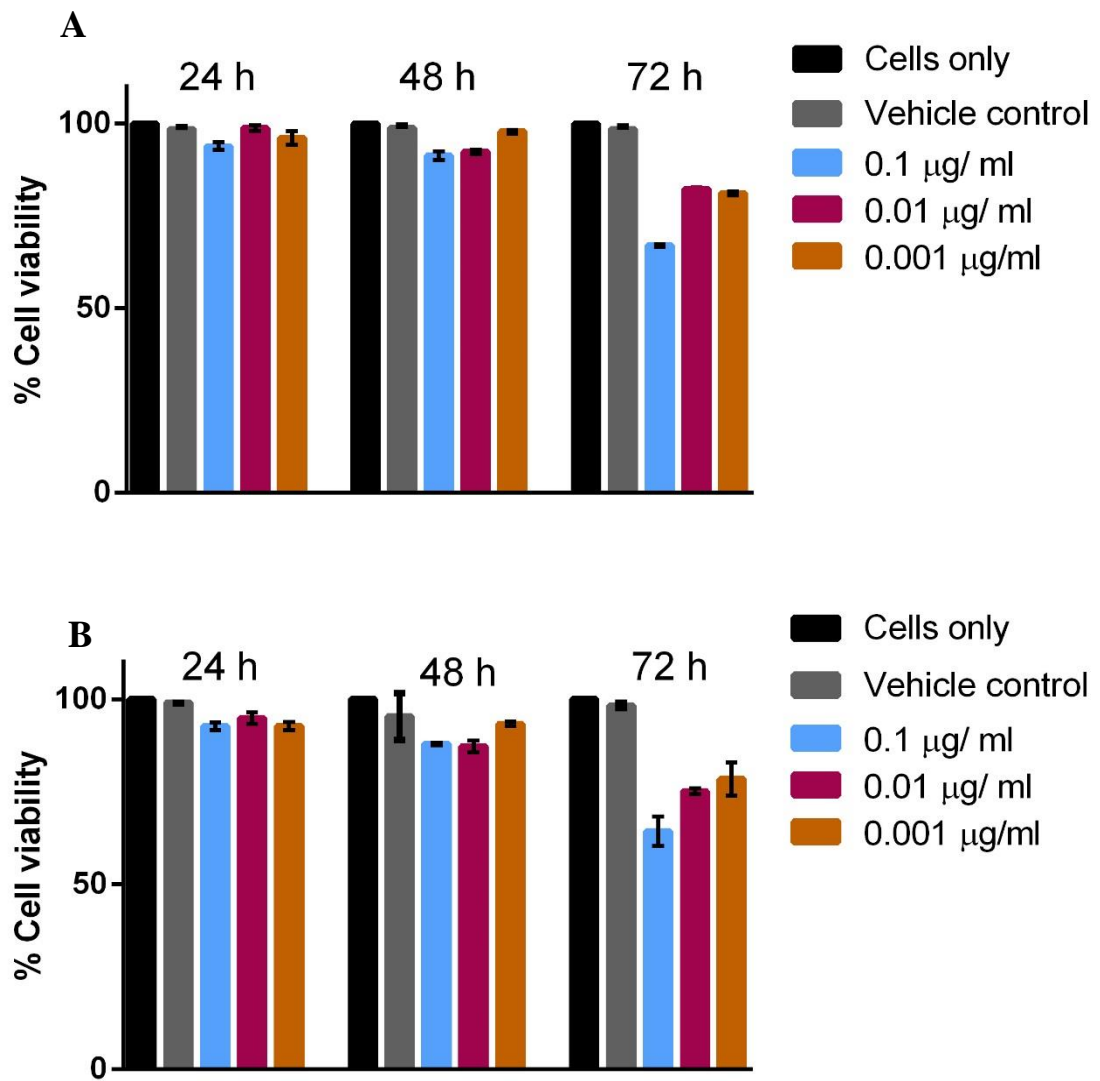


Figure 6.3: Percentage cell viability of endothelial cells relative to vehicle control after treatment with three different concentrations of docetaxel loaded lipid nanoparticle at time points 24 h, 48 h and 72 h determine by the MTS assay.

**A.** docetaxel loaded lipid nanoparticle tagged with fluorescent rhodamine123. **B.** docetaxel loaded lipid nanoparticle tagged with fluorescent rhodamine123 and the ligand transferrin. The vehicle control used in the experiment was 5 % dextrose. The data points are means of three replicated (n=3) and the error bars represent  $\pm$  standard deviation ( $\pm$ SD).

As seen in Figure 6.4, the asiatic acid lipid NPs (A) and empty asiatic acid lipid NPs (B) showed that percentage cell viability decreased with time, with lowest percentage of viable cells at 72 h. At 24 h, all of the different concentration 1.2  $\mu\text{g/ml}$ , 0.12  $\mu\text{g/ml}$  and 0.012  $\mu\text{g/ml}$  of the asiatic acid loaded lipid nanoparticle showed similar percentage of cell viability, however, the cell viability decreased at 48 h and 72 h (Figure 6.4 A). After 72 h, 68.68 % of viable cells were observed with 1.2  $\mu\text{g/ml}$  of asiatic acid loaded lipid nanoparticle. In Figure 6.4 B, empty lipid nanoparticles were tested showed a higher percentage of of viable cells (83.49 %) at 24 h when compared to asiatic acid loaded nanoparticle. The percentage of viable cells decreased with time for all NP except for the cells incubated with empty asiatic acid nanoparticle which did not show any difference in the cell viability (Figure 6.4), where at 24 h, 48 h and 72 h, the per cent viability was 84 %, 83% and 87 % at 1.2  $\mu\text{g/ml}$ , 0.12  $\mu\text{g/ml}$  and 0.012  $\mu\text{g/ml}$  respectively. The concentration of 0.12  $\mu\text{g/ml}$  was used for screening in the models

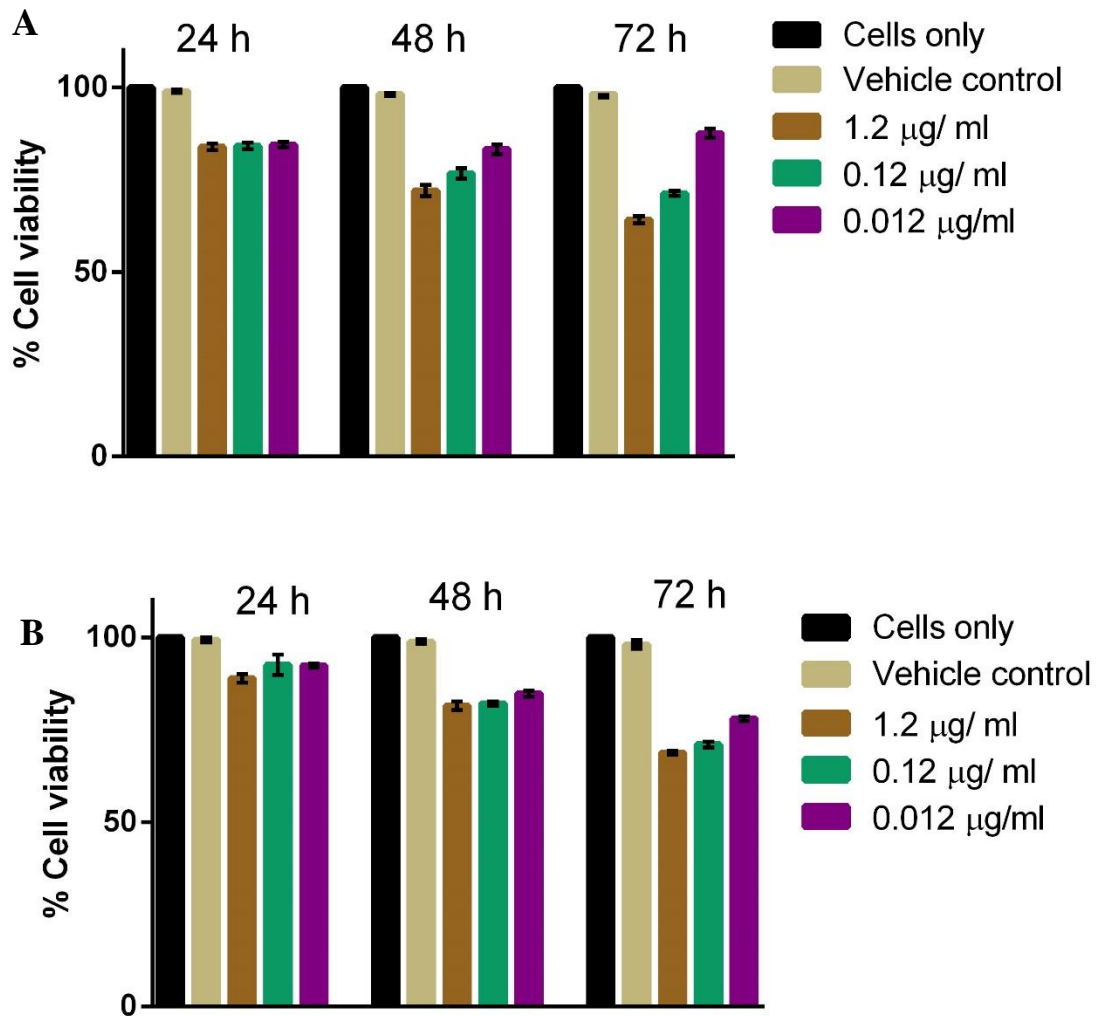


Figure 6.4: Percentage cell viability of endothelial cells relative to vehicle control after treatment with three different concentrations of lipid nanoparticle at time points 24 h, 48 h and 72 h as measured by the MTS assay. **A.** asiatic acid loaded lipid nanoparticle. **B.** empty asiatic acid lipid nanoparticle. The vehicle control used in the experiment was 0.1 % DMSO. The data points are means of three replicates (n=3) and the error bars represent  $\pm$  standard deviation ( $\pm$ SD).

As seen in Figure 6.5 following exposure of curcumin loaded NP, the percentage cell viability decreased with time, showing lowest percentage of 70 % viable cells at 72 h at a concentration of 2.87  $\mu\text{g}/\text{ml}$  (Figure 6.5 A). At 24h and 48 h these NPs showed cell viability of 98 % and 83 % at 2.87  $\mu\text{g}/\text{ml}$ . As seen in Figure 6.5 B, the SA43 aptamer did not show any change in the percentage cell viability up to 48 h. At 72 h, there was a decrease in the cell viability from 98 % to 92 % at a concentration of 100 nM. The concentration of 0.1  $\mu\text{g}/\text{ml}$  of curcumin lipid NPs and 10 nM of SA43 aptamer was used for screening in the models

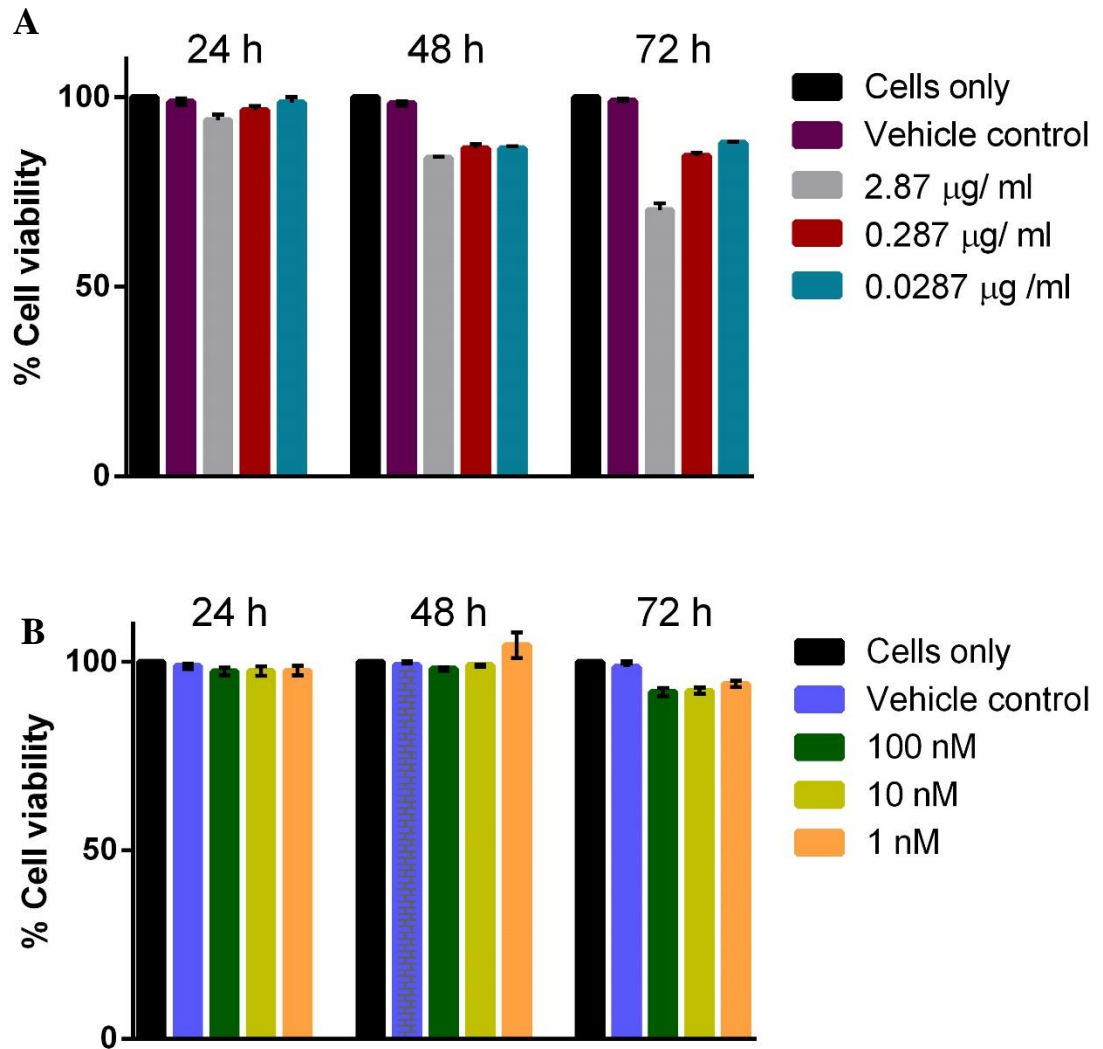


Figure 6.5: Percentage cell viability of endothelial cells relative to vehicle control after treatment with three different concentrations of NPs and SA43 aptamer at time points 24 h, 48 h and 72 h as measured by the MTS assay.

**A.** curcumin loaded lipid nanoparticle, 0.1 % ethanol was used as vehicle control. **B.** SA43 aptamer, 200 µl of culture media was used as vehicle control. The data points are means of three replicates (n=3) and the error bars represent  $\pm$  standard deviation ( $\pm$ SD).

### 6.2.2.2 Permeability of nanoparticles and aptamers

After validating the models for passive diffusion using the FITC-dextran, the aptamer SA43 (cy3 tagged) was tested for its permeability across the *in vitro* BBB tri-culture model. The concentration of the aptamer used for screening was determined by the MTS assay (see Section 2.9.3). The permeability of the aptamers was significantly lower when compared FITC-dextran and a similar trend was seen at all time intervals.

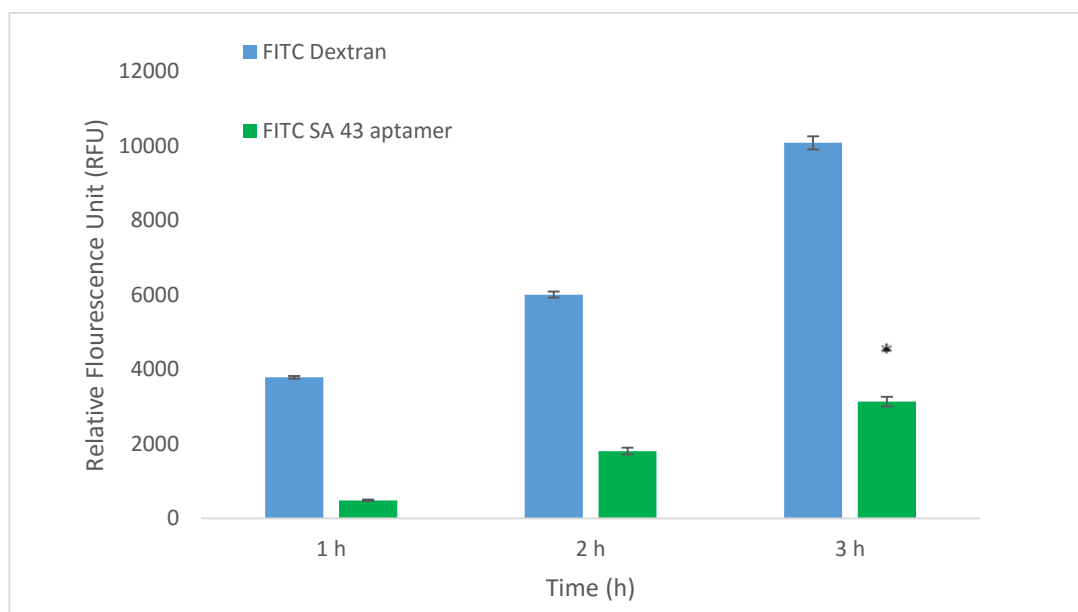


Figure 6.6: Permeability of aptamers SA43 (10nM) and FITC-dextran across different *in vitro* BBB tri-culture model [HBMEC, HA (in contact) and HBVP (out of contact)] at time intervals 1 h, 2 h & 3 h.

The data points are means of three replicates (n=3) and the error bars represent  $\pm$  standard deviation ( $\pm$ SD) of three inter repeats of an experiment.

The  $P_{app}$  value for all the NPs was determined as seen in Table 6.2.

Table 6.2  $P_{app}$  of the NPs and SA43 aptamer

Molecule	$P_{app}$
SA43 Aptamer	$4.32 \pm 3.90 \times 10^{-6}$ cm/ min
Docetaxel loaded lipid nanoparticle with ligand transferrin	$5.76 \pm 7.83 \times 10^{-6}$ cm/ min
Docetaxel loaded lipid nanoparticle	$7.94 \pm 6.72 \times 10^{-6}$ cm/ min
Curcumin loaded lipid nanoparticle	$5.88 \pm 9.31 \times 10^{-6}$ cm/ min

### 6.2.2.3 Cellular uptake of nanoparticles and aptamers

It is essential to develop NPs which are permeable across the BBB and are able to deliver drugs to the tumour site. The NPs can pass through the BBB by paracellular transport via opening of the tight junctions which can be assessed by measuring the TEER values across the barrier. A sharp drop in the TEER values is indicative of the TJs opening, if the TEER stabilises and come back to the initial value it indicates that the opening of the TJs was transient and did not damage the barrier

The NPs and aptamer were tested for their permeability across the BBB, the measurements of TEER was done over a time course of 24 h. The drop in TEER indicated the transient opening of TJs, therefore concluding that the NPs were permeable across the designed *in vitro* BBB model. As seen in Figure 6.7 A, the docetaxel loaded lipid nanoparticle showed a decrease in TEER values from 292  $\Omega/\text{cm}^2$  to 168  $\Omega/\text{cm}^2$  at 1.5 h whereas when tagged with transferrin as a targeting ligand for delivery, the nanoparticle showed a decrease in TEER from 294  $\Omega/\text{cm}^2$  to 157  $\Omega/\text{cm}^2$  at 0.5 h (Figure 6.7 B). In both instances the TEER values gradually increased and stabilised. Asiatic acid loaded lipid nanoparticle and empty nanoparticle both did not show any change in the TEER values (Figure 6.7 C and D). The SA43 aptamer showed a decrease in the TEER values at 1 hr, which gradually increased and stabilised at 6 h (Figure 6.7 F). The curcumin loaded lipid nanoparticle has previously been shown to cross the BBB *in vivo*, and therefore was used as a positive control (Kakkar *et al.*, 2013). It showed a drop in the TEER value at 0.5 h and the TEER values gradually increased and stabilised by 6 h (Figure 6.7 E). Evans Blue Dye (EBD) was used as negative control which is known not to cross the BBB *in vivo* (Bing *et al.*, 2014). EBD did not show any change in the TEER values and TEER remained constant at  $290 \pm 10 \Omega/\text{cm}^2$  (Figure 6.7 G). Cells only, were used as a control to make sure that the barrier was intact at all time during

the measurement and the measures of TEER were true values and not artefacts of a leaky barrier.

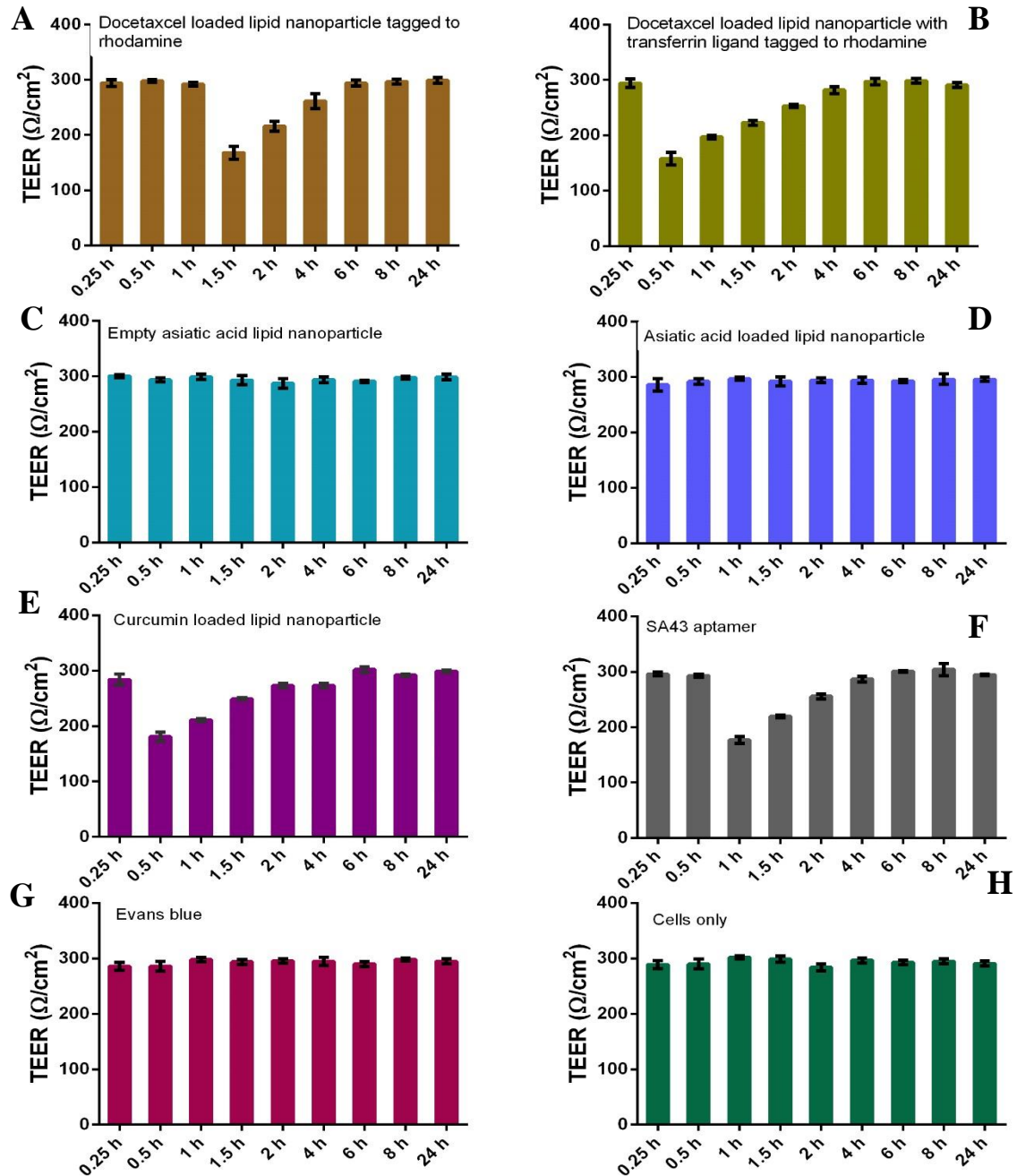


Figure 6.7 Time course TEER measurement of tri-culture BBB model to study the effect of NPs on the resistance of the barrier.

**A.** Docetaxel loaded lipid nanoparticle tagged with rhodamine (0.1 μg/ml) **B.** Docetaxel loaded lipid nanoparticle tagged with rhodamine and transferrin ligand (0.1 μg/ml) **C.** Empty asiatic acid lipid nanoparticle (0.12 μg/ml) **D.** Asiatic acid loaded lipid nanoparticle (0.12 μg/ml) **E.** Curcumin loaded lipid nanoparticle (0.287 μg/ml) **F.** SA43 aptamer (10 nM) **G.** Evans blue (negative control) (1 μg/ml) **H.** Cells only (control).

## 6.3 Discussion and conclusion

An *in vitro* model is needed to predict permeability and concentration of therapeutic drug reaching the site of action for drug-loaded NPs and targeted delivery molecules which can be used as potential therapeutics for glioma. It is essential to fully characterise the models before it is used to screen these novel molecules. The highly selective nature of BBB is a hurdle to the delivery of drugs to CNS tumours, therefore it is essential to study the permeability of drugs and NPs across the BBB. The designed *in vitro* model was characterised to determine the permeability of FITC-dextran, NPs and aptamers across the formed BBB. Macromolecules, conjugated to fluorescent probes, are frequently used to evaluate the permeability of barrier across semi-permeable membranes (Yuan and Rigor, 2011). Dextran is a complex branched hydrophilic glucan molecule which comprises of chains of varying length of polysaccharide ranging between 3 to 2000 kDa, it is a biocompatible and biodegradable molecule largely used to study the concentration gradient of diffusible molecules and subsequent characterisation of gradient slopes (He *et al.*, 2011). The dextran tagged to fluorescent molecules such as FITC or rhodamine can be used to study the permeability of different models (Yuan and Rigor, 2011). These validated models can then be used to commercially screen novel compounds and delivery systems, such as the NPs and aptamers, to study the permeability across the *in vitro* BBB model. In the current study, the co and tri-culture models were tested for their permeability using FITC tagged dextran since these two models showed high resistance (TEER values) indicating that the barrier formed was intact. The tri-culture model showed lower permeability of dextran as compared to the co-culture. The permeability is an important factor for validating a BBB model due to the highly selective nature of the BBB *in vivo*. The permeability data was used to calculate the  $P_{app}$  values for the two designed models. The  $P_{app}$  values showed that the tri-culture model

had significantly lower permeability,  $6.08 \pm 1.40 \times 10^{-6}$  cm/ min when compared to the co-culture model  $15.08 \pm 1.40 \times 10^{-6}$  cm/ min. An *in vitro* BBB model should ideally have a low apparent permeability, this makes the model useful in screening and determining the permeability of novel drugs, NPs. From the above  $P_{app}$  value, it was concluded the tri-culture model was a more intact and rigid model and hence it can be used to screen compounds to determine permeability across the designed barrier. According to the literature, compounds can be typically classed as low permeability with a  $P_{app} < 60 \times 10^{-6}$  cm/ min or high permeability with a  $P_{app} > 60 \times 10^{-6}$  cm/ min, which confirmed that FITC-dextran in the tri and co-culture was still classified as a low permeability molecule, as expected (Di *et al.*, 2003). In the literature the  $P_{app}$  for 20 kDa dextran in the endothelial monoculture was reported to be  $600 \times 10^{-6}$  cm/ min (Ma *et al.*, 2008).

To ensure that the permeability and uptake experiments of nanoparticles and aptamers were made across an intact and viable BBB, the effects of low, mid and high concentrations of NPs and aptamers were assessed with respect to time, using the MTS assay on endothelial cells and the concentrations that were found to be least cytotoxic following 24 h exposure were used for the permeability and cellular uptake studies. Evans blue was used as a negative control, and no permeability was observed either before or after application of NPs or aptamers, proving the barrier had remained intact.

Numerous diseases such as glioma, inflammatory diseases, diabetes and microbial infections can cause the disruption of the BBB. The disruption of the BBB in most circumstances is considered as harmful to the patient since it can lead to influx of leukocytes, potential active neurotoxins and water from the blood (Zlokovic, 2008). This disruption is associated with changes in the endothelial phenotype, decrease in the expression of tight junction proteins and remodelling of the junctional complex (Liebner *et al.*, 2008). It is essential to understand

the significance of opening of TJs in permeability across the BBB since the ability to modulate of the opening of tight junction enables prevention of adverse effects caused due to the BBB disruption and the transport of therapeutics to the brain for the effective treatment of neurological disorders (Zlokovic, 2008; Weidenfeller *et al.*, 2005).

Therapeutics for glioma are limited due to the inability of the drugs to reach the tumour site across the BBB. Recently interest in research into methods of disrupting the BBB have been revisited, such as transient opening of the paracellular pathway, however opening would need to be short in duration and specific to the chemotherapeutic that needs to be delivered (Stamatovic *et al.*, 2008). Several methods have been devised for the transient opening of the BBB for the delivery chemotherapeutics to glioma and other neuroectodermal tumours (Stamatovic *et al.*, 2008). An intra-arterial injection of mannitol arabinose, lactamide, saline, urea and several radiographic contrast agents were used to reversibly disrupt the BBB (Bellavance *et al.*, 2008). These agents are hyperosmolar in nature and cause shrinkage of the endothelial cells, thus opening of tight junction. In the current study, the cellular uptake of the NPs and aptamers across the BBB model via the paracellular permeability was assayed by transient decrease and recovery of TEER, thought to be an indicator of TJs opening. The docetaxel loaded nanoparticle with and without the transferrin ligand and the SA43 aptamer showed a sharp drop in the TEER values as compared to the positive control curcumin loaded NPs. The TEER value of the tri-culture dropped within 1 h from 295  $\Omega/\text{cm}^2$  to 160  $\Omega/\text{cm}^2$  on addition of the aptamer, docetaxel lipid NPs with transferrin ligand and curcumin loaded NPs. The TEER value of the docetaxel loaded NPs dropped to 160  $\Omega/\text{cm}^2$  from 290  $\Omega/\text{cm}^2$  after 1.5 h of incubation with the NP. This indicated the transient opening of the tight junction for the paracellular transport of the NPs and aptamer. In a previous study by Kakkar *et al.* (2013), curcumin loaded lipid NPs. have shown to cross the BBB *in vivo* and these NPs

exhibited similar properties *in vitro* (Kakkar *et al.*, 2013). Both the docetaxel loaded NPs, aptamer showed similar TEER values of the curcumin loaded NPs. The data confirms that both the docetaxel loaded nanoparticles and the SA43 aptamer are permeable through the designed BBB model.

The NPs and the aptamer when introduced in the tri-culture BBB model caused a change in the TEER values which indicated that they interact with the TJs proteins in the endothelial barrier causing them to open transiently. The endothelial barrier comprises of actin-myosin interactions, the junction proteins that contribute to its restrictive properties (Stamatovic *et al.*, 2008). The increase in the paracellular permeability is due to the loss of adhesive properties of the junction proteins and the reorganisation of the actin cytoskeleton that cause formation of minute inter-endothelial gaps in the barrier (Bazzoni, 2006; Garcia and Schaphorst, 1995; Kago *et al.*, 2006). These minute gaps are formed due to change in the adhesive properties of phosphoproteins such as tight junction and gap junction proteins. The alteration in phosphorylation state of these junction proteins causes a change in their interactions, alter transmembrane protein localisation and induces redistribution (Kago *et al.*, 2006; Kroll and Neuwelt, 1998). The phosphorylation causes a redistribution of the junction proteins which disturbs the adhesive contact between the endothelial cells. This is clearly observed by the sharp drop in the TEER values across the barrier and low permeability coefficient of tracer molecules such as FITC-dextran or fluorescent NPs (Stamatovic *et al.*, 2006; Stamatovic *et al.*, 2003; Ye *et al.*, 2014). The TJs comprises of membrane proteins occludin, claudin, JAM-A and intracellular proteins ZO-1. All these proteins together interact to maintain the cell polarity, paracellular permeability and signal transduction at the BBB (Bazzoni, 2006) (Lohmann *et al.*, 2004; Haorah *et al.*, 2007).

Proposed mechanisms for transient TJ opening have focussed on phosphorylation status. The exact phosphorylation site of occludin is still unknown, however, numerous papers have been published in the aim of identifying the target site for phosphorylation (Ma *et al.*, 2007; Hartsock and Nelson, 2008; Raleigh *et al.*, 2011; Liebner *et al.*, 2000). Raleigh *et al.*, explained the occludin S408 on phosphorylation enhances the interaction between tight junction proteins and releases the ZO-1 and causes a flux of negatively charged ions promoting the paracellular cation flux by claudin-1 and claudin-2 based pores. On the other hand on dephosphorylation stabilises the interactions between ZO-1 and occludin thus reducing the paracellular flux of ions and preventing pore assembly or opening of the junctions between the endothelial cells (Raleigh *et al.*, 2011). Stamatovic *et al.* (2006), suggested that VEGF and CCL2 induce Ser/Thr phosphorylation and cause redistribution of TJ protein occludin and ZO-1 and Tyr-phosphorylation causes reorganisation of the TJ complex in murine brain endothelial cells (Stamatovic *et al.*, 2006). There is still no clear evidence on how the redistribution occurs, Smythe *et al.*, suggested that polymerisation of the actin filament, actin and myosin association and generation of intraendothelial contractile forces leads to pulling in of the endothelial cells that causes the redistribution of transmembrane proteins (Smythe and Ayscough, 2006; van Hinsbergh and van Nieuw Amerongen, 2002).

The regulation of permeability by the paracellular transport comprises of interactions between components of endothelial cells and agonist activated signalling pathway. Protein kinase C (PKC) is an important regulator of the TJ and TJ-mediated permeability (Stamatovic *et al.*, 2008). PKC is a family of serine/threonine kinases which involve controlling function of other proteins by phosphorylation of the hydroxyl groups of serine, threonine amino acid residues. Proteins of these families are involved in the regulation of various cell cycles,

apoptosis, and migration (Willis *et al.*, 2010). Signalling molecules, such as Rho kinase, that are involved in the regulation of BBB permeability can also be used as targets for transient opening of the BBB. The molecules involved in the signalling pathways play an important role in the paracellular permeability of the endothelial barrier. Rho kinase is a part of the PKC signalling pathway, it is mainly involved in the regulation of shape and movement of the cell by acting on the cytoskeleton. Others signalling molecules involved disassembly of the TJs include endothelin-1 and PKC isoenzymes ( $\alpha$ ,  $\beta$ I,  $\beta$ II,  $\gamma$ ,  $\delta$ ,  $\epsilon$ ,  $\zeta$ ,  $\eta$ ,  $\lambda$ ,  $\mu$  and  $\iota$ ) (Stamatovic *et al.*, 2008).

In the current study, lipid NPs and asiatic acid loaded lipid NPs did not show any change in the TEER values suggesting that these NPs did not cause a transient opening of the tight junction, it cannot be confirmed that the NPs did not cross the BBB, there are alternate routes which can be used by the NPs to move across the barrier, and unfortunately there was no fluorescent tag on the asiatic acid NPs to assay the flux across the BBB. The transport of NPs across the BBB can also occur through transcellular lipophilic pathway, since the NPs are made of lipids. These can also be transported by transport proteins or receptors located on the cell membrane. The NPs can bind to the receptors located on the cell surface which then engulf the NPs and transport it across the endothelial layer by transcytosis (Abbott *et al.*, 1992; Abbott *et al.*, 2006a; Abbott, 2002). All of these transcellular methods do not affect the TJs assembly between the cells and hence the TEER values remain the same. (Simionescu *et al.*, 1975; Kroll and Neuwelt, 1998; Haluska and Anthony, 2004).

In conclusion, the tri-culture model was utilised to test novel NPs and aptamers for their permeability across the BBB. In future, the mechanism involved in the transfer of nanoparticles across has to be studied in much more detail to understand the transient opening of the barrier induced by the NPs and aptamer.

# CHAPTER 7

# 7. Developing a brain tumour barrier model

## 7.1 Introduction

Major components of the blood brain barrier (BBB) include the endothelial cells, which are interconnected by tight junctions (TJs) and dynamically interact with the astrocytes, pericytes and neurons, forming the neurovascular unit. The BBB maintains homeostasis and protects the brain from xenobiotics and controls the level of neuroactive mediators (Pardridge, 2003; Abbott *et al.*, 2012; Zlokovic, 2008). The highly selective nature of the BBB restricts the delivery of drugs administered for neurological disorders making treatment difficult. Glioblastoma multiforme (GBM) is an example of disorder where the BBB causes treatment issues. A patient suffering from GBM, a malignant form of glioma shows a median survival of 12 -15 month despite of optimal treatment and standard care (Inda *et al.*, 2014). patients with GBM exhibit poor prognosis due to the highly invasive nature of cells, however it is still not clear how the GBM disrupts the BBB while invading to other sites of the normal brain tissue (Vartanian *et al.*, 2014). Even after tumour resection, the GBM cells remain in the peritumoural tissue often causing relapse of GBM.

In this chapter the effect of GBM cells on the newly constructed, optimised and characterised tri-culture *in vitro* BBB model, developed in chapter 5, was studied. The GBM cells; short term cultures of BTNW370 and BTNW914 were added to the tri-culture in the form of spheroids and the effect on the TEER was studied. The GBM spheroids were seeded on the basolateral side of the insert in the setup of the tri-culture model of human microvascular endothelial cells (HBMEC), human astrocytes (HA) (in-contact) and human brain vascular pericytes (HBVP) (out of contact) as described in Section 2.8. These models were also used

to assess the permeability and disposition of nanoparticles (NPs) including docetaxel loaded lipid NPs tagged with rhodamine123 with and without transferrin ligand and curcumin loaded lipid NPs across the BBB and to the glioma.

## 7.2 Results

### 7.2.1 TEER measurements

The TEER measurements of the different brain tumour barrier (BTB) models were conducted to study the influence of the GBM cell spheroid on the resistance across the formed BBB. Since the GBM cells are highly invasive in nature they are expected to show disruption the intact barrier, a phenomenon that has been documented *in vivo* (Inoue *et al.*, 2010). The tri-culture model of HBMEC, HA (in-contact) and HBVP (out of contact) was set up and the TEER measurement were taken on day 1. GBM cells in the form of spheroids; BTNW370 and BTNW914 were seeded in the tri-culture set-up on the basolateral side overlaid on the pericytes. The TEER readings of these models were taken each day up to day 15 with the tri-culture model alone used as a control. The measurement was taken 5 times on each insert with three intra experimental replicates.

As seen in Figure 7.1, TEER readings of all the tri-culture models were plotted together on a scatter plot to compare the TEER values of the different models. The scatter plot compares the trend of TEER measurements for each model over the 15 days. The tri-culture models with the GBM spheroids showed a sharp increase in the TEER values up to day 5, after which the TEER dropped when compared to tri-culture model (control) which showed a steady increase in the TEER values. The tri-culture model with GBM spheroids (basolateral side) showed an increase up to day 6. The TEER values on day 6 was  $116 \Omega/\text{cm}^2$  which dropped after day 6 and continued to decrease up to day 12 to  $34 \Omega/\text{cm}^2$ . On day 13, the model showed

a slight increase to  $47 \Omega/\text{cm}^2$  and decreased until day 15. The tri-culture model (control) showed a steady increase in TEER up to day 12 giving a maximum TEER value of  $265 \Omega/\text{cm}^2$ .

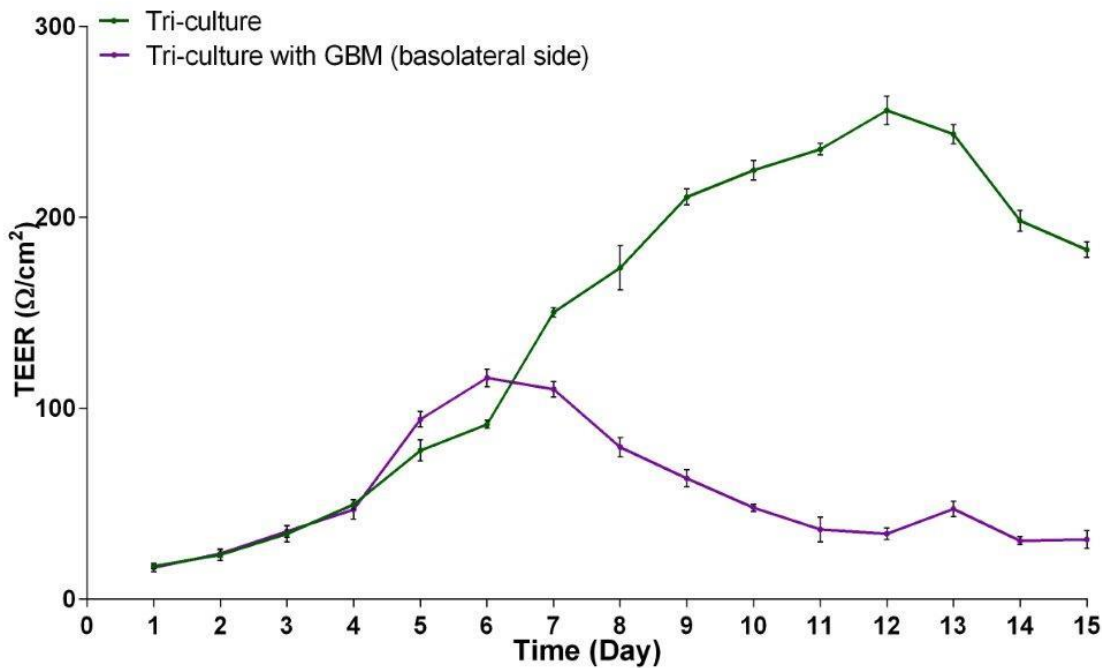


Figure 7.1 Comparison of TEER values in tri-culture model with GBM spheroids (basolateral side) compared to tri-culture alone without GBM.

There was a steady increase in the TEER values for all models up to day 5. After day 6 the tri-culture model with GBM spheroids showed a decrease in the TEER values as compared to tri-culture model. The data points are means of three replicates ( $n=3$ ) and the error bars represent  $\pm$  standard deviation ( $\pm$ SD).

### 7.2.2 Expression of Efflux transporters and DMEs in GBM spheroids.

The tumour shows the presence of efflux transporters and DME expression which will contribute an additional barrier causing drugs efflux and metabolism out of the tumour which leads to further reduction in bioavailability. The expression of efflux transporter; ABCB<sub>1</sub> and ABCG<sub>2</sub> and DMEs; CYP3A4 and CYP2D6 in GBM spheroids was compared with the same GBM cells grown in monolayer was studied by Western blots. As seen in Figure 7.2A & B, GBM spheroids showed a higher expression of both the efflux transporters compared to the monolayer. The expression of ABCB<sub>1</sub> was 124.91 A.U. and ABCG<sub>2</sub> was 99.88 A.U. when

compared to monolayer which had a densitometry value of 28.66 A.U. and 48.63 A.U. respectively, as seen in the densitometry graph (Figure 7.2 E).  $\beta$ -actin was used to normalise the data and to confirm that each well was loaded with equal amount of protein. In Figure 7.2C & D, the expression of CYP3A4 and CYP2D6 was higher in GBM spheroids when compared to monolayer. This was confirmed by densitometry which showed expression of CYP3A4 was 151.59 A.U. and CYP2D6 was 148.27 A.U. (Figure 7.2E).

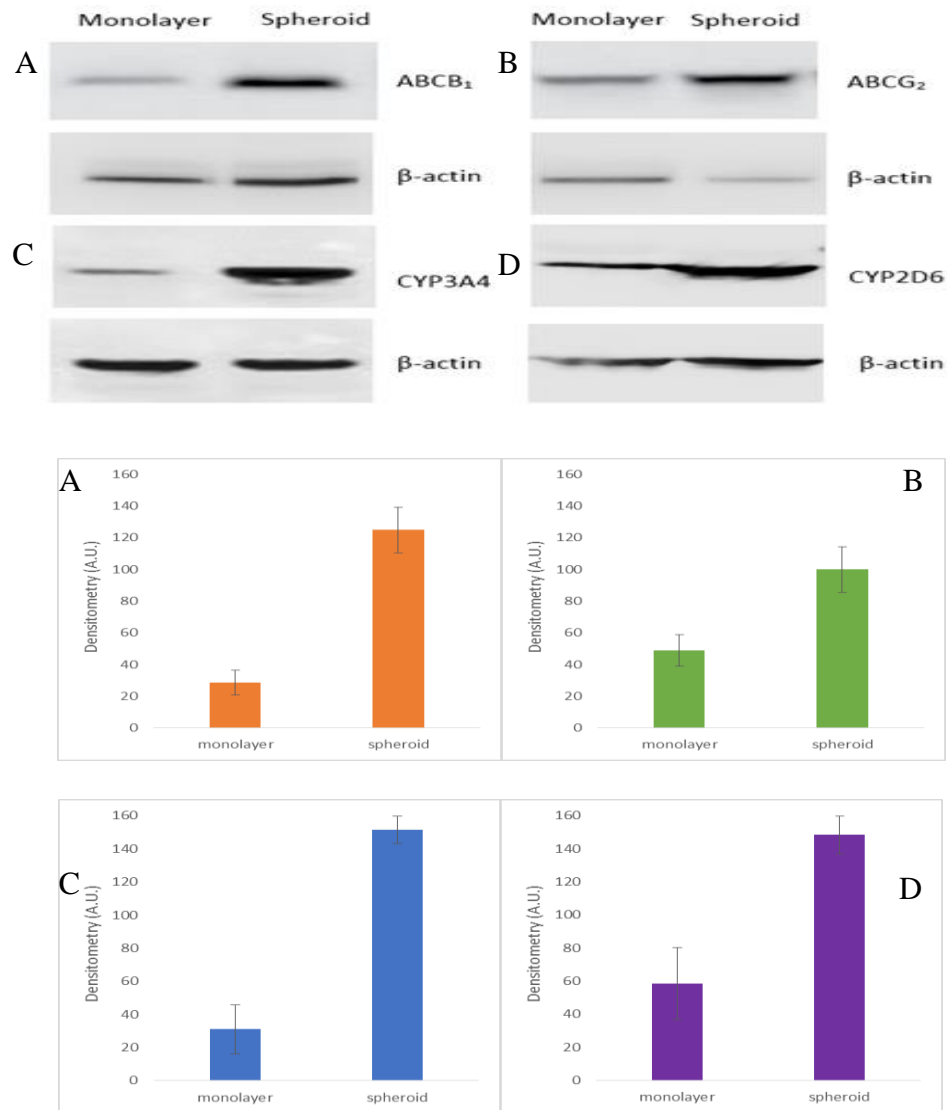


Figure 7.2 Comparison of expression between GBM spheroids and monolayer. **A.** Expression of ABCB<sub>1</sub> transporter. **B.** Expression of ABCG<sub>2</sub> transporter. **C** Expression of CYP3A4 **D** Expression of CYP2D6.  $\beta$ -actin was used as the loading control. E. Densitometry of the expression of efflux transporter; ABCB1 and ABCG2 and DMEs; CYP3A4 and CYP2D6 Each well was loaded with 10  $\mu$ g of protein.

### 7.2.3 Testing of NPs in the developed BTB model

The drugs administered for the treatment of glioma often have CNS bioavailability at the tumour even though the BBB is leaky at the site of tumour (On *et al.*, 2013). This may be due to the activity of efflux transporter at the tumour site. Transporter functional status plays an important role in the disposition of the glioma therapeutics. It is essential to study the role of these efflux transporters and take into account their role while designing a model for prediction of drug efficacy for glioma.

The tri-culture GBM models were tested to determine the uptake of NPs by the GBM spheroids. To determine the role of the efflux transporters, NP uptake was done in the presence and absence of an efflux transporter inhibitor. Vinblastine was used as the inhibitor of efflux transporter. The docetaxel loaded lipid NPs tagged with rhodamine123 with and without transferrin ligand and curcumin loaded lipid NPs were incubated in the tri-culture GBM models on the apical side of the insert. The NPs were also incubated in tri-culture GBM models in the apical side of the insert with an inhibitor for efflux transporters. The inhibitor was seeded along with the NPs. At different time points the fluorescence of the spheroids were read under the plate reader for their fluorescence to determine the uptake of NPs by the GBM. The fluorescence was plotted % fluorescence relative to the stock of NPs.

As seen in Figure 7.3, the fluorescence of the GBM spheroids due to accumulation of NPs were read at different time intervals on tri-culture models with GBM spheroids on the basolateral side. All the GBM spheroids show an increase in fluorescence with time. The fluorescence of NPs was higher in GBM spheroids with the inhibitor. The docetaxel loaded lipid NPs with and without inhibitor at 0.5 h showed a very low fluorescence due accumulation of NPs, 3.47 % and 4.39 % respectively as compared to the other NPs. The NP accumulation shows an increase with respect to time and at 3 hrs the fluorescence reaches

62.71 % and 35.69 % with and without inhibitor respectively (Figure 7.3A). The docetaxel loaded lipid NPs with transferrin ligand showed highest accumulation of NPs at time 0.5 h was 33.91 % and 17.77 % with and without inhibitor respectively. The fluorescence due to NP within cells shows an increase with time and at 3 h the accumulation reaches 77.69 % and 53.79 % with and without inhibitor respectively (Figure 7.3B). The GBM spheroids showed fluorescence due to accumulation of curcumin loaded lipid NPs with transferrin ligand NPs at time 0.5 h was 29.71 % and 15.76 % with and without inhibitor respectively. The accumulation shows an increase with time and at 3 h the accumulation reaches 74.06 % and 52.35 % with and without inhibitor respectively (Figure 7.3C).

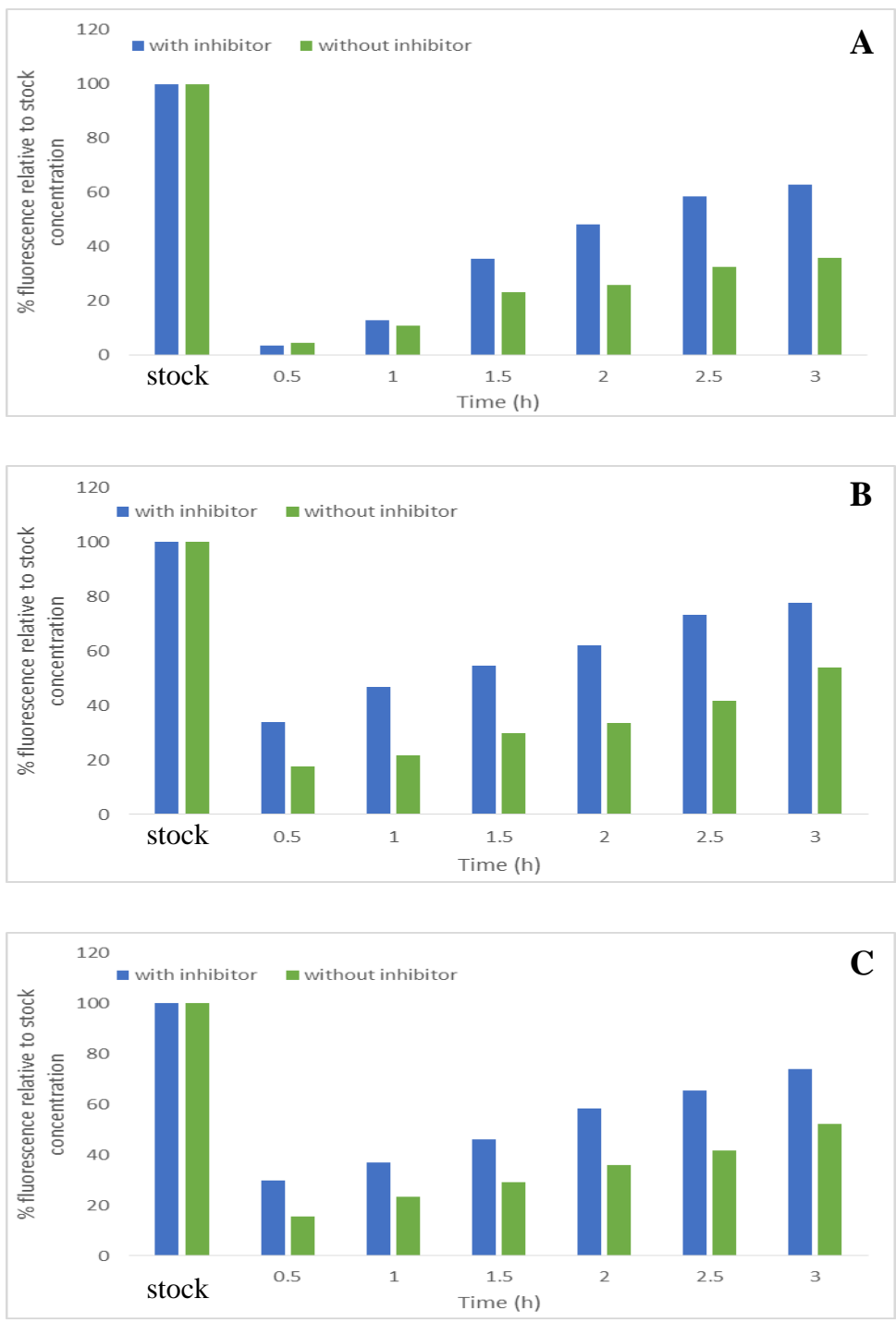


Figure 7.3 NPs uptake by spheroids on tri-culture with GBM (basolateral side).

**A** 0.33 µg/ml Docetaxel loaded lipid nanoparticle tagged to rhodamine123 **B** 0.33 µg/ml Docetaxel loaded lipid nanoparticle tagged to rhodamine123 with transferrin ligand **C** 2.87 µg/ml curcumin loaded lipid nanoparticle. Stock concentration was the concentration of NPs seeded on the apical side of the insert at time 0 h. Data is representative of a single experiment.

## 7.3 Discussion and conclusion

The BBB is a highly selective barrier and regulated by many components which include the tight junction proteins, efflux transporters, cytoskeletal components. The barrier function is regulated in response to any change in the microenvironment such as tumours, inflammatory processes. Nir *et al.*, demonstrated in tumour conditions the capillary endothelial cells are disturbed due to the pressure exerted by the tumour bulk (Nir *et al.*, 1989). This makes the BBB leaky which provides a passage for the glioma therapeutics to reach the tumour site. The functional efflux transporter serves as the transport barrier, which is responsible for the disposition of these glioma drugs at the tumour site.

In this study, the GBM spheroids were added to the tri-culture model, which represents a functional, characterised BBB model (Chapter 5). These GBM spheroids were derived from tumour biopsies from glioma patients. The GBM cells were seeded at the bottom of the culture overlaid on the pericytes or on the apical side overlaid on the endothelial cells. The TEER measurement in the control showed a steady increase up to day 12 which begins to plateau, this is due to the formation of TJs. The TEER measurement of the models, unlike the tri-culture on its own, showed a peak in the first few days of culturing and then show a drop after day 6. The increase in TEER may be due to the expression of the protein, transforming growth factor (TGF). It had been shown that the GBM cells increased secretion of TGF which is a cell growth mediator and plays an important role in proliferation and differentiation of cells (Joseph *et al.*, 2013; Golestaneh and Mishra, 2005). We can assume that TGF secreted by the GBM cells causes the TEER increase due to cell proliferation, the increase in cell proliferation leads to increase in cell-cell communication that increases the TJs proteins. These observations suggest the possible involvement of TGF in blood-tumour

barrier and BBB impairment in GBM. No data was found in the literature with respect to this study so no comparison could be made with other findings.

GBM cells also show overexpression of vascular endothelial growth factor (VEGF), which is an angiogenesis factor. VEGF has been linked with increasing the paracellular permeability in a BBB model (Miao *et al.*, 2014). Increase in paracellular permeability leads to access NPs permeating into the basolateral side thus. Both these factors have not been studied in a brain tumour barrier model before and this could be pivotal in understanding the role of these soluble factors which influence the endothelial cells and basement membrane at the BBB making it leaky (Figure 7.4).

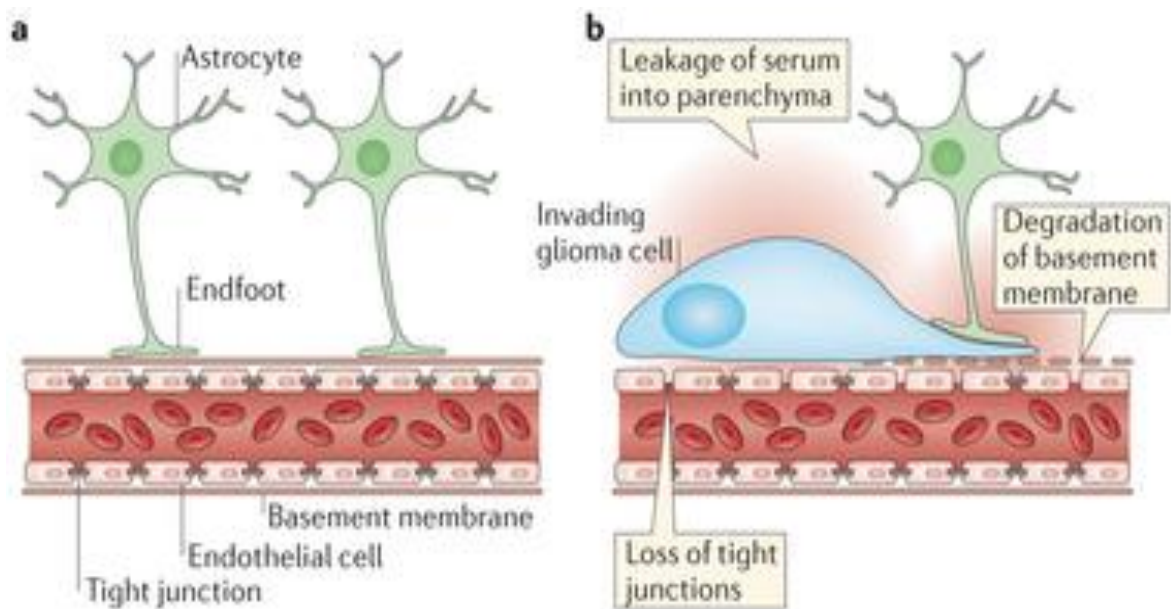


Figure 7.4 BBB structure *in vivo*. a) normal BBB model b) BBB model when leaky.

In glioma, the drugs delivered are able to pass through the leaky BBB, however the drugs are effluxed out of the tumour due the efflux transporters at the tumour site. Another study was conducted to elucidate the role of efflux transporters located at the tumour site involved

testing the uptake of NPs by GBM spheroids. From chapter 6, it was concluded that the NPs were permeable across the robust BBB tri-culture model. The NPs were uptaken by the GBM both in the presence and absence of inhibitor. In glioma, as mentioned before the BBB is leaky and the drug disposition is carried out by the efflux transporters. From the data, we can observe that the GBM spheroids with the inhibitor show high accumulation as compared to GBM cells without the inhibitor due to the high fluorescence of the NPs from the model without the inhibitor. This indicated that the efflux transporters are effluxing the drugs actively out of the cells in the spheroid, however no data was found to compare the findings. In conclusion, this BTB model show very promising role in prediction of drug disposition for glioma. This model currently needs extensive characterisation and protein expression studies to establish it as a fully functional BTB model.

# CHAPTER 8

## 8. Discussion

### 8.1 General discussion

For the last four decades patients with glioma have not shown any improvement in the median survival rate when compared to patients with other cancer types such as colon cancer (Rachet *et al.*, 2009). Glioma are the most common primary malignant brain tumours in adults and comprise of 81 % of the malignant brain tumours (Ostrom *et al.*, 2014). There have been numerous drugs designed to treatment glioma, however, these have not shown a significant improvement in patient survival. The major hurdle in the treatment of glioma is the blood brain barrier which comprises of a physical barrier made up of tight junction proteins and a metabolic barrier consisting of efflux transporters and drug metabolising enzymes (DMEs) that limit the penetration and efficacy of various CNS drugs (Hitchcock, 2008). At molecular level, the function of the barrier at the brain and blood junction mainly involves the efflux transporters localised in the luminal membrane of brain capillary endothelial cells which restrict the brain uptake and extrusion of xenobiotics (Loscher and Potschka, 2005b; Dean *et al.*, 2001). The localised enzymes present at the junction are responsible for metabolising the drugs, therefore leading to poor bioavailability.

There has been an emergence of cell based *in vitro* models as potential tools to study the *in vivo* mechanisms at the BBB. These models are cost effective, versatile and require a simple working environment compared to the *in vivo* systems (Cecchelli *et al.*, 2014). To date, all the research in the BBB field has been focussed on developing a robust *in vitro* BBB model which focuses on the physical barrier and that shows a high expression of tight junction proteins and TEER which makes the model highly selective, however the importance of the metabolic BBB has often been overlooked. Screening of novel anti-cancer drugs on these

models characterised for just the physical barrier only provide us with information about the permeability of the drug. There is an urgent need to develop a model which is physiologically relevant and focusses on the physical, transport and metabolic barrier present at the blood and brain junctions and more importantly a model that is designed with a goal to delivering chemotherapeutics to CNS tumours. The proposed model should take into consideration the role of efflux transporters and metabolic enzymes in drug disposition.

The main aim of the project was to design an all human, fully characterised and physiologically relevant *in vitro* BBB model for the prediction of permeability of drugs across the blood brain barrier to glioma. To date, numerous models have been designed and patented with the desire to construct a fully functional *in vitro* BBB model which can be used to predict efficacy of drugs for neurological disorders, such as those listed in Table 1.5, but as yet no model has been reported to be optimised for metabolic function, including expression and activity of efflux transporters and DMEs.

The primary background work before developing the model was to characterise the cell lines which were to be used to construct the model and study the growth characteristics. The growth curves were used to determine cell population doubling time and exponential growth phase. In the past decade there has been an emerging understanding, about cellular cross-contamination, misidentified cell lines, and the use of cultures at high-passage levels contributing to the generation of erroneous and misleading results (Hughes *et al.*, 2007). Numerous reviews and research articles have been published mentioning the significance of experimental variance between different passage numbers and the need for use of verified, tested and characterised cell lines at low or defined passage number (Rojas, 2011; Apps *et al.*, 2009; Lucey *et al.*, 2009; Wenger *et al.*, 2004; Hughes *et al.*, 2007; Tsujino *et al.*, 1997; Halfter *et al.*, 1998; Grippo *et al.*, 2001).

In the current study, the three cell lines, U87MG (grade IV, glioblastoma), 1321N1 (grade IV, malignant astrocytoma) and SVGp12 (foetal glial astrocyte) were characterised for their origin and type showing positive staining for both HLA and GFAP. The short term glioma cultures derived from patient biopsies were characterised for their phenotype using antibodies raised against CD44 antigen, EMA antigen and GFAP antigen and it was concluded that with the increase in passage number the cells began to lose their characteristic phenotype. These findings were supported by Wenger *et al.* (2004), he reported difference in the phenotype of MCF-7 cell line at two different passage numbers and reiterate the necessity for periodically evaluating cells to confirm their origin (Wenger *et al.*, 2004).

After characterisation of cell line phenotype, the next crucial step in the study was to determine the expression of efflux transporters and DMEs and to maximise their expression by altering culture conditions. Pan *et al.* (2009), reported that Hepa1 cells derived from liver cells were deficient in mitochondria which led to metabolic pathway, drastically up-regulating cell cycle-associated functions and largely shutting down drug metabolizing enzymes (Pan *et al.*, 2009). It was therefore essential to choose cells which were true to the proposed phenotype. Efflux transporters; ABCB<sub>1</sub> and ABCG<sub>2</sub> and DMEs; CYP3A4 and CYP2D6 were chosen to be studied. The expression was studied in cell lines (hCMEC/D3, U87MG, 1321N1 & SVGp12) and short-term cultures (HBMEC, HBVP, HA, BTNW914 & BTNW370). The expression of the efflux transporters; ABCB<sub>1</sub> and ABCG<sub>2</sub> and DMEs; CYP3A4 and CYP2D6 was higher in short term cultures leading to selection of these cells to construct the *in vitro* BBB model. The expression and activity of proteins was higher in short-term cells compared to immortalised cell lines which has also been previously reported by Alge *et al.* (2006), who compared the protein expression profiles of short-term versus

immortalised human retinal pigment epithelial (RPE) cell line and found that expression of proteins was higher in short-term cultures (Alge *et al.*, 2006).

This then led to optimising of culturing conditions to enhance the expression and activity of the DME and transporter proteins. It has been reported by numerous papers that culturing conditions can largely affect the protein expression and activity of cells in culture (Kumar *et al.*, 2008; Kumar *et al.*, 2014; Marini *et al.*, 2014). The conditions were altered, bearing in mind that all the culturing elements were from human origin so that the model developed should be a true representative of human BBB and should not show any elements of inter species variability. Due to inter species variability, such as altered DME and transporter phenotype, the permeability and effects of the novel therapeutics could be misinterpreted, therefore, considerable effort has been put into developing models of human origin (Lacombe *et al.*, 2011; Wilhelm and Krizbai, 2014). The cells were cultured in 5 % human serum, with and without extracellular matrices (MaxGel, poly-L-lysine & fibronectin). The extracellular matrices improves cell attachment and expression of proteins due to improved cell-cell communication (Kavanagh *et al.*, 2006; Schlie-Wolter *et al.*, 2013). The short-term cultures showed higher expression and activity of the proteins of interest when cultured in the presence of fibronectin. Singh *et al.*,(2010) reported the role of fibronectin in protein processing and secretion, binding to cell surface receptors, self-association, and fibril growth which enhances the expression and activity of proteins in the cells (Singh *et al.*, 2010). To conclude, the short-term cultures grown in 5 % human serum and fibronectin as the ECM were selected to translate in the *in vitro* BBB model.

To date, all of the models designed for BBB in the literature have focussed on the TEER expression across the barrier and the expression of TJs proteins. The TEER value *in vivo* is  $>1000 \Omega/\text{cm}^2$ , however various BBB models have been developed to give TEER values

ranging between 20 – 700  $\Omega/\text{cm}^2$ . There are numerous instruments which have been developed to measure the resistance across the *in vitro* BBB. In the current study three measuring systems EVOM, ECIS and CellZscope were compared, thus validating the EVOM instrument as giving reproducible trends in TEER. Naik *et al.*, (2012) reviewed the EVOM instrument and highlight that the resistance is measured in AC current which unlike the DC source used by ECIS and CellZscope is not harmful to the cell layer and does not damage the electrode (Naik and Cucullo, 2012). The EVOM is also the most widely used equipment for measuring TEER, cost-effective and does not involve any complex calculation to determine the TEER across the barrier. The designing of an *in vitro* BBB model required utilising cells in different formations; mono-, co- and tri- culture, to maximise the TEER values and assess the expression of efflux transporters; ABCB<sub>1</sub> and ABCG<sub>2</sub> and DMEs; CYP3A4 and CYP2D6.

Eigenmann *et al.*, (2013) studied properties of different endothelial cells in monoculture for *in vitro* drug disposition studies, and similar to the findings reported here, human microvascular endothelial cells (HBMEC) proved to be the most suitable for modelling *in vitro* BBB models (Eigenmann *et al.*, 2013). Monoculture models are often used in the studies reported in the literature as they are cost effective, simple to establish and have a high throughput screening capacity. The mono-culture of HBMEC established here, gave a TEER of 120  $\Omega/\text{cm}^2$ , which was approximately 10-fold lower than the desired *in vivo* resistance values. The major drawback of the mono-culture model was that the cells were grown without the influence of another cell type unlike the *in vivo* situation and therefore showed a limited expression of the phenotype. The absence of stimulating factors derived from other cellular components of the neurovascular unit leads to low TEER values and high permeability (Kumar *et al.*, 2014; Wilhelm *et al.*, 2011b; Cucullo *et al.*, 2002; Eigenmann *et al.*, 2013).

The monoculture formation of endothelial cells was therefore rejected as a suitable model for the BBB studies presented in this thesis.

It was established that the presence of cerebral components, along with the endothelial cells, were essential for maintenance of the BBB phenotype. All of the BBB models were designed on a porous membrane which enabled the cells to interact with each other physically and chemically thus creating an *in vivo* like environment. The introduction of astrocytes and pericytes enhanced the *in vitro* BBB properties by direct interaction with the endothelial cells as shown here and reported in the literature (Li *et al.*, 2010). *In vivo*, the astrocytes are not in contact with the endothelial cells due to the presence of the basal membrane. To mimic the *in vivo* situation, a number of different experimental setups were designed including an ECM. The different co-cultures of HBMEC (endothelial cells seeded apically) were designed with HA (astrocytes) or HBVP (pericytes) (seeded basolaterally (in-contact) or at bottom of well (out of contact)). The TEER values of HBMEC and HA (in-contact) and HBMEC and HA (out of contact) gave TEER of 208  $\Omega/\text{cm}^2$  and 153  $\Omega/\text{cm}^2$ . The TEER values of HBMEC and HBVP (in-contact) and HBMEC and HBVP (out of contact) gave TEER of 189  $\Omega/\text{cm}^2$  and 115  $\Omega/\text{cm}^2$ . This suggested that when pericytes and astrocytes were cultured in-contact with the endothelial cells the TEER showed a higher value. Some papers suggested culturing astrocytes on the basolateral side of the insert instead of apically, to permitted direct contact of the astrocytic foot process with the endothelial cells (Franke *et al.*, 1999; Duport *et al.*, 1998; Hatherell *et al.*, 2011). Gu *et al.*, (2011) suggested that a co-culture could be set up by seeding astrocyte 'out of contact' at the bottom of the well (Gu *et al.*, 2011), this method would permit the interaction between the astrocyte secreted soluble factors and the endothelial cells only but not the astrocytic foot processes. The TEER values for HBMEC and HA (out of contact) was 153  $\Omega/\text{cm}^2$  which was lower than the HBMEC and HA (in-

contact) giving TEER of  $208 \Omega/\text{cm}^2$ . Although the pericytes are found next to the endothelial cells *in vivo*, their effect on the formation of the barrier is not well understood. The pericytes secrete extracellular matrices like laminin, type IV collagen and glycosaminoglycans, which contribute to the formation of the basement membrane (Sá-Pereira *et al.*, 2012). As found in the studies here and in the literature, introduction of pericytes to the co-culture strengthens the barrier and induces the functional activity of the ABC transporters (Berezowski *et al.*, 2004b; Al Ahmad *et al.*, 2011). Nakagawa *et al.*, described that co-culture of pericytes with endothelial cells gave a high TEER value of  $388 \Omega/\text{cm}^2$  and low permeability (Nakagawa *et al.*, 2007a; Nakagawa *et al.*, 2009b).

After concluding that pericytes and astrocytes both played an important role in modulating the properties of the BBB, the tri-culture models were developed. The HBMEC was cultured with HA (in-contact) and HBVP (out of contact) which gave the highest TEER value of  $258 \Omega/\text{cm}^2$ . A tri-culture model involved the culturing of endothelial cells, astrocytes and pericytes together in a single culture system, and was found to increase the TEER significantly. Many other papers have shown similar findings, traditionally, the endothelial cells are seeded on the apical side of the insert, however the location of astrocyte and pericyte is not predetermined. Nakagawa *et al.* (2009), patented a tri-culture model giving a TEER value of  $350 \Omega/\text{cm}^2$  on day 8 of TEER measurements, the model comprised of endothelial cells on the apical side of the insert, the pericytes on the basolateral side of the insert and the astrocyte seeded at the bottom of the well (Nakagawa *et al.*, 2009a). Hatherell *et al.*, on the other hand reported that culturing of pericytes in an endothelial and astrocyte co-culture disrupted the barrier and decreased the TEER values. According to Hatherell *et al.*, the best model was the co-culture of endothelial cells with the astrocytes seeded on the basolateral

side of the insert since the TEER reading for co-culture was higher than the tri-culture model. (Hatherell *et al.*, 2011).

All these models presented in the thesis were studied for expression and activity of the efflux transporters; ABCB<sub>1</sub> and ABCG<sub>2</sub> and DMEs; CYP3A4 and CYP2D6. The highest expression and activity was exhibited by the tri-culture model indicating that culturing of the three primary cells was the best arrangement to get a high TEER and high protein activity as well as expression. No data was found in the literature reporting expression or activity of efflux transporters; ABCB<sub>1</sub> and ABCG<sub>2</sub> and DMEs; CYP3A4 and CYP2D6 in tri-culture models for comparison, highlighting the originality of the findings presented here.

The structural component of the *in vitro* BBB was designed, however it lacked a component present *in vivo* which was the shear stress on the cells due to the blood flow. The endothelial cells *in vivo* are under constant shear stress due to blood flow through the capillaries. A similar shear stress on the *in vitro* endothelial cells and astrocytes co-cultures cells was induced by perfusion with media. In the current study we utilised the same arrangement of cells but seeded them in a 3D Alvetex fibronectin coated scaffold and applied a shear stress of 20 dyne/cm<sup>2</sup>. The Alvetex perfusion tri-culture model gave a TEER of 710 Ω/ cm<sup>2</sup> which increased from 258 Ω/ cm<sup>2</sup> in a static polycarbonate tri-culture model. The change from a 2D culture surface to a 3D scaffold, more representative of the 3D tissue architecture to provide the cells an *in vivo* like environment; which was reflected in the increase in TEER values. As shown here and reported in the literature, the induction of shear stress improved the expression of tight junction proteins and increased the TEER values in the dynamic *in vitro* BBB model (Davies, 1989; Tarbell, 2010). There have been numerous culture systems available in the market, which involve growing cells on scaffolds, tubular fibres, and polycarbonate membranes with flow causing a shear stress (approximately 5 dyne/ cm<sup>2</sup>).

The protein expression and activity also showed an increase in the Alvetex perfusion model as compared to tri-culture on the polycarbonate membrane. Cucullo *et al.*, used dynamic *in vitro* (DIV) BBB models which include culturing of cell endothelial cell in a polypropylene hollow tube attached to a tunable shear stress. The DIV-BBB model when applied with shear stress of 5 dyne/cm<sup>2</sup> gave a TEER of more than 500 Ω/ cm<sup>2</sup> when grown for a period of 20 days (Cucullo *et al.*, 2008). In spite of having high TEER values, the DIV-BBB system is not suitable for commercial use due to its low throughput capacity. It takes a very long time period for its development (20 days) involves specialist technical skills to culture the cells in the hollow fibre and requires a very large number of cells > 1.5 x 10<sup>6</sup> cells/ tube, initially to be loaded in the hollow fibre (Wilhelm and Krizbai, 2014). In addition, the cells cannot be grown in a 3D formation within the hollow tube.

In conclusion, an all human tri-culture model using only short-term cultures, rather than immortalised cells with incorporated shear stress and 3D environment was validated for maximum TEER, TJ protein expression, DME and transporter expression. This was the model we proposed for the physiologically relevant BBB, however, further characterisation and application was needed to prove its efficiency as an *in vitro* BBB model.

The designed tri-culture was further characterised after studying TEER, expression and activity of efflux transporters; ABCB<sub>1</sub> and ABCG<sub>2</sub> and DMEs; CYP3A4 and CYP2D6 for its paracellular permeability. An appropriate *in vitro* BBB model should show a low apparent permeability (P<sub>app</sub>) which was proved using FITC-Dextran and found to be comparable to others in the literature (Ma *et al.*, 2007). The applicability of the *in vitro* BBB was further confirmed by screening novel NPs and aptamers synthesised in-house for potential use in glioma treatment, in the tri-culture model to determine if the NPs or aptamer were permeable through the BBB model. The reliability of the results was proved by screening a curcumin

loaded lipid NPs through the model which have already been reported to cross the BBB *in vivo* (Kakkar *et al.*, 2013). The model was capable of identifying the NPs which cross the BBB model via paracellular transport. The NPs which were permeable through the paracellular pathway caused a sharp drop in the TEER values. The TEER then slowly increased and stabilised. This sharp drop in TEER was due to transient opening of the BBB. Thus it was confirmed that the molecules were passing through the paracellular pathway. The crossing of BBB can be undertaken by various mechanisms, as seen in Figure 8.1.

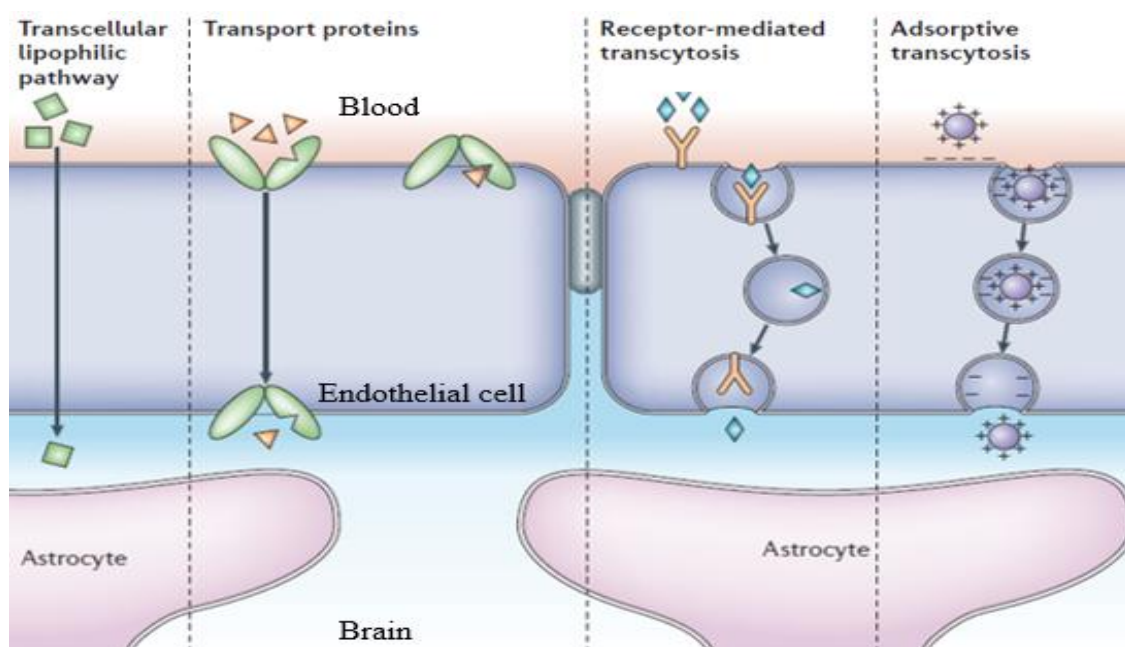


Figure 8.1 Schematic overview of the permeability pathways across the endothelial barrier (Kroll and Neuwelt, 1998).

Drug delivery across BBB by transcytosis and transcellular permeability using enhanced vesicular transport can also be used as a method for delivering compounds into the brain (Gabathuler, 2010). BBB models can be designed to investigate other pathways of transport across the BBB by inhibiting different endocytic pathways. Designed NPs loaded with chemotherapeutics are thought to be delivered across the brain to the tumour site by transcellular or paracellular pathway (Lu *et al.*, 2006). The transcellular route contributes to

both passive and active modes whereas paracellular is an exclusive passive mode of transport. Paracellular transport is less selective and has a higher conductance. Factors contributing to this mode of transport include hydrostatic and osmotic gradient (Bazzoni, 2006). The dynamic interaction of the endothelial cytoskeleton and the adhesive force developed due to cell-cell junction and cell-matrix contact controls the transient opening of the paracellular pathway. This serves as the fundamental mechanism of transport across the blood brain barrier and maintains the exchange between blood and brain (Garcia and Schaphorst, 1995; Garcia-Garcia *et al.*, 2005).

After proving the applicability of the tri-culture BBB model, we wanted to explore the effect of introducing GBM spheroids to an intact *in vitro* barrier of the model, to identify the changes caused at the BBB in presence of a tumour. It has been reported that the BBB is leaky and often not intact at the site of tumour *in vivo* (On *et al.*, 2013). When GBM spheroids, derived from short term cultures of patient glioma biopsies BTNW914 and BTNW370 were added to the *in vitro* BBB model a similar effect was observed. The TEER values were higher as compared to the control and showed increased up to day 6 to  $180 \Omega/\text{cm}^2$  but then shows declined. Similar work had been done in rat *in vitro* BBB model, Toyota *et al.*, developed a tri-culture model using cells from rat, which involved the culturing of endothelial cells on the basolateral side of the insert and pericyte and astrocyte cell on the apical side of the insert. To the tri-culture, human GBM spheroids were added to the basolateral side along with the rat endothelial cells. The addition of human GBM cells in the tri-culture showed an increase in the TEER values in the first 72 h followed by a decrease in the TEER which when compared to culture without GBM did not show that high values. (Toyoda *et al.*, 2013).

To further understand if the role of efflux transporters at the site of tumour, the expression of ABCB<sub>1</sub> and ABCG<sub>2</sub> were studied and the NPs were also screened through the brain tumour barrier model. Such a study is novel and has not been done before and hence there was no available data to compare the behaviour of drug loaded NPs at tumour site. The results showed the presence of active efflux transporters, effluxing the NPs out of the GBM spheroids which was identifiable when the efflux transporters were inhibited and the GBM spheroids showed an increase in the accumulation of NPs.

To summarise, we have established culture conditions under which the brain primary cells show high expression and activity of efflux transporters; ABCB<sub>1</sub> and ABCG<sub>2</sub> and DMEs; CYP3A4 and CYP2D6. We have also established the expression and activity in a multi-cell type model, and provided a connecting link between the physically robust BBB models and the physiologically relevant *in vivo* model. This bridge between *in vitro* and *in vivo* will help it to screen established and novel anticancer glioma therapeutics to predict the efficacy of the drug, based on the therapeutic concentration achieved at the glioma protected by the BBB.

## 8.2 Limitations of the project

Some of the major limitations of the current study is the use of short term cell cultures; the short-term cell cultures used to set up the BBB model were difficult to maintain and only grew up to a certain passage number. The short-term cultures have unmatched value for basic and translational research however, it is not feasible to utilise models comprising of these cultures commercially due to low throughput. It is essential to derive a cell line with matched properties of HBMEC so that the model is easier to set up and can be used on a commercial scale. The EVOM instrument is a robust and reproducible method for the measurement of TEER, however, a TEER measuring system which could determine the value real time would

enable us to understand the TJs formation better. The *in vitro* model is much more expensive and time consuming compared to the most cost-effective method of modelling the BBB by the use of computer aided designing system (Song *et al.*, 2009). *In silico* models mimic all the physiological properties of the blood brain barrier, the computer system incorporates *in vivo* permeability values and simulates the compound interaction in the BBB (Naik and Cucullo, 2012; Palmiotti *et al.*, 2014). The system incorporates essential physiological parameters such as lipophilicity, charge, pH, size of molecule into simulation to get physiologically relevant data (Narayanan and Gunturi, 2005). A large number of compounds can be screened by such systems to determine the permeability co-efficient. The designed *in vitro* model cannot completely replace the use of *in vivo* models. The most widely recognised limitation of *in vitro* model is that the primary cells used to initiate short-term cultures are not the exact dissociated replicates of their *in vivo* counterparts. Finally, the artificial and controlled *in vitro* environment is not the same as what the cells experience *in vivo* and could have an effect, depending upon the measure being assessed (Reichert, 2007).

### 8.3 Future works

The present study involved the development of a functional, fully characterised BBB model which could be used for screening and determining the permeability of NPs and aptamers. Numerous challenges still remain in using this model commercially for screening of glioma therapeutics. Future work in this area could involve studying the mechanism of transport across the BBB; and deciphering whether the permeability of the NP and aptamers was paracellular or transcellular and further assessing the contribution of efflux transporters in the presence of efflux pump inhibitors. In addition, HPLC methods could be established to quantify the release of entrapped drug from the NPs in the BBB model with respect to time. Another interesting study which could be done in future includes; tracking of fluorescent NPs

and aptamers across the BBB by live cell imaging over a time course in combination with co-localisation immunostaining to elucidate the transport mechanism and to prove that NPs had truly been taken across the BBB. The 3D Alvetex scaffold model needs to be further characterised for the polarity of the cells cultured on the 3D scaffold and used for permeability and screening of NPs. In future, the BBB models could be cultured serum free and this would rule out the interferences caused by the growth factors present in the serum which have been shown to disrupt the TJs protein expression (Chang *et al.*, 1997; Jung *et al.*, 2007b). The most essential part which needs to be explored in detail is the applicability of the BTB model and its role in the screening novel glioma therapeutics.

Another system in the literature which has drawn attention is the using of miniaturised microchips to construct a BBB model. The microfluidic models closely mimic the BBB and are comprised of a thin culture membrane with induced shear stress (Booth and Kim, 2012). The microfluidic chip is the smallest model of the BBB available, requiring a very small cell number  $<1 \times 10^4$  cells/chip to setup. Recently, Griep *et al.* (2013), developed a BBB model on a microfluidic device cultivating endothelial cells on a polycarbonate membrane of pore size  $0.4 \mu\text{m}$  and  $10 \mu\text{m}$  thickness. In static conditions the system gave a TEER reading of  $36 \Omega/\text{cm}^2$  however, this value increased to  $120 \Omega/\text{cm}^2$  when a shear stress of  $0.58 \text{ Pa}$  was applied to the model (Griep *et al.*, 2013). In future, we would like to minitourise our optimised and designed BBB model structure to a microfluidic chip, this will make efficient use of HBMEC cells and also give real time TEER measurement.

## 8.4 Conclusion

To conclude the aim of developing an all human, fully characterised and physiologically relevant *in vitro* BBB model was achieved. The model established here is a novel breakthrough in the field of BBB modelling, which was found to be useful for screening novel NP and glioma targeting aptamers. Further research in this area would broaden interests and implications in the field of neuropharmacology.

## 9. References

- Abbott, N., Dolman, D., Drndarski, S. & Fredriksson, S. (2012). An improved in vitro blood-brain barrier model: rat brain endothelial cells co-cultured with astrocytes. *Methods Mol Biol*, 814, 415 - 430.
- Abbott, N., Hughes, C., Revest, P. & Greenwood, J. (1992). Development and characterisation of a rat brain capillary endothelial culture: towards an in vitro blood-brain barrier. *J Cell Sci*, 103, 23 - 37.
- Abbott, N., Ronnback, L. & Hansson, E. (2006a). Astrocyte-endothelial interactions at the blood-brain barrier. *Nature reviews*, 7, 41 - 53.
- Abbott, N., Ronnback, L. & Hansson, E. (2006b). Astrocyte-endothelial interactions at the blood-brain barrier. *Nat Rev Neurosci*, 7, 41 - 53.
- Abbott, N. J. (2002). Astrocyte-endothelial interactions and blood-brain barrier permeability\*. *Journal of Anatomy*, 200, 629-638.
- Abrey, L. E. & Mason, W. P. (2003). *Fast Facts: Brain Tumours*, Oxford, Health Press Limited.
- Agarwal, S., Hartz, A. M., Elmquist, W. F. & Bauer, B. (2011). Breast cancer resistance protein and p-glycoprotein in brain cancer: two gatekeepers team up. *Curr Pharm Des*, 17, 2793-802.
- Agarwal, V., Kommaddi, R. P., Valli, K., Ryder, D., Hyde, T. M., Kleinman, J. E., Strobel, H. W. & Ravindranath, V. (2008). Drug Metabolism in Human Brain: High Levels of Cytochrome P4503A43 in Brain and Metabolism of Anti-Anxiety Drug Alprazolam to Its Active Metabolite. *PLoS ONE*, 3, e2337.
- Al Ahmad, A., Taboada, C. B., Gassmann, M. & Ogunshola, O. O. (2011). Astrocytes and pericytes differentially modulate blood-brain barrier characteristics during development and hypoxic insult. *J Cereb Blood Flow Metab*, 31, 693-705.
- Alge, C. S., Hauck, S. M., Priglinger, S. G., Kampik, A. & Ueffing, M. (2006). Differential Protein Profiling of Primary versus Immortalized Human RPE Cells Identifies Expression Patterns Associated with Cytoskeletal Remodeling and Cell Survival. *Journal of Proteome Research*, 5, 862-878.
- Allt, G. & Lawrenson, J. G. (2000). The blood-nerve barrier: enzymes, transporters and receptors—a comparison with the blood-brain barrier. *Brain Research Bulletin*, 52, 1-12.
- Apps, R., Murphy, S. P., Fernando, R., Gardner, L., Ahad, T. & Moffett, A. (2009). Human leucocyte antigen (HLA) expression of primary trophoblast cells and placental cell lines, determined using single antigen beads to characterize allotype specificities of anti-HLA antibodies. *Immunology*, 127, 26-39.
- Ballabh, P., Braun, A. & Nedergaard, M. (2004). The blood-brain barrier: an overview: structure, regulation, and clinical implications. *Neurobiol Dis*, 16, 1-13.
- Bandopadhyay, R., Orte, C., Lawrenson, J. G., Reid, A. R., De Silva, S. & Allt, G. (2001). Contractile proteins in pericytes at the blood-brain and blood-retinal barriers. *J Neurocytol*, 30, 35-44.

- Banks, W. A. (1999). Physiology and pathology of the blood-brain barrier: implications for microbial pathogenesis, drug delivery and neurodegenerative disorders. *J Neurovirol*, 5, 538-55.
- Bauer, B., Hartz, A. M. S., Fricker, G. & Miller, D. S. (2004). Pregnane X receptor up-regulation of P-glycoprotein expression and transport function at the blood-brain barrier. *Molecular Pharmacology*, 66, 413-419.
- Baxter, M., Withey, S., Harrison, S., Segeritz, C., Zhang, F., Atkinson-Dell, R., Rowe, C., Gerrard, D. T., Sison-Young, R., Jenkins, R., Henry, J., Berry, A. A., Mohamet, L., Best, M., Fenwick, S. W., Malik, H., Kitteringham, N. R., Goldring, C. E., Piper Hanley, K., Vallier, L. & Hanley, N. A. (2014). Phenotypic and functional analyses show stem cell-derived hepatocyte-like cells better mimic fetal rather than adult hepatocytes. *J Hepatol*.
- Bazzoni, G. (2006). Endothelial tight junctions: permeable barriers of the vessel wall. *Thromb Haemost*, 95, 36-42.
- Begley, D. J. (2004). ABC transporters and the blood-brain barrier. *Curr Pharm Des*, 10, 1295-1312.
- Behonick, D. J. & Werb, Z. (2003). A bit of give and take: the relationship between the extracellular matrix and the developing chondrocyte. *Mech Dev*, 120, 1327-36.
- Bellavance, M. A., Blanchette, M. & Fortin, D. (2008). Recent advances in blood-brain barrier disruption as a CNS delivery strategy. *AAPS J*, 10, 166-77.
- Bendayan, R., Lee, G. & Bendayan, M. (2002). Functional expression and localization of P-glycoprotein at the blood brain barrier. *Microscopy Research and Technique*, 57, 365-380.
- Benedetti, M. S., Whomsley, R., Poggesi, I., Cawello, W., Mathy, F.-X., Delporte, M.-L., Papeleu, P. & Watelet, J.-B. (2009). Drug metabolism and pharmacokinetics. *Drug Metabolism Reviews*, 41, 344-390.
- Benson, K., Cramer, S. & Galla, H. J. (2013). Impedance-based cell monitoring: barrier properties and beyond. *Fluids Barriers CNS*, 10, 5.
- Berezowski, V., Landry, C., Dehouck, M. P., Cecchelli, R. & Fenart, L. (2004a). Contribution of glial cells and pericytes to the mRNA profiles of P-glycoprotein and multidrug resistance-associated proteins in an in vitro model of the blood-brain barrier. *Brain Res*, 1018, 1-9.
- Berezowski, V., Landry, C., Lundquist, S., Dehouck, L., Cecchelli, R., Dehouck, M. & Fenart, L. (2004b). Transport screening of drug cocktails through an in vitro blood-brain barrier: is it a good strategy for increasing the throughput of the discovery pipeline? *Pharm Res*, 21, 756 - 760.
- Bhatia, P., Bernier, M., Sanghvi, M., Moaddel, R., Schwarting, R., Ramamoorthy, A. & Wainer, I. W. (2012). Breast cancer resistance protein (BCRP/ABCG2) localises to the nucleus in glioblastoma multiforme cells. *Xenobiotica*, 42, 748-55.
- Bicker, J., Alves, G., Fortuna, A. & Falcao, A. (2014). Blood-brain barrier models and their relevance for a successful development of CNS drug delivery systems: a review. *Eur J Pharm Biopharm*, 87, 409-32.

- Bing, C., Ladouceur-Wodzak, M., Wanner, C. R., Shelton, J. M., Richardson, J. A. & Chopra, R. (2014). Trans-cranial opening of the blood-brain barrier in targeted regions using a stereotaxic brain atlas and focused ultrasound energy. *J Ther Ultrasound*, 2, 13.
- Bodó, A., Bakos, E., Szeri, F., Váradi, A. & Sarkadi, B. (2003). The role of multidrug transporters in drug availability, metabolism and toxicity. *Toxicol Lett*, 140-141, 133-143.
- Booth, R. & Kim, H. (2012). Characterization of a microfluidic in vitro model of the blood-brain barrier (muBBB). *Lab Chip*, 12, 1784-92.
- Borges-Walmsley, M. I., Mckeegan, K. S. & Walmsley, A. R. (2003). Structure and function of efflux pumps that confer resistance to drugs. *Biochemical Journal*, 376, 313-338.
- Bouffet, E., Doumi, N., Thiesse, P., Mottolese, C., Jouvett, A., Lacroze, M., Carrie, C., Frappaz, D. & Brunat-Mentigny, M. (1997). Brain metastases in children with solid tumors. *Cancer*, 79, 403-410.
- Bradford, M. M. (1976). A rapid and sensitive method for the quantitation of microgram quantities of protein utilizing the principle of protein-dye binding. *Analytical Biochemistry*, 72, 248-254.
- Braun, A., Hämmerle, S., Suda, K., Rothen-Rutishauser, B., Günthert, M., Krämer, S. D. & Wunderli-Allenspach, H. (2000). Cell cultures as tools in biopharmacy. *European Journal of Pharmaceutical Sciences*, 11, S51-S60.
- Brimelow, A. H. C. 2011. *Cancer survival: Macmillan hails major improvement* [Online]. BBC News. Available: <http://www.bbc.co.uk/news/health-15726810> [Accessed 06/01/2012 2012].
- Britto, M. R. & Wedlund, P. J. (1992). Cytochrome P-450 in the brain. Potential evolutionary and therapeutic relevance of localization of drug-metabolizing enzymes. *Drug Metab Dispos*, 20, 446-50.
- Brown, M. T., Friedman, H. S., Oakes, W., Boyko, O. B., Hockenberger, B. & Schold, S. C. (1993). Chemotherapy for pilocytic astrocytoma. *Cancer*, 71, 3165 - 3172.
- Burgio, D. E., Gosland, M. P. & Mcnamara A, P. J. (1998). Effects of P-glycoprotein modulators on etoposide elimination and central nervous system distribution. *J Pharmacol Exp Ther*, 287, 911-7.
- Burkhard, C., Di Patre, P. L., Schuler, D., Schuler, G., Yasargil, M. G., Yonekawa, Y., Lutolf, U. M., Kleihues, P. & Ohgaki, H. (2003). A population-based study of the incidence and survival rates in patients with pilocytic astrocytoma. *J Neurosurg*, 98, 1170-4.
- Burns, E. M., Dobben, G. D., Kruckeberg, T. W. & Gaetano, P. K. (1981). Blood-brain barrier: morphology, physiology, and effects of contrast media. *Advances in neurology*, 30, 159-65.
- Calatuzzolo, C., Gelati, M., Ciusani, E., Sciacca, F. L., Pollo, B., Cajola, L., Marras, C., Silvani, A., Vitellaro-Zuccarello, L., Croci, D., Boiardi, A. & Salmaggi, A. (2005). Expression of Drug Resistance Proteins Pgp, MRP1, MRP3, MRP5 AND GST- $\pi$  in Human Glioma. *Journal of Neuro-Oncology*, 74, 113-121.
- Capes-Davis, A., Theodosopoulos, G., Atkin, I., Drexler, H. G., Kohara, A., Macleod, R. A., Masters, J. R., Nakamura, Y., Reid, Y. A., Reddel, R. R. & Freshney, R. I. (2010).

- Check your cultures! A list of cross-contaminated or misidentified cell lines. *Int J Cancer*, 127, 1-8.
- Carman, A. J., Mills, J. H., Krenz, A., Kim, D.-G. & Bynoe, M. S. (2011). Adenosine Receptor Signaling Modulates Permeability of the Blood–Brain Barrier. *The Journal of Neuroscience*, 31, 13272-13280.
- Cecchelli, R., Aday, S., Sevin, E., Almeida, C., Culot, M., Dehouck, L., Coisne, C., Engelhardt, B., Dehouck, M. P. & Ferreira, L. (2014). A stable and reproducible human blood-brain barrier model derived from hematopoietic stem cells. *PLoS One*, 9, e99733.
- Cecchelli, R., Dehouck, B., Descamps, L., Fenart, L., Buée-Scherrer, V., Duhem, C., Lundquist, S., Rentfel, M., Torpier, G. & Dehouck, M. P. (1999). In vitro model for evaluating drug transport across the blood-brain barrier. *Adv Drug Deliv Rev*, 36, 165-178.
- Chaffer, C. L. & Weinberg, R. A. (2011). A perspective on cancer cell metastasis. *Science*, 331, 1559-64.
- Chang, C. W., Ye, L., Defoe, D. M. & Caldwell, R. B. (1997). Serum inhibits tight junction formation in cultured pigment epithelial cells. *Invest Ophthalmol Vis Sci*, 38, 1082-93.
- Chang, G. (2003). Multidrug resistance ABC transporters. *FEBS Letters*, 555, 102-105.
- Chatterjee, M., Gupta, S., Bhar, A. & Das, S. (2012). Optimization of an Efficient Protein Extraction Protocol Compatible with Two-Dimensional Electrophoresis and Mass Spectrometry from Recalcitrant Phenolic Rich Roots of Chickpea (*Cicer arietinum* L.). *International Journal of Proteomics*, 2012, 10.
- Chu, X., Korzekwa, K., Elsbey, R., Fenner, K., Galetin, A., Lai, Y., Matsson, P., Moss, A., Nagar, S., Rosania, G. R., Bai, J. P., Polli, J. W., Sugiyama, Y., Brouwer, K. L. & International Transporter, C. (2013). Intracellular drug concentrations and transporters: measurement, modeling, and implications for the liver. *Clin Pharmacol Ther*, 94, 126-41.
- Cisternino, S., Mercier, C., Bourasset, F., Roux, F. & Scherrmann, J. M. (2004). Expression, up-regulation, and transport activity of the multidrug-resistance protein *Abcg2* at the mouse blood-brain barrier. *Cancer Res*, 64, 3296-301.
- Coecke, S., Blaauboer, B. J., Elaut, G., Freeman, S., Freidig, A., Gensmantel, N., Hoet, P., Kapoulas, V. M., Ladstetter, B., Langley, G., Leahy, D., Mannens, G., Meneguz, A., Monshouwer, M., Nemery, B., Pelkonen, O., Pfaller, W., Prieto, P., Proctor, N., Rogiers, V., Rostami-Hodjegan, A., Sabbioni, E., Steiling, W. & Van De Sandt, J. J. (2005). Toxicokinetics and metabolism. *Altern Lab Anim*, 33 Suppl 1, 147-75.
- Cohen-Kashi Malina, K., Cooper, I. & Teichberg, V. (2009). Closing the gap between the in-vivo and in-vitro blood-brain barrier tightness. *Brain Res*, 1284, 12 - 21.
- Cooray, H. C., Blackmore, C. G., Maskell, L. & Barrand, M. A. (2002). Localisation of breast cancer resistance protein in microvessel endothelium of human brain. *NeuroReport*, 13, 2059-2063.

- Cordon-Cardo, C., O'Brien, J. P., Casals, D., Rittman-Grauer, L., Biedler, J. L., Melamed, M. R. & Bertino, J. R. (1989). Multidrug-resistance gene (P-glycoprotein) is expressed by endothelial cells at blood-brain barrier sites. *Proc Natl Acad Sci U S A*, 86, 695-698.
- Cornford, E. & Hyman, S. (2005). Localization of brain endothelial luminal and abluminal transporters with immunogold electron microscopy. *NeuroRx*, 2, 27 - 43.
- Crocetti, E., Trama, A., Stiller, C., Caldarella, A., Soffiotti, R., Jaal, J., Weber, D. C., Ricardi, U., Slowinski, J. & Brandes, A. (2012). Epidemiology of glial and non-glial brain tumours in Europe. *European Journal of Cancer*.
- Crofton, K. M., Makris, S. L., Sette, W. F., Mendez, E. & Raffaele, K. C. (2004). A qualitative retrospective analysis of positive control data in developmental neurotoxicity studies. *Neurotoxicol Teratol*, 26, 345-52.
- Crone, C. & Olesen, S. P. (1982). Electrical resistance of brain microvascular endothelium. *Brain Res*, 241, 49-55.
- Cucullo, L., Couraud, P.-O., Weksler, B., Romero, I.-A., Hossain, M., Rapp, E. & Janigro, D. (2007). Immortalized human brain endothelial cells and flow-based vascular modeling: a marriage of convenience for rational neurovascular studies. *J Cereb Blood Flow Metab*, 28, 312-328.
- Cucullo, L., Couraud, P., Weksler, B., Romero, I., Hossain, M., Rapp, E. & Janigro, D. (2008). Immortalized human brain endothelial cells and flow-based vascular modeling: a marriage of convenience for rational neurovascular studies. *J Cereb Blood Flow Metab*, 28, 312 - 328.
- Cucullo, L., Mcallister, M. S., Kight, K., Krizanac-Bengez, L., Marroni, M., Mayberg, M. R., Stanness, K. A. & Janigro, D. (2002). A new dynamic in vitro model for the multidimensional study of astrocyte-endothelial cell interactions at the blood-brain barrier. *Brain Res*, 951, 243-54.
- Daniel, W. N. & Timothy, P. D. (2006). The role of cytochrome P450 enzymes in endogenous signalling pathways and environmental carcinogenesis. *Nature Reviews Cancer*, 6, 947-960.
- Davies, P. (1989). *How Do Vascular Endothelial Cells Respond to Flow?*
- De Boer, A. G. & Gaillard, P. J. (2007). Strategies to Improve Drug Delivery Across the Blood-Brain Barrier. *Clinical Pharmacokinetics*, 46, 553-576.
- De Lange, E. C. M. (2004). Potential role of ABC transporters as a detoxification system at the blood-CSF barrier. *Adv Drug Deliv Rev*, 56, 1793-1809.
- Dean, M., Rzhetsky, A. & Allikmets, R. (2001). The human ATP-binding cassette (ABC) transporter superfamily. *Genome Research*, 11, 1156-1166.
- Deenen, M. J., Cats, A., Beijnen, J. H. & Schellens, J. H. (2011a). Part 1: background, methodology, and clinical adoption of pharmacogenetics. *Oncologist*, 16, 811-9.
- Deenen, M. J., Cats, A., Beijnen, J. H. & Schellens, J. H. (2011b). Part 2: pharmacogenetic variability in drug transport and phase I anticancer drug metabolism. *Oncologist*, 16, 820-34.

- Dehouck, M.-P., Jolliet-Riant, P., Brée, F., Fruchart, J.-C., Cecchelli, R. & Tillement, J.-P. (1992). Drug Transfer Across the Blood-Brain Barrier: Correlation Between In Vitro and In Vivo Models. *Journal of Neurochemistry*, 58, 1790-1797.
- Deli, M., Ábrahám, C., Kataoka, Y. & Niwa, M. (2005). Permeability Studies on In Vitro Blood–Brain Barrier Models: Physiology, Pathology, and Pharmacology. *Cellular and Molecular Neurobiology*, 25, 59-127.
- Demeule, M., Régina, A., Jodoin, J., Laplante, A., Dagenais, C., Berthelet, F., Moghrabi, A. & Béliveau, R. (2002). Drug transport to the brain: Key roles for the efflux pump P-glycoprotein in the blood-brain barrier. *Vascul Pharmacol*, 38, 339-348.
- Di, L., Kerns, E. H., Fan, K., McConnell, O. J. & Carter, G. T. (2003). High throughput artificial membrane permeability assay for blood-brain barrier. *Eur J Med Chem*, 38, 223-32.
- Donato, M. T., Jiménez, N., Castell, J. V. & Gómez-Lechón, M. J. (2004). Fluorescence-based assays for screening nine cytochrome P450 (CYP450) activities in intact cells expressing individual human P450 enzymes. *Drug Metabolism and Disposition*, 32, 699-706.
- Doyle, L. & Ross, D. D. (2003). Multidrug resistance mediated by the breast cancer resistance protein BCRP (ABCG2). *Oncogene*, 22, 7340-58.
- Duffner, P. K., Cohen, M. E. & Freeman, A. I. (1985). Pediatric brain tumors: An overview. *CA: A Cancer Journal for Clinicians*, 35, 287-301.
- Duport, S., Robert, F., Muller, D., Grau, G., Parisi, L. & Stoppini, L. (1998). An in vitro blood–brain barrier model: Cocultures between endothelial cells and organotypic brain slice cultures. *Proceedings of the National Academy of Sciences*, 95, 1840-1845.
- Dutheil, F., Beaune, P. & Lorient, M.-A. (2008). Xenobiotic metabolizing enzymes in the central nervous system: Contribution of cytochrome P450 enzymes in normal and pathological human brain. *Biochimie*, 90, 426-436.
- Eggstein, G. R., Liebner, S. & Wolburg, H. 2004. 27 - The Blood-Brain Barrier in the Human Glioma. In: Hari Shanker, S. & Jan, W. (eds.) *Blood-Spinal Cord and Brain Barriers in Health and Disease*. San Diego: Academic Press.
- Eigenmann, D. E., Xue, G., Kim, K. S., Moses, A. V., Hamburger, M. & Oufir, M. (2013). Comparative study of four immortalized human brain capillary endothelial cell lines, hCMEC/D3, hBMEC, TY10, and BB19, and optimization of culture conditions, for an in vitro blood-brain barrier model for drug permeability studies. *Fluids Barriers CNS*, 10, 33.
- Eisenblatter, T. & Galla, H. J. (2002). A new multidrug resistance protein at the blood-brain barrier. *Biochem Biophys Res Commun*, 293, 1273-8.
- Eisenblatter, T., Huwel, S. & Galla, H. J. (2003). Characterisation of the brain multidrug resistance protein (BMDP/ABCG2/BCRP) expressed at the blood-brain barrier. *Brain Res*, 971, 221-31.
- Ekins, S. & Erickson, J. A. (2002). A pharmacophore for human pregnane X receptor ligands. *Drug Metab Dispos*, 30, 96-9.

- Erben, M., Decker, S., Franke, H. & Galla, H.-J. (1995). Electrical resistance measurements on cerebral capillary endothelial cells — a new technique to study small surface areas. *Journal of Biochemical and Biophysical Methods*, 30, 227-238.
- Esquenet, M., Swinnen, J. V., Heyns, W. & Verhoeven, G. (1997). LNCaP prostatic adenocarcinoma cells derived from low and high passage numbers display divergent responses not only to androgens but also to retinoids. *The Journal of Steroid Biochemistry and Molecular Biology*, 62, 391-399.
- Eyupoglu, I. Y., Buchfelder, M. & Savaskan, N. E. (2013). Surgical resection of malignant gliomas—role in optimizing patient outcome. *Nat Rev Neurol*, 9, 141-151.
- Ferguson, C. S. & Tyndale, R. F. (2011). Cytochrome P450 enzymes in the brain: emerging evidence of biological significance. *Trends Pharmacol Sci*, 32, 708-14.
- Fidler, I. J. (2003). The pathogenesis of cancer metastasis: the 'seed and soil' hypothesis revisited. *Nat Rev Cancer*, 3, 453-8.
- Franke, H., Galla, H. J. & Beuckmann, C. T. (1999). An improved low-permeability in vitro-model of the blood-brain barrier: transport studies on retinoids, sucrose, haloperidol, caffeine and mannitol. *Brain Res*, 818, 65-71.
- Freshney, R. (2000). New York, N.Y.: Wiley-Liss.
- Fromm, M. F. (2004). Importance of P-glycoprotein at blood-tissue barriers. *Trends Pharmacol Sci*, 25, 423-9.
- Gabathuler, R. (2010). Approaches to transport therapeutic drugs across the blood-brain barrier to treat brain diseases. *Neurobiol Dis*, 37, 48-57.
- Gaillard, P. & De Boer, A. (2000). Relationship between permeability status of the blood-brain barrier and in vitro permeability coefficient of a drug. *Eur J Pharm Sci*, 12, 95 - 102.
- Gaillard, P., Voorwinden, L., Nielsen, J., Ivanov, A., Atsumi, R., Engman, H., Ringbom, C., De Boer, A. & Breimer, D. (2001). Establishment and functional characterization of an in vitro model of the blood-brain barrier, comprising a co-culture of brain capillary endothelial cells and astrocytes. *Eur J Pharm Sci*, 12, 215 - 222.
- Garberg, P., Ball, M., Borg, N., Cecchelli, R., Fenart, L., Hurst, R., Lindmark, T., Mabondzo, A., Nilsson, J. & Raub, T. (2005a). In vitro models for the blood-brain barrier. *Toxicol In Vitro*, 19, 299 - 334.
- Garberg, P., Ball, M., Borg, N., Cecchelli, R., Fenart, L., Hurst, R. D., Lindmark, T., Mabondzo, A., Nilsson, J. E., Raub, T. J., Stanimirovic, D., Terasaki, T., Öberg, J. O. & Österberg, T. (2005b). In vitro models for the blood-brain barrier. *Toxicology in Vitro*, 19, 299-334.
- Garcia-Garcia, E., Gil, S., Andrieux, K., Desmaele, D., Nicolas, V., Taran, F., Georgin, D., Andrieux, J., Roux, F. & Couvreur, P. (2005). A relevant in vitro rat model for the evaluation of blood-brain barrier translocation of nanoparticles. *Cell Mol Life Sci*, 62, 1400 - 1408.
- Garcia, J. G. & Schaphorst, K. L. (1995). Regulation of endothelial cell gap formation and paracellular permeability. *J Invest Med*, 43, 117-26.

- Gerk, P. M. & Vore, M. (2002). Regulation of Expression of the Multidrug Resistance-Associated Protein 2 (MRP2) and Its Role in Drug Disposition. *Journal of Pharmacology and Experimental Therapeutics*, 302, 407-415.
- Gherzi-Egea, J. F., Leninger-Muller, B., Suleman, G., Siest, G. & Minn, A. (1994). Localization of drug-metabolizing enzyme activities to blood-brain interfaces and circumventricular organs. *J Neurochem*, 62, 1089-96.
- Gil-Gil, M. J., Martinez-Garcia, M., Sierra, A., Conesa, G., Del Barco, S., González-Jimenez, S. & Villà, S. (2014). Breast cancer brain metastases: a review of the literature and a current multidisciplinary management guideline. *Clinical and Translational Oncology*, 16, 436-446.
- Godoy, P., Hewitt, N. J., Albrecht, U., Andersen, M. E., Ansari, N., Bhattacharya, S., Bode, J. G., Bolleyn, J., Borner, C., Bottger, J., Braeuning, A., Budinsky, R. A., Burkhardt, B., Cameron, N. R., Camussi, G., Cho, C. S., Choi, Y. J., Craig Rowlands, J., Dahmen, U., Damm, G., Dirsch, O., Donato, M. T., Dong, J., Dooley, S., Drasdo, D., Eakins, R., Ferreira, K. S., Fonsato, V., Fraczek, J., Gebhardt, R., Gibson, A., Glanemann, M., Goldring, C. E., Gomez-Lechon, M. J., Groothuis, G. M., Gustavsson, L., Guyot, C., Hallifax, D., Hammad, S., Hayward, A., Haussinger, D., Hellerbrand, C., Hewitt, P., Hoehme, S., Holzhutter, H. G., Houston, J. B., Hrach, J., Ito, K., Jaeschke, H., Keitel, V., Kelm, J. M., Kevin Park, B., Kordes, C., Kullak-Ublick, G. A., Lecluyse, E. L., Lu, P., Luebke-Wheeler, J., Lutz, A., Maltman, D. J., Matz-Soja, M., McMullen, P., Merfort, I., Messner, S., Meyer, C., Mwinyi, J., Naisbitt, D. J., Nussler, A. K., Olinga, P., Pampaloni, F., Pi, J., Pluta, L., Przyborski, S. A., Ramachandran, A., Rogiers, V., Rowe, C., Schelcher, C., Schmich, K., Schwarz, M., Singh, B., Stelzer, E. H., Stieger, B., Stober, R., Sugiyama, Y., Tetta, C., Thasler, W. E., Vanhaecke, T., Vinken, M., Weiss, T. S., Widera, A., Woods, C. G., Xu, J. J., Yarborough, K. M. & Hengstler, J. G. (2013). Recent advances in 2D and 3D in vitro systems using primary hepatocytes, alternative hepatocyte sources and non-parenchymal liver cells and their use in investigating mechanisms of hepatotoxicity, cell signaling and ADME. *Arch Toxicol*, 87, 1315-530.
- Goldstein, G. W. (1988). Endothelial Cell-Astrocyte Interactions. *Annals of the New York Academy of Sciences*, 529, 31-39.
- Golestaneh, N. & Mishra, B. (2005). TGF-[beta], Neuronal Stem Cells and Glioblastoma. *Oncogene*, 24, 5722-5730.
- Gomes, F. C. A., Paulin, D. & Moura Neto, V. (1999). Glial fibrillary acidic protein (GFAP): modulation by growth factors and its implication in astrocyte differentiation. *Brazilian Journal of Medical and Biological Research*, 32, 619-631.
- Gomes, J., Al Zayadi, A. & Guzman, A. (2011). Occupational and environmental risk factors of adult primary brain cancers: a systematic review. *Int J Occup Environ Med*, 2, 82-111.
- Gonzalez, F. J. & Gelboin, H. V. (1994). Role of human cytochromes P450 in the metabolic activation of chemical carcinogens and toxins. *Drug Metab Rev*, 26, 165-83.

- Graham, C. A. & Cloughesy, T. F. (2004). Brain tumor treatment: chemotherapy and other new developments. *Semin Oncol Nurs*, 20, 260-72.
- Griep, L. M., Wolbers, F., De Wagenaar, B., Ter Braak, P. M., Weksler, B. B., Romero, I. A., Couraud, P. O., Vermes, I., Van Der Meer, A. D. & Van Den Berg, A. (2013). BBB on chip: microfluidic platform to mechanically and biochemically modulate blood-brain barrier function. *Biomed Microdevices*, 15, 145-50.
- Grier, J. T. & Batchelor, T. (2006). Low-Grade Gliomas in Adults. *The Oncologist*, 11, 681-693.
- Grippo, M., Penteado, P., Carelli, E., Cruz-Hofling, M. & Verinaud, L. (2001). Establishment and Partial Characterization of a Continuous Human Malignant Glioma Cell Line: NG97. *Cell Mol Neurobiol*, 21, 421 - 428.
- Grover, A., Hirani, A., Pathak, Y. & Sutariya, V. (2014). Brain-Targeted Delivery of Docetaxel by Glutathione-Coated Nanoparticles for Brain Cancer. *AAPS PharmSciTech*.
- Grzmil, M. & Hemmings, B. A. (2010). Deregulated signalling networks in human brain tumours. *Biochimica et Biophysica Acta (BBA) - Proteins and Proteomics*, 1804, 476-483.
- Gu, F., Wang, J., Fu, L. & Ma, Y. J. (2011). Co-culture with microglia promotes neural stem cells differentiation into astrocytes. *Chin Med J (Engl)*, 124, 3394-8.
- Gunaratna, C. (2000). Drug metabolism and pharmacokinetics in drug discovery: A primer for bioanalytical chemists, Part I. *Current separations*, 19, 17- 23.
- Gupta, T. & Sarin, R. (2002). Poor-prognosis high-grade gliomas: evolving an evidence-based standard of care. *The Lancet Oncology*, 3, 557-564.
- Gynther, M. (2010). *Blood-Brain Barrier Transporters in CNS Drug Delivery : Design and Biological Evaluation of LAT1 and GluT1 –Targeted Prodrugs*. University of Eastern Finland.
- Haimeur, A., Conseil, G., Deeley, R. G. & Cole, S. P. C. (2004). The MRP-related and BCRP/ABCG2 multidrug resistance proteins: Biology, substrate specificity and regulation. *Curr Drug Metab*, 5, 21-53.
- Halfter, H., Kremerskothen, J., Webwe, J., Hacker-Klom, U., Barnekow, A., Ringlestein, E. & Stogbauer, F. (1998). Growth inhibition of newly established human glioma cell lines by leukemia inhibitory factor. *J Neuro-Oncol*, 39, 1 - 18.
- Haluska, M. & Anthony, M. L. (2004). Osmotic blood-brain barrier modification for the treatment of malignant brain tumors. *Clin J Oncol Nurs*, 8, 263-7.
- Hanada, S., Fujoka, K., Inoue, Y., Kanaya, F., Manome, Y. & Yamamoto, K. (2013). Application of in vitro BBB model to measure permeability of nanoparticles. *Journal of Physics: Conference Series*, 429, 012028.
- Hanahan, D. & Weinberg, R. A. (2000). The hallmarks of cancer. *Cell*, 100, 57-70.
- Hanahan, D. & Weinberg, Robert a. (2011). Hallmarks of Cancer: The Next Generation. *Cell*, 144, 646-674.

- Haorah, J., Ramirez, S. H., Schall, K., Smith, D., Pandya, R. & Persidsky, Y. (2007). Oxidative stress activates protein tyrosine kinase and matrix metalloproteinases leading to blood-brain barrier dysfunction. *J Neurochem*, 101, 566-76.
- Hartsock, A. & Nelson, W. J. (2008). Adherens and tight junctions: structure, function and connections to the actin cytoskeleton. *Biochim Biophys Acta*, 1778, 660-9.
- Hartz, A. M. & Bauer, B. (2010). Regulation of ABC transporters at the blood-brain barrier: new targets for CNS therapy. *Mol Interv*, 10, 293-304.
- Harvey, K., Siddiqui, R. A., Sliva, D., Garcia, J. G. & English, D. (2002). Serum factors involved in human microvascular endothelial cell morphogenesis. *J Lab Clin Med*, 140, 188-98.
- Haseloff, R. F., Blasig, I. E., Bauer, H. C. & Bauer, H. (2005). In search of the astrocytic factor(s) modulating blood-brain barrier functions in brain capillary endothelial cells in vitro. *Cell Mol Neurobiol*, 25, 25-39.
- Hass, R. & Bertram, C. (2009). Characterization of human breast cancer epithelial cells (HBCEC) derived from long term cultured biopsies. *Journal of Experimental & Clinical Cancer Research*, 28, 127.
- Hatherell, K., Couraud, P., Romero, I., Weksler, B. & Pilkington, G. (2011). Development of a three-dimensional, all-human in vitro model of the blood-brain barrier using mono-, co- and tri-Transwell cultivation methods. *J Neurosci Meth*, 199, 223 - 229.
- Hayashi, K., Nakao, S., Nakaoke, R., Nakagawa, S., Kitagawa, N. & Niwa, M. (2004). Effects of hypoxia on endothelial/pericytic co-culture model of the blood-brain barrier. *Regulatory Peptides*, 123, 77-83.
- He, J., Du, Y., Guo, Y., Hancock, M. J., Wang, B., Shin, H., Wu, J., Li, D. & Khademhosseini, A. (2011). Microfluidic synthesis of composite cross-gradient materials for investigating cell-biomaterial interactions. *Biotechnol Bioeng*, 108, 175-85.
- Healey, J. (2010). Editorial: The Imperative to Authenticate Cell Lines. *Clinical Orthopaedics and Related Research®*, 468, 3413-3414.
- Hedlund, E., Gustafsson, J. A. & Warner, M. (2001). Cytochrome P450 in the brain; a review. *Curr Drug Metab*, 2, 245-63.
- Higgins, S. C., Steingrimsdottir, H. & Pilkington, G. J. (2010). Human, mouse or rat? Species authentication of glioma-derived cell cultures. *J Neurosci Methods*, 194, 139-43.
- Hitchcock, S. A. (2008). Blood-brain barrier permeability considerations for CNS-targeted compound library design. *Curr Opin Chem Biol*, 12, 318-23.
- Hoffmann, A., Bredno, J., Wendland, M., Derugin, N., Ohara, P. & Wintermark, M. (2011). High and Low Molecular Weight Fluorescein Isothiocyanate (FITC)-Dextrans to Assess Blood-Brain Barrier Disruption: Technical Considerations. *Transl Stroke Res*, 2, 106-11.
- Huang, H.-L., Hsing, H.-W., Lai, T.-C., Chen, Y.-W., Lee, T.-R., Chan, H.-T., Lyu, P.-C., Wu, C.-L., Lu, Y.-C., Lin, S.-T., Lin, C.-W., Lai, C.-H., Chang, H.-T., Chou, H.-C. & Chan, H.-L. (2010). Trypsin-induced proteome alteration during cell subculture in mammalian cells. *Journal of Biomedical Science*, 17, 36.

- Hughes, P., Marshall, D., Reid, Y., Parkes, H. & Gelber, C. (2007). The costs of using unauthenticated, over-passaged cell lines: how much more data do we need? *Biotechniques*, 43, 575, 577-8, 581-2 passim.
- Huse, J. T. & Holland, E. C. (2010). Targeting brain cancer: advances in the molecular pathology of malignant glioma and medulloblastoma. *Nat Rev Cancer*, 10, 319-331.
- Ignatova, T. N., Kukekov, V. G., Laywell, E. D., Suslov, O. N., Vrionis, F. D. & Steindler, D. A. (2002). Human cortical glial tumors contain neural stem-like cells expressing astroglial and neuronal markers in vitro. *Glia*, 39, 193-206.
- Inda, M. M., Bonavia, R. & Seoane, J. (2014). Glioblastoma multiforme: a look inside its heterogeneous nature. *Cancers (Basel)*, 6, 226-39.
- Ingelman-Sundberg, M. (2004). Pharmacogenetics of cytochrome P450 and its applications in drug therapy: the past, present and future. *Trends Pharmacol Sci*, 25, 193-200.
- Inoue, A., Takahashi, H., Harada, H., Kohno, S., Ohue, S., Kobayashi, K., Yano, H., Tanaka, J. & Ohnishi, T. (2010). Cancer stem-like cells of glioblastoma characteristically express MMP-13 and display highly invasive activity. *Int J Oncol*, 37, 1121-31.
- Ishihara, H., Kubota, H., Lindberg, R. L., Leppert, D., Gloor, S. M., Errede, M., Virgintino, D., Fontana, A., Yonekawa, Y. & Frei, K. (2008). Endothelial cell barrier impairment induced by glioblastomas and transforming growth factor beta2 involves matrix metalloproteinases and tight junction proteins. *J Neuropathol Exp Neurol*, 67, 435-48.
- Ishikawa, T., Onishi, Y., Hirano, H., Oosumi, K., Nagakura, M. & Tarui, S. (2004). Pharmacogenomics of drug transporters: A new approach to functional analysis of the genetic polymorphisms of ABCB1 (P-glycoprotein/MDR1). *Biological and Pharmaceutical Bulletin*, 27, 939-948.
- Jemal, A., Siegel, R., Xu, J. & Ward, E. (2010). Cancer statistics, 2010. *CA Cancer J Clin*, 60, 277-300.
- Jensen, R. & Chkheidze, R. 2011. The Role of Glucose Transporter-1 (GLUT-1) in Malignant Gliomas. In: Hayat, M. A. (ed.) *Tumors of the Central Nervous System, Volume 1*. Springer Netherlands.
- Joseph, J. V., Balasubramanian, V., Walenkamp, A. & Kruyt, F. A. (2013). TGF-beta as a therapeutic target in high grade gliomas - promises and challenges. *Biochem Pharmacol*, 85, 478-85.
- Jung, C. S., Foerch, C., Schänzer, A., Heck, A., Plate, K. H., Seifert, V., Steinmetz, H., Raabe, A. & Sitzer, M. (2007a). *Serum GFAP is a diagnostic marker for glioblastoma multiforme*.
- Jung, S., Moon, K.-S., Kim, S.-T., Ryu, H.-H., Lee, Y.-H., Jeong, Y.-I., Jung, T.-Y., Kim, I.-Y., Kim, K.-K. & Kang, S.-S. (2007b). Increased expression of intracystic matrix metalloproteinases in brain tumors: relationship to the pathogenesis of brain tumor-associated cysts and peritumoral edema. *Journal of Clinical Neuroscience*, 14, 1192-1198.
- Kago, T., Takagi, N., Date, I., Takenaga, Y., Takagi, K. & Takeo, S. (2006). Cerebral ischemia enhances tyrosine phosphorylation of occludin in brain capillaries. *Biochem Biophys Res Commun*, 339, 1197-203.

- Kakkar, V., Mishra, A. K., Chuttani, K. & Kaur, I. P. (2013). Proof of concept studies to confirm the delivery of curcumin loaded solid lipid nanoparticles (C-SLNs) to brain. *Int J Pharm*, 448, 354-9.
- Kaplan, J. & Hukku, B. (1998). Cell line characterization and authentication. *Methods Cell Biol*, 57, 203-16.
- Kapoor, N., Pant, A., Dhawan, A., Dwivedi, U., Seth, P. & Parmar, D. (2007). Differences in the expression and inducibility of cytochrome P450 2B isoenzymes in cultured rat brain neuronal and glial cells. *Molecular and Cellular Biochemistry*, 305, 199-207.
- Karnezis, T., Shayan, R., Caesar, C., Roufail, S., Harris, Nicole c., Ardipradja, K., Zhang, You f., Williams, Steven p., Farnsworth, Rae h., Chai, Ming g., Rupasinghe, Thusitha w. T., Tull, Dedreia l., Baldwin, Megan e., Sloan, Erica k., Fox, Stephen b., Achen, Marc g. & Stacker, Steven a. (2012). VEGF-D Promotes Tumor Metastasis by Regulating Prostaglandins Produced by the Collecting Lymphatic Endothelium. *Cancer cell*, 21, 181-195.
- Kavanagh, E., Tsapara, A., Matter, K. & Balda, M. 2006. Tight Junctions and the Regulation of Epithelial Cell Proliferation and Gene Expression. *Tight Junctions*. Springer US.
- Kemper, E. M., Van Zandbergen, A. E., Cleypool, C., Mos, H. A., Boogerd, W., Beijnen, J. H. & Van Tellingen, O. (2003). Increased penetration of paclitaxel into the brain by inhibition of P-Glycoprotein. *Clin Cancer Res*, 9, 2849-55.
- Kido, Y., Tamai, I., Nakanishi, T., Kagami, T., Hirosawa, I., Sai, Y. & Tsuji, A. (2002). Evaluation of blood-brain barrier transporters by co-culture of brain capillary endothelial cells with astrocytes. *Drug Metab Pharmacokinet*, 17, 34-41.
- Kim, L. & Glantz, M. (2006). Chemotherapeutic options for primary brain tumors. *Current Treatment Options in Oncology*, 7, 467-478.
- Kimelberg, H. K. & Nedergaard, M. (2010). Functions of astrocytes and their potential as therapeutic targets. *Neurotherapeutics*, 7, 338-53.
- Kleihues, P. & Ohgaki, H. (1999). Primary and secondary glioblastomas: from concept to clinical diagnosis. *Neuro Oncol*, 1, 44-51.
- Krizanac-Bengez, L., Kapural, M., Parkinson, F., Cucullo, L., Hossain, M., Mayberg, M. R. & Janigro, D. (2003). Effects of transient loss of shear stress on blood-brain barrier endothelium: role of nitric oxide and IL-6. *Brain Res*, 977, 239-46.
- Kroll, R. A. & Neuwelt, E. A. (1998). Outwitting the blood-brain barrier for therapeutic purposes: osmotic opening and other means. *Neurosurgery*, 42, 1083-99; discussion 1099-100.
- Kumar, N., Gammell, P., Meleady, P., Henry, M. & Clynes, M. (2008). Differential protein expression following low temperature culture of suspension CHO-K1 cells. *BMC Biotechnology*, 8, 42.
- Kumar, S., Shaw, L., Lawrence, C., Lea, R. & Alder, J. (2014). P50DEVELOPING A PHYSIOLOGICALLY RELEVANT BLOOD BRAIN BARRIER MODEL FOR THE STUDY OF DRUG DISPOSITION IN GLIOMA. *Neuro-Oncology*, 16, vi8.
- Kuteykin-Teplyakov, K., Luna-Tortos, C., Ambroziak, K. & Loscher, W. (2010). Differences in the expression of endogenous efflux transporters in MDR1-transfected

- versus wildtype cell lines affect P-glycoprotein mediated drug transport. *Br J Pharmacol*, 160, 1453-63.
- Lacombe, O., Videau, O., Chevillon, D., Guyot, A., Contreras, C., Blondel, S., Nicolas, L., Ghetas, A., Benech, H. & Thevenot, E. (2011). In vitro primary human and animal cell-based blood-brain barrier models as a screening tool in drug discovery. *Mol Pharm*, 8, 651 - 663.
- Lai, C. H. & Kuo, K. H. (2005). The critical component to establish in vitro BBB model: Pericyte. *Brain Res Brain Res Rev*, 50, 258-65.
- Langner, C., Ratschek, M., Rehak, P., Schips, L. & Zigeuner, R. (2003). Expression of MUC1 (EMA) and E-cadherin in renal cell carcinoma: a systematic immunohistochemical analysis of 188 cases. *Mod Pathol*, 17, 180-188.
- Lee, G., Babakhanian, K., Ramaswamy, M., Prat, A., Wosik, K. & Bendayan, R. (2007). Expression of the ATP-binding cassette membrane transporter, ABCG2, in human and rodent brain microvessel endothelial and glial cell culture systems. *Pharm Res*, 24, 1262-74.
- Lee, J., Lilly, G. D., Doty, R. C., Podsiadlo, P. & Kotov, N. A. (2009). In vitro toxicity testing of nanoparticles in 3D cell culture. *Small*, 5, 1213-21.
- Lee, Y. J., Kusuhara, H., Jonker, J. W., Schinkel, A. H. & Sugiyama, Y. (2005). Investigation of efflux transport of dehydroepiandrosterone sulfate and mitoxantrone at the mouse blood-brain barrier: a minor role of breast cancer resistance protein. *J Pharmacol Exp Ther*, 312, 44-52.
- Li, G., Simon, M. J., Cancel, L. M., Shi, Z. D., Ji, X., Tarbell, J. M., Morrison, B., 3rd & Fu, B. M. (2010). Permeability of endothelial and astrocyte cocultures: in vitro blood-brain barrier models for drug delivery studies. *Ann Biomed Eng*, 38, 2499-511.
- Liebner, S., Corada, M., Bangsow, T., Babbage, J., Taddei, A., Czupalla, C., Reis, M., Felici, A., Wolburg, H., Fruttiger, M., Taketo, M., Von Melchner, H., Plate, K., Gerhardt, H. & Dejana, E. (2008). Wnt/beta-catenin signaling controls development of the blood-brain barrier. *J Cell Biol*, 183, 409 - 417.
- Liebner, S., Fischmann, A., Rascher, G., Duffner, F., Grote, E. H., Kalbacher, H. & Wolburg, H. (2000). Claudin-1 and claudin-5 expression and tight junction morphology are altered in blood vessels of human glioblastoma multiforme. *Acta Neuropathol*, 100, 323-31.
- Lin, J. H. & Lu, A. Y. H. (1997). Role of Pharmacokinetics and Metabolism in Drug Discovery and Development. *Pharmacological Reviews*, 49, 403-449.
- Lockhart, A. C., Tirona, R. G. & Kim, R. B. (2003). Pharmacogenetics of ATP-binding cassette transporters in cancer and chemotherapy. *Molecular cancer therapeutics*, 2, 685-698.
- Lohmann, C., Krischke, M., Wegener, J. & Galla, H. J. (2004). Tyrosine phosphatase inhibition induces loss of blood-brain barrier integrity by matrix metalloproteinase-dependent and -independent pathways. *Brain Res*, 995, 184-96.
- Loscher, W. & Potschka, H. (2005a). Blood-brain barrier active efflux transporters: ATP-binding cassette gene family. *NeuroRx*, 2, 86-98.

- Loscher, W. & Potschka, H. (2005b). Drug resistance in brain diseases and the role of drug efflux transporters. *Nat Rev Neurosci*, 6, 591-602.
- Loscher, W. & Potschka, H. (2005c). Role of drug efflux transporters in the brain for drug disposition and treatment of brain diseases. *Prog Neurobiol*, 76, 22-76.
- Löscher, W. & Potschka, H. (2005). Role of drug efflux transporters in the brain for drug disposition and treatment of brain diseases. *Progress in Neurobiology*, 76, 22-76.
- Louis, D., Ohgaki, H., Wiestler, O., Cavenee, W., Burger, P., Jouvet, A., Scheithauer, B. & Kleihues, P. (2007). The 2007 WHO Classification of Tumours of the Central Nervous System. *Acta Neuropathologica*, 114, 97-109.
- Lu, W., Tan, Y. Z. & Jiang, X. G. (2006). Establishment of coculture model of blood-brain barrier in vitro for nanoparticle's transcytosis and toxicity evaluation. *Yao Xue Xue Bao*, 41, 296-304.
- Lucey, B. P., Nelson-Rees, W. A. & Hutchins, G. M. (2009). Henrietta Lacks, HeLa cells, and cell culture contamination. *Arch Pathol Lab Med*, 133, 1463-7.
- Luissint, A., Artus, C., Glacial, F., Ganeshamoorthy, K. & Couraud, P. (2012a). Tight junctions of the blood-brain barrier: physiological architecture and disease-associated dysregulation. *Fluids Barriers CNS*, 9, 23.
- Luissint, A., Federici, C., Guillonnet, F., Chretien, F., Camoin, L., Glacial, F., Ganeshamoorthy, K. & Couraud, P. (2012b). Guanine nucleotide-binding protein Galphai2: a new partner of claudin-5 that regulates tight junction integrity in human brain endothelial cells. *J Cereb Blood Flow Metab*, 32, 860 - 873.
- Lundquist, S. & Renftel, M. (2002). The use of in vitro cell culture models for mechanistic studies and as permeability screens for the blood-brain barrier in the pharmaceutical industry - Background and current status in the drug discovery process. *Vascul Pharmacol*, 38, 355-364.
- Ma, L., Kuang, K., Smith, R. W., Rittenband, D., Iserovich, P., Diecke, F. P. & Fischberg, J. (2007). Modulation of tight junction properties relevant to fluid transport across rabbit corneal endothelium. *Exp Eye Res*, 84, 790-8.
- Macleod, R. A., Dirks, W. G., Matsuo, Y., Kaufmann, M., Milch, H. & Drexler, H. G. (1999). Widespread intraspecies cross-contamination of human tumor cell lines arising at source. *Int J Cancer*, 83, 555-63.
- Malina, K. C. K., Cooper, I. & Teichberg, V. I. (2009). Closing the gap between the in-vivo and in-vitro blood-brain barrier tightness. *Brain Res*, 1284, 12-21.
- Mann, A., Miksys, S. L., Gaedigk, A., Kish, S. J., Mash, D. C. & Tyndale, R. F. (2012). The neuroprotective enzyme CYP2D6 increases in the brain with age and is lower in Parkinson's disease patients. *Neurobiol Aging*, 33, 2160-71.
- Marini, G., Luchese, M., Argondizzo, A. P., De Goes, A. C. M. A., Galler, R., Alves, T. L., Medeiros, M. & Larentis, A. (2014). Experimental design approach in recombinant protein expression: determining medium composition and induction conditions for expression of pneumolysin from *Streptococcus pneumoniae* in *Escherichia coli* and preliminary purification process. *BMC Biotechnology*, 14, 1.
- Masserini, M. (2013). Nanoparticles for Brain Drug Delivery. *ISRN Biochemistry*, 2013, 18.

- Masters, J. R. W. (2000). Human cancer cell lines: fact and fantasy. *Nat Rev Mol Cell Biol*, 1, 233-236.
- Mather, J. P. & Roberts, P. E. 1998. Standard Cell Culture Techniques. *Introduction to Cell and Tissue Culture*. Springer US.
- Mcfadyen, M. C. E., Melvin, W. T. & Murray, G. I. (2004). Cytochrome P450 enzymes: Novel options for cancer therapeutics. *Molecular Cancer Therapeutics*, 3, 363-371.
- Medical Research Council Brain Tumor Working, P. (2001). Randomized trial of procarbazine, lomustine, and vincristine in the adjuvant treatment of high-grade astrocytoma: a Medical Research Council trial. *J Clin Oncol*, 19, 509-18.
- Mertsch, K. & Maas, J. (2002). Blood-Brain Barrier Penetration and Drug Development from an Industrial Point of View. *Current Medicinal Chemistry -Central Nervous System Agents*, 2, 187-201.
- Meyer, R., Gehlhaus, M., Knoth, R. & Volk, B. (2007). Expression and function of cytochrome p450 in brain drug metabolism. *Curr Drug Metab*, 8, 297 - 306.
- Miao, Z., Dong, Y., Fang, W., Shang, D., Liu, D., Zhang, K., Li, B. & Chen, Y. H. (2014). VEGF increases paracellular permeability in brain endothelial cells via upregulation of EphA2. *Anat Rec (Hoboken)*, 297, 964-72.
- Miksys, S. & Tyndale, R. F. (2004). The Unique Regulation of Brain Cytochrome P450 2 (CYP2) Family Enzymes by Drugs and Genetics. *Drug Metabolism Reviews*, 36, 313-333.
- Miksys, S. & Tyndale, R. F. (2009). Brain drug-metabolizing cytochrome P450 enzymes are active in vivo, demonstrated by mechanism-based enzyme inhibition. *Neuropsychopharmacology*, 34, 634-40.
- Miller, D. S. (2010). Regulation of P-glycoprotein and other ABC drug transporters at the blood-brain barrier. *Trends Pharmacol Sci*, 31, 246-54.
- Miller, G. (2002). Drug targeting. Breaking down barriers. *Science*, 297, 1116-8.
- Modi, G., Pillay, V., Choonara, Y. E., Ndesendo, V. M., Du Toit, L. C. & Naidoo, D. (2009). Nanotechnological applications for the treatment of neurodegenerative disorders. *Prog Neurobiol*, 88, 272-85.
- Montgomery, D. L. (1994). Astrocytes: form, functions, and roles in disease. *Vet Pathol*, 31, 145-67.
- Moore, K. & Kim, L. (2010). *Primary Brain Tumors: Characteristics Practical Diagnostic and Treatment Approaches*, New York NY, Springer Science.
- Naik, P. & Cucullo, L. (2012). In vitro blood-brain barrier models: current and perspective technologies. *J Pharm Sci*, 101, 1337-54.
- Nakada, M., Kita, D., Watanabe, T., Hayashi, Y., Teng, L., Pyko, I. V. & Hamada, J.-I. (2011). Aberrant Signaling Pathways in Glioma. *Cancers*, 3, 3242-3278.
- Nakagawa, S., Deli, M., Kawaguchi, H., Shimizudani, T., Shimono, T., Kittel, A., Tanaka, K. & Niwa, M. (2009a). A new blood-brain barrier model using primary rat brain endothelial cells, pericytes and astrocytes. *Neurochem Int*, 54, 253 - 263.

- Nakagawa, S., Deli, M., Nakao, S., Honda, M., Hayashi, K., Nakaoka, R., Kataoka, Y. & Niwa, M. (2007a). Pericytes from brain microvessels strengthen the barrier integrity in primary cultures of rat brain endothelial cells. *Cell Mol Neurobiol*, 27, 687 - 694.
- Nakagawa, S., Deli, M. A., Kawaguchi, H., Shimizudani, T., Shimono, T., Kittel, A., Tanaka, K. & Niwa, M. (2009b). A new blood-brain barrier model using primary rat brain endothelial cells, pericytes and astrocytes. *Neurochemistry International*, 54, 253-263.
- Nakagawa, S., Deli, M. A., Nakao, S., Honda, M., Hayashi, K., Nakaoka, R., Kataoka, Y. & Niwa, M. (2007b). Pericytes from brain microvessels strengthen the barrier integrity in primary cultures of rat brain endothelial cells. *Cellular and Molecular Neurobiology*, 27, 687-694.
- Narayanan, R. & Gunturi, S. B. (2005). In silico ADME modelling: prediction models for blood-brain barrier permeation using a systematic variable selection method. *Bioorg Med Chem*, 13, 3017-28.
- Nathoo, N., Toms, S. A. & Barnett, G. H. (2004). Metastases to the brain: current management perspectives. *Expert Rev Neurother*, 4, 633-40.
- Nebert, D. W., Wikvall, K. & Miller, W. L. (2013). Human cytochromes P450 in health and disease. *Philos Trans R Soc Lond B Biol Sci*, 368, 20120431.
- Nelson, S. D. & Gordon, W. P. (1983). Mammalian Drug Metabolism. *Journal of Natural Products*, 46, 71-78.
- Nir, I., Levanon, D. & Iosilevsky, G. (1989). Permeability of blood vessels in experimental gliomas: uptake of <sup>99m</sup>Tc-glucoheptonate and alteration in blood-brain barrier as determined by cytochemistry and electron microscopy. *Neurosurgery*, 25, 523-31; discussion 531-2.
- Noguchi, K., Katayama, K., Mitsuhashi, J. & Sugimoto, Y. (2009). Functions of the breast cancer resistance protein (BCRP/ABCG2) in chemotherapy. *Adv Drug Deliv Rev*, 61, 26-33.
- Oberdorster, G., Elder, A. & Rinderknecht, A. (2009). Nanoparticles and the brain: cause for concern? *J Nanosci Nanotechnol*, 9, 4996-5007.
- Obermeier, B., Daneman, R. & Ransohoff, R. M. (2013). Development, maintenance and disruption of the blood-brain barrier. *Nat Med*, 19, 1584-1596.
- Ohgaki, H. & Kleihues, P. (2005). Epidemiology and etiology of gliomas. *Acta Neuropathologica*, 109, 93-108.
- Ohgaki, H. & Kleihues, P. (2007). Genetic pathways to primary and secondary glioblastoma. *Am J Pathol*, 170, 1445-53.
- Ohgaki, H. & Kleihues, P. (2013). The definition of primary and secondary glioblastoma. *Clin Cancer Res*, 19, 764-72.
- Oldendorf, W. H. (1971). Blood Brain Barrier Permeability to Lactate. *European Neurology*, 6, 49-55.
- Omidi, Y. & Barar, J. (2012). Impacts of blood-brain barrier in drug delivery and targeting of brain tumors. *Bioimpacts*, 2, 5-22.

- On, N. H., Mitchell, R., Savant, S. D., Bachmeier, C. J., Hatch, G. M. & Miller, D. W. (2013). Examination of blood-brain barrier (BBB) integrity in a mouse brain tumor model. *J Neurooncol*, 111, 133-43.
- Ostrom, Q. T., Bauchet, L., Davis, F. G., Deltour, I., Fisher, J. L., Langer, C. E., Pekmezci, M., Schwartzbaum, J. A., Turner, M. C., Walsh, K. M., Wrensch, M. R. & Barnholtz-Sloan, J. S. (2014). The epidemiology of glioma in adults: a “state of the science” review. *Neuro-Oncology*, 16, 896-913.
- Oyama, T., Kagawa, N., Kunugita, N., Kitagawa, K., Ogawa, M., Yamaguchi, T., Suzuki, R., Kinaga, T., Yashima, Y., Ozaki, S., Isse, T., Kim, Y. D., Kim, H. & Kawamoto, T. (2004). Expression of cytochrome P450 in tumor tissues and its association with cancer development. *Front Biosci*, 9, 1967-76.
- Palmiotti, C. A., Prasad, S., Naik, P., Abul, K. M., Sajja, R. K., Achyuta, A. H. & Cucullo, L. (2014). In Vitro Cerebrovascular Modeling in the 21st Century: Current and Prospective Technologies. *Pharm Res*.
- Pan, C., Kumar, C., Bohl, S., Klingmueller, U. & Mann, M. (2009). Comparative proteomic phenotyping of cell lines and primary cells to assess preservation of cell type-specific functions. *Mol Cell Proteomics*, 8, 443-50.
- Pardridge, W. M. (1999). Blood-brain barrier biology and methodology. *J Neurovirol*, 5, 556-69.
- Pardridge, W. M. (2003). Blood-brain barrier drug targeting: the future of brain drug development. *Mol Interv*, 3, 90-105, 51.
- Pardridge, W. M. (2005). The blood-brain barrier: bottleneck in brain drug development. *NeuroRx*, 2, 3-14.
- Parkinson, F. E., Ferguson, J., Zamzow, C. R. & Xiong, W. (2006). Gene expression for enzymes and transporters involved in regulating adenosine and inosine levels in rat forebrain neurons, astrocytes and C6 glioma cells. *J Neurosci Res*, 84, 801-8.
- Patabendige, A., Skinner, R. A., Morgan, L. & Joan Abbott, N. (2013). A detailed method for preparation of a functional and flexible blood–brain barrier model using porcine brain endothelial cells. *Brain Research*.
- Poller, B., Gutmann, H., Krähenbühl, S., Weksler, B., Romero, I., Couraud, P.-O., Tuffin, G., Drewe, J. & Huwyler, J. (2008). The human brain endothelial cell line hCMEC/D3 as a human blood-brain barrier model for drug transport studies. *Journal of Neurochemistry*, 107, 1358-1368.
- Rachet, B., Maringe, C., Nur, U., Quaresma, M., Shah, A., Woods, L. M., Ellis, L., Walters, S., Forman, D., Steward, J. & Coleman, M. P. (2009). Population-based cancer survival trends in England and Wales up to 2007: an assessment of the NHS cancer plan for England. *Lancet Oncol*, 10, 351-69.
- Ragnaill, M. N., Brown, M., Ye, D., Bramini, M., Callanan, S., Lynch, I. & Dawson, K. A. (2011). Internal benchmarking of a human blood–brain barrier cell model for screening of nanoparticle uptake and transcytosis. *European Journal of Pharmaceutics and Biopharmaceutics*, 77, 360-367.

- Rajkumar, S. V., Buckner, J. C., Schomberg, P. J., Reid, J. M., Bagniewski, P. J., Ames, M. M., Cascino, T. L. & Marks, R. S. (1998). Phase I and pharmacokinetic study of preirradiation chemotherapy with BCNU, cisplatin, etoposide, and accelerated radiation therapy in patients with high-grade glioma. *Int J Radiat Oncol Biol Phys*, 42, 969-75.
- Raleigh, D. R., Boe, D. M., Yu, D., Weber, C. R., Marchiando, A. M., Bradford, E. M., Wang, Y., Wu, L., Schneeberger, E. E., Shen, L. & Turner, J. R. (2011). Occludin S408 phosphorylation regulates tight junction protein interactions and barrier function. *J Cell Biol*, 193, 565-82.
- Reichel, A., Begley, D. J. & Abbott, N. J. (2003). An overview of in vitro techniques for blood-brain barrier studies. *Methods in molecular medicine*, 89, 307-324.
- Reichert, W. M. (2007). *Indwelling Neural Implants: Strategies for Contending with the In Vivo Environment*, CRC Press.
- Reni, M., Ferreri, A. J., Guha-Thakurta, N., Blay, J. Y., Dell'oro, S., Biron, P. & Hochberg, F. H. (2001). Clinical relevance of consolidation radiotherapy and other main therapeutic issues in primary central nervous system lymphomas treated with upfront high-dose methotrexate. *Int J Radiat Oncol Biol Phys*, 51, 419-25.
- Rieder, C. R., Ramsden, D. B. & Williams, A. C. (1998). Cytochrome P450 1B1 mRNA in the human central nervous system. *Mol Pathol*, 51, 138-42.
- Ritschel & Kerns (2004). *Handbook of Basic Pharmacokinetics including Clinical applications*, Washington, DC, Americal Pharmaceutical Association.
- Rivlin, N., Brosh, R., Oren, M. & Rotter, V. (2011). Mutations in the p53 Tumor Suppressor Gene: Important Milestones at the Various Steps of Tumorigenesis. *Genes & Cancer*, 2, 466-474.
- Robertson, G. R., Field, J., Goodwin, B., Bierach, S., Tran, M., Lehnert, A. & Liddle, C. (2003). Transgenic Mouse Models of Human CYP3A4 Gene Regulation. *Molecular Pharmacology*, 64, 42-50.
- Rodríguez-Escudero, I., Oliver, M. D., Andrés-Pons, A., Molina, M., Cid, V. J. & Pulido, R. (2011). A comprehensive functional analysis of PTEN mutations: implications in tumor- and autism-related syndromes. *Human Molecular Genetics*.
- Rojas, A. (2011). Cell line cross-contamination: who wins? *J Biol Chem*, 286, le20; author reply le21.
- Roth, M., Obaidat, A. & Hagenbuch, B. (2012). OATPs, OATs and OCTs: the organic anion and cation transporters of the SLCO and SLC22A gene superfamilies. *Br J Pharmacol*, 165, 1260-87.
- Roux, F. & Couraud, P. (2005). Rat brain endothelial cell lines for the study of blood-brain barrier permeability and transport functions. *Cell Mol Neurobiol*, 25, 41 - 58.
- Rubenstein, B. M. & Kaufman, L. J. (2008). The Role of Extracellular Matrix in Glioma Invasion: A Cellular Potts Model Approach. *Biophysical Journal*, 95, 5661-5680.
- Rubin, L., Hall, D., Porter, S., Barbu, K., Cannon, C., Horner, H., Janatpour, M., Liaw, C., Manning, K. & Morales, J. (1991). A cell culture model of the blood-brain barrier. *J Cell Biol*, 115, 1725 - 1735.

- Rucker, H. K., Wynder, H. J. & Thomas, W. E. (2000). Cellular mechanisms of CNS pericytes. *Brain Research Bulletin*, 51, 363-369.
- Ruoslahti, E. (1996). Brain extracellular matrix. *Glycobiology*, 6, 489-92.
- Sá-Pereira, I., Brites, D. & Brito, M. A. (2012). Neurovascular unit: a focus on pericytes. *Molecular neurobiology*, 45, 327-347.
- Scherer, H. J. (1938). Structural Development in Gliomas. *The American Journal of Cancer*, 34, 333-351.
- Scherer, H. J. (1940). Cerebral Astrocytomas and Their Derivatives. *The American Journal of Cancer*, 40, 159-198.
- Schinkel, A. H. (1999). P-Glycoprotein, a gatekeeper in the blood-brain barrier. *Adv Drug Deliv Rev*, 36, 179-194.
- Schlie-Wolter, S., Ngezahayo, A. & Chichkov, B. N. (2013). The selective role of ECM components on cell adhesion, morphology, proliferation and communication in vitro. *Experimental Cell Research*, 319, 1553-1561.
- Schuetz, E. & Strom, S. (2001). Promiscuous regulator of xenobiotic removal. *Nat Med*, 7, 536-7.
- Schwartzbaum, J. A., Fisher, J. L., Aldape, K. D. & Wrensch, M. (2006). Epidemiology and molecular pathology of glioma. *Nat Clin Pract Neuro*, 2, 494-503.
- Scotto, K. W. (2003). Transcriptional regulation of ABC drug transporters. *Oncogene*, 22, 7496-7511.
- Shawahna, R., Decleves, X. & Scherrmann, J. M. (2012). Hurdles with Using In Vitro Models to Predict Human Blood-brain Barrier Drug Permeability: A Special Focus on Transporters and Metabolizing Enzymes. *Curr Drug Metab*.
- Shen, S. & Zhang, W. (2010). ABC transporters and drug efflux at the blood-brain barrier. *Rev Neurosci*, 21, 29-53.
- Siddharthan, V., Kim, Y. V., Liu, S. & Kim, K. S. (2007). Human astrocytes/astrocyte-conditioned medium and shear stress enhance the barrier properties of human brain microvascular endothelial cells. *Brain Res*, 1147, 39-50.
- Simionescu, N., Simionescu, M. & Palade, G. E. (1975). Permeability of muscle capillaries to small heme-peptides. Evidence for the existence of patent transendothelial channels. *J Cell Biol*, 64, 586-607.
- Singh, P., Carraher, C. & Schwarzbauer, J. E. (2010). Assembly of fibronectin extracellular matrix. *Annu Rev Cell Dev Biol*, 26, 397-419.
- Smythe, E. & Ayscough, K. R. (2006). Actin regulation in endocytosis. *J Cell Sci*, 119, 4589-98.
- Sobue, K., Yamamoto, N., Yoneda, K., Hodgson, M., Yamashiro, K., Tsuruoka, N., Tsuda, T., Katsuya, H., Miura, Y. & Asai, K. (1999). Induction of blood-brain barrier properties in immortalized bovine brain endothelial cells by astrocytic factors. *Neurosci Res*, 35, 155 - 164.
- Song, C. M., Lim, S. J. & Tong, J. C. (2009). Recent advances in computer-aided drug design. *Briefings in Bioinformatics*, 10, 579-591.

- Sonoda, J., Rosenfeld, J. M., Xu, L., Evans, R. M. & Xie, W. (2003). A nuclear receptor-mediated xenobiotic response and its implication in drug metabolism and host protection. *Curr Drug Metab*, 4, 59-72.
- Stacey, G. 2001. Primary Cell Cultures and Immortal Cell Lines. *eLS*. John Wiley & Sons, Ltd.
- Stamatovic, S. M., Dimitrijevic, O. B., Keep, R. F. & Andjelkovic, A. V. (2006). Protein kinase Calpha-RhoA cross-talk in CCL2-induced alterations in brain endothelial permeability. *J Biol Chem*, 281, 8379-88.
- Stamatovic, S. M., Keep, R. F. & Andjelkovic, A. V. (2008). Brain endothelial cell-cell junctions: how to "open" the blood brain barrier. *Curr Neuropharmacol*, 6, 179-92.
- Stamatovic, S. M., Keep, R. F., Kunkel, S. L. & Andjelkovic, A. V. (2003). Potential role of MCP-1 in endothelial cell tight junction 'opening': signaling via Rho and Rho kinase. *J Cell Sci*, 116, 4615-28.
- Staud, F., Ceckova, M., Micuda, S. & Pavsek, P. (2010). Expression and function of p-glycoprotein in normal tissues: effect on pharmacokinetics. *Methods Mol Biol*, 596, 199-222.
- Strobel, H. W., Kawashima, H., Geng, J., Sequeira, D., Bergh, A., Hodgson, A. V., Wang, H. & Shen, S. (1995). Expression of multiple forms of brain cytochrome P450. *Toxicol Lett*, 82-83, 639-43.
- Strobel, H. W., Thompson, C. M. & Antonovic, L. (2001). Cytochromes P450 in brain: function and significance. *Curr Drug Metab*, 2, 199-214.
- Stummer, W. & Kamp, M. A. (2009). The importance of surgical resection in malignant glioma. *Curr Opin Neurol*, 22, 645-9.
- Stupp, R., Mason, W. P., Van Den Bent, M. J., Weller, M., Fisher, B., Taphoorn, M. J., Belanger, K., Brandes, A. A., Marosi, C., Bogdahn, U., Curschmann, J., Janzer, R. C., Ludwin, S. K., Gorlia, T., Allgeier, A., Lacombe, D., Cairncross, J. G., Eisenhauer, E., Mirimanoff, R. O., European Organisation For, R., Treatment of Cancer Brain, T., Radiotherapy, G. & National Cancer Institute of Canada Clinical Trials, G. (2005). Radiotherapy plus concomitant and adjuvant temozolomide for glioblastoma. *N Engl J Med*, 352, 987-96.
- Swartz, A. M., Li, Q. J. & Sampson, J. H. (2014). Rindopepimut: a promising immunotherapeutic for the treatment of glioblastoma multiforme. *Immunotherapy*, 6, 679-90.
- Synold, T. W., Dussault, I. & Forman, B. M. (2001). The orphan nuclear receptor SXR coordinately regulates drug metabolism and efflux. *Nat Med*, 7, 584-90.
- Takakura, Y., Audus, K. L. & Borchardt, R. T. (1991). Blood-Brain Barrier: Transport Studies in Isolated Brain Capillaries and in Cultured Brain Endothelial Cells.
- Tarbell, J. M. (2010). Shear stress and the endothelial transport barrier. *Cardiovasc Res*, 87, 320-30.
- Taylor, L. P. (2010). Diagnosis, treatment, and prognosis of glioma: Five new things. *Neurology*, 75, S28-S32.

- Theaker, J. M., Gatter, K. C., Esiri, M. M. & Fleming, K. A. (1986). Epithelial membrane antigen and cytokeratin expression by meningiomas: an immunohistological study. *J Clin Pathol*, 39, 435-9.
- Tian, X. H., Wei, F., Wang, T. X., Wang, P., Lin, X. N., Wang, J., Wang, D. & Ren, L. (2012). In vitro and in vivo studies on gelatin-siloxane nanoparticles conjugated with SynB peptide to increase drug delivery to the brain. *Int J Nanomedicine*, 7, 1031-41.
- Toth, A., Veszelka, S., Nakagawa, S., Niwa, M. & Deli, M. (2011). Patented in vitro blood-brain barrier models in CNS drug discovery. *Recent Pat CNS Drug Discov*, 6, 107 - 118.
- Toyoda, K., Tanaka, K., Nakagawa, S., Thuy, D. H., Ujifuku, K., Kamada, K., Hayashi, K., Matsuo, T., Nagata, I. & Niwa, M. (2013). Initial contact of glioblastoma cells with existing normal brain endothelial cells strengthen the barrier function via fibroblast growth factor 2 secretion: a new in vitro blood-brain barrier model. *Cell Mol Neurobiol*, 33, 489-501.
- Tsujino, K., Yamate, J., Tsukamoto, Y., Kumagai, D., Kannan, Y., Jippo, T., Kuwamura, M., Kotani, T., Takeya, M. & Sakuma, S. (1997). Establishment and Characterization of cell lines derived from a transplantable rat malignant meningioma: morphological heterogeneity and production of nerve growth factor. *Acta Neuropathol*, 93, 461 - 470.
- Tsuneki, M. & Madri, J. A. (2014). CD44 regulation of endothelial cell proliferation and apoptosis via modulation of CD31 and VE-cadherin expression. *Journal of Biological Chemistry*.
- Ulbrich, K., Hekmatara, T., Herbert, E. & Kreuter, J. (2009). Transferrin- and transferrin-receptor-antibody-modified nanoparticles enable drug delivery across the blood-brain barrier (BBB). *Eur J Pharm Biopharm*, 71, 251-6.
- Ulrich, T. A., De Juan Pardo, E. M. & Kumar, S. (2009). The mechanical rigidity of the extracellular matrix regulates the structure, motility, and proliferation of glioma cells. *Cancer Res*, 69, 4167-74.
- Urich, E., Lazic, S., Molnos, J., Wells, I. & Freskgard, P. (2012). Transcriptional profiling of human brain endothelial cells reveals key properties crucial for predictive in vitro blood-brain barrier models. *PLoS One*, 7, e38149.
- Van Hinsbergh, V. W. & Van Nieuw Amerongen, G. P. (2002). Intracellular signalling involved in modulating human endothelial barrier function. *J Anat*, 200, 549-60.
- Van Schaik, R. H. (2008). CYP450 pharmacogenetics for personalizing cancer therapy. *Drug Resist Updat*, 11, 77-98.
- Vartanian, A., Singh, S. K., Agnihotri, S., Jalali, S., Burrell, K., Aldape, K. D. & Zadeh, G. (2014). GBM's multifaceted landscape: highlighting regional and microenvironmental heterogeneity. *Neuro-Oncology*, 16, 1167-1175.
- Veringa, S. J. E., Biesmans, D., Van Vuurden, D. G., Jansen, M. H. A., Wedekind, L. E., Horsman, I., Wesseling, P., Vandertop, W. P., Noske, D. P., Kaspers, G. J. L. & Hulleman, E. (2013). *In Vitro* Drug Response and Efflux Transporters Associated with Drug Resistance in Pediatric High Grade Glioma and Diffuse Intrinsic Pontine Glioma. *PLoS ONE*, 8, e61512.

- Vescovi, A. L., Galli, R. & Reynolds, B. A. (2006). Brain tumour stem cells. *Nat Rev Cancer*, 6, 425-36.
- Vierck, J. L. & Dodson, M. V. (2000). Interpretation of cell culture phenomena. *Methods Cell Sci*, 22, 79-81.
- Virgintino, D., Robertson, D., Errede, M., Benagiano, V., Girolamo, F., Maiorano, E., Roncali, L. & Bertossi, M. (2002). Expression of P-glycoprotein in human cerebral cortex microvessels. *J Histochem Cytochem*, 50, 1671-6.
- Vulic, M. & Kolter, R. (2002). Alcohol-induced delay of viability loss in stationary-phase cultures of *Escherichia coli*. *J Bacteriol*, 184, 2898-905.
- Warren, M., Zerangue, N., Woodford, K., Roberts, L., Tate, E. & Feng, B. (2009). Comparative gene expression profiles of ABC transporters in brain microvessel endothelial cells and brain in five species including human. *Pharmacol Res*, 59, 404 - 413.
- Weidenfeller, C., Schrot, S., Zozulya, A. & Galla, H. (2005). Murine brain capillary endothelial cells exhibit improved barrier properties under the influence of hydrocortisone. *Brain Res*, 1053, 162 - 174.
- Weksler, B., Romero, I. & Couraud, P.-O. (2013). The hCMEC/D3 cell line as a model of the human blood brain barrier. *Fluids and Barriers of the CNS*, 10, 16.
- Wen, P. Y. & Loeffler, J. S. (2000). Brain metastases. *Curr Treat Options Oncol*, 1, 447-58.
- Wenger, S. L., Senft, J. R., Sargent, L. M., Bamezai, R., Bairwa, N. & Grant, S. G. (2004). Comparison of established cell lines at different passages by karyotype and comparative genomic hybridization. *Biosci Rep*, 24, 631-9.
- Wilhelm, I., Fazakas, C. & Krizbai, I. (2011a). In vitro models of the blood-brain barrier. *Acta Neurobiol Exp*, 71, 113 - 128.
- Wilhelm, I., Fazakas, C. & Krizbai, I. A. (2011b). In vitro models of the blood-brain barrier. *Acta Neurobiol Exp (Wars)*, 71, 113-28.
- Wilhelm, I. & Krizbai, I. A. (2014). In Vitro Models of the Blood–Brain Barrier for the Study of Drug Delivery to the Brain. *Molecular Pharmaceutics*, 11, 1949-1963.
- Williams, R. T. (1959). *Detoxification Mechanisms*, New York, Wiley.
- Willis, C. L., Meske, D. S. & Davis, T. P. (2010). Protein kinase C activation modulates reversible increase in cortical blood-brain barrier permeability and tight junction protein expression during hypoxia and posthypoxic reoxygenation. *J Cereb Blood Flow Metab*, 30, 1847-59.
- Wolburg, H., Neuhaus, J., Kniesel, U., Krauss, B., Schmid, E. M., Ocalan, M., Farrell, C. & Risau, W. (1994). Modulation of tight junction structure in blood-brain barrier endothelial cells. Effects of tissue culture, second messengers and cocultured astrocytes. *Journal of Cell Science*, 107, 1347-1357.
- Wong, A., Ye, M., Levy, A., Rothstein, J., Bergles, D. & Searson, P. C. (2013). The Blood-Brain Barrier: An Engineering Perspective. *Frontiers in Neuroengineering*, 6.
- Xiao, G. & Gan, L.-S. (2013). Receptor-Mediated Endocytosis and Brain Delivery of Therapeutic Biologics. *International Journal of Cell Biology*, 2013, 14.

- Xu, C., Li, C. Y. & Kong, A. N. (2005). Induction of phase I, II and III drug metabolism/transport by xenobiotics. *Arch Pharm Res*, 28, 249-68.
- Xu, F., Wu, J., Wang, S., Durmus, N. G., Gurkan, U. A. & Demirci, U. (2011). Microengineering methods for cell-based microarrays and high-throughput drug-screening applications. *Biofabrication*, 3, 034101.
- Ye, D., Dawson, K. A. & Lynch, I. (2014). A TEM protocol for quality assurance of in vitro cellular barrier models and its application to the assessment of nanoparticle transport mechanisms across barriers. *Analyst*.
- Yuan, S. Y. & Rigor, R. R. (2011). *Regulation of Endothelial Barrier Function*, Morgan & Claypool.
- Zenker, D., Begley, D., Bratzke, H., Rubsamen-Waigmann, H. & Von Briesen, H. (2003). Human blood-derived macrophages enhance barrier function of cultured primary bovine and human brain capillary endothelial cells. *J Physiol*, 551, 1023-32.
- Zlokovic, B. (2008). The blood-brain barrier in health and chronic neurodegenerative disorders. *Neuron*, 57, 178 - 201.

# 10. Appendices

## 1) Cell culture

### Cell Counting

From the trypsinised cell suspension, 10  $\mu\text{l}$  was aliquotted in a 1 mL sterile eppendorf tube to which 10  $\mu\text{l}$  of trypan blue dye was added. Trypan blue is a vital dye with a negatively charged chromophore (Strober, 2001). It reacts only with cells with a lysed membrane and stains them blue. Hence, the cells that exclude the dye were counted as viable. The Neubauer counting chamber / haemocytometer was used for counting cells.

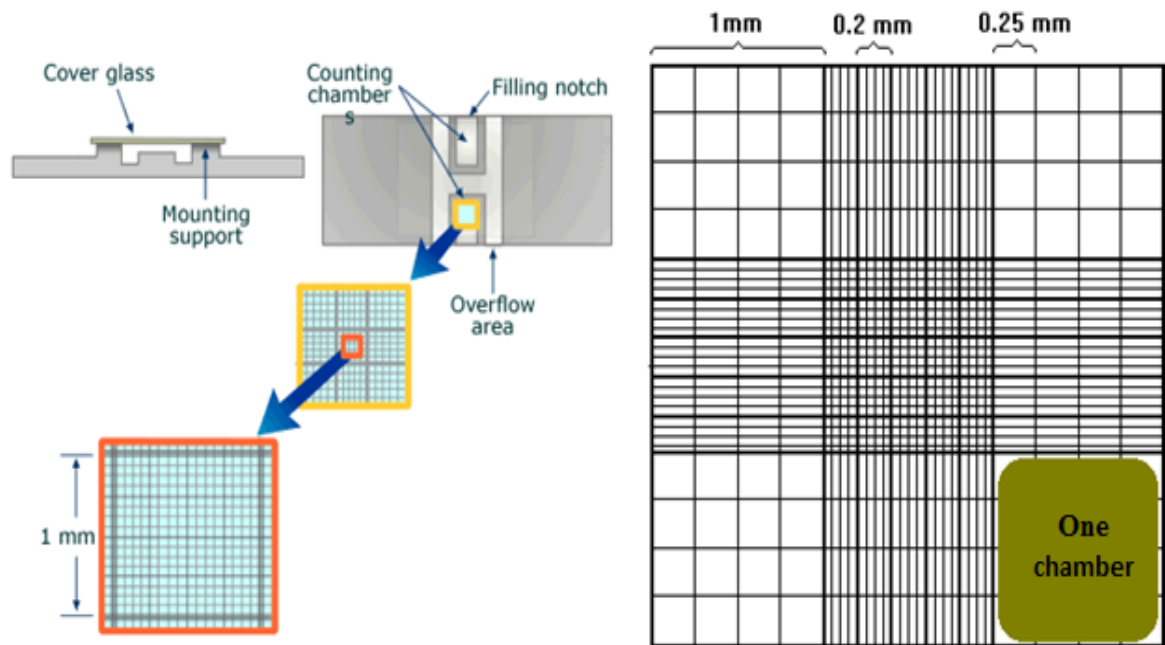


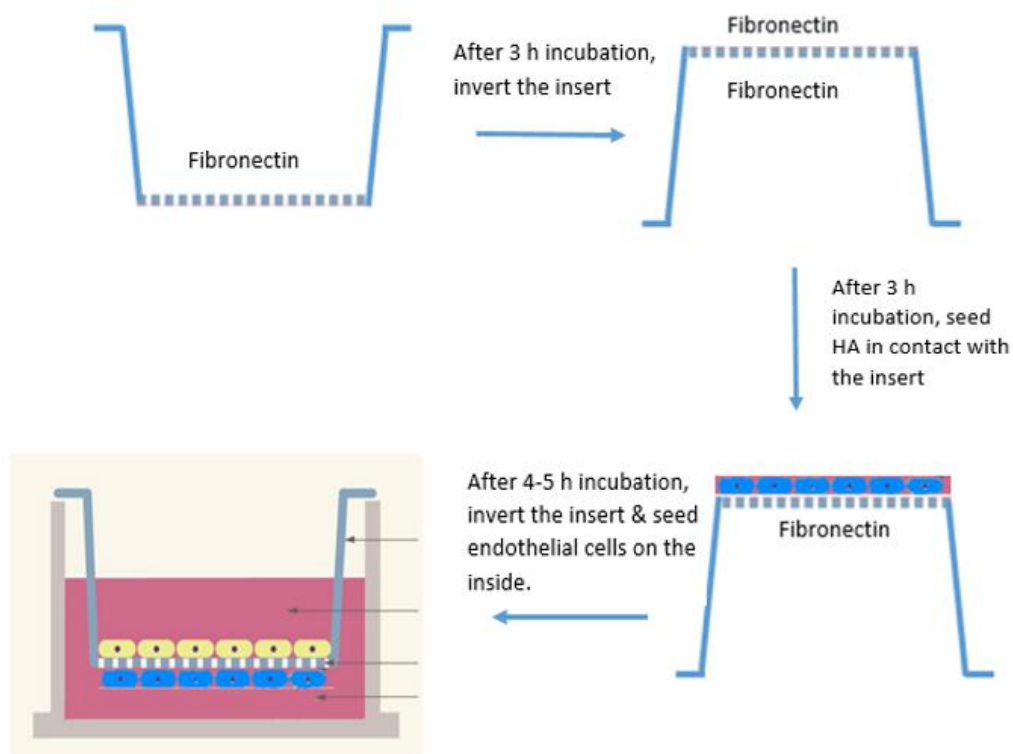
Diagram showing haemocytometer and its dimensions.

Ten microliter of trypan blue stained suspension was loaded on to the haemocytometer and the cells were counted under the inverted light microscope at 10 X magnification (Leica DMIL, Bucks, UK). The microscope was focused on 25 squares of one chamber and the number of cells in these squares were counted, this step was then repeated for the other chambers as well (Figure 26). The average number of cells in the centre grid (1  $\text{mm}^2$ ) of each

chamber was counted and this number was multiplied with the haemocytometer factor  $1 \times 10^4$  and then cell count was corrected for dilution factors to obtain the number of cells per 1 mL of suspension. This number would then be used either for seeding the cells in 96 microtiter well plates, tissue culture flasks or for cryopreservation. The cells were seeded at density of 2000 cells/ 200  $\mu\text{L}$ / well in 96 microtiter plate, 20,000 cells/ mL/ well in 24 well plate and  $1 \times 10^6$  cells/ mL/ flask in 75  $\text{cm}^2$  flask.

## 2) Setting up Transwell inserts for in contact co-cultures

Diagrammatic representation of the protocol to set up transwell cultures



### 3) HBSS buffer recipe

400 mg Potassium Chloride (KCl, FW=75; Sigma #P-4504)

60 mg Potassium Phosphate, monobasic (KH<sub>2</sub>PO<sub>4</sub>, FW=136; Sigma #P-8416)

350 mg Sodium Bicarbonate (NaHCO<sub>3</sub>, FW=84; Sigma #S-5761)

8000 mg Sodium Chloride (NaCl, FW=158; Sigma #S-5629)

48 mg Sodium Phosphate, dibasic, anhydrous (Na<sub>2</sub>HPO<sub>4</sub>, FW=142; Sigma #S-5136)

1000 mg D-Glucose (Dextrose, FW=180; Sigma #G-7021)

10 mg Phenol Red (FW=376.4; Sigma #P-5530)

### 4) Western blotting

#### 10 % SDS PAGE gel recipe

*Recipe for casting resolving and stacking gel for SDS-PAGE.*

Materials	10% Resolving Gel (for two gels)	4% Stacking Gel (for two gels)
dH <sub>2</sub> O	4.7 mL	4.5 mL
1.5M Tris Buffer (pH 8.8)	2.6 mL	-
1M Tris Buffer (pH 6.8)	-	0.76 mL
10% SDS	100 µl	60 µl
40% Acrylamide	2.5 mL	0.6 mL
10% APS (freshly made only)	100 µl	60 µl
TEMED (added prior to pouring gel)	10 µl	6 µl
Total Volume	10 mL	6 mL

### 5) Buffer recipe used in Western blotting

	Buffer	Recipe
1	RIPA buffer	150 mM sodium chloride 1.0% Triton X-100 0.5% sodium deoxycholate 0.1% SDS (sodium dodecyl sulphate) 50 mM Tris, pH 8.0
2	Sample loading buffer	4% SDS 10% 2-mercaptoethanol 20% glycerol 0.004% bromophenol blue 0.125 M Tris HCl
3	Electrophoresis buffer (10X)	303 g Trisbase (FW 121.1) 1440 g glycine (FW 75.07) 100 g SDS
4	Transfer buffer (10X)	303 g Trisbase, 1440 g glycine
5	Wash buffer (10X)	24.23 g Trizma HCl 80.06 g NaCl 800 ml distilled water. pH to 7.6
6	Blocking buffer	Wash buffer + 5 % milk powder
7	Stripping buffer	15 g glycine 1 g SDS 10 ml Tween 20 800ml with ultrapure water Adjust pH to 2.2